Universität Konstanz

Systems Biological Analysis of Bcl-2 Family Interactions and Effector Oligomerization

Doctoral thesis for obtaining the academic degree
Doctor of Natural Sciences

submitted by
Hantusch, Annika

at the University of Konstanz
Faculty of Sciences
Department of Biology

Konstanz, 2017

Date of the oral examination: February 27, 2018

1. Reviewer: Prof. Dr. Thomas Brunner
2. Reviewer: Prof. Dr. Markus Morrison (Rehm), University of Stuttgart
3. Reviewer: PD Dr. Aswin Mangerich

We must accept finite disappointment,
but never lose infinite hope.

Martin Luther King Jr.

Contents

Summary

The Bcl-2 protein family controls mitochondrial outer membrane permeabilization (MOMP), a point of no return in apoptosis regulation. Despite a vast amount of available experimental studies investigating the interactions within the family, an encompassing understanding of the regulatory processes occurring in aqueous and membrane environments remains elusive. Here, a systems biological approach of quantitative kinetic modeling in combination with retro- and prospective experimental data was used to gain mechanistic insights into the Bcl-2 interactome. Novel and currently underappreciated mechanisms of action were identified within the interaction network of the Bcl-2 family members tBid, Bax, Bcl-xL and a sensitizer BH3-only protein. Furthermore, a comprehensive database encompassing 15 well-defined family members was developed (Bcl-2-Ome), which facilitates navigation and detailed analysis of published experimental data on the Bcl-2 interactome. These results were obtained in three independent studies:
(1) In Chapter 2, the Bcl-2-Ome web service is presented. It comprises 353 curated experimental outcomes with detailed information on experimental conditions to allow comparison of multiple and seemingly conflicting studies in their contexts. (2) A computational model based on ordinary differential equations was developed, which accurately captures Bax membrane-recruitment, activation and oligomerization (Chapter 3). Extension of the model by the prosurvival protein Bcl-xL revealed that Bcl-xL's retrotranslocation activity is indispensable to reproduce the disassembly of Bax pores. Moreover, incorporation of retrotranslocation into the model enables prediction of sharp decision thresholds of MOMP competency as well as synergies arising by combinations of tBid and sensitizer BH3-only input. (3) In Chapter 4, different plausible interaction scenarios were modeled based on time-resolved data on tBid and Bcl-xL homo- and heterodimerizations. Model selection criteria supported a novel mechanism of action of tBid interaction with Bcl-xL homodimers in aqueous environment, which induces heterodimer formation.
Taken together, the results of this thesis provide a web service for dissection of the Bcl-2 interactome at an unprecedented level of detail, suggest a novel interaction mechanism of tBid and Bcl-xL in solution, and highlight the importance of Bcl-xL retrotranslocation activity for MOMP regulation.

Zusammenfassung

Die Bcl-2 Proteinfamilie übt eine wichtige Funktion in der Apoptoseregulation aus, indem sie die irreversible Permeabilisierung der äußeren mitochondrialen Membran (MOMP) vermittelt. Trotz einer Vielzahl experimenteller Studien über die Interaktionen innerhalb der Proteinfamilie bleibt ein umfassendes Verständnis der regulatorischen Prozesse, die sich in Membranen oder wässrigen Lösungen abspielen können, zurzeit nicht greifbar. In der vorliegenden Arbeit wurde ein systembiologischer Ansatz verwendet, bestehend aus quantitativer kinetischer Modellierung in Kombination mit retro- und prospektiven experimentellen Daten, um mechanistische Prozesse innerhalb des Bcl-2 Interaktoms zu ergründen. Durch diesen Ansatz wurden neue sowie aktuell unterschätzte regulatorische Mechanismen innerhalb des Interaktionsnetzwerkes der Bcl-2 Familienmitglieder tBid, Bax, Bcl-xL und einem sensitizer BH3-only Protein ermittelt. Des Weiteren wurde eine Datenbank entwickelt, die Protein-Protein-Interaktionsdaten über 15 Bcl-2 Familienmitglieder beinhaltet (Bcl-2-Ome). Sie erleichtert einen umfassenden Überblick und die Analyse von publizierten experimentellen Daten, die das Bcl-2 Interaktom betreffen. Diese Ergebnisse wurden durch drei voneinander unabhängigen Studien erzielt:
(1) In Kapitel 2 wird der Bcl-2-Ome Webservice beschrieben. Er umfasst 353 experimentelle Ergebnisse mit detaillierten Informationen über die experimentellen Bedingungen des Versuchs und erlaubt dadurch den Vergleich mehrerer und sich scheinbar widersprechender Studien. (2) Ein auf gewöhnlichen Differentialgleichungen basierendes mathematisches Modell wurde entwickelt, welches die Membranrekrutierung, Aktivierung und Oligomerisation von Bax akkurat erfasst (Kapitel 3). Erweiterung des Modells um das antiapoptotische Protein Bcl-xL ergab des Weiteren, dass die retrotranslozierende Aktivität von Bcl-xL unabdingbar ist, um die Auflösung von Bax Poren zu reproduzieren und um den plötzlichen Umschwung der MOMP-Induktion innerhalb eines engen Konzentrationsbereichs und die durch kombinierte Stimulation mit tBid und sensitizer BH3-only entstehenden Synergien vorherzusagen. (3) In Kapitel 4 wurden verschiedene plausible Interaktionsszenarien, basierend auf zeitaufgelösten experimentellen Daten über die Homo- und Heterodimerisierung von tBid und Bcl-xL, modelliert. Modellselektionskriterien legen einen bislang unvermuteten molekularen Mechanismus nahe, bei dem tBid mit

Bcl-xL heterodimerisiert, indem es an Bcl-xL Homodimere bindet.
Zusammenfassend wurde durch die in dieser Dissertation präsentierte Arbeit ein Webservice entwickelt, der es erlaubt, publizierte Daten über das Bcl-2 Interaktom einfach und detailliert zu analysieren. Überdies wurden ein neuer Interaktionsmechanismus von tBid und Bcl-xL in Lösung vorgeschlagen und ein hoher Stellenwert von Bcl-xL vermittelter Retrotranslokation für die MOMP-Regulation hervorgehoben.

Acknowledgments

Thank you Thomi for your continuous support throughout my whole PhD, without you, this project would not have been possible. You were a constant source of scientific enthusiasm and reliability and I believe there are few group leaders with such a sense of humanity as you have it. You made not only my project, but the whole FOR2036 consortium a success and a place where people collaboratively work together and are not afraid to share their ideas. I enjoyed every moment since I could join your group and it is hard for me to leave.

Thank you Markus for your willingness to supervise my project and all the thoughts, effort and time you spent on it. With you I had the most enjoyable scientific discussions. From the moment you became my supervisor, there was not a single occasion when I could not rely on your scientific and personal support.

I would like to thank Tancred, who taught me my first programming steps and who enabled me to make the step into systems biology.

Thank you to Christine Peter for joining my thesis committee and her helpful comments and input.

Many thanks go to the Membrane Biophysics group at University of Tübingen, whose quantitative data built the basis for the computational models presented in this thesis. I would especially like to thank Stephanie, Ana and Kushal for very fruitful collaborations and testing of model predictions.

Thank you Eugenia, for being the best officemate I could have hoped for! With you every day in the office was a good one, no matter the scientific results.

Thank you Janine for a wonderful time in the lab, in Obergurgl and Fiuggi. And thank you to all members of the Brunner lab, you build a wonderful and familiar atmosphere.

Many thanks to all members of the FOR2036 research consortium, it was a great place to pursue a PhD project. And thank you to all the people I met on conferences and workshops and who inspired me.

There are so many people I would like to thank, many of which will probably never read this thesis, but greatly contributed to its outcome.

Vielen Dank an meine Familie, die mich kennt, die mit mir durch dick und dünn geht, bei der ich ich sein darf, die immer für mich da ist. Es ist schön, eine so große und tolle Familie zu haben!

Ich danke all meinen Freunden und Marco dafür, dass ich sie habe und ich auf sie bauen kann. Ich danke dir, Kathrin, für deine unglaubliche Energie und greif-nach-den-Sternen-Einstellung, die mich immer wieder inspiriert.

Furthermore, I would like to thank the authors of the following books, which have been constant sources of inspiration for me during my thesis, in chronological order:

- E. Klipp, W. Liebermeister, C. Wierling, A. Kowald, H. Lehrach, and R. Herwig, editors. *Systems biology: a textbook*. Wiley-VCH, Weinheim, 1. reprint edition, 2010
- A. Saltelli, editor. *Global sensitivity analysis: the primer*. John Wiley, Chichester, England ; Hoboken, NJ, 2008
- D. Holtom and E. Fisher. *Enjoy writing your science thesis or dissertation! a step by step guide to planning and writing dissertations and theses for undergraduate and graduate science students*. Imperial College Press, London, repr edition, 2006. OCLC: 837634836

List of Publications

The work presented in this thesis encompasses the following publications and manuscripts:

Chapter 2

Annika Hantusch, Thomas Brunner, Tancred Frickey*, and Markus Rehm*. Bcl-2-Ome - a database and interactive web service for dissecting the Bcl-2 interactome. *Cell Death and Differentiation*, 24(1):192-192, January 2017.

Chapter 3

Annika Hantusch, Kushal Kumar Das, Ana J. Garcia-Saez, Thomas Brunner*, and Markus Rehm*. Bax retrotranslocation potentiates Bcl-xL activity and is essential for systems-level switching of apoptosis competency. *Manuscript submitted.*

Chapter 4

Stephanie Bleicken, **Annika Hantusch**, Kushal Kumar Das, Tancred Frickey, and Ana J. Garcia-Saez. Quantitative interactome of a membrane Bcl-2 network identifies a hierarchy of complexes for apoptosis regulation. *Nature Communications.* 8(1):73, July 2017.

*joint senior authors

Declaration of Author's Contributions

Chapter 2

Annika Hantusch collected primary experimental data, designed the xml file, programmed the web service and wrote the manuscript. Thomas Brunner, Tancred Frickey and Markus Rehm contributed to design the web service and to write the manuscript.

Chapter 3

Annika Hantusch performed the modeling, designed the simulations and wrote the manuscript. Kushal Kumar Das performed experiments and analyzed data. Ana J. Garcia-Saez contributed to design experiments and write the manuscript. Thomas Brunner and Markus Rehm contributed to design the study and simulation experiments and to write the manuscript.

Chapter 4

Stefanie Bleicken designed and performed experiments, analyzed data, and wrote the manuscript. Kushal Kumar Das performed experiments and analyzed data. Annika Hantusch and Tancred Frickey did the modeling and wrote the modeling part of the manuscript. Ana J. Garcia-Saez designed the study, planned experiments, and wrote the manuscript.

Abbreviations

Apaf-1	apoptotic protease activating factor 1
ATP	adenosine triphosphate
Bad	Bcl-2 associated death promoter
Bak	Bcl-2 homologous antagonist killer
Bax	Bcl-2 associated X protein
Bcl-2	B-cell lymphoma 2
Bcl-w	Bcl-2-like protein 2
Bcl-xL	B-cell lymphoma-extra large
Bfl-1/A1	Bcl-2-related protein A1
BH	Bcl-2 homology
BH3	Bcl-2 homology domain 3
Bid	BH3 interacting-domain death agonist
Bik	Bcl-2-interacting killer
Bim	Bcl2-interacting mediator of cell death
Bmf	Bcl-2-modifying factor
Bok	Bcl-2 related ovarian killer
caspase	cysteine-dependent aspartate-directed proteases
cBid	caspase-8 cleaved Bid
cFLIP	cellular FLICE-like inhibitory protein
cIAP	cellular inhibitor of apoptosis
CLL	chronic lymphocytic leukemia
COPASI	complex pathway simulator
DAMP	damage-associated molecular pattern
dATP	deoxyadenosine triphosphate

DED	death effector domain
DISC	death inducing signaling complex
DLC	dynein light chain
DNA	deoxyribonucleic acid
DR	death receptor
ER	endoplasmic reticulum
ERAD	ER-associated degradation
ERK	extracellular signal-regulated kinase
FADD	FAS-associated death domain protein
FAS	tumor necrosis factor receptor superfamily member 6
GFP	green fluorescent protein
Hrk	activator of apoptosis harakiri
JNK	c-Jun N-terminal kinase
K_M	Michaelis-Menten constant
k_{off}	dissociation rate constant
k_{on}	association rate constant
kDa	kilo Dalton
LUBAC	linear ubiquitin chain assembly complex
MAP	mitogen-activated protein
Mcl-1	induced myeloid leukemia cell differentiation protein Mcl-1
MLKL	mixed lineage kinase domain-like
MOM	mitochondrial outer membrane
MOMP	mitochondrial outer membrane permeabilization
NF-$\varkappa$B	nuclear factor kappa-light-chain-enhancer of activated B cells
NIK	NF-$\varkappa$B-inducing kinase
Noxa	phorbol-12-myristate-13-acetate-induced protein 1
ODE	ordinary differential equations
p53	cellular tumor antigen p53

PCD	programmed cell death
PDE	partial differential equations
PKB/Akt	protein kinase B
Puma	p53 upregulated modulator of apoptosis
RIPK1	receptor-interacting serine/threonine-protein kinase 1
RIPK3	receptor-interacting serine/threonine-protein kinase 3
SBML	systems biology markup language
Smac	second mitochondria-derived activator of caspases
SSR	sum of squared residuals
tBid	truncated Bid
TIRF	total internal reflection fluorescence
TNF	tumor necrosis factor
TNFR1	tumor necrosis factor receptor superfamily member 1A
TRADD	tumor necrosis factor receptor type 1-associated death domain protein
TRAF	TNF receptor-associated factor
TRAIL	tumor necrosis factor-related apoptosis-inducing ligand
TRAILR	TRAIL receptor
VDAC2	voltage-dependent anion channel 2
XIAP	X-linked inhibitor of apoptosis protein

List of Figures

List of Tables

1 Introduction

The cell, the functional unit of our body, is a highly complex entity, which can adapt to its environment by translating incoming signals via a multitude of intertwined signaling pathways. Whether the outside conditions of the cell change by different nutrient supply or exposure to hormones, or if intracellular perturbations arise due to heat shock or radiation, cellular strategies exist that regulate sensing, signaling and adaption (Alberts, 2015). Major regulators of these signaling pathways are proteins and their dynamic interplay. A mammalian cell expresses more than 100,000 distinct proteins (Sims and Allbritton, 2007), and fascinatingly only a small, yet important, fraction of around 4% of the human proteome mediates cell signaling (Liebermeister et al., 2014).

The cell is not solitary, but part of higher order organizational structures, forming tissues, organs and the whole body. It provides its functions jointly with on the order of 10^{13} other, differently or similarly specialized human cells in the body (Sender et al., 2016). Irrespective of the cell's specialized function, adaption and cellular decision making in response to stimuli is common in all cell types. Signaling pathways are not only similar in the whole human body, but even conserved across species (Babonis and Martindale, 2017). In multicellular organisms, a remarkable and drastic cellular decision that can be mediated by its signaling circuits is the cell's decision to die. This process is termed programmed cell death, and its best described form is apoptosis, in which the cell prepares its own removal by phagocytosis. The cell death pathway might be employed when a cell is damaged to an irreversible extent or unneeded in the further development process of the organism. By triggering the highly conserved apoptotic program, the cell possesses the ability to induce and mediate its stepwise decomposition (Green and Fitzgerald, 2016).

Interestingly, although apoptosis triggering stimuli can be registered and processed by the cell through a variety of different receptors at the cell membrane as well as intracellular sensors and connected pathways, in most cases, efficient apoptosis execution requires an activation of the Bcl-2 (B-cell lymphoma 2) protein family (Delbridge and Strasser, 2015). This major player of the apoptotic program guards a point of no return in the cell's decision to die and is part of the intrinsic apoptosis pathway. A highly complex network of protein-protein interactions within the Bcl-2 family can irreversibly induce

the apoptotic program by triggering the formation of pores in the outer mitochondrial membrane. Given the importance of this molecular checkpoint in deciding cellular fate, it is hardly surprising that health and disease states critically depend on the functioning or malfunctioning of the apoptotic pathways and especially the members of the Bcl-2 family (Czabotar et al., 2014).

This thesis is dedicated to deciphering and capturing the complex interplay of pro- and antiapoptotic Bcl-2 family members in a systems biological approach, by computational modeling based on experimental data. In the following sections, the molecular pathways mediating programmed cell death will be described. It will furthermore be discussed, how strategic exploitation of extended knowledge of mechanisms of action in apoptosis regulation can be utilized for the development of targeted therapies. After putting the intrinsic pathway of apoptosis into context, the focus of the following sections will be a thorough analysis of the molecular mechanisms within the Bcl-2 family (section 1.2) and the use of systems modeling approaches to enhance the understanding of those (section 1.3). Although the Bcl-2 family has been heavily investigated since the identification of its first family member decades ago (Tsujimoto et al., 1984a), quantitative computational models capturing its regulatory mechanisms can now be used to aid in predicting the cellular response to disturbances. Highly specific drugs targeted at individual Bcl-2 family members are currently FDA approved, investigated in clinical trials and in further development (Roberts et al., 2016; Kotschy et al., 2016).

1.1 Apoptosis and its relevance in health and disease

Apoptosis can be induced by two distinct apoptosis signaling pathways, an extrinsic and an intrinsic one (see following sections and Figure 1.1), and represents the best understood form of programmed cell death (PCD). Also other forms of PCD exist, such as regulated necrosis and autophagic cell death. While autophagy merely seems to play auxiliary roles in apoptosis-mediated cell death, regulated necrosis might serve as a back-up program for apoptosis and is mediated by molecular players that have considerable overlap with those of the apoptotic pathway (see section 1.1.2).

Several processes in the human body depend on the regulated removal of cells. In fetal mammalian development, cells comprising the interdigital webs are removed via the apoptotic program (Duprez et al., 2009). Also the number of oocytes of human females is regulated by apoptosis, and the chambers of the heart are shaped as cells undergo programmed cell death (Fuchs and Steller, 2011).

Furthermore, the possibility to induce apoptosis allows the body to explore beneficial

or harmful cellular functions in a trial and error-like manner. In this way, the immune system induces apoptotic cell death during lymphocyte selection (Opferman, 2008). By selectively killing autoreactive cells, the generation of specialized lymphocytes that highly specifically recognize and combat pathogens is enabled, while autoimmune reactions are prevented.

Homeostasis of the adult body relies on continuous proliferation and growth, but also destruction of cells (Duprez et al., 2009). Tissue in which cells are constantly produced throughout life requires continuous regulated removal of cells. This is especially important if cells accumulated mutations or irreparable DNA (deoxyribonucleic acid) damage. Apoptosis can then serve as a quality control mechanism by allowing the removal of malfunctioning cells (Fuchs and Steller, 2011).

At the same time, execution of programmed cell death requires tight regulation. If more cells die than are replaced, this can result in atrophy. Additionally, some cell types in the human body are not subject to a high turnover and increased cell death rates can cause irreparable damage in the affected tissues. Neurodegenerative diseases, such as Alzheimer's, have been linked to excessive execution of apoptosis in neurons (Mattson et al., 2008; Green et al., 2011).

Importantly, the intrinsic capability of cells to induce their own death can be beneficially exploited in a pharmaceutical context to kill unwanted cells in the human body. Induction of apoptosis is a highly attractive approach in cancer therapy, especially as it has been shown that cancer cells are often more prone to undergo apoptosis than healthy cells (Holohan et al., 2013).

1.1.1 Extrinsic and intrinsic apoptosis pathway

The execution of apoptosis by definition results in the activation of cysteine-dependent aspartate-directed proteases, termed caspases. These caspases cleave approximately 1,000 distinct substrates in the cell, leading to organized cellular destruction (Crawford and Wells, 2011). Induction of the caspase cascade is caused by activation of initiator caspases (8, 9 and 10), which in turn cleave and activate effector caspase (3 and 7) (Crawford and Wells, 2011; Tummers and Green, 2017). The cleavage of crucial cellular components by caspases also mediates the morphological characteristics by which cells undergoing apoptosis have been characterized early on in apoptosis research. These include membrane blebbing, DNA fragmentation, the exposure of phosphatidylserine in the cellular membrane to the extracellular environment and cell shrinkage (Green and Fitzgerald, 2016). Cellular components remaining from the dead cells are recycled by phagocytosis and an inflammatory response is prevented (Park and Kim, 2017).

While the biochemical understanding of processes occurring during apoptosis has increased substantially, the Nomenclature Committee on Cell Death has proposed a definition of the apoptotic pathways based on functional rather than morphological characteristics (Galluzzi et al., 2012), as will be described in the following paragraphs.

Extrinsic apoptosis is usually triggered by external ligands binding to death receptors (DR), which are members of the TNF (tumor necrosis factor) receptor super family. It thus commences with receptor ligand interactions at the cellular membrane, justifying the term 'extrinsic' pathway. This pathway leads to activation of the so called caspase cascade immediately downstream of ligand engagement and the formation of a multiprotein complex at the death receptor (Fulda, 2015). Initiator caspases are recruited to and activated within this complex, and subsequently cleave and thereby activate effector caspases (Crawford and Wells, 2011). The second, intrinsic pathway, is defined by a phenomenon called mitochondrial outer membrane permeabilization (MOMP), the formation of pores in the mitochondrial outer membrane (MOM). MOMP has been defined as a point of no return, as it leads to the irreversible release of proteins from the mitochondrial intermembrane space into the cytosol and is usually widespread across the cell (Tait and Green, 2010). The Bcl-2 protein family regulates MOMP and receives input stimuli from various intracellular signaling pathways through its approximately 15 family members. Thus the term 'intrinsic' pathway, although the triggering stimulus leading to information processing that ultimately reaches the Bcl-2 protein family, obviously might as well have been an extrinsic one (Czabotar et al., 2014).

Interestingly, while MOMP has been defined as a point of no return, induction of the caspase cascade can still be prevented under certain conditions. Recently, permeabilization of a minority of mitochondria ('minority MOMP') in single cells upon treatment with subthreshold amounts of apoptotic stimuli has been described (Ichim et al., 2015). Upon inefficient initiator caspase activation, instead a caspase-independent form of apoptosis might occur, by other factors that mediate large-scale DNA fragmentation and cleavage of cellular substrates (Galluzzi et al., 2012). However, DNA damage induced by low levels of initiator caspases or other proteins can also be insufficient to induce cell death and instead promote genomic instability (Ichim et al., 2015).

Last but not least, significant interplay and regulatory potential exists in the combination of the two pathways (Sprick and Walczak, 2004), rendering apoptosis regulation a highly complex process with many obstacles on the way to predict how a cell will respond to single or combined stimuli.

Extrinsic or death receptor pathway

The initiator caspase-8 (and maybe caspase-10) is the starting point of the caspase cascade that is induced by the extrinsic apoptosis pathway (Figure 1.1). While caspase-8 is known to play a significant role in most if not all cell types, the importance of caspase-10 is far less well described and remains controversial. The zymogen (i.e. almost inactive form) of caspase-8, also called procaspase-8, resides as a monomer in the cytosol of healthy cells (Tummers and Green, 2017).

Initiator caspase activation via the death receptor apoptotic pathway occurs within a multiprotein complex, the death inducing signaling complex (DISC). The DISC serves as an activation platform of the initiator caspase and is formed subsequently to ligand engagement and trimerization of death receptors. Trimeric death receptors recruit adapter proteins to their cytosolic domains, these include FAS-associated death domain protein (FADD) and, in case of ligand binding to the tumor necrosis factor receptor type 1, TRADD (tumor necrosis factor receptor type 1-associated death domain protein) (Tummers and Green, 2017).

Procaspase-8 can bind to the death effector domain (DED) of FADD, as soon as FADD binds to the cytosolic region of a trimerized receptor. This interaction occurs via one of its own two DED domains (DED1). DED2 of bound procaspase-8 thereby forms an anchor point and can recruit further procaspase-8 molecules that will bind via their DED1 domain. In this manner, a unidirectional filamentous structure of multiple procaspases is formed (Siegel et al., 1998; Dickens et al., 2012). The whole complex of death receptor, adapter proteins and initiator caspases constitutes the DISC. One multiprotein DISC consists of around six procaspase-8 molecules, one FADD and three death receptors (Hughes et al., 2016). Interestingly, also dependence receptors have been identified as mediators of extrinsic apoptosis. In contrast to the above described mechanism, these receptors remain inactive as long as they are engaged by their ligands. Upon ligand deprivation and monomerization, dependence receptors shift from prosurvival to apoptosis signaling (Gibert and Mehlen, 2015).

The molecular mechanism of pro-caspase 8 activation commences with an autoproteolytic cleavage step, which is stimulated by the induced proximity of several procaspase molecules in the filamentous structures at the DISC. Cleavage between DED2 and the large procaspase-8 subunit then results in the fully catalytically active initiator caspase-8 (Tummers and Green, 2017). The extent of caspase-8 activation in a cell can be regulated by cFLIP (cellular FLICE-like inhibitory protein), a homolog of procaspase-8 that lacks proteolytic activity (Chaudhary et al., 2000). The long and short isoforms of cFLIP ($cFLIP_L$ and $cFLIP_S$) can either block or promote caspase-8 activation. $cFLIP_S$ dis-

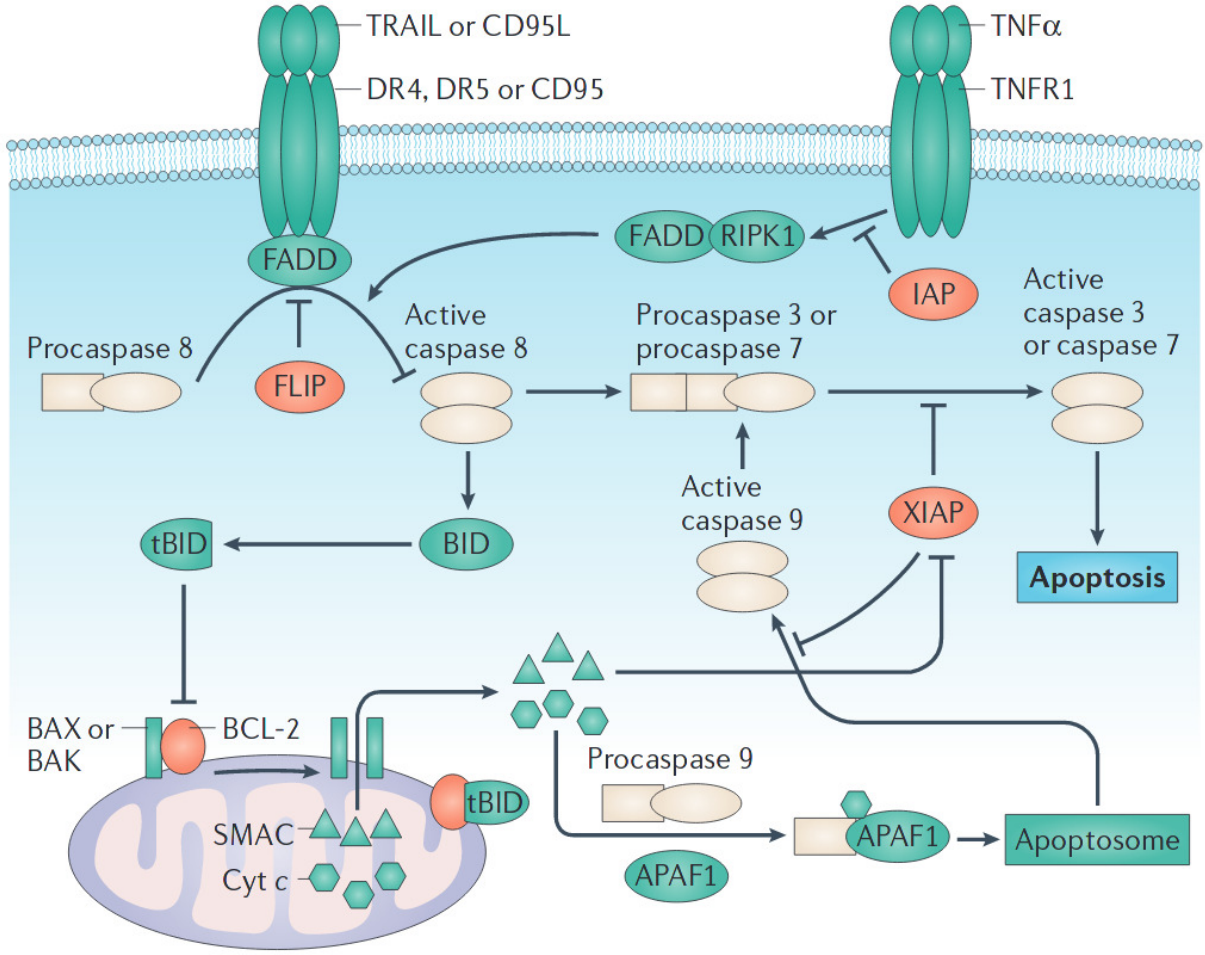

Figure 1.1: **Extrinsic and intrinsic apoptosis pathway.** The extrinsic pathway can be triggered by ligands binding to death receptors, resulting in receptor trimerization, adapter protein recruitment and initiator caspase-8 activation. The intrinsic pathway mediates initiator caspase-9 activation by Bcl-2 family regulated permeabilization of the outer mitochondrial membrane and apoptosome formation. Sufficient initiator caspase activation leads to effector caspase activation and apoptotic cell death. Figure modified and taken from Holohan et al. (2013).

rupts caspase-8 filaments and thereby prevents caspase activation. A substantial increase in the catalytic activity of procaspase-8 can be promoted by the formation of cFLIP$_L$-procaspase-8 heterodimers, but high levels of cFLIP$_L$ can also inhibit caspase-8 activity (Hughes et al., 2016).

Catalytically active caspase-8 cleaves and thereby activates the zymogens of effector caspases-3 and -7. The usually inactive dimeric effector procaspases are thereby divided into their large and small subunits, which afterwards form the tertiary structure of the active effector caspase homodimer (Tummers and Green, 2017).

Intrinsic or mitochondrial pathway

Similarly to the extrinsic pathway, also MOMP, the defining event of the mitochondrial pathway (Figure 1.1), can lead to the formation of a multiprotein complex that serves as an activation platform for initiator caspases. Pore formation in the mitochondrial outer membrane is carried out directly by oligomerization of effector proteins of the Bcl-2 family in the outer mitochondrial membrane. This process is regulated by a complex interaction network of proapoptotic and prosurvival family members (see section 1.2). In brief, the Bcl-2 family comprises three functional subgroups, the BH3-only proteins, prosurvivals and effectors. Prosurvival proteins bind to the effectors (Bax (Bcl-2 associated X protein) and Bak (Bcl-2 homologous antagonist killer)) and thereby prevent their oligomerization. BH3-only proteins promote apoptosis induction by sequestering prosurvivals and/or activating effectors (Czabotar et al., 2014).

Through the perforated mitochondrial outer membrane, proteins are released from the intermembrane space into the cytosol. The most prominent of these proteins is cytochrome *c*, which in a single cell is released from the intermembrane space into the cytosol within the order of five minutes (Goldstein et al., 2000). When investigating this release on a second-scale resolution, different pore formation kinetics for different apoptosis-inducing stimuli can be identified (Rehm et al., 2009).

The perforation of the outer mitochondrial membrane and accompanied release of proteins implicate a breakdown of the mitochondrial transmembrane potential and thus depolarization of the mitochondria (Düssmann et al., 2003). Additionally, with the release of cytochrome *c* and thereby loss of a crucial member of the electron transport chain, cellular ATP (adenosine triphosphate) levels decrease following MOMP (Waterhouse et al., 2001). The cytosolic localization of cytochrome *c* then instead enables the formation of the activation platform for procaspase-9, the initiator caspase of intrinsic apoptosis: By binding to monomeric Apaf-1 (apoptotic protease activating factor 1) molecules together with ATP or dATP, cytochrome *c* induces the assembly of the apoptosome, which displays a heptameric wheel-like structure (Acehan et al., 2002).

Dispute exists on the exact activation mechanism of caspase-9. Although initiator caspases were conventionally considered to be activated by enforced homodimerization, an additional, allosteric activation of caspase-9 or procaspase-9 by Apaf-1 subunits of the apoptosome was suggested (Rodriguez and Lazebnik, 1999). This allosteric activation of procaspase-9 by the apoptosome backbone was supported by mathematical modeling (Würstle and Rehm, 2014) and experimentally identified as a step enhancing the activity of the initiator caspase by two orders of magnitude (Hu et al., 2014; Wu et al., 2016). It was furthermore shown that procaspase-9 must remain bound to the apoptosome to

display its full catalytic activity. Only then it can efficiently cleave effector caspase-3 and trigger the caspase cascade. As soon as it is autoprocessed to caspase-9, it dissociates from the apoptosome and looses a significant amount of its activity. It was thus suggested that the amount of procaspase-9 together with the apoptosome serves as a molecular timer that determines the amount and extent of initiator caspase activity during mitochondrial apoptosis (Malladi et al., 2009).
Initiator caspase-9 as well as effector caspases-3 and 7 can be blocked if they are bound to X-linked inhibitor of apoptosis protein (XIAP). Sufficient caspase activation therefore has to occur in a cell to overcome the prosurvival effect of XIAP and induce apoptosis via the caspase cascade (Eckelman et al., 2006).
A further protein released from the intermembrane space during MOMP is Smac (second mitochondria-derived activator of caspases, also known as DIABLO), which due to its larger molecular size requires more time to be released than cytochrome *c* (Rehm et al., 2003). It acts proapoptotically by binding to XIAP and thereby freeing initiator and effector caspases.

Crosstalk

Caspase-8 constitutes an important link between extrinsic and intrinsic apoptosis signaling (Figure 1.1). It cleaves Bid (BH3 interacting-domain death agonist), a major regulator among the Bcl-2 family proteins, into truncated Bid (tBid, 15 kDa fragment) and a shorter 7 kDa fragment (Li et al., 1998). tBid is the active form of Bid and can potently induce activation of effector Bcl-2 family proteins and MOMP (see section 1.2). Some cell types, such as lymphocytes, can accumulate sufficient amounts of active initiator caspase-8 via DISC formation. They potently trigger the caspase cascade without engaging the Bcl-2 protein family and have been termed type I cells. But a variety of cell lines (e.g. hepatocytes, pancreatic β-cells), called type II cells, even require the additional induction of MOMP and subsequent caspase-9 activation to efficiently induce effector caspase activation (Scaffidi et al., 1998). Interestingly, the time between initiator and effector caspase activation, in type II cells measurable by the time point of MOMP execution, is subject to considerable delays, lasting up to several hours. The duration of this delay is highly heterogeneous in a cell population and has been mostly attributed to variable protein expression in individual cells (Albeck et al., 2008a). In sibling cells that have just emerged from cellular division, however, this event is timed in a highly synchronous manner (Rehm et al., 2009).
Cellular stresses that induce intrinsic apoptosis also affect signaling components of the extrinsic apoptosis pathway. The transcription factor and tumor suppressor p53 (cellular

tumor antigen p53) induces the expression of several proteins upon DNA damage and also directly upregulates proapoptotic Bcl-2 family members (see section 1.2.3). Additionally, p53 has been shown to induce upregulation of death receptors, such as DR5, and thereby also sensitizes cells to extrinsic apoptosis stimuli (Wu et al., 1997).
Several mitogen-activated protein (MAP) kinases are activated in response to DNA damage and can trigger mitochondrial apoptosis by phosphorylating pro- and antiapoptotic Bcl-2 family members (Roos et al., 2015). As an example, the Bcl-2 family member Bim (Bcl-2-interacting mediator of cell death) can be phosphorylated by c-Jun N-terminal kinase (JNK), which increases its proapoptotic potential (Dhanasekaran and Reddy, 2008). But also following extrinsic apoptosis induction, JNK can be phosphorylated and thereby activated (Vivo et al., 2003; Corazza et al., 2006).
Consequently, combination of chemotherapy with DR-engaging ligands, such as tumor necrosis factor-related apoptosis-inducing ligand (TRAIL), has been identified as a treatment strategy exerting high toxicity. For instance, the two stimuli synergistically induce apoptosis in otherwise resistant liver tumor cells, but also primary hepatocytes, by engaging multiple proapoptotic Bcl-2 family members (Schneider-Jakob et al., 2010). Of note, synergistic induction of apoptosis by TRAIL and chemotherapy in these cells was observed irrespective of the order of treatment with the two stimuli.
The combination of drugs in the treatment of cancers has evolved to be standard practice (NCI, 2013). Due to the central role of the Bcl-2 family in mediating apoptosis, many of the cellular processes triggered by standard or targeted chemotherapeutic drugs culminate in Bcl-2 family member activation and make the protein family an attractive direct target for chemotherapy (Hata et al., 2015).

1.1.2 Other forms of cell death

Although apoptosis is the most prominent and best studied form of programmed cell death, other regulated cell death programs have been discovered in the course of investigation. The two best described forms are regulated necrosis and autophagic cell death.
Necrosis was traditionally identified as the death of cells by accident, for example by mechanical disruption. The morphological features of necrosis are, in contrast to apoptosis, cellular swelling and rupture of the cell membrane. As a result, the intracellular components of a necrotic cell are released into the surrounding tissue, stimulating an immune response and processes such as wound healing (Fuchs and Steller, 2015). However, also a regulated cell death form displaying the morphological features of necrosis has been identified. The best studied form of regulated necrosis is mediated by the proteins RIPK1 and -3 (receptor-interacting serine/threonine-protein kinases 1 and 3) and has been termed

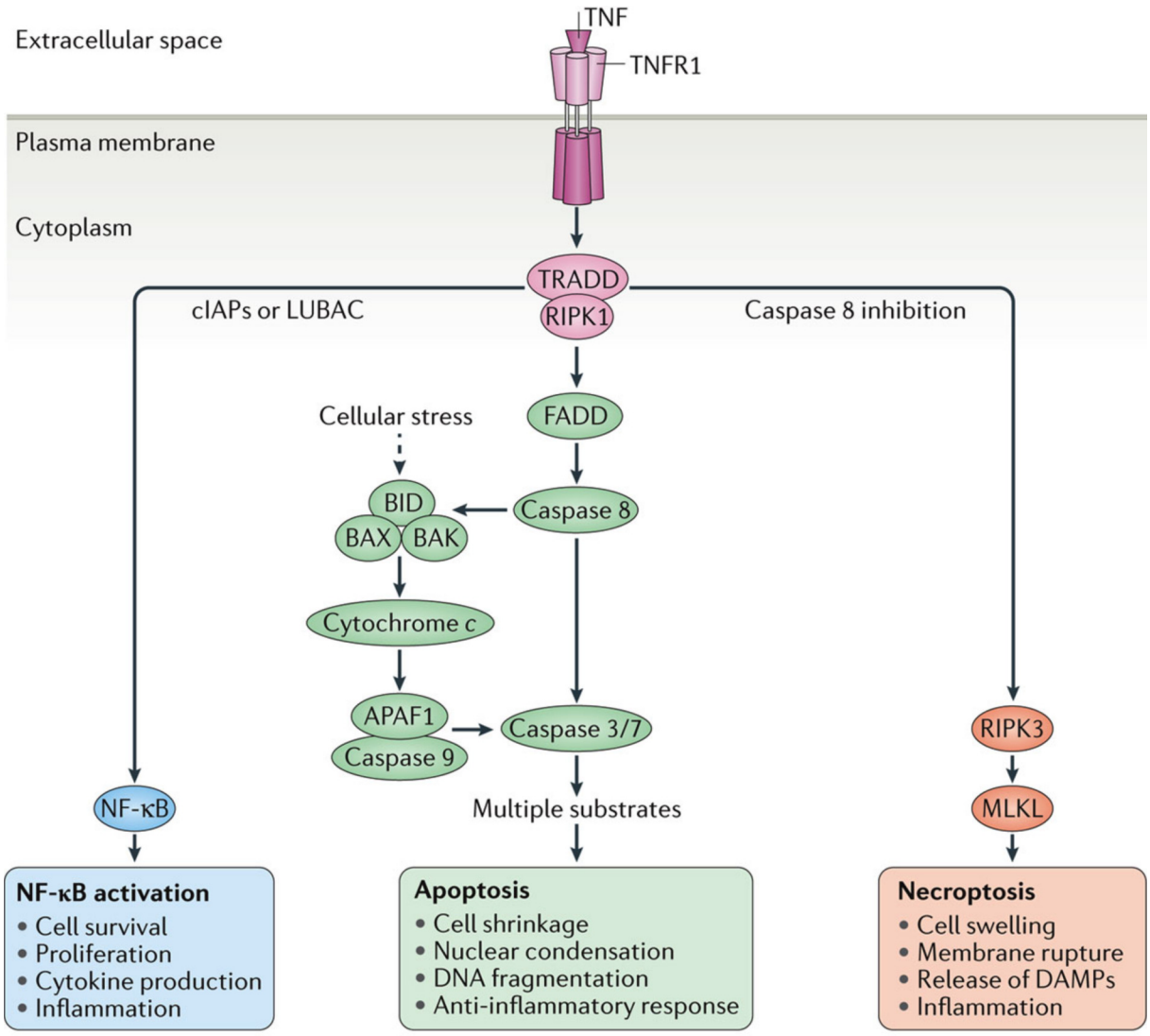

Figure 1.2: **Simplified overview of cellular decision making in response to apoptotic stimuli.** Multiple intracellular pathways trigger Bcl-2 family activation and intrinsic apoptosis in response to stress. Extrinsic apoptosis can be induced by death receptor signaling. cIAPs counteract apoptosis induction and promote prosurvival signaling and cell survival by NF-κB activation. Necroptosis instead of apoptosis can be triggered by TNF in case of caspase-8 inhibition and induces an inflammatory response due to the release of intracellular DAMPs (damage-associated molecular patterns) upon rupture of the cell membrane. Figure taken from Weinlich et al. (2016).

'necroptosis' (Galluzzi et al., 2012). Triggering of necroptosis is achieved via a complex signaling network that has considerable overlap with components of the apoptotic machinery (Peter, 2011). Necroptosis can be induced by ligation of death receptors at the cell membrane, including TNFR1 (tumor necrosis factor receptor superfamily member 1A), FAS (tumor necrosis factor receptor superfamily member 6) and TRAILR. But also intracellular stress signals have been identified as necroptosis triggers (Vanden Berghe et al., 2014). In the best understood form of necroptosis induction, TNF binds to TNFR, which leads to the formation of a multiprotein complex called complex I. This complex

contains RIPK1 and TRADD and recruits cIAP1 and cIAP2 (cellular inhibitor of apoptosis 1 and 2) (Vanden Berghe et al., 2014). cIAP1 and cIAP2 contain, just like their family member XIAP, an intrinsic E3 ubiquitin ligase activity (Eckelman et al., 2006) and polyubiquitinate RIPK1 (Silke and Meier, 2013). The polyubiquitin chains allow docking of further proteins to the multiprotein complex (e.g. LUBAC (linear ubiquitin chain assembly complex)) and result in NF-κB (nuclear factor kappa-light-chain-enhancer of activated B cells) activation (Haas et al., 2009).

Activation of members of the NF-κB family of transcription factors is generally associated with prosurvival signaling and cell survival, as it leads to upregulation of antiapoptotic proteins such as cIAPs and Bcl-2 (Hoesel and Schmid, 2013). NF-κB also mediates upregulation of $cFLIP_L$ (Micheau et al., 2001) and in presence of procaspase-8 the two proteins can form a heterodimer that cleaves and inactivates RIPK1 and 3. Intriguingly, also caspase-8 homodimerization and activation can be induced, leading to apoptotic cell death by effector caspase activation (Vanden Berghe et al., 2014). Caspase-8 activation or heterodimerization with $cFLIP_L$ in this regard is mediated by formation of one of two currently known cytosolic complexes (Micheau and Tschopp, 2003; Feoktistova et al., 2011; Tenev et al., 2011): The cytosolic TRADD-dependent complex IIa is formed upon deubiquitination and subsequent dissociation of RIPK1 from complex I. But also upon pharmacological cIAP inhibition or cIAP depletion, caspase-8 activation or heterodimerization with $cFLIP_L$ can occur in a cytosolic complex termed the 'ripoptosome', or complex IIb. In this case, RIPK1 dissociates from complex I due to a lack of cIAP-mediated ubiquitination. cIAP inhibition furthermore leads to increased levels of TRAF2 and 3 (TNF receptor-associated factor), causing NIK accumulation (NF-κB-inducing kinase) and non-canonical NF-κB activation (Zarnegar et al., 2008).

In this signaling pathway, necroptosis can occur instead of apoptosis only when caspase-8 is inhibited (Figure 1.2). Absence of caspase-8 enables auto- and transphosphorylation of RIPK1 and 3, their association into microfilaments (the necrosome) (Li et al., 2012), and recruitment of MLKL (mixed lineage kinase domain-like) (Sun et al., 2012; Zhao et al., 2012). MLKL recruitment is the key determinant of necroptotic cell death and the protein can mediate the subsequent necroptotic cell death processes leading to cell swelling and rupture in various ways (Vanden Berghe et al., 2014).

Of note, regulated forms of necrosis other than necropotosis have been identified, such as pyroptosis and ferroptosis. They can occur independently of RIPK1 and RIPK3 but share the same morphological features of necrosis (Vanden Berghe et al., 2014).

Autophagic cell death is a process still under debate for its independent role in triggering programmed cell death. Autophagy in general is induced by cellular stress and is depen-

dent on a variety of evolutionary conserved genes that regulate the autophagic process. It is characterized by the formation of autophagosomes, vesicles that fuse with lysosomes and thereby recycle the contained cellular components (Su et al., 2015). Autophagy is thus a catabolic process. Proteins or even whole mitochondria might be subjected to autophagy. In the latter case, the process is termed mitophagy and might be employed by the cell to remove damaged mitochondria and thereby counteract intrinsic apoptosis (Mariño et al., 2014). The rate of autophagosome formation and fusion with lysosomes is called autophagic flux and can be measured in autophagy assays (Fitzwalter and Thorburn, 2015). In mammalian cells, a large number of autophagosomes was observed during the cell death process, rather than death mediated by autophagy itself (Mariño et al., 2014). The provision of ATP by autophagy might also contribute to ATP-dependent apoptotic processes such as apoptosome formation and membrane blebbing (Fuchs and Steller, 2015).

1.1.3 Dysregulation of apoptosis in cancer and targeted therapeutics

Evasion of apoptosis is one of the classical hallmarks of cancer (Hanahan and Weinberg, 2000). Indeed, differences in anti- and proapoptotic protein expression in cancerous in comparison to healthy cells have been identified. These differences can be caused by direct mutations of genes encoding proteins of the apoptosis pathway, or due to downstream effects of dysregulated transcription factors. The tumor suppressor p53 for instance is critical for mediating expression of BH3-only proteins and has been shown to be inactive in many cancers (Muller and Vousden, 2013). Similarly, NF-$\varkappa$B is constitutively active in various cancers and is known to induce upregulation of prosurvival proteins such as cIAPs, Bcl-2 and cFLIP (Hoesel and Schmid, 2013).

Interestingly, individual cancer types often display altered expression of a few specific proteins involved in apoptosis. This renders rational drug design in apoptosis research a promising approach to treat cancer (Holohan et al., 2013). A detailed understanding of the molecular processes is crucial for the identification of potential drug targets. This new approach to chemotherapy (targeted treatments) thus commenced in the late 1980's and now enables effective cancer treatments (Chabner and Roberts, 2005). In fact, since the millenium, of the FDA-approved drugs that target a new molecular player (first-in-class drugs), the majority was discovered by target-based approaches (Eder et al. (2014) and Figure 1.3A).

To specifically and directly target the dysfunctional apoptotic pathway in cancer, a num-

ber of targeted therapeutics have been developed that reached clinical trials. In the following sections, the extrinsic apoptosis stimulus TRAIL, as well as the small molecule drugs Smac mimetics and BH3 mimetics will be described.

TRAIL

TRAIL (Figure 1.3B) was first described two decades ago, when it was identified by the sequence homology it shares with the extracellular domains of TNF and FAS (Wiley et al., 1995; Pitti et al., 1996). Trimerized recombinant TRAIL could selectively induce apoptosis in cancer cells by binding to TRAILR1 and 2 and displayed low toxicity to healthy cells *in vitro* and in mouse xenograft models (Walczak et al., 1999). TRAIL can also bind to TRAILR3 and 4, which does not induce apoptosis but might rather inhibit TRAIL activity (Lemke et al., 2014).
Despite the promising preclinical results, recombinant TRAIL and antibodies directed against TRAILR1 and 2 failed in clinical trials, as they showed low cytotoxicity in primary cancers when administered as monotherapy (Holohan et al., 2013). Current research efforts utilize TRAILR ligands with improved agonistic properties, such as trimerized recombinant TRAIL versions, and in combination therapy with conventional chemotherapy, Smac mimetics, or BH3 mimetics (Lemke et al., 2014).

Smac mimetics

Smac is released into the cytosol upon MOMP induction and acts proapoptotically by binding to IAPs and inducing their proteasomal degradation (Kocab and Duckett, 2016). Overexpression of IAPs has been been attributed to resistance of cancer cells to chemotherapy. Thus, small molecules have been developed based on the AVPI tetrapeptide motif that mediates Smac binding to IAPs (Holohan et al., 2013). These Smac mimetics (e.g. birinapant) are currently tested in clinical trials as IAP antagonists that induce apoptotic death in cancer cells (Derakhshan et al., 2017). They exert their proapoptotic function by binding to XIAP and thereby freeing bound caspases (3, 7 and 9), as well as by binding to cIAPs. In the latter case they induce a conformational change in cIAP1 or 2, which results in their autoubiquitination and proteasomal degradation (Silke and Meier (2013); Holohan et al. (2013) and Figure 1.3C).
Response to Smac mimetic treatment depends on cell type-specific intracellular signaling. In some cells, Smac mimetics can induce death by activating NF-$\varkappa$B, which upregulates TNF. The availability of a death agonist like TNF (or TRAIL) is crucial for the treatment response. If cells do not induce autokrine TNF induction, they require an external death agonist for stimulation and are merely sensitized to apoptosis (Derakhshan et al., 2017).

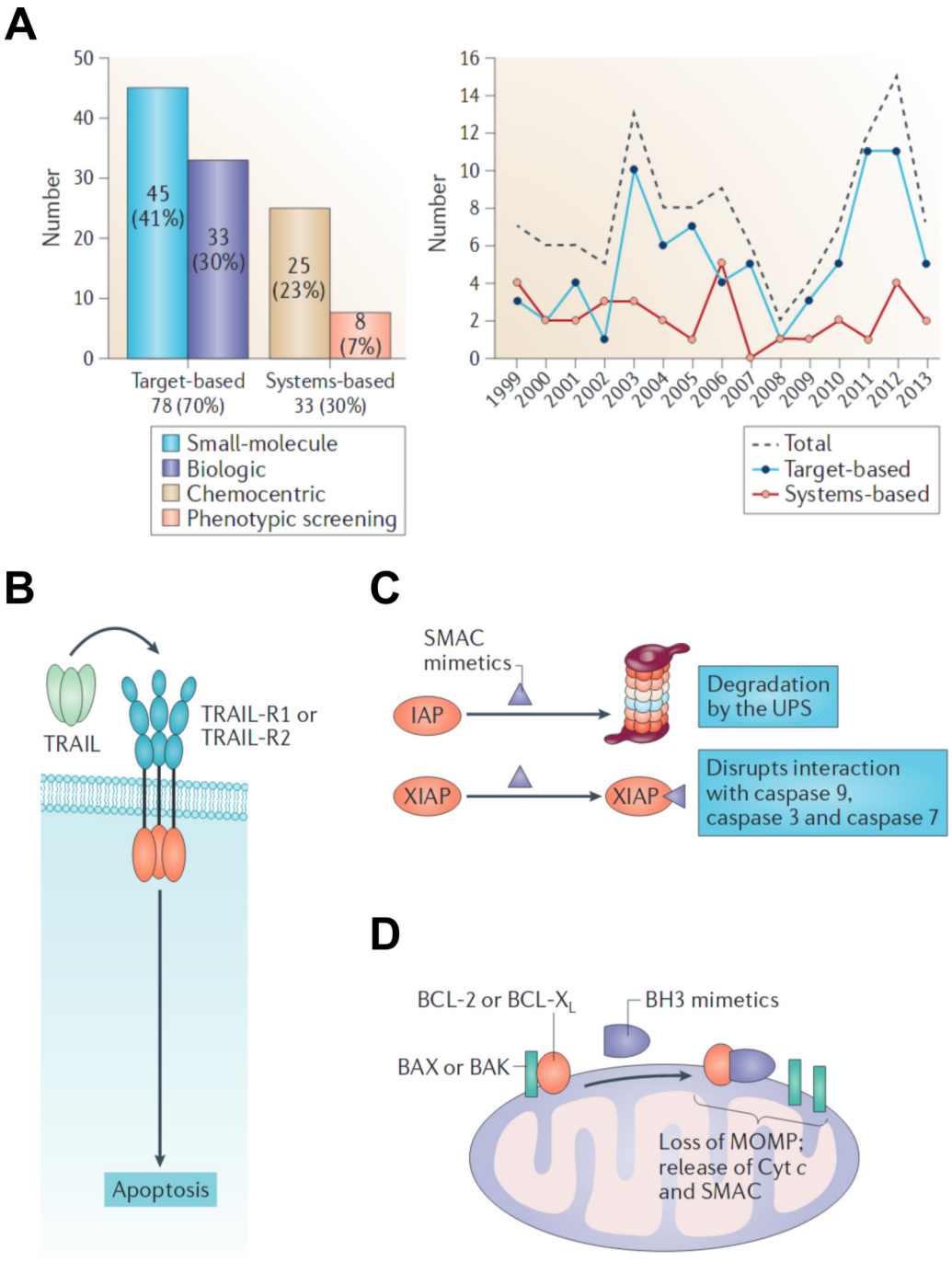

Figure 1.3: **Targeted therapeutics. A**, The number of FDA approved new-in-class drugs from target-based approaches outnumbers those resulting from phenotypic screens in recent years. In the bar graph, all 113 new-in-class drugs from 1999-2013 are summarized. **B**, TRAIL induces apoptosis by binding to and trimerizing TRAILR1 or 2 (TRAIL receptor 1/2). **C**, Smac mimetics act by (1) inducing proteasomal degradation of cIAP1 and -2 and (2) sequestering XIAP. **D**, BH3 mimetics bind to prosurvival Bcl-2 family members, thereby enabling activation of effector proteins Bax and Bak (here: MOMP denotes mitochondrial membrane potential). Subfigures modified and taken from **A** Eder et al. (2014), **B** von Karstedt et al. (2017), **C,D** Holohan et al. (2013).

Moreover, treatment with Smac mimetics can also sensitize cells to death by inducing formation of the ripoptosome, as described in section 1.1.2 (Silke and Meier, 2013; Kocab

and Duckett, 2016).

BH3 mimetics

The Bcl-2 family is an especially attractive target for cancer therapy. First of all, the protein family fulfills a central role by mediating MOMP induction and thereby a point of no return in programmed cell death. But even more importantly, it has been observed that successful engagement of the Bcl-2 family by intracellular signaling pathways is crucial for the efficacy of most conventional therapies, as well as targeted therapies that inhibit upstream oncogenic kinases (Czabotar et al., 2014; Hata et al., 2015).
Furthermore, prosurvival Bcl-2 family members were shown to be overexpressed in many cancers (Delbridge and Strasser, 2015). At the same time, these cancer cells are sometimes even more susceptible to apoptosis inducing stimuli. This might be due to increased expression of BH3-only proteins, which are sequestered by the prosurvival family members (Letai, 2008). This cellular state has been dubbed 'primed to death'. Primed cells are sensitive to sensitizing molecules such as BH3 peptides which do not directly activate Bax and Bak but bind to prosurvival proteins, thereby freeing previously bound BH3-only activators. This mechanism is employed by small molecules that have been developed to act like sensitizers by binding to specific prosurival Bcl-2 family members and are called BH3 mimetics (Figure 1.3D). The general therapeutic potential of BH3 mimetics has been further promoted by the finding that cellular apoptosis susceptibility determined by 'BH3 profiling', the application of BH3 peptides on digitonin-permeabilized cells, is capable of determining if cells are in a primed state and can even predict responsiveness to conventional chemotherapy (Certo et al., 2006; Deng et al., 2007).
BH3 mimetics have already entered successful clinical trials. The bioavailable BH3 mimetic venetoclax (ABT-199), which specifically binds to Bcl-2 with high affinity, is now approved for the treatment of CLL (chronic lymphocytic leukemia) (Roberts et al., 2016). A further BH3 mimetic specifically targeting Mcl-1 (induced myeloid leukemia cell differentiation protein Mcl-1) was recently developed and showed promising results *in vitro* and *in vivo* (Kotschy et al., 2016).

1.2 The Bcl-2 protein family

Pro- and antiapoptotic Bcl-2 protein family members form a complex interaction network that can mediate permeabilization of the mitochondrial outer membrane. Sequence similarities within the Bcl-2 family have led to the characterization of four Bcl-2 homology (BH) domains. The occurrence of multiple or only the BH3 domain, together with

the protein functions, allows classification into three subgroups (Figure 1.4A). These are the pore forming effectors, proapoptotic BH3-only proteins and antagonizing prosurvivals (Czabotar et al., 2014). Of note, the definition of the BH domains is loose and sequence similarity searches reveal a multitude of potential further BH-containing proteins that do not show binding affinity to other Bcl-2 family members or direct implications on pore formation regulation (Aouacheria et al., 2013).
Associations within the family are mediated by interactions of their amphipatic BH3 domains with the hydrophobic binding grooves at the surface of multidomain family members (Czabotar et al., 2014; Luna-Vargas and Chipuk, 2016). Those allow a variety of homo- and heterodimerizations within the family and control among the functional subgroups. The Bcl-2 interactome and regulation of MOMP are subject to many levels of regulation. These include posttranslational modifications, subcellular localization and tissue and cell line-specific expression of the proteins. The following sections will provide an overview of the current knowledge of mechanisms of action within and regulation of the members of the Bcl-2 family.

Suggested models of regulation

The two effectors Bax and Bak have been shown to be components of the mitochondrial outer membrane pores. For long, a debate existed on the regulatory mechanisms that lead to effector activation, oligomerization and irreversible induction of MOMP. A direct activation model (Kuwana et al., 2002; Letai et al., 2002), in which BH3-only proteins induce a conformational change in the effectors, as opposed to an indirect activation model (Willis et al., 2007) was proposed (Figure 1.4B). The latter assumed that in healthy cells MOMP is prevented by prosurvival proteins, which constantly antagonize active effectors. Increasing amounts of BH3-only proteins that bind to prosurvivals would then lead to the release of active Bax and Bak and subsequent pore formation.
In fact, however, the BH3-only proteins tBid and Bim were early on identified as direct activators, which upon binding to the effectors induce a conformational change in Bax and Bak (Letai et al., 2002; Kuwana et al., 2005). This step is a prerequirement for binding of effectors to prosurvivals as well as the formation of oligomers (Czabotar et al., 2013). Nevertheless, an important role in the sequestration of active effectors for MOMP prevention could be attributed to prosurvival proteins (Billen et al., 2008b). More recently, a unified model of effector regulation highlighted the influence of both direct as well as indirect components (Llambi et al., 2011). Further suggested models additionally stressed the importance of the mitochondrial outer membrane (Leber et al., 2007) or effector autoactivation and direct activation by Noxa (phorbol-12-myristate-13-acetate-induced protein

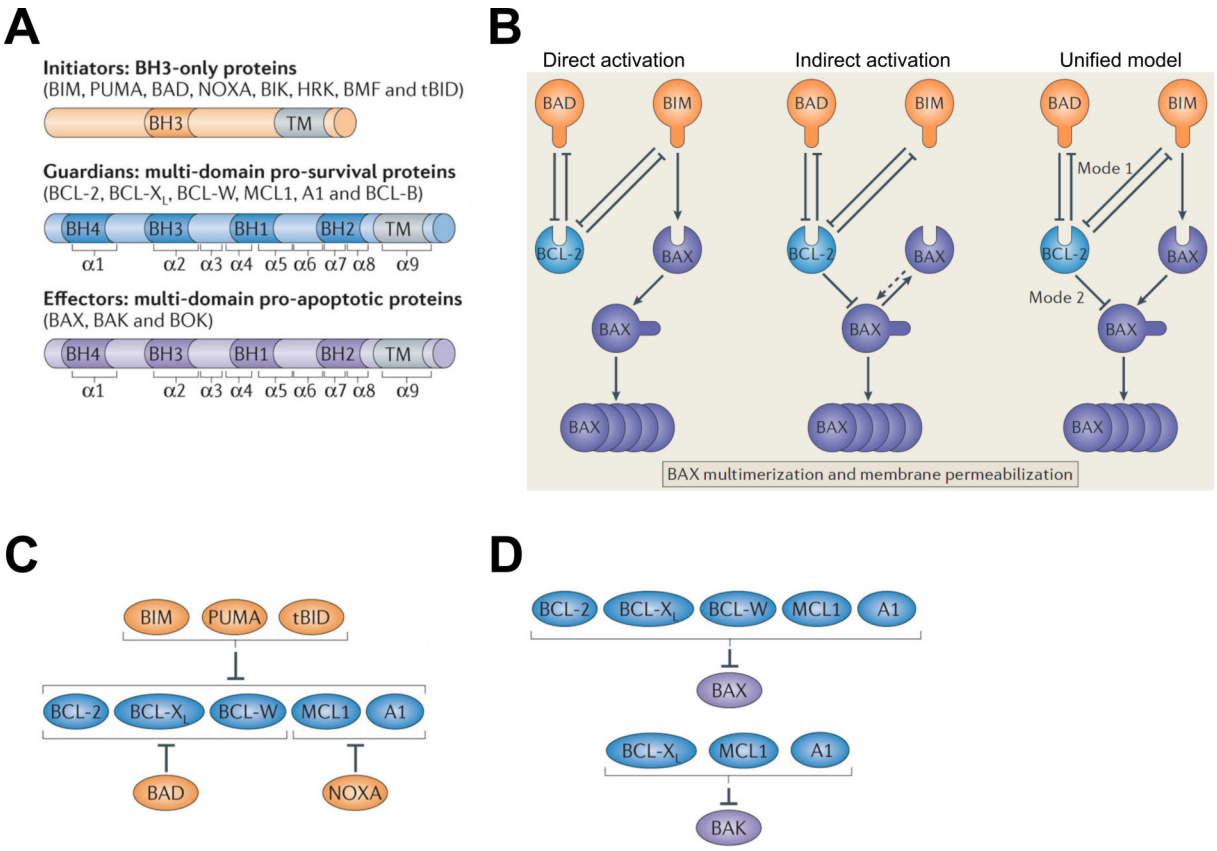

Figure 1.4: **Bcl-2 protein family, interactions and models of regulation.** **A**, Functional subgroups within the Bcl-2 family and their BH domains (A1 is the murine version of Bfl-1). **B**, Suggested models of regulation within the Bcl-2 protein family. **C,D**, Differential binding of prosurvivals to BH3-only proteins (**C**) and to effectors (**D**). Subfigures modified and taken from Czabotar et al. (2014).

1) (Chen et al., 2015).

A clear picture of effector activation has however been challenged by the observation that cells lacking all potential activator BH3-only proteins could still undergo Bax/Bak dependent apoptosis by antagonizing prosurvival proteins (O'Neill et al., 2016).

In this chapter, first the activation and oligomerization processes of the effectors Bax and Bak will be described in detail (section 1.2.1). Then, details will be given on the BH3-only proteins, prosurvival proteins and interactions within the family (see also Figure 1.4C,D) that control oligomerization (section 1.2.2). Ultimately, an overview of the various forms of regulation of all family members is presented (section 1.2.3).

1.2.1 Effector activation and oligomerization

Activation and oligomerization of Bax

In non-apoptotic cells, Bax is mainly located in the cytosol and only a minor fraction can be detected at mitochondrial membranes (Wolter et al., 1997). Bax comprises nine

α helices and the C-terminal α9 helix serves as a transmembrane anchor for association with the mitochondrial outer membrane. The transmembrane anchor remains buried in the hydrophobic groove of cytosolic Bax (Suzuki et al., 2000). Recent studies revealed that a dynamic equilibrium of cytosolic Bax and MOM-bound effector exists in healthy cells (Edlich et al., 2011; Schellenberg et al., 2013).

Bax can be efficiently activated by activator BH3-only proteins at the membrane, when its α9 helix is membrane-inserted and the hydrophobic binding groove free for interactions. The activators induce a conformational change in Bax that transforms the globular protein to a membrane spanning molecule. Bax in its active and membrane bound conformation then associates with further active Bax molecules and forms pores in the membrane (Lovell et al., 2008; Kim et al., 2009; Czabotar et al., 2013).

Recent insights revealed the structural changes in Bax upon binding of an activator BH3 peptide to the hydrophobic groove: The core and latch domains of the effector dissociate and its BH3 domain is released from the hydrophobic core of the protein (Czabotar et al. (2013) and Figure 1.5). This activating interaction was early on suggested to be a transient step, a 'hit and run' manner of BH3-only mediated activation of effectors (Wei et al., 2000). This might be due to fast release of the activator once the conformational change is induced. A lipidic environment promotes the active effector conformation, in which hydrophobic amino acid stretches such as the α5 and α2 helices (the latter also contains the BH3 domain) of the protein are rearranged and released from the protein core to the surface. After release of the BH3-only protein, two Bax molecules with unlatched core domains can form symmetric BH3-in-groove homodimers (Czabotar et al., 2013). These form the building blocks of higher order oligomers (Subburaj et al., 2015). By providing a two-dimensional planar surface for orientation, the mitochondrial outer membrane most likely aids in mediating BH3-domain-groove interactions of two active Bax molecules (Czabotar et al., 2013). In line with these results are previous observations from *in vitro* studies which showed that soluble Bax can be recruited into the membrane by membrane bound tBid (Lovell et al., 2008). Insertion of Bax into a lipid bilayer occurs via a two-step reversible interaction mechanism. First, Bax is loosely attached to tBid and the membrane, then it undergoes a conformational change together with membrane-insertion, and subsequently dissociates from tBid (Lovell et al., 2008). The same study also provided the first proof of a direct interaction of tBid and Bax. The interaction could only be observed in a membrane environment and not in solution. The membrane integration step of Bax was suggested to be rate-limiting in the multistep process of membrane recruitment and activation (Lovell et al., 2008; Subburaj et al., 2015). The active conformation of Bax can furthermore be induced artificially *in vitro*, by the application of mild heat (Subburaj

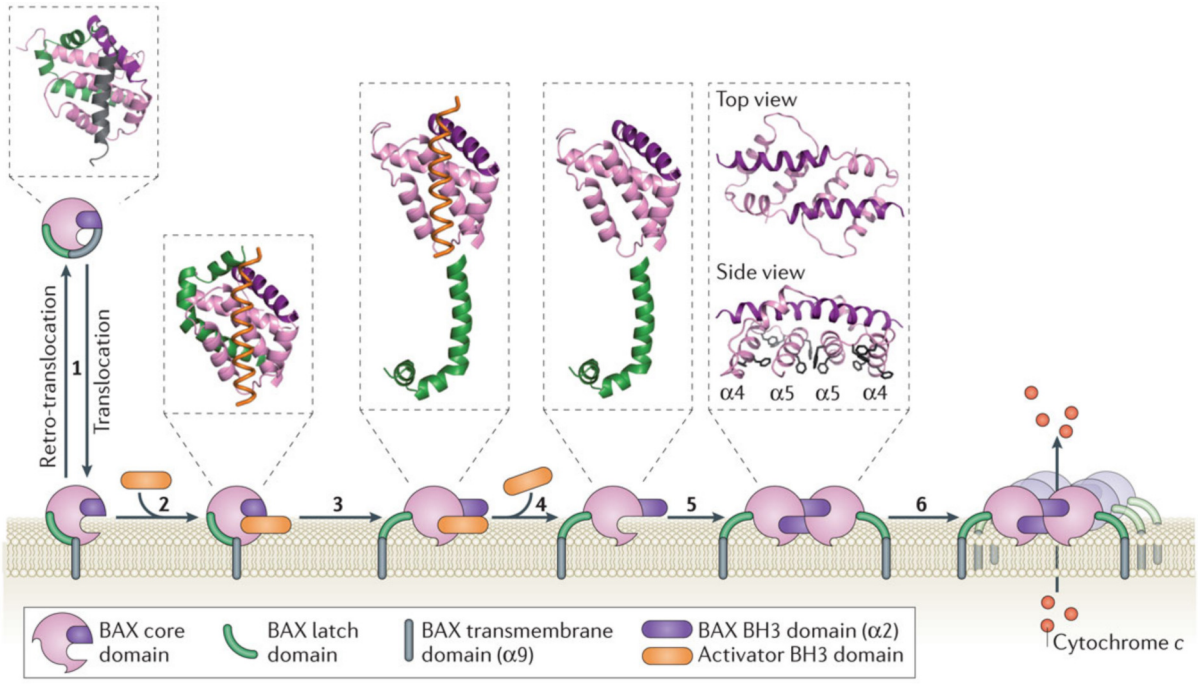

Figure 1.5: **Bax activation and oligomerization.** Bax dynamically interacts with and detaches from the mitochondrial outer membrane (1). Membrane associated Bax can bind to an activator BH3-only protein, which stimulates Bax to adopt its active conformation (2). Within this process, the latch domain is separated from the core domain and Bax exposes its BH3 domain (3). Upon release of the activator from the hydrophobic binding groove of Bax (4), this interaction site is free for association with the BH3 domain of another active Bax molecule (5). Symmetric BH3-in-groove homodimers form the building blocks of higher order oligomers that allow the release of cytochrome *c* and other factors from the mitochondrial intermembrane space into the cytosol (6). Figure taken from Czabotar et al. (2014).

et al., 2015), or the use of non-ionic detergents (Hsu and Youle, 1997).

Interestingly, an autoactivation mechanism of Bax has further been identified. It might contribute to the all-or-none control of MOMP by the Bcl-2 protein family (Valentijn et al., 2008). Further evidence for autoactivation is provided by studies showing that BH3-only peptides of Bax can induce a conformational change in Bax molecules similar to the Bid BH3 peptide (Gavathiotis et al., 2010; Llambi et al., 2011; Czabotar et al., 2013; Leshchiner et al., 2013). Also *in vitro* findings showed that in a solution containing multiple liposomes, active Bax molecules cluster on a few liposomes instead of being evenly distributed on different liposomes (Subburaj et al., 2015).

A further binding site in Bax exists opposite of its canoncial hydrophobic groove. BH3 peptides have been shown to bind to this site that is formed by the α1 and α6 helices. This 'rear pocket' was suggested to serve as an allosteric binding site for BH3-only proteins. They thereby induce the release of the transmembrane domain of Bax and a reorganization in the α1-α2 loop (Gavathiotis et al., 2008, 2010). The subsequent Bax activation step however, seems to be mediated through interaction of a BH3 peptide with the canonical hydrophobic binding groove (Leshchiner et al., 2013).

The irreversibility of effector activation is supported by the fact that Bax continues to insert into membranes of liposomes that have already been permeabilized (Lovell et al., 2008). In a cellular setting, only a small fraction of the whole Bax pool was found associated at the MOM in single cells at the onset of cytochrome *c* release and continued to be recruited to the MOM even minutes after cytochrome *c* had already been completely released from the intermembrane space into the cytosol (Düssmann et al., 2010).
The stoichiometry of building blocks of Bax oligomers was recently analyzed *in vitro* by TIRF (Total Internal Reflection Fluorescence) microscopy (Subburaj et al., 2015). By analyzing fluorescently labeled mono- and multimeric Bax species at the membrane it was shown that although Bax inserts into the MOM as a monomer, afterwards dimers, tetramers, hexamers and higher oligomeric species of Bax are formed with fast kinetics. Another recent study reported findings from *in vitro* electron-microscopy experiments utilizing gold labeled Bax that showed that Bax oligomeric pores could be detected with a number of different stoichiometries and that further Bax is recruited to the rims of such pores (Kuwana et al., 2016). In agreement with the previous study, also this method could not detect monomeric Bax in the membrane outside the pores.
Debate exists on the size of functional Bax pores that are capable of releasing small globular proteins, such as cytochrome *c*, or larger molecules. It has been shown that pores consisting of four Bax molecules should be sufficient to allow the diffusion of small globular proteins such as cytochrome *c* (Saito et al., 2000). Additionally, a role of lipids in shaping the pores has been proposed (Bleicken et al., 2013a). The existence of these toroidal pores, consisting of proteins as well as lipids, might explain how even a single Bax molecule was reported to be sufficient to permeabilize the membrane for small proteins (Xu et al., 2013). But also higher-oligomeric Bax pores exist (Kuwana et al., 2016). Whether those are relevant during the fast process of cytochrome *c* release or not remains to be investigated.

Activation and oligomerization of Bak

Bak is anchored to the MOM with its α9 transmembrane helix in healthy cells, but apart from that also adopts a globular inactive fold just like Bax (Wei et al., 2000; Moldoveanu et al., 2006). Upon binding of an activating BH3 peptide, structural reorganizations of its nine α helices, dissociation of latch and core domain as well as BH3 domain exposure occur as described above for Bax (Brouwer et al. (2014) and Figure 1.5).
The hit and run model of BH3-only protein mediated Bak activation has been supported by the fact that a conformational change in Bak could not be induced if the BH3 peptide remained bound to the hydrophobic binding groove (Moldoveanu et al., 2013). In con-

trast to Bax, BH3 peptides do not bind to a further site in Bak (Leshchiner et al., 2013). After release of a BH3-only protein, active Bak molecules interact with the mitochondrial outer membrane in plane and associate to form stable BH3-in-groove Bak homodimers (Brouwer et al., 2014). These can permeabilize the membrane by the formation of high molecular weight complexes.
Interactions of Bak with MOM proteins, such as voltage-dependent anion channel 2 (VDAC2), have been reported to be involved in the regulation of its proapoptotic potential (Cheng, 2003; Roy et al., 2009). Furthermore, Bak has been shown to be part of higher molecular weight oligomers in different unstimulated cell lines. In this context, an autoactivation mechanism without the necessity of activator BH3-only proteins was suggested for Bak (Dai et al., 2015).
Also a daisy-chain mechanism of Bak and Bax oligomerization has been suggested, in which the BH3 domain of one protein interacts with α1/α6 of another molecule (Pang et al., 2012). However, the recent structural findings show that this model is unlikely to play a dominant role in the formation of oligomers. The basic unit of Bak oligomers is, as in the case of Bax, a homodimer (Ma et al., 2013) that is formed by BH3-in-groove interactions. The α3/α5 interface for assembly of homodimers to higher order oligomers was suggested by distance measurements (Mandal et al., 2016). In contrast, a recent study showed that Bak dimers can loosely interact with each other on multiple possible sites (Uren et al., 2017). Interestingly, homodimers could be detached from one another by Bax molecules, but not by prosurvivals such as Mcl-1 and Bcl-xL (B-cell lymphoma-extra large) (Uren et al., 2017). The formation of Bax-Bak pores and how those would assemble has not been shown to date.

Bok - a further potential family member

Sequence similarity suggested that a further protein, Bok (Bcl-2 related ovarian killer), might belong to the effector subclass of Bcl-2 family proteins and is involved in the induction of intrinsic apoptosis (Hsu et al., 1997). Indeed, many human cancers show reduced somatic copy-numbers of the *BOK* gene, supporting a proapoptotic role of this multi-BH-domain protein (Beroukhim et al., 2010). Recent insights into the pore formation activity of Bok highlight its capability to oligomerize and perforate membranes in the absence of the effectors Bax and Bak (Einsele-Scholz et al., 2016; Llambi et al., 2016; Fernández-Marrero et al., 2017). However, experimental evidence consistently supports the notion that regulation of Bok-mediated pore formation underlies other mechanisms than that of Bax and Bak: One study suggested an intrinsic pore formation activity of Bok at the MOM and that this activity is held in check by a high protein turnover, which

is mediated by the endoplasmic reticulum (ER)-associated degradation (ERAD) pathway (Llambi et al., 2016). A further recent study could not confirm that Bok can form pores in liposomes with a lipid composition akin that of the MOM in the absence of further cofactors (Fernández-Marrero et al., 2017). Additionally, the major fraction of Bok is not located at the mitochondrial, but other intracellular membranes such as the ER and Golgi (Echeverry et al., 2013). So far, the exact role and capability of Bok in mediating intrinsic apoptosis remains unclear (Haschka and Villunger, 2017).

1.2.2 Interplay of Bcl-2 family subgroups

BH3-only proteins

At least eight proteins fulfill a proapoptotic function within the Bcl-2 family and contain solely the BH3 domain (Figure 1.4A). A unique property of the BH3-only protein Bid is that the structure of the full-length protein resembles more that of a multidomain family member than that of other BH3-only proteins (Billen et al., 2008a). After the discovery of tBid and Bim as activator BH3-only proteins, also Puma (p53 upregulated modulator of apoptosis) was shown to activate Bax and Bak (Cartron et al., 2004a; Kim et al., 2006, 2009). While an activator function of Noxa has been postulated by some groups (Dai et al., 2011; Chen et al., 2015), this result could not be reported consistently among the scientific community (Kuwana et al., 2005; Du et al., 2011). Whether Puma and Noxa mainly exert their proapoptotic role by binding to prosurvival proteins, or activation of effectors additionally plays a significant role in their mechanism of action remains unclear to date.

The remaining BH3-only proteins Bmf (Bcl-2-modifying factor), Hrk (activator of apoptosis harakiri), Bad (Bcl-2 associated death promoter) and Bik (Bcl-2-interacting killer) do not directly bind to Bax or Bak, but instead promote apoptosis by binding and thereby antagonizing prosurvival Bcl-2 family members and are called sensitizers (Letai et al., 2002).

It has been shown that different BH3-only proteins sense cellular stresses from different pathways (Happo et al., 2012). Their proapoptotic function is utilized in 'BH3 profiling' to determine the responsiveness of cells to BH3-only proteins and BH3 mimetics. This approach applies BH3 peptides derived from BH3-only proteins on digitonin-permeabilized cells and can be used to investigate the overall responsiveness to apoptosis-inducing stimuli as well as detect cellular dependencies to certain prosurvival proteins (Certo et al., 2006; Del Gaizo Moore and Letai, 2013).

Prosurvival Bcl-2 Family Members

Five Bcl-2 proteins mediate prosurvival functions within the family (Figure 1.4A). These are Bcl-xL, Bcl-2, Bcl-w (Bcl-2-like protein 2), Mcl-1 and Bfl-1 (Bcl-2-related protein A1). Bcl-2 is also the founding family member and was discovered in association with the survival of B-cells in B-cell lymphoma (Tsujimoto et al., 1984b,a).
Prosurvival proteins were shown to heterodimerize with BH3-only proteins and with active effectors. They thereby prevent Bax and Bak activation and the oligomerization of active effectors (Chen et al., 2005; Billen et al., 2008b). For Bcl-xL also self-association and formation of homodimers has been reported (Jeong et al., 2004; O'Neill et al., 2006). In addition to sequestration of proapoptotic proteins, a further regulatory mechanism of prosurvival family members has been identified. Bcl-xL, Bcl-2 and Mcl-1 were shown to mediate retrotranslocation of Bax from the mitochondria to the cytosol (Edlich et al., 2011). The best studied prosurvival protein in this regard is Bcl-xL. For retrotranslocation, a direct interaction of Bax with Bcl-xL seems to be necessary at two interaction sites, namely the hydrophobic groove and the C-terminal membrane anchor of Bcl-xL (Todt et al., 2013). Recently, also prosurvival-mediated retrotranslocation of Bak has been described, albeit at far lower rates (Todt et al., 2015). Although a study found that the abundantly expressed protein VDAC2 is necessary to mediate Bax retrotranslocation in living cells (Lauterwasser et al., 2016), Bcl-xL mediated retrotranslocation was observed in *in vitro* system on artificial liposomes lacking additional molecular players (Subburaj et al., 2015). To date, it remains unclear how much this additional function of prosurvival proteins adds to their prosurvival function.

Differential interaction patterns

At first sight multiple Bcl-2 family members have redundant functions. However, differential binding affinities have been identified within the Bcl-2 proteins and were intensively investigated. *In vitro* and *in cellulo* studies revealed that the activators Bim, Puma and tBid bind to all five prosurvival proteins. Bad is only bound by Bcl-xL, Bcl-w and Bcl-2, and Noxa only binds to Mcl-1 and A1/Bfl-1 (Chen et al. (2005); Certo et al. (2006) and Figure 1.4C).
Interestingly, it has been shown that binding of Noxa to Mcl-1 can lead to proteasomal degradation of the prosurvival protein (Willis et al. (2005) and section 1.2.3). Although experiments suggested that interactions between BH3-only proteins and other family members are mainly regulated via the interaction of their BH3 domain with the hydrophobic groove of a multidomain family member, a BH3 peptide of Bim in contrast

to the Noxa peptide cannot induce the degradation of Mcl-1 (Czabotar et al., 2007). Additionally, binding of the full-length Bim protein to prosurvivals was not impaired by mutations that impair binding of its BH3 domain to these proteins *in vitro* (Aranovich et al., 2012). These results indicate that interaction sites outside the BH3 region might add to the regulatory function of BH3-only proteins.
The interactions between the larger multidomain family members were more difficult to study on a quantitative scale, due to the necessity of purified recombinant proteins in *in vitro* settings. While Bax is bound and thereby antagonized by all prosurvival family members, Bak is preferentially bound by a subset consisting of Bcl-xL, Mcl-1 and Bfl-1 (Willis et al. (2005); Ku et al. (2011) and Figure 1.4D).
Yet, reported quantitative as well as qualitative results vary due to multiple factors that influence binding capabilities of Bcl-2 family members (Chen et al., 2005; Certo et al., 2006; Ku et al., 2011). The length of BH3 peptide stretches (Ku et al., 2011) was shown to significantly impact the observed results and rigorous analysis of binding partners is available only for some, but not the neglected family members Hrk, Bik, Bmf, Bcl-w and Bfl-1. Importantly, the use of detergents can alter the conformations and binding behavior of multidomain Bcl-2 family members (Hsu and Youle, 1997). This might be due to hydrophobic grooves which are formed by the BH1-3 domains and potentially also bind amphipatic molecules. In higher concentrations as used in biochemical assays, non-ionic detergents induce conformational changes in Bcl-2 family members and lead to significantly altered interaction profiles, which might mimic those occuring in a lipid environment (Lindsay et al., 2011).

1.2.3 Levels of regulation

A detailed mechanistic understanding of Bcl-2 family regulated cell death induction is further complicated by several levels of regulatory control of the proteins. Family members are differentially expressed in a cell line and tissue-specific manner and can be further up- or downregulated by various processes. These include direct transcriptional regulation by transcription factors that are activated by cellular signaling pathways, as well as targeted degradation of proteins. The availability of proteins for interactions is further on regulated via sequestration by proteins not belonging to the Bcl-2 protein family. Posttranslational modifications can mediate those interactions and additionally play a role in recruitment of the proteins to their main site of action, the mitochondrial outer membrane.
In the following sections, a non-exhaustive overview of different forms of regulation of family members is given, with a more detailed focus on the well-studied family members Bax, Bak, Bcl-xL, Bcl-2, Mcl-1, Bid, Bim and Bad.

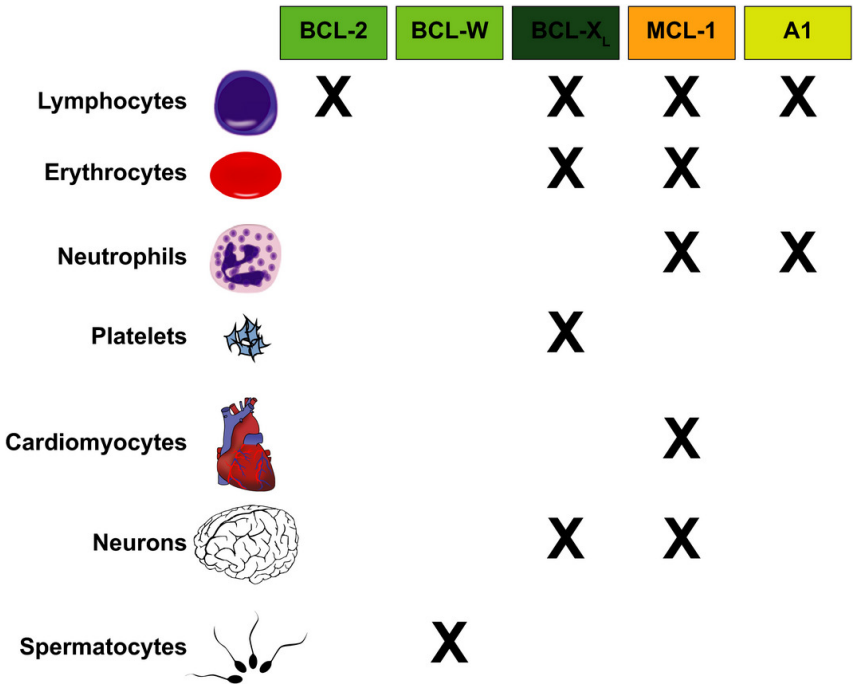

Figure 1.6: **Role of prosurvival Bcl-2 family members in survival of cellular lineages.** While Bcl-xL and Mcl-1 critically regulate the survival of several cellular lineages, dependency on Bcl-2, Bcl-w and Bfl-1 was shown only for certain cell types. Figure taken from Opferman (2016).

Differential expression and stimulus-induced upregulation

Both Bax and Bak are ubiquitously expressed among cell types and only the knockout of both proteins in mice leads to a high lethality rate after birth, development of autoimmune diseases and developmental defects. The knockout of only Bax instead leads to excess platelets and knockout of Bak to infertile male mice due to excess primordial germ cells (Czabotar et al., 2014).

Prosurvival proteins have been shown to mediate survival in a cell line- and differentiation-dependent manner. While a dominant role of Bcl-w and Bfl-1 mediated survival could be identified in only a few cellular lineages, the family members Bcl-xL and Mcl-1 were found to be main regulators across a variety of cell lines (Opferman (2016) and Figure 1.6). Platelet survival critically depends on Bcl-xL and explains the induction of thrombocytopenia by the BH3 mimetic ABT-737 (specifically binds to Bcl-2 and Bcl-xL), which lead to failure of this BH3 mimetic in clinical trials (Mason et al., 2007). The first FDA approved small molecule BH3 mimetic, venetoclax, specifically targets Bcl-2 and potently induces apoptosis in CLL (Roberts et al., 2016). Expression of Mcl-1 has been identified as a resistance mechanism against treatments with BH3 mimetics that target other prosurvival proteins (Opferman, 2016). At the same time, its absolute expression in tumor tissue and cell lines was reported to be low in comparison to Bcl-2 and Bcl-xL (Lindner et al., 2013a). The expression of A1 seems to be mainly restricted to hematopoietic cell

lines in adult mice, where it can be transcriptionally induced by NF-κB signaling (Ottina et al., 2012).
Also distinct BH3-only proteins were reported to play a dominant role in the regulation of MOMP in different cell types (Happo et al., 2012). Basal levels of the BH3-only proteins Bim, Bad, Bid, Bik and Bmf are expressed in unstimulated cells (Puthalakath and Strasser, 2002). Bim furthermore occurs in at least three different isoforms, namely Bim_{EL}, Bim_{L} and Bim_{S}, which result from alternative splicing (Hsu et al., 1998; O'Connor et al., 1998). The three isoforms are all proapoptotic but differently regulated by post-translational modifications (Gillings et al., 2009). Bim expression is especially relevant for the efficacy of chemotherapeutic agents targeting oncogenic kinases (Czabotar et al., 2014; Hata et al., 2015). Transcription of Puma, and further expression of Bim, can be induced by FOXO3a upon cytokine withdrawal (You et al., 2006). In response to DNA damage, the tumor suppressor and transcription factor p53 induces expression of the BH3-only proteins Noxa, Puma and Bik (Oda et al., 2000; Yu et al., 2001; Mathai et al., 2002). Hrk expression can be induced in a JNK-dependent manner (Harris and Johnson, 2001; Chang et al., 2013).

Regulation by subcellular localization

The primary site of action of the Bcl-2 protein family is the mitochondrial outer membrane. Different mechanisms regulate the recruitment of family members to the membrane, either constitutively, or during induction of apoptosis.
The Bcl-2 family member Bak is almost exclusively found as an integral membrane protein and insertion into the mitochondrial outer membrane is mediated by its C-terminal transmembrane anchor (Lindsay et al., 2011). VDAC2 was identified as a critical component for Bak targeting to the MOM. It supposedly interacts with Bak and maybe even prevents Bak activation in healthy cells (Cheng, 2003; Roy et al., 2009). In contrast to Bak, only a minor fraction of Bax can be found attached to the MOM in healthy cells (Wolter et al., 1997). A proline residue in the sequence of Bax, that is not present in Bak, enables intramolecular interaction of the C-terminal transmembrane anchor with the hydrophobic groove of Bax (Schinzel et al., 2004).
As described in section 1.2.2, Bcl-xL and further prosurvival family members such as Bcl-2 and Mcl-1 can mediate constant retrotranslocation of Bax and Bak molecules from the MOM to the cytosol (Edlich et al., 2011; Todt et al., 2013, 2015).
Also the subcellular localization within the prosurvival subgroup of Bcl-2 family members is distinct. Bcl-2 has been reported to partially translocate to the MOM and partially to the membrane of the ER (Kaufmann et al., 2003). Bcl-xL occurs in a cytosolic and a

membrane-inserted fraction in healthy cells (Aranovich et al., 2012), in the latter case it is mainly targeted to the MOM (Kaufmann et al., 2003). The differential targeting of intracellular membranes is likely explained by a more hydrophobic C-terminal tail anchor of Bcl-xL in comparison to that of Bcl-2 (Lindsay et al., 2011). The C-terminus of A1/Bfl-1 contains both polar and charged amino acid residues and the investigation of specificity of membrane association or cytosolic localization led to inconsistent results (Yang et al., 2005; Herold et al., 2006).

Mcl-1 is the only prosurvival family member possessing an extended N-terminal sequence and this domain additionally mediates its functions. Cleavage of the elongated sequence leads to translocation of Mcl-1 to the mitochondrial intermatrix space, where it is involved in further functions, such as mitochondrial fusion processes or ATP production (Perciavalle and Opferman, 2013).

For tBid it has been shown that cardiolipin-rich domains in the membrane increase its binding affinity to the membrane and effector activating potential (Kuwana et al., 2002; Gonzalvez et al., 2005). Cardiolipin is a negatively charged lipid and might be present in increased concentrations at ER-mitochondria contact sites, where a high concentration of positively charged Ca^{2+} accumulates (Cosentino and García-Sáez, 2014; Csordás et al., 2010).

In contrast to tBid, Bim binding to different lipid compositions within a membrane is more promiscuous (Shamas-Din et al., 2015). However, the Bim isoforms Bim_{EL} and Bim_{L} contain a domain that might enable binding to the dynein light chain (DLC) 1 and thereby promote a cytoplasmatic localization (Puthalakath et al., 1999). Similarly, Bmf was shown to be sequestered by dynein light chain 2 (Puthalakath et al., 2001). Release from DLC1 and 2 might be necessary to free these proteins before they can exert their proapoptotic activity at the membrane and in interactions with the other Bcl-2 family members.

In *in vitro* settings, binding of a BH3-protein to the membrane is required for recruitment of multidomain family members (Lovell et al., 2008). This finding is supported by studies which showed that Bad induces the accumulation of Bcl-xL at the MOM (Jeong et al., 2004). Also Bim induces Bcl-w binding to the membrane, which under unstimulated conditions is only loosely attached to the MOM (Wilson-Annan et al., 2003).

Of note, further cofactors and microdomains in the MOM that contain specific compositions of lipids and proteins might influence targeting of family members to the membrane (Cosentino and García-Sáez, 2014). Moreover, specific posttranslational modifications enable or complicate membrane recruitment of Bcl-2 proteins.

Regulation by posttranslational modifications

Besides ubiquitination, phosphorylation of Bcl-2 proteins is an important posttranslational modification. A variety of regulating kinases have been shown to phosphorylate Bcl-2 family members and influence their pro- and antiapoptotic activities. The most prominent kinases reported to influence Bcl-2 family signaling are the serine/threonine-specific protein kinases JNKs, extracellular signal-regulated kinases (ERKs), and protein kinase B (PKB, or Akt).

Bax phosphorylation at S184 by Akt interferes with its membrane binding and conformational change to the active Bax molecule (Arokium et al., 2007; Wang et al., 2010). The Bax mutants S184A and S184E therefore became important tools in studying the molecular mechanisms that regulate Bax targeting to and permeabilization of the MOM. Dephosphorylation of Bak at Y108 has been reported to promote its activation and pore formation activity (Fox et al., 2010).

Mcl-1 displays the by far highest protein turnover rate within the Bcl-2 family, with reported half-lives of 20-40 min (Nijhawan et al., 2003; Schwickart et al., 2010). Regulation of Mcl-1 protein levels in response to survival or apoptosis signaling are mainly regulated by posttranslational modifications that affect the half-life of the protein (Maurer et al., 2006; Nijhawan et al., 2003). Phosphorylation of Mcl-1 at multiple sites was suggested to be important for its ubiquitination by E3 ligases and subsequent proteasomal degradation during mitotic arrest (Wertz et al., 2011). Yet, in a recent study, only Noxa, and not single or double phosphorylation of Mcl-1 was identified as the major regulator of Mcl-1 degradation (Haschka et al., 2015). Usp9x was identified as a deubiquitinase of Mcl-1 and a correlation between Usp9x expression and Mcl-1 protein levels was observed in lymphomas (Schwickart et al., 2010).

Although the full-length protein Bid exerts only a limited proapoptotic potential and remains in the cytosol in healthy cells, phosphorylation of Bid at S66 was shown to sensitize cells to apoptosis during mitotic arrest (Wang et al., 2014). Upon cleavage of Bid by Caspase-8, the p15 fragment tBid is translocated to the MOM (Li et al., 1998; Wei et al., 2000). tBid is targeted for proteasomal degradation by ubiquitination, its proapoptotic potential is thereby limited through a half-life of less than 90 minutes (Breitschopf, 2000).

The BH3-only protein Bim is regulated by multiple upstream signaling processes. ERK was shown to phosphorylate Bim_{EL} at S69 and further sites, thereby targeting it for ubiquitination and proteasomal degradation as well as lowering its affinity to prosurvival family members (Luciano et al., 2003; Ewings et al., 2007). In turn, the deubiquitinase Usp27x can bind to ERK phosphorylated Bim and stabilize Bim protein levels (Weber et al., 2016). Further phosphorylation of Bim_{EL} and Bim_{L} (and also of Bmf) by JNK,

which increases their proapoptotic activity by releasing them from the dynein motor complex, has also been reported (Lei and Davis, 2003).
Prosurvival signaling mediates Bad phosphorylation by the IP3K/Akt pathway (Harada et al., 1999). Phosphorylated Bad interacts with 14-3-3 proteins, which through their sequestration of phosphorylated Bad prevent it from fulfilling its proapoptotic functions (Zha et al., 1996). Upon insufficient prosurvival signaling, Bad is dephosphorylated and can then translocate to the MOM where it binds with its C-terminal transmembrane anchor.

1.3 Systems biology of molecular networks and the Bcl-2 family

1.3.1 Molecular systems biology

Mathematical models can greatly contribute to the understanding of mechanisms of action in molecular biology and even predict cellular responses. The interdisciplinary field combining molecular biology with computational modeling has been termed 'systems biology'. Systems biological approaches combine the experimental analysis of biomolecular processes with methods from systems or graph theory (Klipp et al., 2010).
The network of interactions within the Bcl-2 protein family is highly complex and the mitochondrial outer membrane constitutes an additional interaction partner complicating experimental investigations (Czabotar et al. (2014) and section 1.2). Mathematical modeling can advance biological insight in such complex regulatory networks by rigorously describing and modeling the known molecular mechanisms.
Simulations from computational models are usually compared with experimental outcomes in an iterative procedure. Should the model fail to fit or predict experimental data, this indicates that important players or mechanisms of action have not been taken into account yet. Similarly, the incorporated processes and reactions might be oversimplified, or even prove to be wrong upon closer experimental investigation. In this manner, already the modeling process itself can yield valuable insights in the investigation of cellular processes (Rehm and Prehn, 2013). Still, a model is always a simplification of the biological system it simulates. Especially for detailed kinetic models considerable biological knowledge and a precise research question are necessary to decide if processes could potentially be neglected in a model or not (Klipp et al., 2010).
Ultimately, as soon as a model has been established that is in agreement with available experimental data, it can be used as a predictive tool. Due to reduced investment of

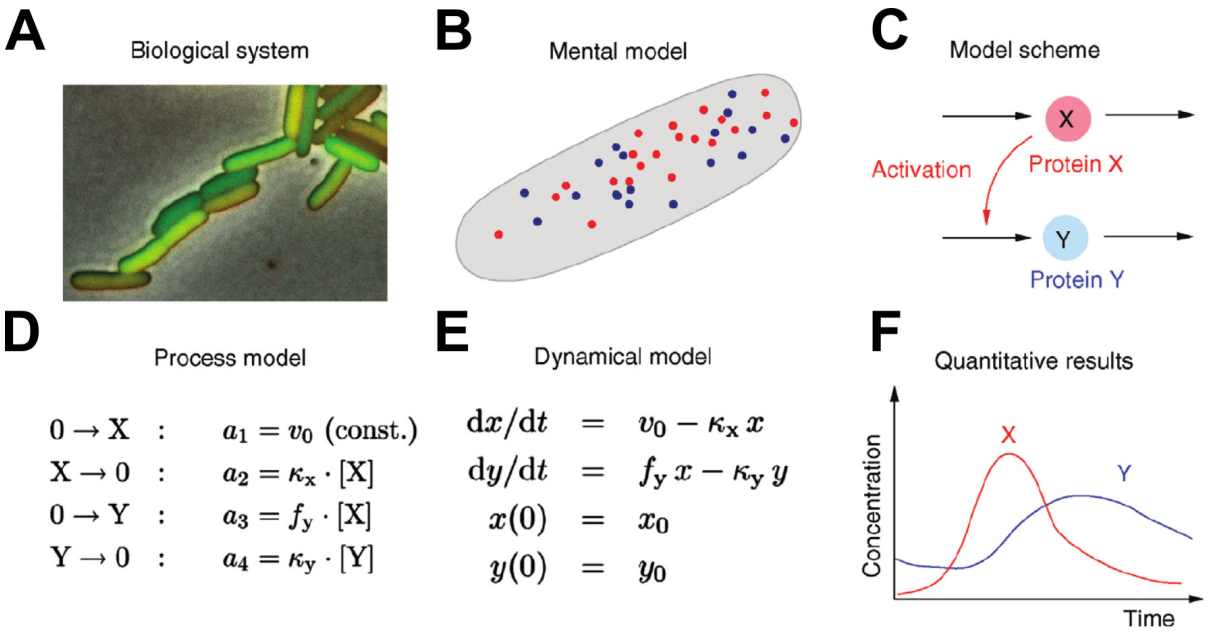

Figure 1.7: **ODE modeling of biological systems.** **A**, A biological process of interest (here: expression of a GFP (green fluorescent protein) tagged protein in *Escherichia coli*) can be captured in a mathematical model. **B**, A mental model first simplifies the biological process, here by considering that only one further protein is involved in regulation of the protein's expression. **C**, A model scheme then adds mechanistic biological knowledge to the model. **D**, The biochemical steps involved in each of the mechanisms are assigned model parameters (rate constants). **E**, Subsequently the processes are translated into differential equations describing the change of protein concentrations by time increment. These sets of ODEs, supplemented with knowledge of the starting concentrations at time point zero (x(0) and y(0)), are then numerically integrated and quantitative deterministic simulations are obtained (**E**). Figure modified and taken from Klipp et al. (2016).

time and costs of model simulation compared to experimentation (Klipp et al., 2010), biological processes of interest can be rigorously screened computationally and relevant findings ultimately tested in experimental setups (Rehm and Prehn, 2013).
Furthermore, established mathematical models have been shown to be of potential use in a clinical setting as prognostic tools outperforming biomarkers (Lindner et al., 2016). This is especially promising with regard to personalized medicine, as *in silico* mediated improvement of treatment prognosis would allow faster and noninvasive identification of optimal treatment strategies for individual patients (Gonzalez-Angulo et al., 2010).

Modeling frameworks

Depending on the scope of the research question to be answered in a systems biological approach, different modeling frameworks can be applied. Commonly used modeling approaches in apoptosis research are ordinary differential equations (ODE)-based models, Boolean networks, cellular automata, partial differential equations (PDE)-based models and agent-based models (Würstle et al., 2014; Huber et al., 2011).

In order to model the temporal behavior of cellular signal transduction processes, ODE models are often applied (Chen et al., 2010). For every species (e.g. a protein or protein complex) incorporated in an ODE model, a mathematical equation accounts for the processes that contribute to formation or dissolution of this species over time in a quantitative manner (Rehm and Prehn (2013) and Figure 1.7). Mathematical expressions for individual reactions in the interaction network can be derived from mass-action or Michaelis-Menten kinetics. The assigned parameter values (of e.g. k_{on}, k_{off} and K_M) are then biologically meaningful numbers that might have been determined experimentally.
Due to their qualitative nature, Boolean networks are suitable if merely qualitative data are available and an analysis of rather large regulatory networks is desired. They are thus also often employed to analyze gene-regulatory networks (Karlebach and Shamir, 2008). PDE models use reaction diffusion equations to incorporate not only temporal but also spatial resolution (Rehm and Prehn, 2013). This is important if spatial processes are to be investigated, or if a homogeneous distribution of particles can not be assumed and thus does not allow the use of ODE models. Cellular automata and agent-based models additionally account for stochasticity in biological systems, making them especially useful when analyzing processes involving a small number of particles (An et al., 2009; Machado et al., 2011). ODE models in turn usually deal with nanomolar or micromolar concentrations, i.e. when assuming a volume of around one picoliter of a mammalian cell (Sims and Allbritton, 2007), in the order of 10,000-100,000 entities of a specific protein per cell. In addition to the possibility to implement and analyze a computational model by using programming languages and associated packages, editors with graphical user interfaces for setting up and analyzing models of biological processes have been developed (e.g. COPASI and CellDesigner) (Hoops et al., 2006; Funahashi et al., 2008). The exchange of models throughout different modeling environments has been facilitated with the invention of the systems biology markup language (SBML) (Hucka et al., 2003).

1.3.2 Analysis of ordinary differential equations-based models

ODE-based models are used to simulate the temporal behavior of species (e.g. proteins) incorporated in the model. The ordinary differential equations can be set up by applying the law of mass action. It states that the reaction rate of each biochemical step (e.g. the association of two proteins) is proportional to the concentration of the two proteins to the power of their stoichiometry. In the simple case where two proteins X and Y reversibly

interact, the reaction rate ν would thus be:

$$X + Y \leftrightharpoons XY$$
$$\nu = k_{on} \cdot [X] \cdot [Y] - k_{off} \cdot [XY]$$

This would result in the following set of ordinary differential equations:

$$\frac{d[X]}{dt} = -\nu$$
$$\frac{d[Y]}{dt} = -\nu$$
$$\frac{d[XY]}{dt} = \nu$$

Addition of further species and reactions then leads to more equations, mathematical expressions and parameters. Values need to be assigned to the biochemical parameters to perform simulations. These might be found in the literature, if they were measured in *in vitro* systems. Sometimes also *in cellulo* determined rate constants are available. Although these provide important information on the rate of biochemical reactions in endogenous systems, care needs to be taken when integrating such effective rate constants into mathematical models. The biochemical parameters in ODE models account for the isolated individual reactions, whereas effective rate constants define the rate in presence of competing reactions (Klipp et al., 2010).

Structural and practical identifiability

When parameter values are completely undefined, they need to be estimated either from similar reactions with known biochemical parameters or by fitting the model to experimental data. Depending on the model structure, it might be impossible to obtain a unique parameter value from model fitting. This problem has been termed structural non-identifiability. Furthermore, even if a parameter is structurally identifiable, given a limited amount of experimental data the model can be fitted to, it might still be impossible to identify a unique solution for the parameter value (i.e. practical non-identifiability) (Raue et al., 2009). Methods have been developed to address this problem, such as the determination of the profile likelihood of each parameter. First, a model parameterization has to be obtained that yields the best possible fit to the experimental data (for instance by minimization of the SSR (sum of squared residuals) between model simulations and data points). To determine the profile likelihood of a parameter, the SSR of the model's fit to experimental data is then reassessed for variations in the parameter value. Through

95 % confidence levels it can be determined which of the parameters are identifiable given the experimental data (Raue et al., 2009; Schaber, 2012).
However, most often model predictions rather than the exact values of model parameters are of interest. When using a model to make predictions, the uncertainties in parameter values should be accounted for in predictive simulations. To address this need, the calculation of prediction profile likelihoods has been suggested (Kreutz et al., 2012). The method assesses the prediction confidence by continuously comparing predicted values to the fit of the model to experimental data. This approach is valid given that the asymptotic criterion applies, i.e. a large amount of experimental data points is available or parameter dependencies are linear. If those criteria do not apply, which is often the case in systems biology approaches, other, more computationally expensive methods have to be employed, e.g. by densely sampling plausible parameterizations in parameter space.
Despite of the various attempts and developed methods to identify and achieve practical parameter identifiability (Raue et al., 2014), uncertainty in many parameter values might be an intrinsic but unproblematic property of many systems biological models. In a study investigating a range of published mathematical models, consistently 'sloppy' parameter sensitivities have been identified (Gutenkunst et al., 2007). This means that for a given biological research question (or simulation), only small subsets of the model's parameters critically influence the prediction of interest. Those parameter values in turn need to be determined precisely to obtain accurate predictions. The major part of parameter values in systems biological models, however, could be anywhere within a plausible range spanning up to orders of magnitude without affecting the model output.

Model selection

The most obvious criterion to reject a computational model is its inability to comply with or correctly predict experimental data. In this case, the model might oversimplify processes or neglect important molecular players or processes (Klipp et al., 2010). However, it might also be that several models are in line with experimental data, but assume different model structures and represent different hypotheses of the underlying biological mechanisms. In this case, statistical methods as well as approaches from information theory exist that enable comparison and discrimination of models.
The two main methods to compare models are the application of likelihood ratio tests (i.e. null hypothesis testing) and model selection criteria (e.g. Akaike information criterion or Bayesian information criterion). When trying to identify which one in a set of models is best supported by experimental data, it is important to account for the complexity of each model. If a model contains more parameters, it in general allows an improved fit

to the data, irrespective of the underlying biological hypotheses (Dyson, 2004). In likelihood ratio tests the more complex model is chosen, if the null hypothesis that the simple and more complex model perform equally well can be rejected. Model selection criteria additionally allow ranking of competing models and account for quality of the model fit as well as model complexity (Johnson and Omland, 2004; Klipp et al., 2010).

Global and local sensitivity analysis

To determine model robustness to perturbations or identify modeled components to which certain biological processes are most sensitive to, sensitivity analyses can be employed (Rehm and Prehn, 2013). Local sensitivity analyses identify altered behavior upon changes in each individual parameter value separately. This is a valid approach, if one can be certain about all other parameter values in the model, which is often not the case. Global sensitivity analyses circumvent this problem by testing the effect of each parameter on model predictions with respect to a variability in all other parameters (Saltelli, 2008). Global approaches are far more computationally demanding than local methods, but can even be implemented in modeling software such as COPASI (Sahle et al., 2008).
Global sensitivity analyses can furthermore aid in the modeling process by identifying parameters that are (un-)critical for model predictions. They can also enable experimental design by revealing those unknown parameters that would reduce uncertainty in predictions (Saltelli, 2008).

1.3.3 Systems biological studies of the Bcl-2 family

Models of different scope have been developed to investigate the regulation of MOMP by the Bcl-2 protein family. Qualitative Boolean networks as well as quantitative approaches were used and studies range from pure *in silico* approaches to experimentally validated models with predictive or even prognostic value (Würstle et al., 2014).
In a Boolean network-based model the impact of single Bcl-2 family members on decision outcomes could be theoretically assessed when assuming fixed qualitative interaction patterns within the whole protein family (Tokar et al., 2013). By extending such qualitative models to more realistic representations of cellular processes through implementing quantitative kinetic rate constants, experimentally observed features such as nonlinearity in stimulus response curves and switch-like apoptosis induction could be reproduced (Tokar and Ulicny, 2013).
Using both a mass action-based as well as cellular automaton model, the oligomerization of Bax was identified to make its activation irreversible upon apoptosis induction. Fur-

thermore, the feedback loop of tBid that continuously activates further Bax was identified as a component that drives Bax activation in a switch-like manner (Chen et al., 2007a). By investigating prosurvival-mediated sequestration and inhibition of constitutively active effectors as opposed to the necessity of a direct activation of Bax or Bak, only the direct but not the indirect activation model was identified to robustly display ultrasensitive pore formation behavior (Chen et al., 2007b).

A large model focusing mainly on the extrinsic apoptosis pathway, which was validated with experimental data, also shed light on aspects of Bcl-2 family mediated MOMP. The main purpose of this mass-action based modeling approach was to investigate the long and variable delay between initiator caspase activation at the DISC and efficient effector caspase activation that ultimately causes cellular destruction (Albeck et al., 2008a,b). Besides a crucial role of the regulation of caspase-8 activity, a strict all-or-none induction of MOMP, mediated by prosurvival mechanisms within the Bcl-2 family, was identified (Albeck et al., 2008b). A threshold level of proapoptotic proteins that is needed to overcome inhibition by the prosurvival proteins was identified to determine the time point of pore formation, cytochrome *c* release and subsequent effector caspase activation (Albeck et al., 2008a).

Furthermore, potential causes of cell-to-cell variability in apoptosis responsiveness were analyzed by sampling protein expression levels from log-normal distributions and using them as model inputs (Gaudet et al., 2012). High abundance of Bcl-2 was associated with an inability to induce MOMP, while an only modest increase in Bcl-2 compared to the measured population mean lead to Bax-dependent MOMP decisions. These results might explain how in a cell population the response to apoptosis inducing triggers is determined by the ratio of prosurvival and proapoptotic Bcl-2 family proteins in single cells. Insensitivity of cells to a stimulus would then result from tremendous prosurvival overexpression.

In a study investigating cell-to-cell heterogeneity in response to anti-mitotic drugs, the oligomerization of Bak and its control by Mcl-1 and Bcl-xL was modeled. The respective concentration ratio of prosurvival protein to Bak was identified as the cause for the resulting variability in cell populations (Kueh et al., 2016).

A striking experimental observation was that in single cells only a minor fraction of Bax has translocated to the MOM upon MOMP induction. Instead, the majority of Bax is recruited to the membrane when cytochrome *c* is already completely released into the cytosol. In line with the experimental finding, a cellular automaton model could simulate the formation of pores by low amounts of Bax molecules at the membrane (Düssmann et al., 2010).

Importantly, when observed on a single-cell level, wide-spread MOMP commences at in-

dividual and then extends to further mitochondria. Interestingly, implementing reaction-diffusion processes of BH3-only proteins was sufficient to remodel the kinetics of wave-like MOMP spreads throughout the cell in a model based on partial differential equations (Rehm et al., 2009).

Focusing less on the kinetic behavior of MOMP induction but more the overall threshold of proapoptotic input that is necessary to overcome inhibition by prosurvivals, the so far most elaborate quantitative model on Bcl-2 family mediated MOMP was developed. Based on quantitative protein expression data and kinetic interaction data, the model ('DR_MOMP') calculates cell line or tissue-specific BH3-stress doses (Lindner et al., 2013a). These were shown to correlate with cell death responsiveness upon genotoxic drug treatment. This model was also used to investigate consistency with the indirect instead of the direct activation model. However, constitutively active effectors resulted in a scenario that required strong constraints to keep active effectors in check and prevent pore formation in unstimulated cells. Assuming varying protein expression to account for cell-to-cell heterogeneities further complicated inhibition of spontaneous MOMP induction (Lindner et al., 2013b).

When the calculation of BH3-stress doses using DR_MOMP was applied to primary colorectal cancer tumor tissue, the model displayed prognostic value in the stratification of patients into low- and high-risk groups (Lindner et al., 2016). This does not only show that Bcl-2 family regulated MOMP induction is indeed an important bottleneck in apoptosis signaling that critically determines susceptibility to chemotherapy. It also highlights that capturing the molecular processes that control MOMP in a mathematical model can open possibilities to translate findings from basic research to clinical applications. These might later extend to guide personalized treatment decisions.

1.4 Aim of this study

The overall aim of this thesis was to apply a systems biological and computational approach to elucidate and structure interactions within the Bcl-2 protein family and the mechanisms of action governing effector pore formation. To this end, published data from the scientific community and unpublished experimental data from collaborators within the FOR2036 research consortium "New insights into Bcl-2 family interactions: from biophysics to function" were available. In particular, this research question was divided into three subaims, as presented in Chapters 2-4:

Chapter 2: A wealth of studies have been published, which investigated Bcl-2 family interactions and the transient interactions of BH3-only proteins with effector proteins that might cause activation and subsequent oligomerization of effectors. A consistent picture of the Bcl-2 interactome yet remains elusive due to the use of varying experimental conditions and recombinant proteins or peptide stretches. The aim of this part was to provide a structured overview of Bcl-2 family interactions to facilitate our understanding of and accelerate research on the Bcl-2 interactome.

Chapter 3: A quantitative understanding of the mechanistic processes governing Bax membrane recruitment and oligomerization is key to understanding MOMP control and cellular decisions in response to chemotherapeutic treatments. Experimental constraints render it difficult to quantify the influence of different prosurvival and proapoptotic molecular mechanisms within the Bcl-2 protein family on MOMP decisions. To address this problem, the aim was to build a mathematical model that can accurately reproduce available quantitative data and provide testable predictions on MOMP control. The resulting model should furthermore be applied to test if a rationale can be provided for the experimentally observed synergies of distinct BH3-only proteins in mediating apoptotic cell death.

Chapter 4: Computational modeling should be employed to shed light on the dynamic processes occurring between tBid, Bcl-xL and Bcl-xL homodimers in solution. Quantitative and time-resolved *in vitro* data on particle concentrations detected in solution were provided by Dr. Stephanie Bleicken from the Membrane Biophysics group at University of Tübingen.

2 Bcl-2-Ome - A database and interactive web service for dissecting the Bcl-2 interactome

Annika Hantusch, Thomas Brunner, Tancred Frickey*, and Markus Rehm*.

Cell Death and Differentiation, 24(1):192-192, January 2017

*joint senior authors

2.1 Bcl-2-Ome

The interactome of the Bcl-2 protein family regulates mitochondrial outer membrane permeabilisation and apoptotic cell death and, following decades of research, now takes center stage in the development of targeted anti-cancer therapeutics (Czabotar et al., 2014; Delbridge et al., 2016). Bcl-2 family members physiologically interact in aqueous and lipid membrane environments and also at interfaces between both phases. Consequently, a broad range of methodological approaches is employed to study the Bcl-2 family interactome, with differences in experimental conditions and reaction environments strongly affecting interaction kinetics and steady states. Since detailed insight into the Bcl-2 family interactome is crucial not only for understanding signal transduction, but also for the further development of targeted therapeutics and the context-dependent identification of optimal interventions, tools are required that assist in navigating through the large amount of available, complex and frequently conflicting data. We address this need by offering a comprehensive database and interactive web service (Bcl-2-Ome) that provides structured, annotated and expert-curated data on the Bcl-2 interactome, a framework for prospective community-assisted data integration and database expansion, and a user-friendly interface for searches, data filtering and interactome visualization. All database entries are linked back to primary source literature and include detailed information on experimental conditions and reagents used for data generation. Bcl-2-Ome therefore allows the exploration of the Bcl-2 family interactome at an unprecedented level of convenience and detail. Bcl-2-Ome is implemented as a Java Web Start application and is freely accessible at **http://for2036.uni-konstanz.de/Bcl2Ome/**. All contents are available for download as xml file, and the web service also links to less specific but global interactome resources (STRING, IntAct) and the BCL2DB repository for sequence and structural information, ensuring that Bcl-2-Ome is offered within the context of existing repositories.

By now, 353 quantitative and qualitative experimental outcomes are integrated in Bcl-2-Ome. Three hundred and six entries describe the outcome of interaction studies and 47 entries describe effector (Bax, Bak) activation, such as the transient interactions with BH3-only proteins. Bcl-2-Ome can be accessed and interrogated through a user interface, which provides comprehensive data exploration possibilities. Search and filter criteria can be defined, the Bcl-2 interactome is graphically illustrated accordingly and provides access to detailed underlying original data (Figure 2.1). The web service provides step-by-step instructions for representative use cases online. Since Bcl-2-Ome enables the convenient comparison of findings from multiple studies, information on reproducibly reported interactions can easily be sourced. Likewise, poorly defined or conflicting data on interactions

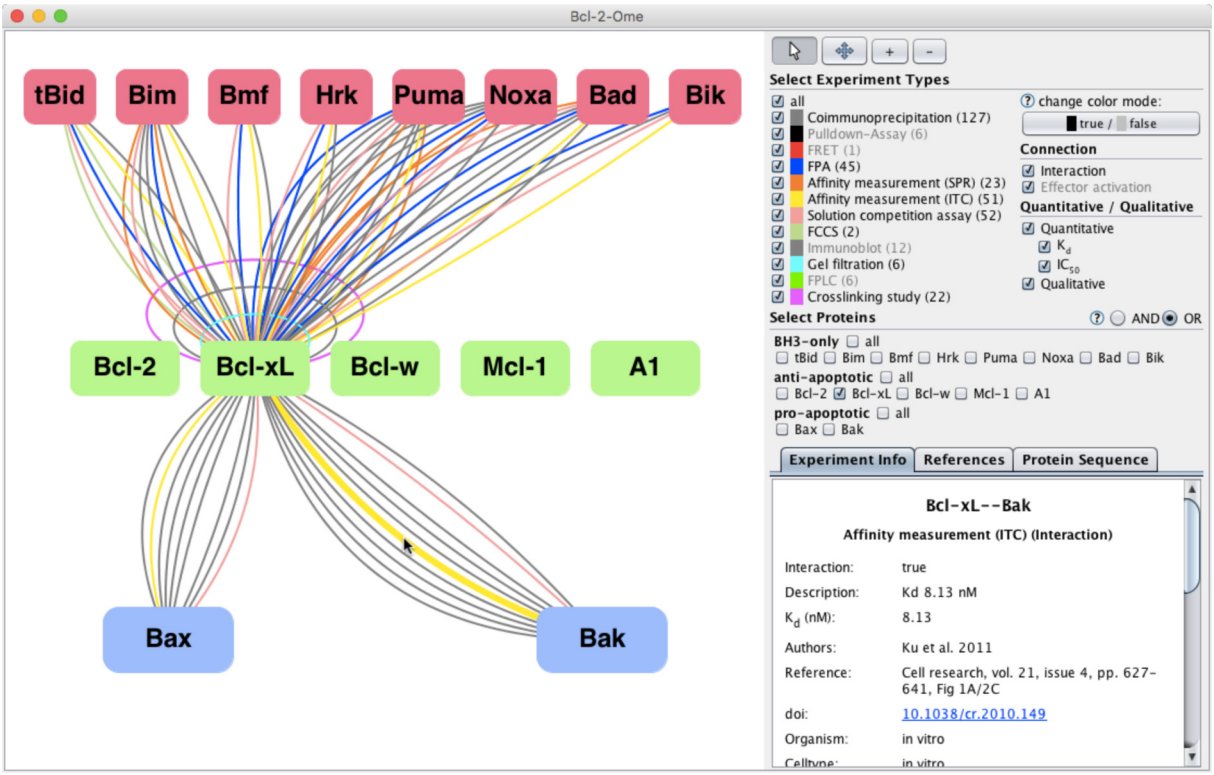

Figure 2.1: **Graphical User Interface of the Bcl-2-Ome web service.** Bcl-2 family members are displayed as a graph on the left. Connecting lines (edges) represent individual experimental outcomes from the peer reviewed literature. Interactions and effector activation are denoted by undirected and directed edges, respectively. The example shows the interactions for the Bcl-2 family member Bcl-x_L. Edges can be selected via mouse clicks, resulting in the corresponding experimental details being displayed in the lower right corner of the user interface. The information depicted therein describes the relation of the two proteins as identified in the respective experiment, the type of experimental approach taken to obtain the data, a Boolean value specifying whether an interaction/effector activation was observed in this experiment and the associated literature reference. A short description of the experimental outcome adds further details to each result. Depending on the experimental approach and the data availability, additional information are given: a quantitative value such as the K_D or IC_{50} value, information on the cell line, detergents, antibodies and instrumentation used. Finally, details on whether and which recombinant or endogenous proteins were used are given, including sequence information and origin of the sequences. The top right panel provides a set of filters that allow users to focus on subsets of the data, e.g. limit the display to only quantitative or qualitative results, or interactions between specific proteins and to include or exclude results obtained by specific methods. A color code assists in differentiating between experimental approaches. Numbers in brackets denote the number of entries present in the database for the respective experimental approaches. The lower part of the right panel contains additional tabs to select experiments by reference or to retrieve Bcl-2 protein sequences of human or mouse origin as defined by UniProt (http://www.uniprot.org). Detailed step-by-step instructions on how to operate the webservice are provided online.

within the Bcl-2 family can be evaluated within the context of the different assays, reactants, reaction conditions and cellular models used in the original research studies. Through a data submission interface, Bcl-2-Ome allows community-assisted expansion and regular updating. Submissions are reviewed for completeness, and curated as needed before inclusion. Taken together, we therefore believe that Bcl-2-Ome and its functionalities will be useful to a wide community of cell death researchers that may approach the

field from a background of cell biology, biochemistry, biophysics or systems biology.

2.2 Community-Assisted Database Expansion

This Bcl-2-Ome database and web service is designed to allow community- assisted expansion. To this end, a data submission form (http://for2036.uni-konstanz.de/Bcl2DB/submit) enables users to provide data for inclusion into Bcl-2-Ome. In addition, a template xml form is provided on the website to enable convenient submission of multiple entries in parallel. Submissions will be reviewed for completeness, and curated as needed prior to inclusion.
Bcl-2-Ome is regularly being updated as part of the FOR2036 research consortium "New insights into Bcl-2 family interactions: from biophysics to function".
http://for2036.uni-konstanz.de

2.3 Discussion

The aim of Bcl-2-Ome is to provide users with an up-to-date overview of our current understanding of the Bcl-2 protein family interactome and an interactive means of exploring its complexity. Providing structured access to experimental data at currently unparalleled detail, Bcl-2-Ome is also a unique tool that can provide the basis for facilitating and directing the design of complex experimental and mathematical analyses, such as biophysical, biochemical, cell biological and systems biological studies on Bcl-2 protein ensembles and their interplay in governing cell fate decisions between life and death.

3 Bax retrotranslocation potentiates Bcl-xL activity and is essential for systems-level switching of apoptosis competency

Annika Hantusch, Kushal Kumar Das, Ana J. Garcia-Saez,
Thomas Brunner*, and Markus Rehm*.

Manuscript submitted

*joint senior authors

3.1 Abstract

The rapid, typically all-or-none process of mitochondrial outer membrane permeabilization (MOMP) constitutes a primary cell death decision that is controlled by the Bcl-2 family interactome. However, how strict all-or-none MOMP decisions are governed by and emanate from the dynamic interplay of pro- and antiapoptotic Bcl-2 family members remains incompletely understood. In particular, it is unclear to which extent the shuttling of Bcl-2 family species between lipid and aqueous phases contributes to regulating MOMP sensitivity. Here, we studied the interplay of tBid, Bax and Bcl-xL, using a combined approach of deterministic mathematical modeling and retrospective as well as prospective experimental testing of model predictions. Systems modeling of the tBid-Bax interplay and their fluxes between cytosol and mitochondrial membranes reproduced experimental data on tBid-triggered Bax activation and oligomerization highly accurately. Extending these studies to analyze the cell-protective role of Bcl-xL strikingly revealed that the activity of Bcl-xL to retrotranslocate activated Bax from membranes back into the cytosol is essential to reproduce or correctly predict experimental outcomes. These included the potency of Bcl-xL in suppressing Bax oligomerization, its role in limiting Bax membrane recruitment, the resistance threshold to low concentrations of MOMP triggers as well as response synergies arising from combinations of tBid and sensitizer BH3-only peptides. Importantly, retrotranslocation activity of Bcl-xL is necessary to strictly separate conditions of MOMP competency and resistance. Our results therefore identify Bax retrotranslocation by Bcl-xL as an indispensable component of the molecular switch by which Bcl-2 family members govern cellular death decisions.

3.2 Introduction

Pro- and antiapoptotic members of the Bcl-2 (B-cell lymphoma 2) protein family gather signals from pathways sensing stresses, such as DNA damage or cytokine deprivation, and regulate the mitochondrial pathway of apoptosis (Roos et al., 2015; Cory et al., 2016). The primary mediators of incoming stress signals are Bcl-2 family members with a single Bcl-2 homology (BH) domain, the so-called BH3-only proteins. The subgroup of activator BH3-only proteins, such as truncated Bid (tBid), Bim or Puma, directly activate the effector Bcl-2 family proteins Bax and Bak (Czabotar et al., 2013; Luna-Vargas and Chipuk, 2016). These in turn oligomerize to form pores in the outer mitochondrial membrane, causing the release of cytochrome *c* and other proapoptotic factors into the cytosol (Lopez and Tait, 2015). This process of mitochondrial outer membrane permeabilization

(MOMP) typically is an all-or-none event, resulting in the rapid and efficient activation of effector caspases and apoptosis execution (Goldstein et al., 2000; Rehm et al., 2009). Prosurvival family members, such as Bcl-xL, Bcl-2 and Mcl-1, efficiently antagonize both activator and sensitizer BH3-only proteins as well as Bax and Bak, thereby protecting cells from unwanted MOMP. However, their increased expression might also completely prevent apoptosis and thereby the elimination of excessively stressed and damaged cells (Opferman, 2016; Hata et al., 2015). Imbalances in the expression of Bcl-2 family members therefore interfere with normal cellular homeostasis in multicellular organisms and can contribute to the complex etiologies of diverse degenerative and proliferative diseases (Czabotar et al., 2014).

Importantly, the majority of critical interactions between Bcl-2 family members occur at or within the outer mitochondrial membrane. Membrane association and integration significantly affect protein conformations and binding affinities of Bcl-2 family members, so that authentic interaction data cannot be obtained from studies carried out solely in aqueous environments (García-Sáez et al., 2009; Chi et al., 2014). For example, membrane environments dramatically promote the association of tBid with Bcl-xL (García-Sáez et al., 2009). Furthermore, membrane bound proteins induce the recruitment of further family members, and membrane insertion leads to altered interaction patterns (Bleicken et al., 2017). Similar findings regarding the regulatory role of the membrane were made for various Bcl-2 family members and interactions, using NMR structure elucidation in artificial micelles (Wang and Tjandra, 2013), subcellular fractionation (Jeong et al., 2004; Wilson-Annan et al., 2003), or by studying GFP fusion proteins and their recruitment to the outer mitochondrial membrane (Wilfling et al., 2012).

Recently, Bax activation was described at greater mechanistic detail. Binding of the tBid BH3 domain to Bax unlatches the Bax core domain, thereby exposing the Bax BH3 domain and preparing Bax to form BH3-in-groove homodimers (Czabotar et al., 2013). Strikingly, the lipidic environment at the mitochondrial outer membrane appears to facilitate the disengagement of core and latch domains and provides a surface to preorientate Bax for homooligomerisation (Czabotar et al., 2013). Bak is likely activated by a similar molecular mechanism in mitochondrial membranes (Brouwer et al., 2014). Even though technologies such as scanning fluorescence cross correlation spectroscopy (sFCCS) or FRET-based assays in lipid environments now begin to provide reliable data from well-controlled experimental conditions (Bogner et al., 2010; Bleicken et al., 2017; Shamas-Din et al., 2015), obtaining a quantitative and kinetic understanding of the Bcl-2 interactome and MOMP regulation remains challenging (Luna-Vargas and Chipuk, 2016; Volkmann et al., 2014).

A further layer of complexity in the regulation of MOMP sensitivity might be added by the recently reported shuttling of Bcl-2 family members. Most prominently, it was demonstrated that the cytosolic fraction of Bax and Bax bound to the mitochondrial outer membrane exist in a dynamic equilibrium in healthy cells (Edlich et al., 2011; Schellenberg et al., 2013; Todt et al., 2015). Bcl-xL, a predominantly membrane integrated family member, promotes retrotranslocation of Bax from the mitochondria into the cytosol and thereby limits Bax cytotoxicity (Edlich et al., 2011; Todt et al., 2013). However, to which extent retrotranslocation contributes to the antiapoptotic potential of Bcl-xL remains so far undetermined.

Here, we studied the regulation of MOMP by the interplay of tBid, Bax and Bcl-xL at and within membranes, using a combined approach of deterministic mathematical modeling and experimental validation of model predictions. We were able to quantify for the first time the contribution of Bax retrotranslocation to the overall antiapoptotic potential of Bcl-xL. Bax retrotranslocation functionally appears to be essential to provide MOMP resistance to residual, basal BH3-only protein stress while still allowing rapid and synergistic MOMP induction in response to combinations of activator and sensitizer BH3-only protein inputs. Furthermore, retrotranslocation activity is required to control switch-like transitions from MOMP competency to MOMP resistance across a narrow Bcl-xL concentration range.

3.3 Results

3.3.1 Quantitative kinetic modeling of the tBid-Bax interplay accurately simulates Bax activation and oligomerization

We initially developed a core mathematical model of the tBid-Bax interplay at and within membranes to study if membrane recruitment, activation and oligomerization of Bax, leading to MOMP, can be simulated authentically. This core model subsequently was used to analyze the potency of Bcl-xL in preventing MOMP and to determine the contribution of Bax retrotranslocation to the antiapoptotic function of Bcl-xL. All processes were modeled using ordinary differential equations (see methods section and Supplementary Material for detailed information).

The activator BH3-only protein tBid was implemented to promote the insertion of monomeric Bax into the outer mitochondrial membrane (Lovell et al., 2008) (Fig. 3.1A). In the model, this process comprised serial reversible reactions, including tBid-mediated Bax membrane association and subsequent membrane insertion to yield Bax in its fully

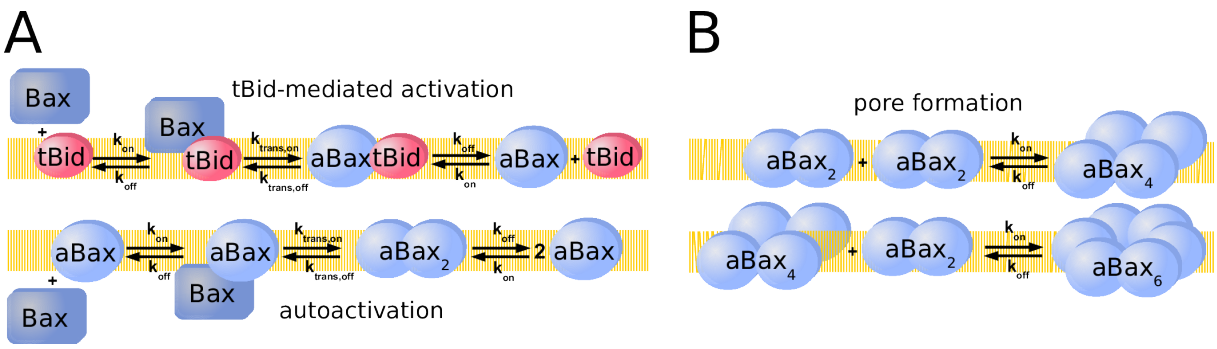

Figure 3.1: **Molecular mechanisms of the tBid-Bax interplay and Bax pore formation captured in the core mathematical model A**, Signaling processes providing active Bax species. Cytosolic Bax in its inactive conformation can be integrated into the membrane and activated either by interaction with tBid or with active Bax molecules (aBax) that already reside in the membrane. These processes were implemented as two-step reversible mechanisms, taking into account intermediate Bax species that are attached to but not yet fully integrated into the membrane. **B**, Bax oligomerization and pore formation. Dimers of aBax were implemented to from higher order oligomers (tetramers, hexamers). Tetramers and hexamers were considered as a minimum requirement for pore formation.

active conformation (aBax). The two-step activation process of Bax is in agreement with the recently proposed core/latch disengagement mechanism, in which the BH3 domain of tBid first binds to Bax and thereby induces the dissociation of Bax's core and latch domains (Czabotar et al., 2013). aBax subsequently can form symmetric homodimers with other aBax molecules by BH3 domain/binding groove interactions (Czabotar et al., 2013). In line with experimental evidence, aBax was assumed to recruit further Bax molecules to the membrane, thereby driving a Bax autoactivation loop (Gavathiotis et al., 2010; Tan et al., 2006; Valentijn et al., 2008) (Fig. 3.1A). Since Bax autoactivation relies on the Bax BH3 domain (Gavathiotis et al., 2010), the reaction sequence was implemented analogous to Bax activation by tBid (Fig. 3.1A). Experimentally, mostly even-numbered oligomers of aBax can be detected in membranes (Subburaj et al., 2015). We thus modeled aBax oligomerization by assuming dimeric aBax species aggregating into tetramers ($aBax_4$) and hexamers ($aBax_6$) (Fig. 3.1B). Higher order oligomers were not explicitly modeled, since $aBax_4$ and $aBax_6$ appear to be sufficient for pore formation and cytochrome *c* release into the cytosol (Saito et al., 2000; Xu et al., 2013). The amounts of $aBax_4$ and $aBax_6$ were therefore regarded as a final output of the model, indicative of the extent of membrane permeabilization (Fig. 3.1B).

Bax multimers rapidly accumulate in membranes in response to tBid addition, as was demonstrated by measuring oligomerization kinetics in lipid bilayers (Subburaj et al., 2015). However, the rate and dissociation constants for the underlying reactions and interactions so far can only be estimated within biologically plausible and justifiable parameter ranges. We therefore tested if model parameterizations could be obtained from these ranges that allowed us to reproduce experimental kinetics of Bax oligomerization. A

detailed description of this procedure and the definition of suitable parameter ranges are provided in the methods section and in Supplementary Material. Results from ensemble simulations (n = 340) using optimized parameter ranges demonstrate that oligomerization of membrane bound aBax proceeds swiftly upon addition of tBid, with $aBax_4$ and $aBax_6$ species rapidly reaching equilibrium concentrations within 1-2 min of triggering the reaction network (Fig. 3.2A), thus closely matching reported kinetics (Subburaj et al., 2015). The distribution of oligomeric Bax species indicated that predominantly Bax tetramers and, albeit in lower amounts, Bax hexamers are formed. This distribution agreed well with the distribution of Bax oligomers measured experimentally (Fig. 3.2B). Next, we used this core model to study oligomerization of aBax resulting from autoactivation. To this end, we ran simulations in absence of tBid and used small amounts of aBax as model inputs. For inputs of up to 10-20% aBax, we noted roughly equimolar amounts of $aBax_2$ and $aBax_4$ forming. To validate these predictions, we examined experimental data in which heat-activated aBax was used to initiate Bax oligomerization and pore formation in absence of tBid (Subburaj et al., 2015). Comparison of model predictions and experimentally observed distributions confirmed a close match of the results, with $aBax_2$ and $aBax_4$ being the predominant species (Fig. 3.2C). For conditions with high amounts of aBax inputs (80%), it would be assumed that oligomer distributions similar to those in presence of tBid would be obtained. Control simulations indeed confirmed this assumption (not shown).

To conclude, our core model of the tBid-Bax interplay therefore reproduces experimental findings on tBid-induced Bax oligomerization, kinetically and quantitatively, and, without further modification of its structure or parameter values, accurately predicts Bax oligomer distributions obtained by autoactivation.

3.3.2 Bcl-xL-mediated Bax retrotranslocation is critical for limiting Bax oligomerization

We next integrated Bcl-xL into the model to study the interplay of this classical triad of activator, effector and prosurvival Bcl-2 family members, and to assess the potency of Bcl-xL in preventing Bax pore formation in this signaling context. Bcl-xL mediates its prosurvival function by at least two well-characterized mechanisms, i.e. (i) by binding to aBax and thereby preventing oligomerization and pore formation (Ding et al., 2014; Zhou et al., 2005), as well as (ii) by sequestering BH3-only proteins such as tBid (Lovell et al., 2008; Bleicken et al., 2013b). We thus accounted for heterodimerization of Bcl-xL with tBid and aBax in the extended model (Fig. 3.3A). Recent experimental studies inter-

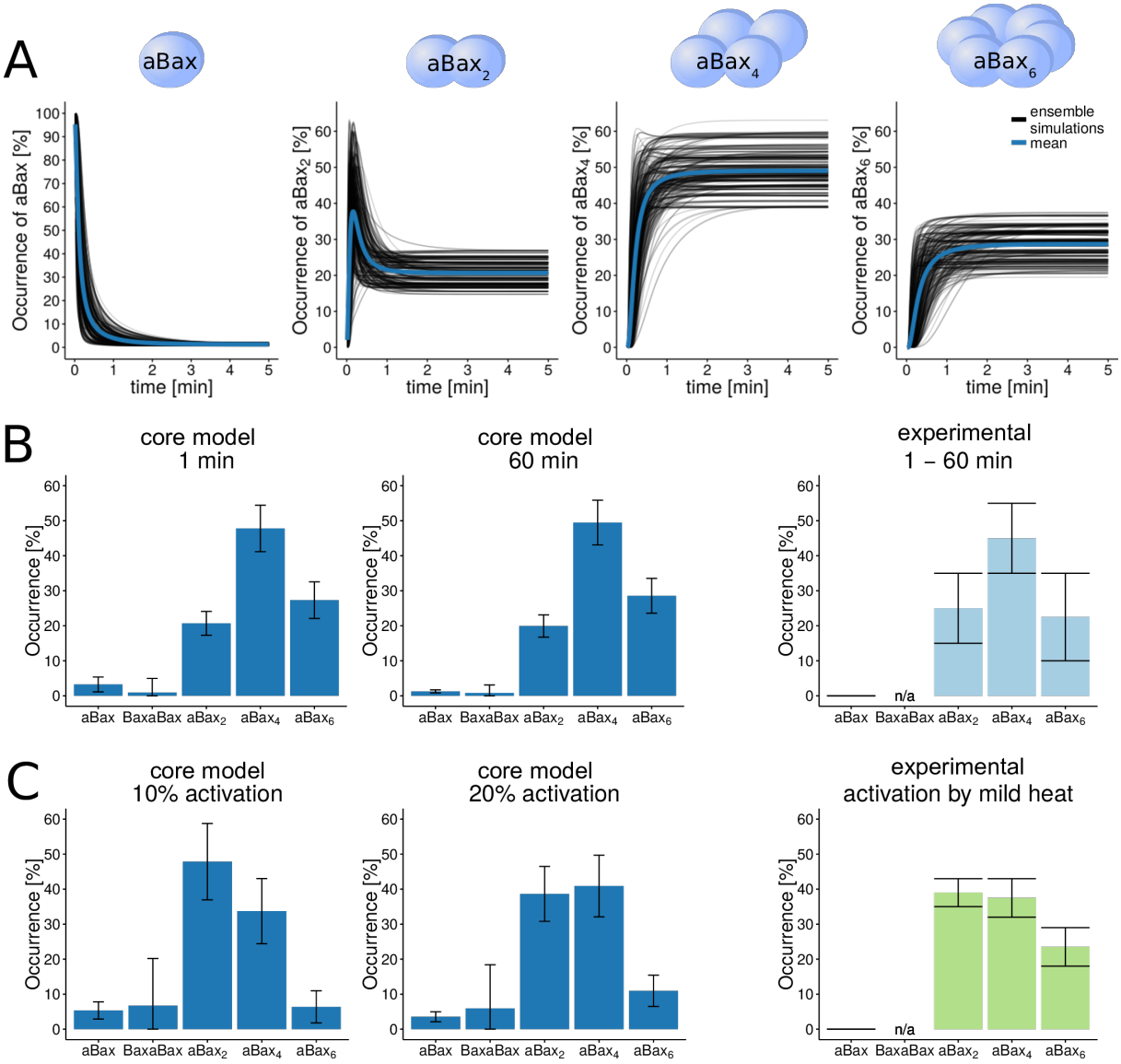

Figure 3.2: **Ensemble simulations accurately reproduce tBid-induced Bax oligomerization kinetics and reliably predict Bax autoactivation A**, Rapid oligomerization of Bax. Oligomerization kinetics are shown for an ensemble of 340 individual simulations. The mean kinetic is shown in blue. Input protein concentrations were 2.5 nM Bax and 5 nM tBid (Subburaj et al., 2015). **B**, Distribution of tBid-induced Bax oligomeric species obtained from the trained model at 1 and 60 min. Data are shown as mean and SD of the ensemble simulations. Quantitative experimental data were estimated from (Subburaj et al., 2015) and are shown for comparison. **C**, Distribution of Bax oligomeric species obtained by autoactivation. Model predictions are shown for inputs of 10% and 20% aBax. Experimental data as estimated from (Subburaj et al., 2015) are shown for comparison and validation of predictions. Experimentally valid observations were assumed to be within the shown errorbars. Data are shown as means and SD.

estingly revealed that Bcl-xL also retrotranslocates aBax from mitochondrial membranes into the cytosol, a process that could add to the antiapoptotic potency of Bcl-xL (Edlich et al., 2011; Todt et al., 2013, 2015). Retrotranslocation was therefore implemented as an optional model extension (Fig. 3.3A, black box). Experimentally, the ability of Bcl-xL to disassemble tBid-induced, pre-formed aBax oligomers can be quantified in lipid

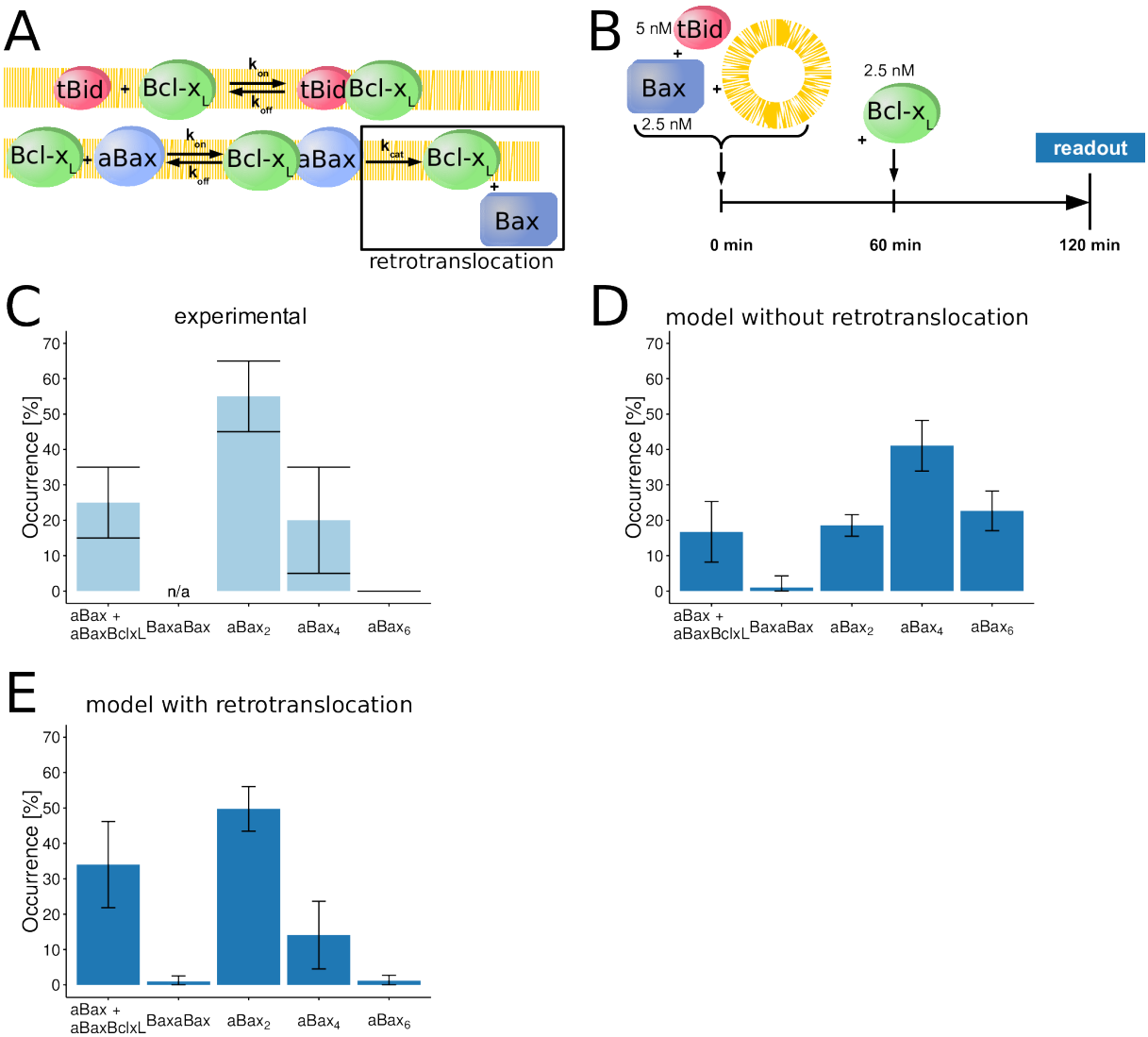

Figure 3.3: **Retrotranslocation of Bax by Bcl-xL is required to significantly impair Bax oligomerization A**, Model extension by Bcl-xL. Bcl-xL exerts its prosurvival function by binding to tBid as well as to active Bax monomers. The extension of the model by Bcl-xL was implemented in two variants, including the retrotranslocation of mitochondrial Bax into the cytosol (black box) or not. **B**, Experimental conditions for studying the influence of Bcl-xL on Bax oligomerization, as described in (Subburaj et al., 2015). This scenario served as the reference for in silico studies. **C**, Experimentally measured Bax oligomer distribution in presence of Bcl-xL, as estimated from (Subburaj et al., 2015). Experimentally valid observations were assumed to be within the shown errorbars. **D**, Bax oligomer distribution obtained from the model without Bcl-xL retrotranslocation activity. Model predictions and additional model fitting approaches failed to replicate experimental data shown in C. Shown are simulation assuming rapid binding of Bcl-xL to aBax and high affinity of the resulting complex (k_{on} 10 $nM^{-1}s^{-1}$, K_D 0.1 nM). **E**, Bax oligomer distribution obtained from the trained model with Bcl-xL retrotranslocation activity. Experimental data shown in C can be reproduced. Data are shown as means and SD of ensemble simulations.

bilayers isolated from large unilamellar vesicles (Subburaj et al., 2015) (Fig. 3.3B). Data on steady state distributions of aBax oligomers and heterodimers with Bcl-xL indicate that aBax hexamers cannot be observed upon addition of Bcl-xL and that the majority of aBax resides within $aBax_2$ and Bcl-xL-aBax species (Fig. 3.3C). Interestingly, simulations

conducted with our core model, extended by the tBid-Bcl-xL and aBax-Bcl-xL interplay, failed to reproduce such data (Fig. 3.3D). Instead, we found that the majority of aBax still formed tetramers and hexamers (Fig. 3.3D). Even when searching a large parameter space, we failed to fit the model to the experimental data shown in Fig. 3.3C. We next tested if the model variant that included the possibility for Bcl-xL to retrotranslocate membrane-bound Bax into the cytosol was better suited to provide outputs that correspond to experimental findings. Indeed, results obtained with this model variant agreed very well with experimentally observed aBax oligomer distributions when assuming retrotranslocation rates of 5 to 10 s^{-1} (Fig. 3.3E).
In summary, these results demonstrate that the interplay of tBid, Bax and Bcl-xL at and within membranes can be quantitatively recapitulated by mathematical modeling, and that the ability of Bcl-xL to retrotranslocate aBax from membranes into the cytosol needs to be taken into account to reproduce experimental data on Bax oligomerization.

3.3.3 Mathematical modeling accurately predicts limited Bax membrane recruitment in presence of Bcl-xL

We next used our model to estimate the overall amount of Bax recruitment to membranes in presence of Bcl-xL. To this end, we studied conditions at which small amounts of tBid (20 nM) activate higher concentrations of Bax (100 nM), in absence or presence of increasing amounts of Bcl-xL. To determine the overall recruitment of Bax, we took into account all Bax containing species at or within membranes (ΣBax_M) (Fig. 3.4A). Without inclusion of Bax retrotranslocation, Bcl-xL was not able to limit Bax membrane recruitment (Fig. 3.4B), even when assuming rapid association of Bcl-xL with tBid and aBax, and high affinity of the resulting complexes (k_{on} 10 $nM^{-1}s^{-1}$, K_D 0.1 nM). In contrast, ensemble simulations that took Bax retrotranslocation into account predicted that Bax membrane recruitment would be antagonized very potently already at concentrations of 20 nM Bcl-xL (Fig. 3.4C). In comparison to previously reported experimental findings (Billen et al., 2008b), these predictions seemed to be highly accurate (Fig. 3.4D). We next eliminated the binding of tBid to Bcl-xL in the model to study the contribution of this interaction to the potency of Bcl-xL in limiting Bax membrane recruitment. For these conditions, higher amounts of Bax were predicted to accumulate at membranes, with high Bcl-xL concentrations nevertheless efficiently limiting overall Bax recruitment to approximately 15% (Fig. 3.4E). Very similar trends were observed experimentally using the tBid variant tBid-mt1 (Billen et al., 2008b), albeit with our predictions slightly overestimating the potency of Bcl-xL at lower concentrations (Fig. 3.4E,F).

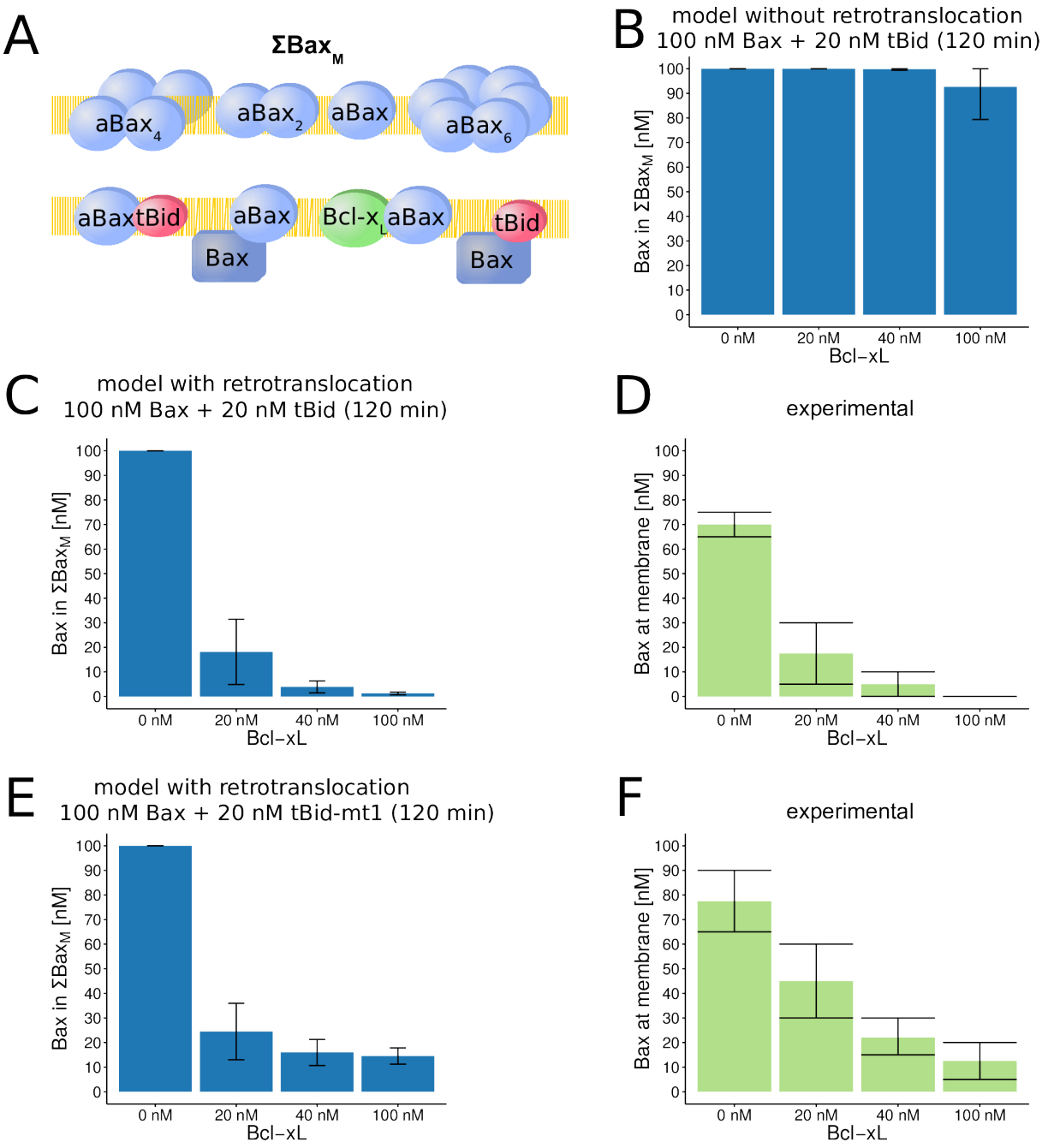

Figure 3.4: **Systems modeling can accurately predict Bax membrane recruitment when taking Bax retrotranslocation activity of Bcl-xL into account A**, Definition of Bax membrane recruitment. As readout for Bax membrane recruitment, all Bax containing species residing at or in the membrane were considered (ΣBax_M). **B**, In the mathematical model lacking retrotranslocation activity, Bax translocation to membranes cannot be prevented. **C**,**D** The mathematical model including retrotranslocation activity of Bcl-xL accurately predicts tBid-induced ΣBax_M at different concentrations of Bcl-xL (C) when compared to the experimental data estimated from (Billen et al., 2008b) (D). **E**,**F** Model predictions for conditions in which a tBid variant was implemented that cannot bind to Bcl-xL. Predictions (E) correspond to trends observed experimentally as estimated from (Billen et al., 2008b) (F). Data are shown as means and SD from ensemble simulations or experimental data estimated from (Billen et al., 2008b), where experimental valid observations were assumed to be within the shown errorbars.

Overall, these findings demonstrate that the capability of Bcl-xL to retrotranslocate Bax from membranes into the cytosol significantly contributes to its antiapoptotic potential and that overall Bax membrane recruitment can be accurately predicted by mathematically modeling the tBid-Bax-Bcl-xL interplay.

3.3.4 Activator/sensitizer BH3-only synergies can be predicted if retrotranslocation activity of Bcl-xL is taken into account

Sensitizer BH3-only proteins play major cell type- and tissue-specific roles in the regulation of apoptosis susceptibility (Happo et al., 2012). We therefore studied how sensitizer BH3 peptides (Das et al., 2017) co-regulate Bax oligomerization together with activator BH3-only protein tBid, and how the retrotranslocation activity of Bcl-xL influences Bax oligomerization in this scenario. For implementation into the mathematical model, we assumed that sensitizers and activators bind to Bcl-xL with identical affinity, but that sensitizers cannot interact with or activate Bax (Fig. 3.5A). We first calculated if a sensitizer alone would be sufficient to trigger efficient Bax oligomerization in presence of Bcl-xL and limited amounts of aBax (10%). At these conditions, even high amounts of sensitizer failed to induce Bax oligomerization (Fig. 3.5B). In contrast, low concentrations of >20 nM tBid were sufficient to oligomerize nearly the entire pool of Bax (approx. 95%) (Fig. 3.5B). We next tested if these predictions could be confirmed experimentally by testing tBid and an Hrk-derived BH3 peptide (Das et al., 2017). Indeed, Bax pores only formed when activator BH3-only protein tBid was added to Bax and Bcl-xL, as evidenced by the release of calcein from large unilamellar vesicles (LUVs) (Fig. 3.5C). Simulations for various combinations of sensitizer and activator concentrations suggested that sensitizers would be expected to potently enhance tBid-induced Bax oligomerization and pore formation, with sensitizer in nM amounts sufficient for significantly decreasing the concentration of tBid required for Bax pore formation (Fig. 3.5D). In comparison to the theoretical additive isobole for half-maximal Bax recruitment into pores (Fig. 3.5D, blue line), the interaction between activator and sensitizer reveals a highly synergistic behavior. Additional simulations predicted that synergies can be expected as long as the retrotranslocation activity of Bcl-xL is taken into account, since otherwise the reaction system was hypersensitive to residual amounts of activator BH3-only proteins (Fig. 3.5E, Fig. 3.8). Subsequent experiments confirmed these predictions, with combinations of suboptimal amounts of tBid and Hrk peptide inducing efficient calcein release from liposomes (Fig. 3.5F). Of note, we utilized the Hrk peptide at micromolar concentrations, as it was shown previously that BH3 peptides are orders of magnitude less potent than

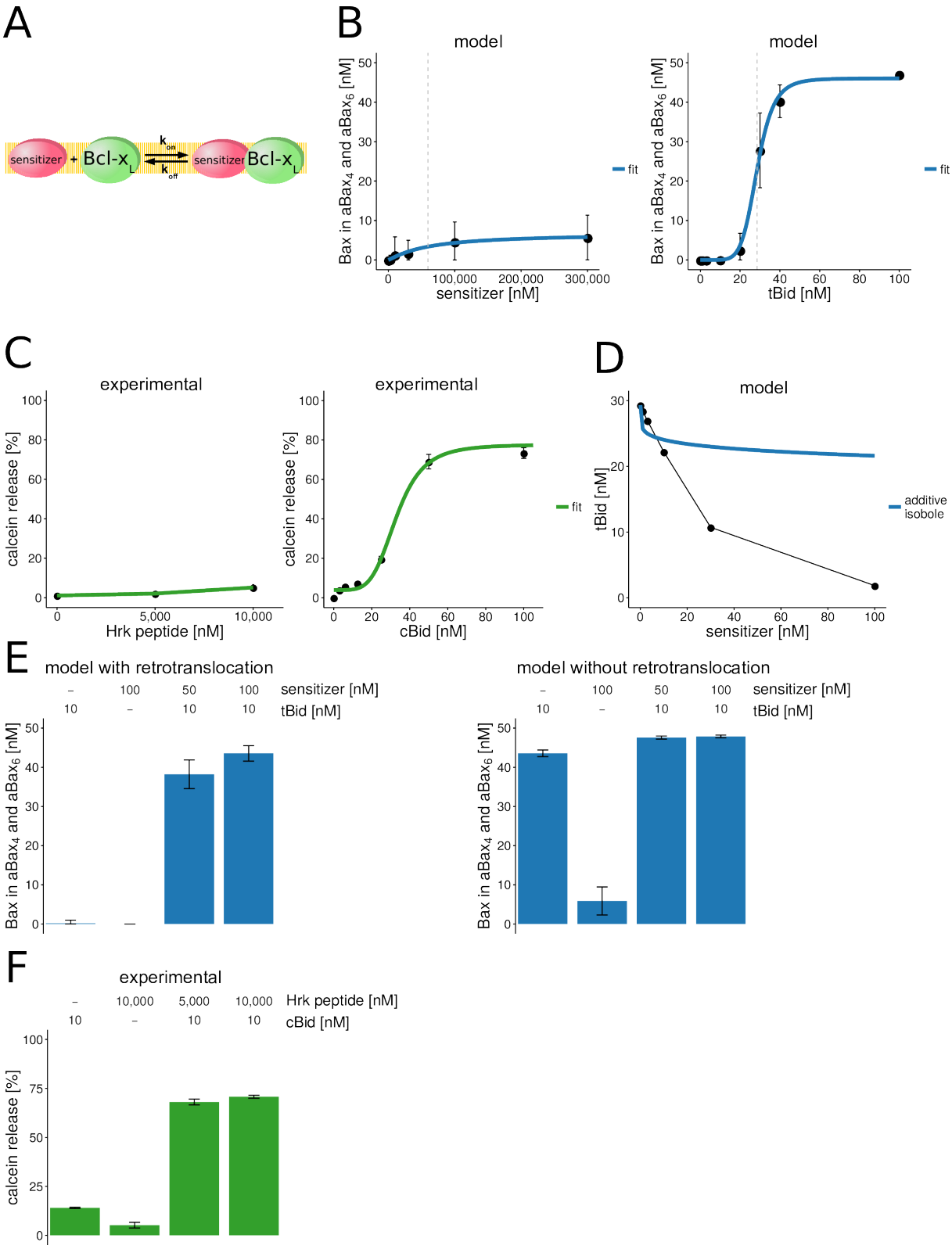

Figure legend on next page

the full length proteins (Kuwana et al., 2005), most likely due to decreased membrane binding affinity of the soluble peptides (Oh et al., 2006). Taken together, these results therefore demonstrate that upon inclusion of retrotranslocation into the model, experi-

Figure 3.5: **Mathematical modeling reliably predicts activator/sensitizer BH3-only synergies** **A**, Model extension for inclusion of BH3-only sensitizer. The sensitizer was implemented to reversibly bind Bcl-xL, with kinetics identical to tBid. **B**, Bax oligomerization predictions in response to sensitizer or tBid. Starting conditions were 45 nM Bax, 5 nM aBax and 20 nM Bcl-xL. Vertical grey dashed lines indicate EC_{50} concentrations. **C**, Experimental validation of model predictions. Dose response curves of calcein release from large unilamellar vesicles after incubation with 50 nM Bax, 20 nM Bcl-xL and varying amounts of Hrk peptide or cBid (cleaved Bid, consisting of tBid and a p7 fragment). **D**, Isobologram of simulations with combined tBid and sensitizer addition. Black dots correspond to EC_{50} Bax oligomerization. The additive isobole (blue) was calculated from data shown in B (see methods for details). **E**, Prediction of Bax oligomerization for single or combined addition of tBid and sensitizer, when added to a system of 20 nM Bcl-xL, 45 nM Bax and 5 nM aBax. **F**, Experimental validation of model predictions. Bax pore formation was experimentally determined by release of calcein from large unilamellar vesicles. LUVs were incubated with 20 nM Bcl-xL, 50 nM Bax, and cBid and/or Hrk peptide as indicated. Data are shown as means and SD of ensemble simulations or experimental data.

mentally observed synergies between activator and sensitizer BH3-only proteins can be predicted.

3.3.5 Bax retrotranslocation is essential to separate conditions of MOMP competency and resistance

As reported previously (Goldstein et al., 2000; Lopez and Tait, 2015), MOMP typically is a rapid, all-or-none cell fate decision to initiate the apoptosis execution phase. The binary nature of death decisions (yes vs. no) implies that conditions of MOMP competency and resistance must be strictly separated to avoid or minimize the chance for an inefficient or submaximal induction of apoptosis execution (Ichim et al., 2015). We therefore studied if the signaling system would be capable of controlling Bax oligomerization and pore formation competency in a switch-like manner, and to which extent this decision switch relies on the capacity of Bcl-xL to retrotranslocate Bax into the cytosol. In these simulations, we steadily upregulated Bcl-xL and calculated whether Bax oligomerization was inhibited. The results from these analyses demonstrate that as long as Bcl-xL is capable of retrotranslocating Bax, conditions of complete Bax oligomerization and absence of Bax oligomerization are separated by a very narrow concentration range of sub-stoichiometric amounts of Bcl-xL (Fig. 3.6A,B). In contrast, loss of retrotranslocation activity resulted in an approximately inversely proportional relationship between the amounts of oligomerized Bax and the amounts of Bcl-xL, with super-stoichiometric amounts of Bcl-xL being required to prevent Bax oligomerization and pore formation (Fig. 3.6A,B). This threshold behavior was observed regardless of whether sensitizer BH3-only contributions were taken into account or not. Based on the conditions studied here, we can estimate that retrotranslocation activity increases the antiapoptotic potency of Bcl-xL at least 10-fold

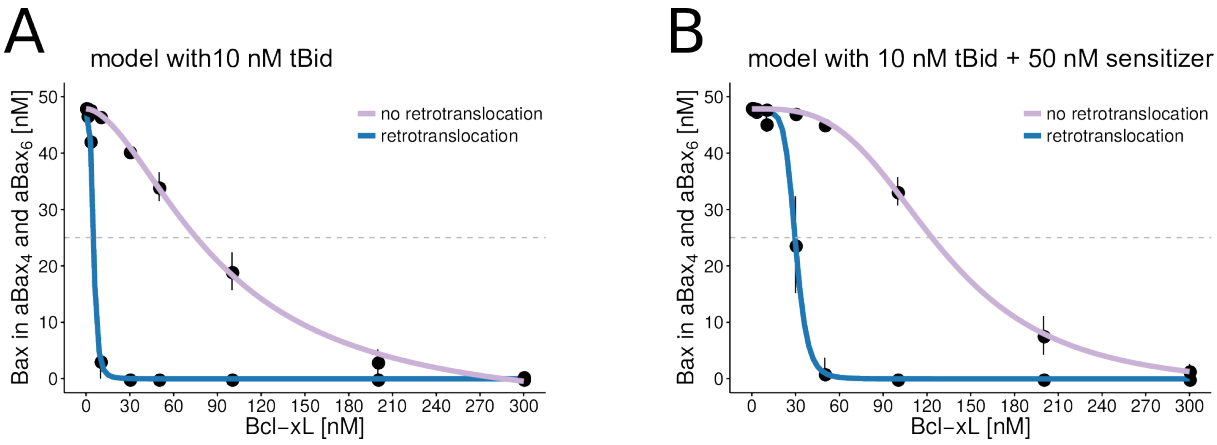

Figure 3.6: **Retrotranslocation activity of Bcl-xL is essential to strictly separate conditions of MOMP competency and resistance** Simulations of Bax oligomerization into pores (MOMP competency) in relation to increasing amounts of Bcl-xL. Simulations are performed for 50 nM Bax and 10 nM tBid (**A**) or 10 nM tBid plus 50 nM sensitizer (**B**). The negative hill curve was fitted to simulated data points to determine IC_{50} values (see methods for details). Blue lines refer to results from the model variant including retrotranslocation activity of Bcl-xL. Data are shown as means and SD of ensemble simulations.

(30 nM vs. 300 nM to prevent Bax oligomerization). These findings therefore demonstrate that Bax retrotranslocation is essential to generate sharp decision thresholds that separate MOMP competency from MOMP resistance, with near-binary characteristics.

3.4 Discussion

Here, we studied the interplay of activator BH3-only protein tBid, multi-domain effector Bax and their antagonist Bcl-xL, using a combined approach of mathematical systems modeling as well as retrospective and prospective experimental validation of model predictions (summarized in Fig. 3.7). The results of our simulations demonstrate that inclusion of Bax retrotranslocation by Bcl-xL is indispensable for reproducing Bax membrane integration and oligomerization quantitatively and kinetically. We furthermore determined that, under the conditions studied here, retrotranslocation enhances the antiapoptotic potential of Bcl-xL approximately 10-fold, indicating a highly significant and currently still underestimated contribution of Bax shuttling towards defining cellular apoptosis resistance. Furthermore, the process of Bax retrotranslocation is essential for the MOMP decision to display near-binary, switch-like characteristics, with the signaling system transitioning from high MOMP competency to complete MOMP resistance across a narrow Bcl-xL concentration range. Even though Bax and Bcl-xL have long been identified as key regulators of MOMP and apoptosis susceptibility (Oltval et al., 1993; Boise et al., 1993), evidence for continuous shuttling of Bax from mitochondrial membranes back into the

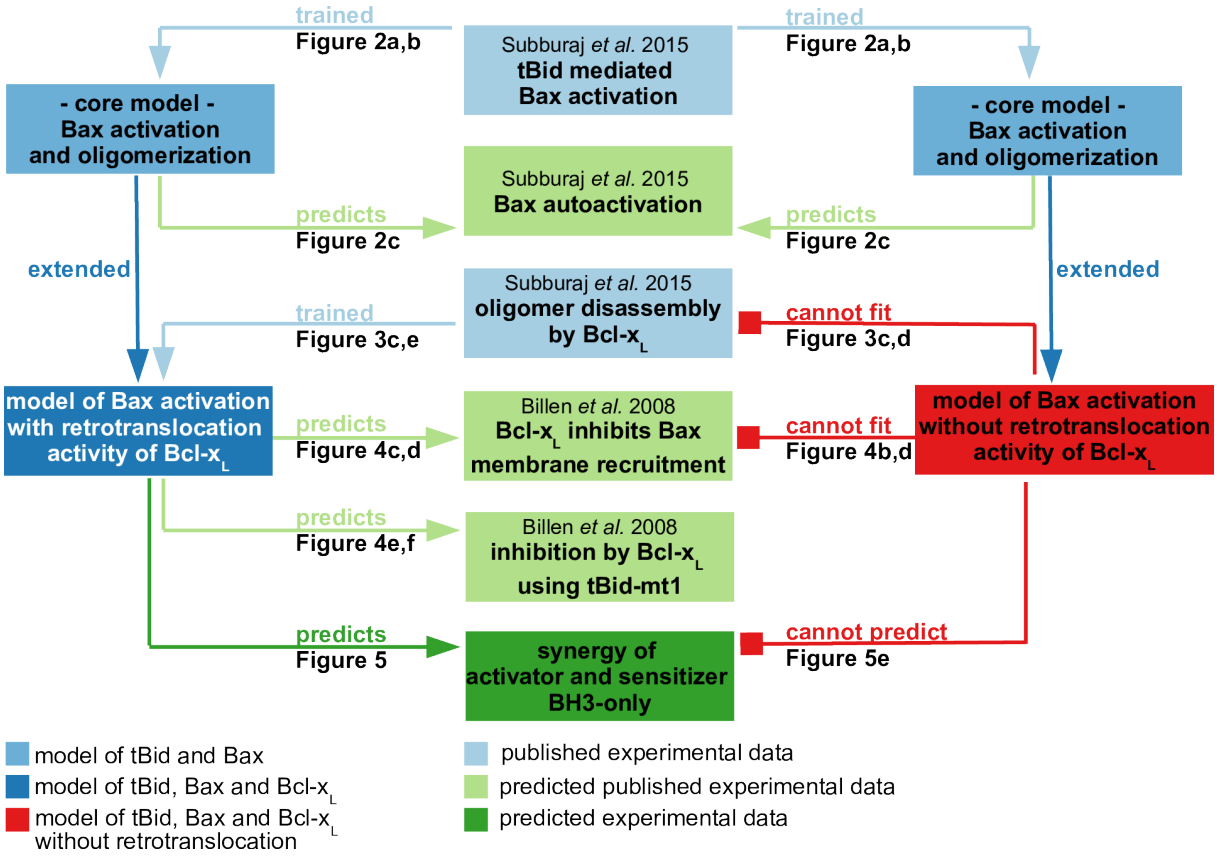

Figure 3.7: **Flow chart providing an overview of model training, successful predictions and experimental validation.**

cytosol emerged only in recent years (Edlich et al., 2011; Schellenberg et al., 2013). While other antiapoptotic Bcl-2 family members might likewise possess retrotranslocation activity, the molecular mechanisms have been studied predominantly for Bcl-xL (Todt et al., 2013; Renault et al., 2015; Todt et al., 2015). For retrotranslocation to occur, Bax must interact with the hydrophobic groove of Bcl-xL via its BH3 domain and additionally with Bcl-xL's COOH-terminal membrane anchor, since preventing any of these interactions results in mitochondrial Bax accumulation (Todt et al., 2013). Retrotranslocation can be observed in minimalistic, but well-controlled *in vitro* experimental settings, as evidenced by a decrease in Bax binding to the membrane in giant unilamellar vesicles upon Bcl-xL membrane insertion (Bleicken et al., 2014). However, within the complexity of living cells additional processes might undoubtedly play coregulatory roles. Indeed, some evidence in this direction has been provided. Mitochondrial specificity and membrane affinity for Bax may rely on additional cofactors such as VDAC2, which recently was reported to also contribute to Bax retrotranslocation (Lauterwasser et al., 2016). Additionally, mitochondria-ER contact sites seem to be preferential binding sites for Bcl-2 family proteins, probably through the local accumulation of Ca2+, which might foster

the formation of membrane microdomains rich in negatively charged cardiolipin (Grijalba et al., 1999; Csordás et al., 2010; Cosentino and García-Sáez, 2014). Cardiolipin indeed promotes tBid recruitment to membranes and efficient Bax activation (Kuwana et al., 2002; Gonzalvez et al., 2005). Furthermore, posttranslational modifications of Bax, such as phosphorylation of S184, were proposed to interfere with its membrane binding and apoptotic activity (Arokium et al., 2007; Wang et al., 2010).

Interestingly, in living cells engineered to be devoid of all known BH3-only activator proteins, antagonizing antiapoptotic family members alone is sufficient to induce Bax translocation and apoptotic cell death (O'Neill et al., 2016). *In vitro*, however, Bax does not spontaneously form pores (Kuwana et al., 2005; Lovell et al., 2008). These results therefore hint at additional processes contributing to Bax activation *in cellulo*, or at environments more prone to induce basal rates of Bax membrane insertion. These observations further support an important role of retrotranslocation activity in preventing apoptosis hypersensitivity and unwanted cell death. Retrotranslocation activity is not restricted to Bcl-xL, since other antiapoptotic family members, such as Bcl-2 and Mcl-1, retrotranslocate Bax at similar rates (Edlich et al., 2011). Effector protein Bak, closely related to Bax, likewise is retrotranslocated from mitochondria into the cytosol, albeit at far lower rates (Todt et al., 2015). Overall, this indicates a continuous shuttling to and from mitochondrial membranes, including all major multi-domain Bcl-2 family members. Based on our results on the relevance of retrotanslocation, it is therefore likely that the continuous interplay of pro- and antiapoptotic fluxes establishes a steady state that prevents MOMP in stress-free scenarios. Indeed, replacing the C-terminal membrane anchor of Bax with that of Bak, not only targets Bax to mitochondria, but also reduces Bax retrotranslocation and is sufficient to trigger spontaneous MOMP and apoptosis execution (Todt et al., 2015).

Another notable finding of our study is that retrotranslocation generates a signaling system in which conditions of MOMP competency and MOMP resistance are separated in a near binary, switch-like manner by small changes in the amounts of Bcl-xL. The binary nature of the MOMP decision is well known from studies on mitochondrial permeabilization during intrinsic and extrinsic apoptosis. Typically, all or no mitochondria in individual cells commit complete MOMP (Goldstein et al., 2000; Rehm et al., 2009). Conditions of submaximal or incomplete MOMP instead appear to be exceptions (Ichim et al., 2015). We furthermore show that sensitizer and activator BH3-only proteins can act synergistically in overcoming the threshold for effective MOMP execution. By sequestering Bcl-xL and thereby blocking its prosurvival functions, sensitizers efficiently lower the amount of tBid necessary for MOMP competence. This may explain the effectiveness of sensitizer

BH3-mimetics in promoting apoptosis induction in cells that are addicted to prosurvival Bcl-2 family proteins, where the latter hold in check subthreshold amounts of activator BH3-only proteins (Sarosiek and Letai, 2016). Synergies between sensitizer and activator BH3-only proteins were also described for various combination treatments for which signal transduction pathways culminate at the level of Bcl-2 family members, resulting in improved apoptosis responses of otherwise resistant tumors (Schneider-Jakob et al., 2010; Inoue-Yamauchi et al., 2017).

The Bcl-2 family interplay and the control of the MOMP decision have been the subject of previous systems biological studies (Würstle et al., 2014; Huber et al., 2011). However, the detail at which the interactions were modeled varied greatly, and model development served different purposes. Additionally, quantitative and time-resolved data, especially for the oligomerization processes of full-length proteins in membrane environments, only recently became available by the use of biophysical methods in *in vitro* systems (Subburaj et al., 2015).

In an early theoretical study, a cellular automaton as well as an ODE-based modeling approach were employed to study robustness properties of Bax-induced MOMP. The positive feedback of activator BH3-only proteins that are freed by binding of aBax to Bcl-2 was identified to contribute substantially to a swift accumulation of active Bax molecules (Chen et al., 2007a). At the time of the study, experimental information on membrane recruitment, insertion and kinetics of oligomerization of active Bax molecules were not available, but the simulations nevertheless emphasized that non-linear causation is very likely an important driver of Bax pore formation. An expansion of this modeling strategy, using a combined experimental and mathematical approach, demonstrated that the amounts of mitochondrial Bax measured at the time of MOMP would indeed be sufficient to allow higher order oligomers to form by lateral aBax diffusion and aggregation, linking for the first time mitochondrial Bax amouts to pore formation propensity and MOMP competence (Düssmann et al., 2010). However, whether switching between full MOMP competency and resistance can be achieved by small changes in antiapoptotic family members was outside of the scope of the study. The so far most sophisticated and detailed model of the Bcl-2 family interplay successfully linked chemotherapy responsiveness to calculated resistances to BH3-only stress doses in colorectal cancer (Lindner et al., 2013a). These resistances were determined from the antiapoptotic thresholds that emerge from the interplay of prosurvival and effector Bcl-2 family protein concentrations. Interestingly, a calculated resistance to high stress doses correlated with a higher risk for disease recurrence in stage III colorectal cancer patients that received adjuvant chemotherapy, indicating the potential of mathematical models of protein interaction networks as inno-

vative systems-based biomarkers (Lindner et al., 2013a, 2016). Since we demonstrated that retrotranslocation of Bax and, by extension, possibly Bak is crucial to strictly separate conditions of MOMP competency and resistance, it is tempting to speculate that including information on steady-state dynamics and shuttling rates of Bcl-2 family members might improve the prognostic power of translationally relevant systems models.

3.5 Methods

3.5.1 Model Implementation

The model was implemented as an ordinary differential equations (ODE)-based model in R (version 3.3.2). Supplementary Material (Fig. 3.9 and Tables 3.1-3.3) provides detailed information on all species, interactions and rate constants. ODEs were integrated numerically using R's routine lsoda (package deSolve, version 1.13), which provides an interface to the lsoda FORTRAN ODE solver, which switches automatically between stiff and nonstiff methods.

3.5.2 Parameter estimates, sampling procedure and model training

Biologically plausible parameter ranges were chosen as described in Supplementary Material. Ensemble simulations were performed as part of model training, using the following procedure. Biologically plausible parameter ranges were transformed to be $\log_{10}$ uniformly distributed in [0,1] and parameters were sampled from these distributions. We discretized the parameter space into a 20-level grid. Two hundred trajectories were sampled in parameter space following a previously described procedure (Saltelli, 2008): In brief, for each trajectory a random grid point was selected. From this point one parameter was changed (in- or decreased) at a time by a value of d=20/[2*(20-1)] until each parameter was changed exactly once. This provides a trajectory through parameter space with (n+1) sampling points, were n is the number of parameters in the respective model used for the simulation. The choice of d as 20/[2*(20-1)] (for a 20-level grid) ensured that all levels have equal probability of being selected in the sampling strategy (Saltelli, 2008). This resulted in an ensemble size of 200*(n+1) model parameterizations. A function written in R generating trajectories in parameter space is provided as Supplementary Material.
For each output of interest (e.g. aBax [%]), dot plots of ensemble simulations were generated, where each dot corresponds to one simulation. This allowed us to assess the influence of each parameter on model outputs. Regions of the parameter space not pro-

viding outputs in agreement with experimental training data were excluded. Restriction of parameter ranges, simulation and analysis of dot plots in an iterative procedure lead to the parameter ranges of the trained model (see also section on parameter ranges of the trained core and complete model in Supplementary Material, Fig. 3.10-3.32).

3.5.3 Simulations and Model Predictions

Ensemble predictions were generated by sampling from parameter ranges of the trained models as defined in Table 3.1 (Supplementary Material). 20 trajectories in parameter space were generated for simulations shown in Fig. 3.2A, 3.5 and 3.6; 200 trajectories were generated for all other simulations. Associated protein amounts used as model inputs are listed in Table 3.2 (Supplementary Material). All results were reproducible by independent resampling in parameter space.

3.5.4 Testing for Synergy

Dose response curves for tBid and sensitizer addition alone or in combination were generated by evaluating the amounts of $aBax_4$ and $aBax_6$ at 2 h of modeled reaction time. A hill curve was fitted to these data using R's built-in function nls (package stats, version 3.3.2, algorithm 'port'):

$$E = \frac{E_{max} \cdot A^h}{A^h + EC_{50}^h}$$

With E = effect (Bax recruitment into tetrameric and hexameric pores), h = hill coefficient, E_{max} = maximal effect, E_{50}= halfmaximal effect, A = BH3-only concentration, l = baseline effect.

As described previously (Grabovsky and Tallarida, 2004), the theoretical additive isobole was calculated from the hill curves for tBid and sensitizer inputs:

$$b = EC_{50,tBid} - \frac{EC_{50,tBid}}{\left[\frac{E_{max,tBid}}{E_{max,sensitizer}}\left(1 + \frac{A_c^{h_{sensitizer}}}{a^{h_{sensitizer}}}\right) - 1\right]^{\frac{1}{h_{tBid}}}}$$

With b = sensitizer [nM], a = tBid [nM], $E_{max,tBid}$ and $E_{max,sensitizer}$ = maximal effects achieved with tBid alone or sensitizer alone (including baseline effect), $EC_{50,tBid}$ = concentration of tBid alone that induced half of $E_{max,tBid}$, A_C = concentration of sensitizer that induced half of $E_{max,sensitizer}$, h_{tBid} and $h_{sensitizer}$ = hill coefficient of single treatments.

3.5.5 Peptides and Proteins

Hrk peptide H-LRSSAAQLTAARLKALGDELH-OH was ordered with > 95% purity from AnaSpec Inc (Fremont, CA).
Purification of cleaved Bid, Bax and Bcl-xL was described by us previously (Bleicken et al., 2017).

3.5.6 LUV permeabilization assay / Calcein release assay

LUVs of a size of approximately 100 nm were prepared, composed of 80% phosphatidyl choline and 20% cardiolipin. The dried lipid mixture was dissolved in buffer (20 nM HEPES, pH7.4) and 80 mM calcein (fluorescein-bis-methyl-iminodiaceticacid at pH7.5) was entrapped in lipid vesicles at a self-quenching concentration, so that its release into the external medium is accompanied by an increase in fluorescence intensity. To form the vesicles, the solution with lipids at a final concentration of 4 mg ml^{-1} was vortexed and passed through 5 cycles of freezing and thawing. The generated multilamellar vesicles were extruded >30 times with a 100 nm membrane filter (Avestin). LUVs were incubated with Bid, Bax, Bcl-xL and Hrk peptide at room temperature. The kinetics of calcein release were studied using a Tecan Infinite M200 microplate reader (Tecan, Switzerland). The percentage of release R was calculated from:

$$R = (FS - F0) \div (Fmax - F0) \times 100$$

Where F0 is the initial fluorescence of LUVs; Fmax is the maximum fluorescence after final addition of 5% TritionX-100; FS is the equilibrium fluorescence following addition of Bcl-2 family proteins.

3.6 Supplementary Information

3.6.1 Information on prior estimates of parameter values

Biologically plausible parameter ranges were chosen within which subsequent model training was performed. K_D values were assumed to lie within 0.1 - 1000 nM, as affinity constants for interactions within the Bcl-2 family were reported in the low to high nM range (Hantusch et al., 2017). For k_{on} rate constants, values between $1e^{-6}$ - 1 $nM^{-1}s^{-1}$ were assumed to be reasonable ranges for protein-protein associations (Schreiber et al., 2009). The in-membrane association of Bcl-xL with aBax was allowed to reach a rate constant of up to 10 $nM^{-1}s^{-1}$, taking into account that these proteins are pre-oriented within two-

dimensional membrane planes, contributing to faster association kinetics (Schreiber et al., 2009). k_{off} values were calculated from $k_{off} = k_{on} * K_D$.

Insertion of Bax into the membrane or release back into the cytosol was assumed with rates of $1e^{-5}$ - $1e^{-1}s^{-1}$, with exception of translocation of the tBidBax complex into the fully membrane inserted tBidaBax ($1e^{-5}$ - 1 s^{-1}). Retrotranslocation of Bax by Bcl-xL was assumed to be within $1e^{-5}$ - 10 s^{-1}. For all of these processes, rate constants of the isolated reactions are unavailable and due to sparse information about the velocity of such processes, parameters spanning several orders of magnitude and approximately in the same range as k_{off} constants and the effective rate constant of Bax retrotranslocation in living cells (Edlich et al., 2011) were assumed.

3.6.2 Supplementary Tables

Table 3.1: **Parameter ranges after model training** Parameter ranges after model training used for simulations in the respective Figures. k_{off} values were calculated from K_D and k_{on}. K_D values are given in nM, k_{on} in $nM^{-1}s^{-1}$

	Fig. 3.2	Fig. 3.3E,3.4C,3.5,3.6	Fig. 3.3D	Fig. 3.4B	Fig. 3.4E	Fig. 3.5*,3.6* *without retrotranslocation
$K_{D,1}$	0.1 - 1000	10 – 1,000	0.1 - 1000	0.1 - 1000	10 – 1,000	10 – 1,000
$K_{D,2}$	0.001 – 0.01	0.006 – 0.01	0.001 – 0.01	0.001 – 0.01	0.006 – 0.01	0.006 – 0.01
$K_{D,3}$	0.1 – 0.4	0.1 – 0.4	0.1 – 0.4	0.1 – 0.4	0.1 – 0.4	0.1 – 0.4
$K_{D,4}$	0.4 - 1	0.4 - 1	0.4 - 1	0.4 - 1	0.4 - 1	0.4 - 1
$K_{D,5}$	0.1 - 50	0.1 - 50	0.1 - 50	0.1 - 50	0.1 - 50	0.1 - 50
$K_{D,6}$	30 – 1,000	30 – 1,000	30 – 1,000	30 – 1,000	30 – 1,000	30 – 1,000
$K_{D,7}$	-	1.58 - 3	0.1 - 1,000	0.1	-	1.58 - 3
$K_{D,8}$	-	0.1 – 0.2	0.1	0.1	0.1 – 0.2	0.1 – 0.2
$k_{on,1}$	$1e^{-6}$ - 1	$1e^{-6}$ - 1	$1e^{-6}$ - 1	$1e^{-6}$ - 1	$1e^{-6}$ - 1	$1e^{-6}$ - 1
$k_{on,2}$	0.16 - 1	0.4 - 1	0.16 - 1	0.16 - 1	0.4 - 1	0.4 - 1
$k_{on,3}$	0.1 - 1	0.1 - 1	0.1 - 1	0.1 - 1	0.1 - 1	0.1 - 1
$k_{on,4}$	$6e^{-2}$ - 1	$6e^{-2}$ - 1	$6e^{-2}$ - 1	$6e^{-2}$ - 1	$6e^{-2}$ - 1	$6e^{-2}$ - 1
$k_{on,5}$	$1e^{-2}$ - 1	$1e^{-2}$ - 0.02	$1e^{-2}$ - 1	$1e^{-2}$ - 1	$1e^{-2}$ - 0.02	$1e^{-2}$ - 0.02
$k_{on,6}$	$3e^{-3}$ - 1	0.1 - 1	$3e^{-3}$ - 1	$3e^{-3}$ - 1	0.1 - 1	0.1 - 1
$k_{on,7}$	-	$1e^{-4}$ - 1	$1e^{-6}$ - 1	10	-	$1e^{-4}$ - 1
$k_{on,8}$	-	7.08 - 10	10	10	7.08 - 10	7.08 - 10
$k_{tron,1}$	$1e^{-5}$ - $1e^{-1}$	$1e^{-3}$ - $1e^{-1}$	$1e^{-5}$ - $1e^{-1}$	$1e^{-5}$ - $1e^{-1}$	$1e^{-3}$ - $1e^{-1}$	$1e^{-3}$ - $1e^{-1}$
$k_{troff,1}$	$1e^{-5}$ - $3e^{-4}$	$1e^{-5}$ - $3e^{-4}$	$1e^{-5}$ - $3e^{-4}$	$1e^{-5}$ - $3e^{-4}$	$1e^{-5}$ - $3e^{-4}$	$1e^{-5}$ - $3e^{-4}$
$k_{tron,2}$	0.3 - 1	0.3 - 1	0.3 - 1	0.3 - 1	0.3 - 1	0.3 - 1
$k_{troff,2}$	$1e^{-5}$ - $1e^{-1}$	$1e^{-5}$ - $1e^{-1}$	$1e^{-5}$ - $1e^{-1}$	$1e^{-5}$ - $1e^{-1}$	$1e^{-5}$ - $1e^{-1}$	$1e^{-5}$ - $1e^{-1}$
$k_{cat,1}$	-	43013	-	-	43013	-

Table 3.2: **Modeled protein concentrations at t_0** Protein concentrations at t = 0 min (t_0) used for simulations in the respective Figures. All (hetero- and homo-) dimers, tetramers, hexamers were considered to be absent at time t_0 (0 nM).

	Fig. 3.2A,B	Fig. 3.2C	Fig. 3.3	Fig. 3.4	Fig. 3.5	Fig. 3.6
Bax [nM]	2.5	2.5 - aBax	2.5	100	45	50
aBax [nM]	0	varying % of Bax	0	0	5	0
tBid [nM]	5	0	5	20	varying	10
Bcl-x_L [nM]	-	-	2.5 (at t_{60})	0/20/40/100	20	varying
sensitizer [nM]	-	-	-	-	varying	0/50
simulation [min]	1/5/10/60	60	120	120	120	120

Table 3.3: **Definition of outputs of simulations presented in the respective Figures**

Fig.	Output	Unit	Formula	If applicable: as % of
3.2	aBax	%	aBax + aBaxtBid	aBax + aBaxtBid + 2 BaxaBax + 2 $aBax_2$ + 4 aBax4 + 6 $aBax_6$
3.2	BaxaBax	%	2 BaxaBax	aBax + aBaxtBid + 2 BaxaBax + 2 $aBax_2$ + 4 aBax4 + 6 $aBax_6$
3.2	$aBax_2$	%	2 $aBax_2$	aBax + aBaxtBid + 2 BaxaBax + 2 $aBax_2$ + 4 aBax4 + 6 $aBax_6$
3.2	$aBax_4$	%	4 $aBax_4$	aBax + aBaxtBid + 2 BaxaBax + 2 $aBax_2$ + 4 aBax4 + 6 $aBax_6$
3.2	$aBax_6$	%	6 $aBax_6$	aBax + aBaxtBid + 2 BaxaBax + 2 $aBax_2$ + 4 aBax4 + 6 $aBax_6$
3.3	aBax + aBaxBclxL	%	aBax + aBaxtBid + aBaxBclxL	aBax + aBaxtBid + 2 BaxaBax + 2 $aBax_2$ + 4 aBax4 + 6 $aBax_6$ + aBaxBclxL
3.3	BaxaBax	%	2 BaxaBax	aBax + aBaxtBid + 2 BaxaBax + 2 $aBax_2$ + 4 aBax4 + 6 $aBax_6$ + aBaxBclxL
3.3	$aBax_2$	%	2 $aBax_2$	aBax + aBaxtBid + 2 BaxaBax + 2 $aBax_2$ + 4 aBax4 + 6 $aBax_6$ + aBaxBclxL
3.3	$aBax_4$	%	4 $aBax_4$	aBax + aBaxtBid + 2 BaxaBax + 2 $aBax_2$ + 4 aBax4 + 6 $aBax_6$ + aBaxBclxL
3.3	$aBax_6$	%	6 $aBax_6$	aBax + aBaxtBid + 2 BaxaBax + 2 $aBax_2$ + 4 aBax4 + 6 $aBax_6$ + aBaxBclxL
3.4	ΣBax_M	nM	aBax + aBaxtBid + 2 BaxaBax + 2 $aBax_2$ + 4 aBax4 + 6 $aBax_6$ + aBaxBclxL + BaxtBid	-
3.5,3.6	Bax in $aBax_4$ and$aBax_6$	nM	4 aBax4 + 6 $aBax_6$	-

3.6.3 Supplementary Figures

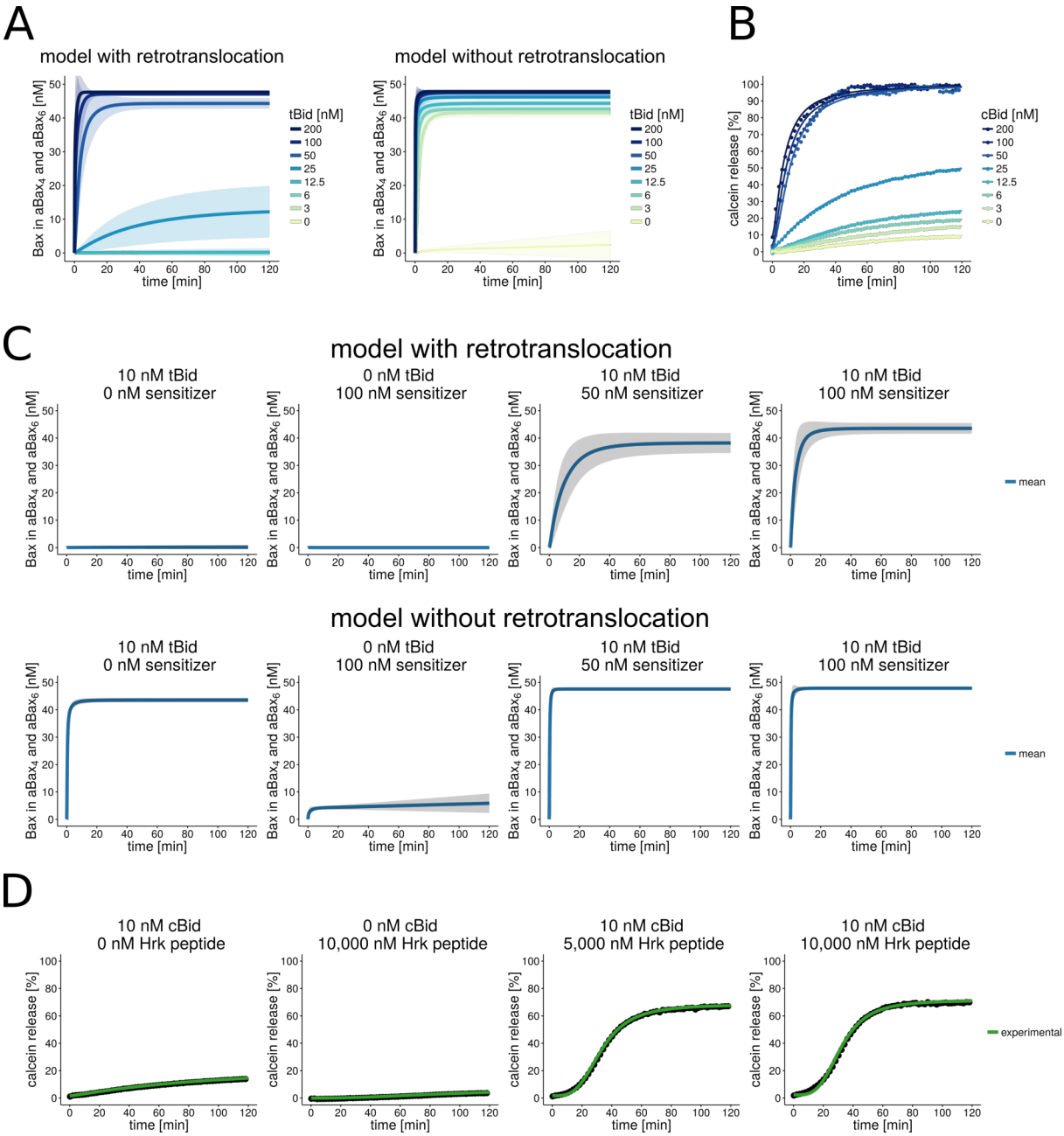

Figure 3.8: **Time courses of modeled Bax recruitment into pores and experimentally measured calcein release** Time courses of modeled Bax recruitment into pores (A,C) and experimentally measured calcein release from large unilamellar vesicles (B,D). **A**, Simulations for 45 nM Bax and 5 nM aBax with 20 nM Bcl-xL and varying amounts of tBid, with and without accounting for retrotranslocation in the model. **B**, Calcein release as measured for 50 nM Bax, 20 nM Bcl-xL and varying amounts of cBid. **C**,**D** Time courses of simulation and experimental measurements corresponding to simulations shown in Fig. 3.5E,F. Shaded areas in simulation plots correspond to SD of ensemble predictions, lines correspond to the means.

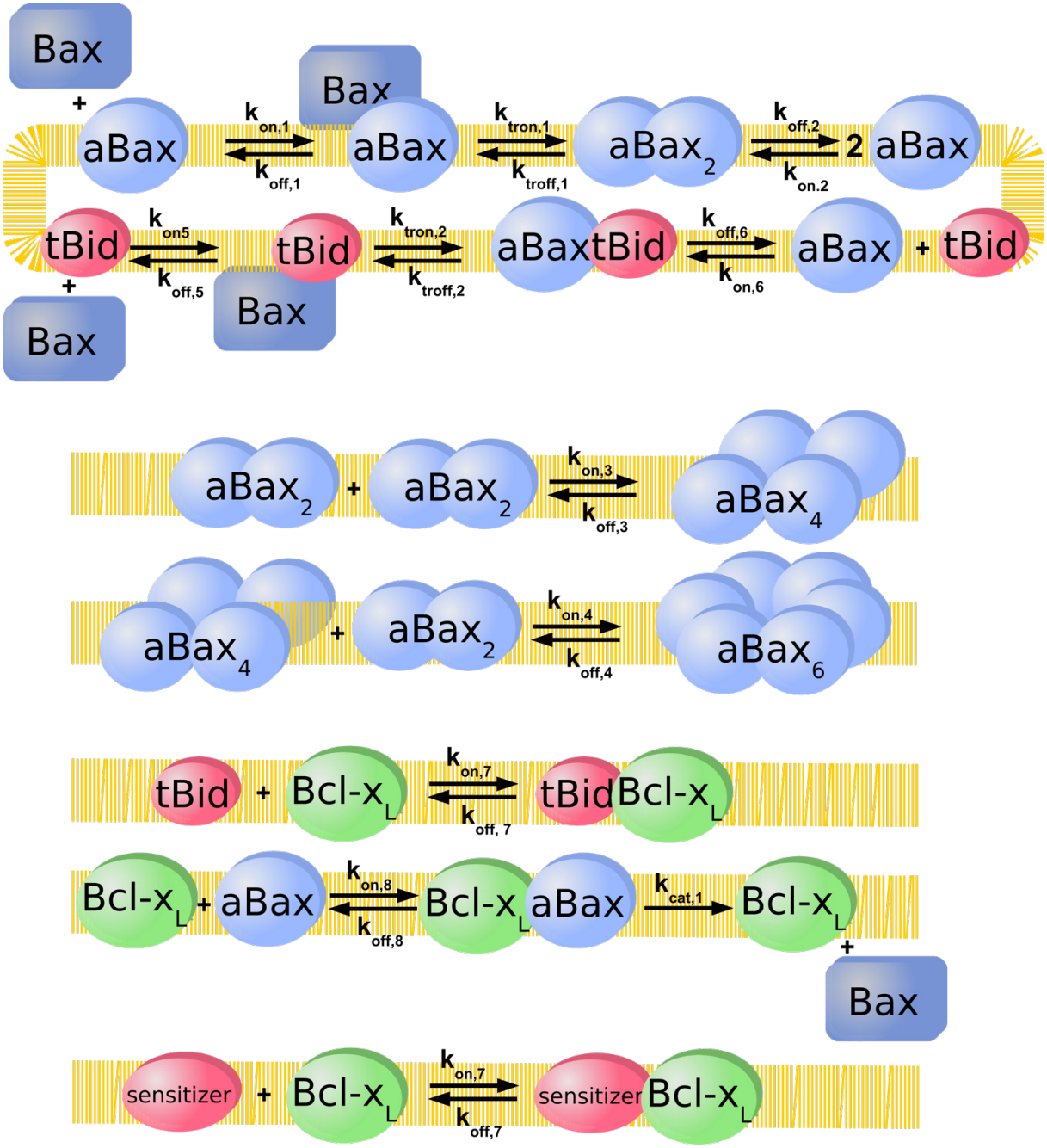

Figure 3.9: **Overview of model parameters** Overview of all interactions, translocations into and from the membrane to the aqueous phase, as well as retrotranslocation process that were integrated in the model. Numbers of rate constants serve as identifiers for the supplementary tables.

Analysis of parameter ranges of trained core model and model with Bcl-xL retrotranslocation activity

Shown are simulation results for all parameters whose values were restricted in the model training procedure. Each dot in the following dot plots corresponds to one model simulation. Black vertical lines correspond to boundaries of the parameter range after model training. Shown are the simulation results of outputs for which experimental data were

available (such as the occurrence $aBax_2$ in %) and which implicated a restriction of the respective parameter to train the model.

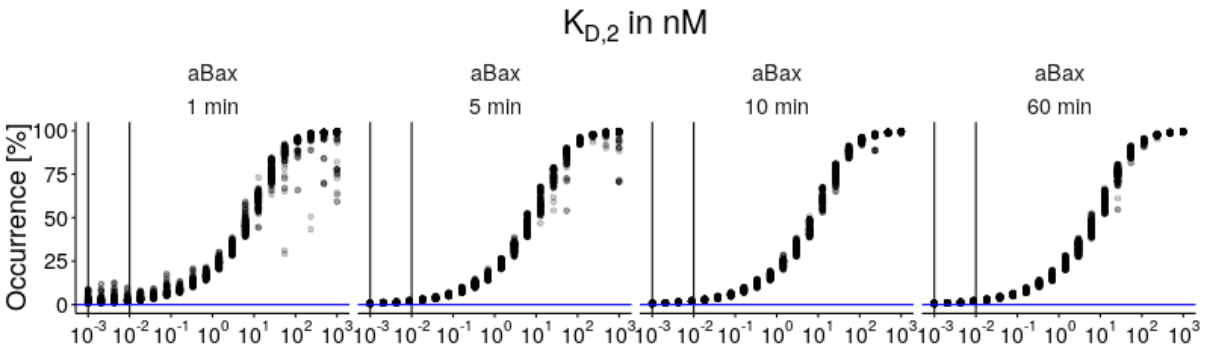

Figure 3.10: **Analysis of $K_{D,2}$ parameter range of trained core model** Simulation results using the starting conditions as in Fig. 3.2A,B and readout at the indicated time points. Shown are sampled parameterizations across the original assumed plausible range of parameter $K_{D,2}$ of the core model (before model training). Blue horizontal lines indicate experimentally valid range for the respective model outputs as estimated from original publication (Subburaj et al., 2015).

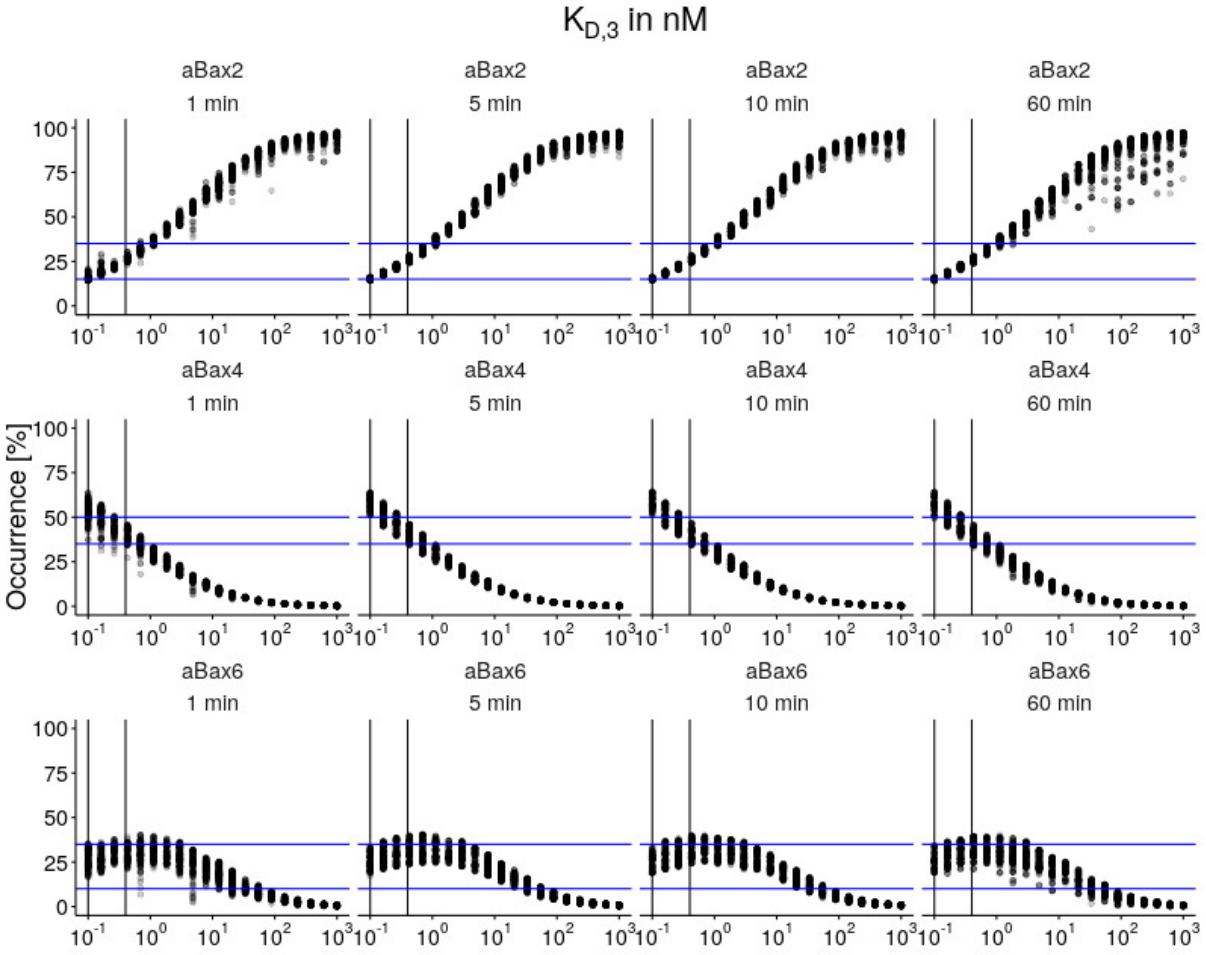

Figure 3.11: **Analysis of $K_{D,3}$ parameter range of trained core model** Simulation results using the starting conditions as in Fig. 3.2A,B and readout at the indicated time points. Shown are sampled parameterizations across the original assumed plausible range of parameter $K_{D,3}$ of the core model (before model training). Blue horizontal lines indicate experimentally valid range for the respective model outputs as estimated from original publication (Subburaj et al., 2015).

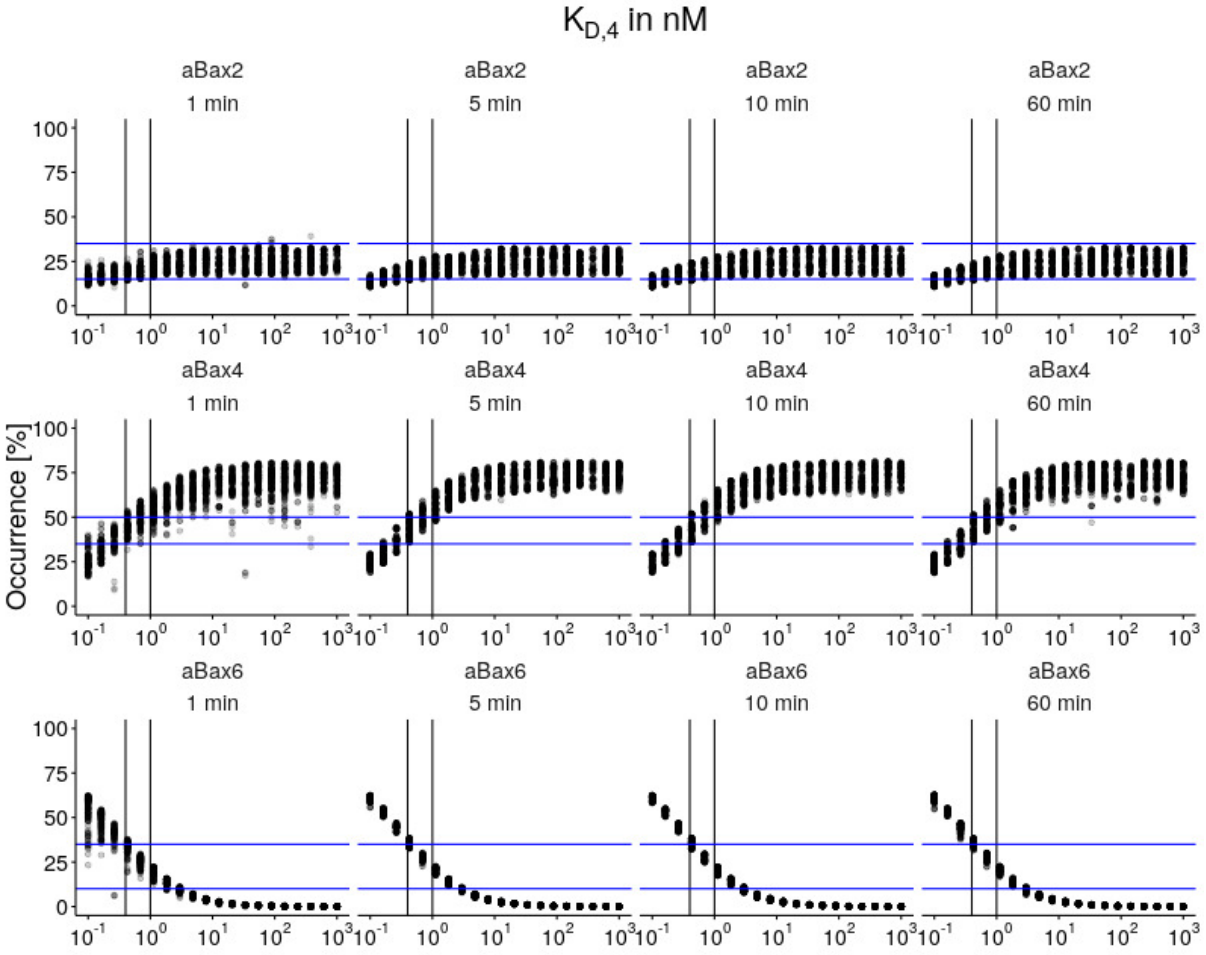

Figure 3.12: **Analysis of $K_{D,4}$ parameter range of trained core model** Simulation results using the starting conditions as in Fig. 3.2A,B and readout at the indicated time points. Shown are sampled parameterizations across the original assumed plausible range of parameter $K_{D,4}$ of the core model (before model training). Blue horizontal lines indicate experimentally valid range for the respective model outputs as estimated from original publication (Subburaj et al., 2015).

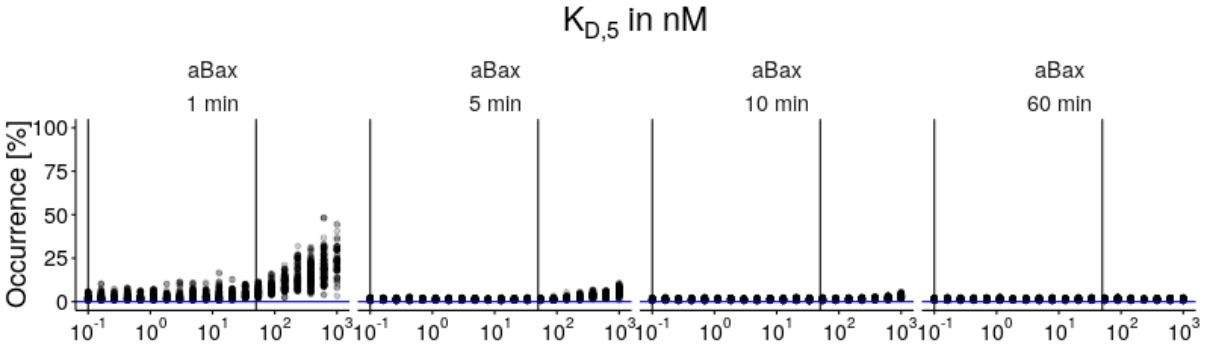

Figure 3.13: **Analysis of $K_{D,5}$ parameter range of trained core model** Simulation results using the starting conditions as in Fig. 3.2A,B and readout at the indicated time points. Shown are sampled parameterizations across the original assumed plausible range of parameter $K_{D,5}$ of the core model (before model training). Blue horizontal lines indicate experimentally valid range for the respective model outputs as estimated from original publication (Subburaj et al., 2015).

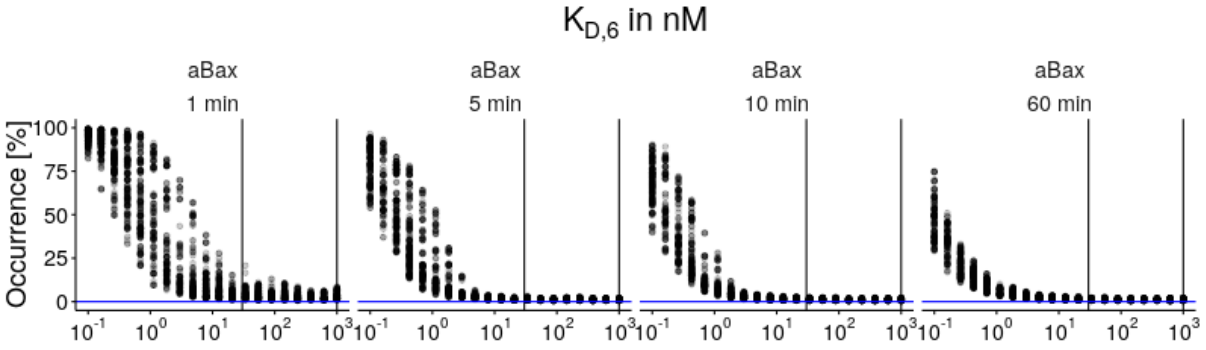

Figure 3.14: **Analysis of $K_{D,6}$ parameter range of trained core model** Simulation results using the starting conditions as in Fig. 3.2A,B and readout at the indicated time points. Shown are sampled parameterizations across the original assumed plausible range of parameter $K_{D,6}$ of the core model (before model training). Blue horizontal lines indicate experimentally valid range for the respective model outputs as estimated from original publication (Subburaj et al., 2015).

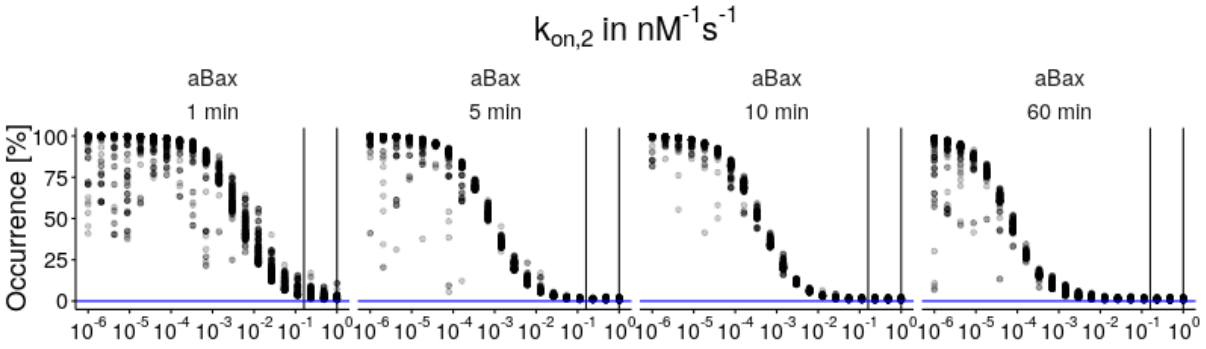

Figure 3.15: **Analysis of $k_{on,2}$ parameter range of trained core model** Simulation results using the starting conditions as in Fig. 3.2A,B and readout at the indicated time points. Shown are sampled parameterizations across the original assumed plausible range of parameter $k_{on,2}$ of the core model (before model training). Blue horizontal lines indicate experimentally valid range for the respective model outputs as estimated from original publication (Subburaj et al., 2015).

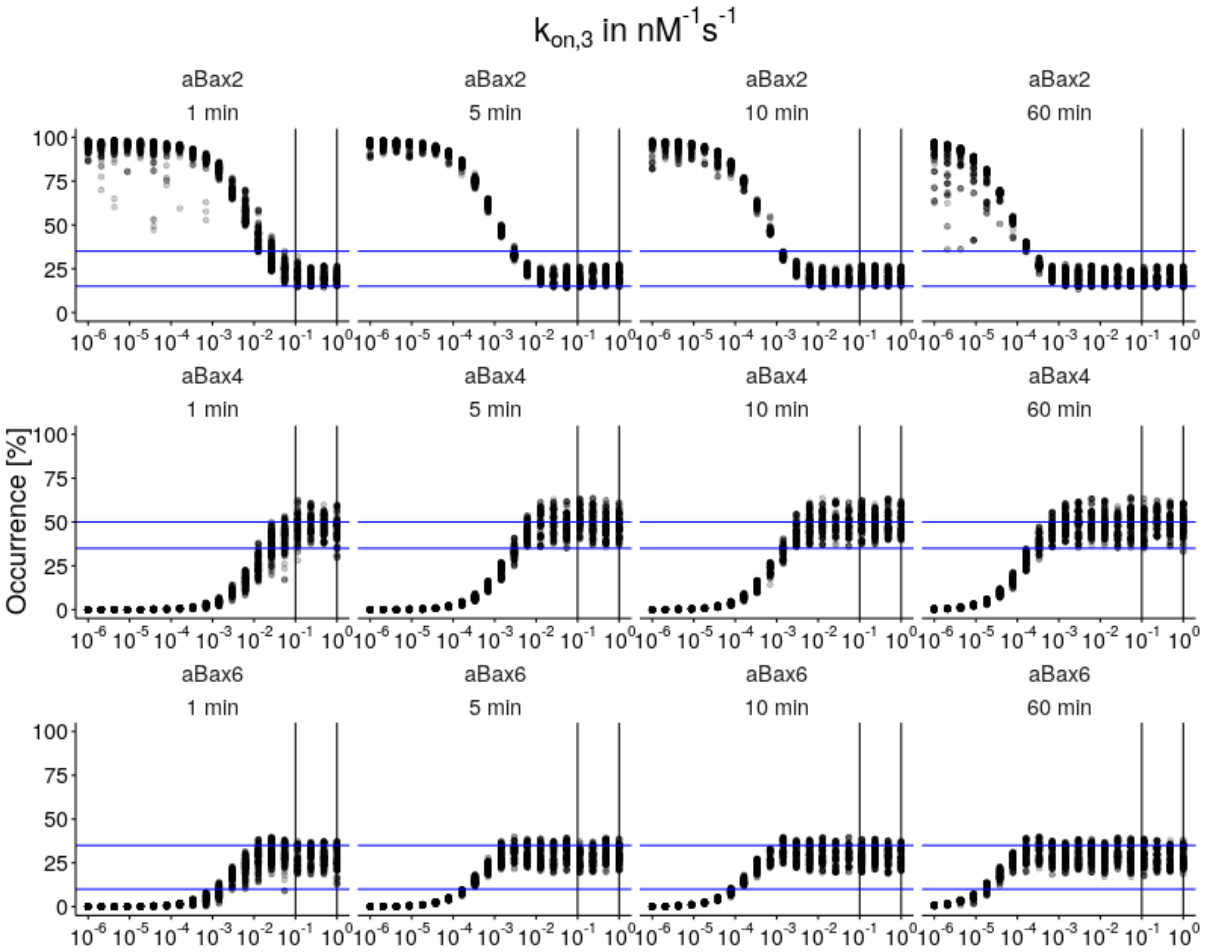

Figure 3.16: **Analysis of $k_{on,3}$ parameter range of trained core model** Simulation results using the starting conditions as in Fig. 3.2A,B and readout at the indicated time points. Shown are sampled parameterizations across the original assumed plausible range of parameter $k_{on,3}$ of the core model (before model training). Blue horizontal lines indicate experimentally valid range for the respective model outputs as estimated from original publication (Subburaj et al., 2015).

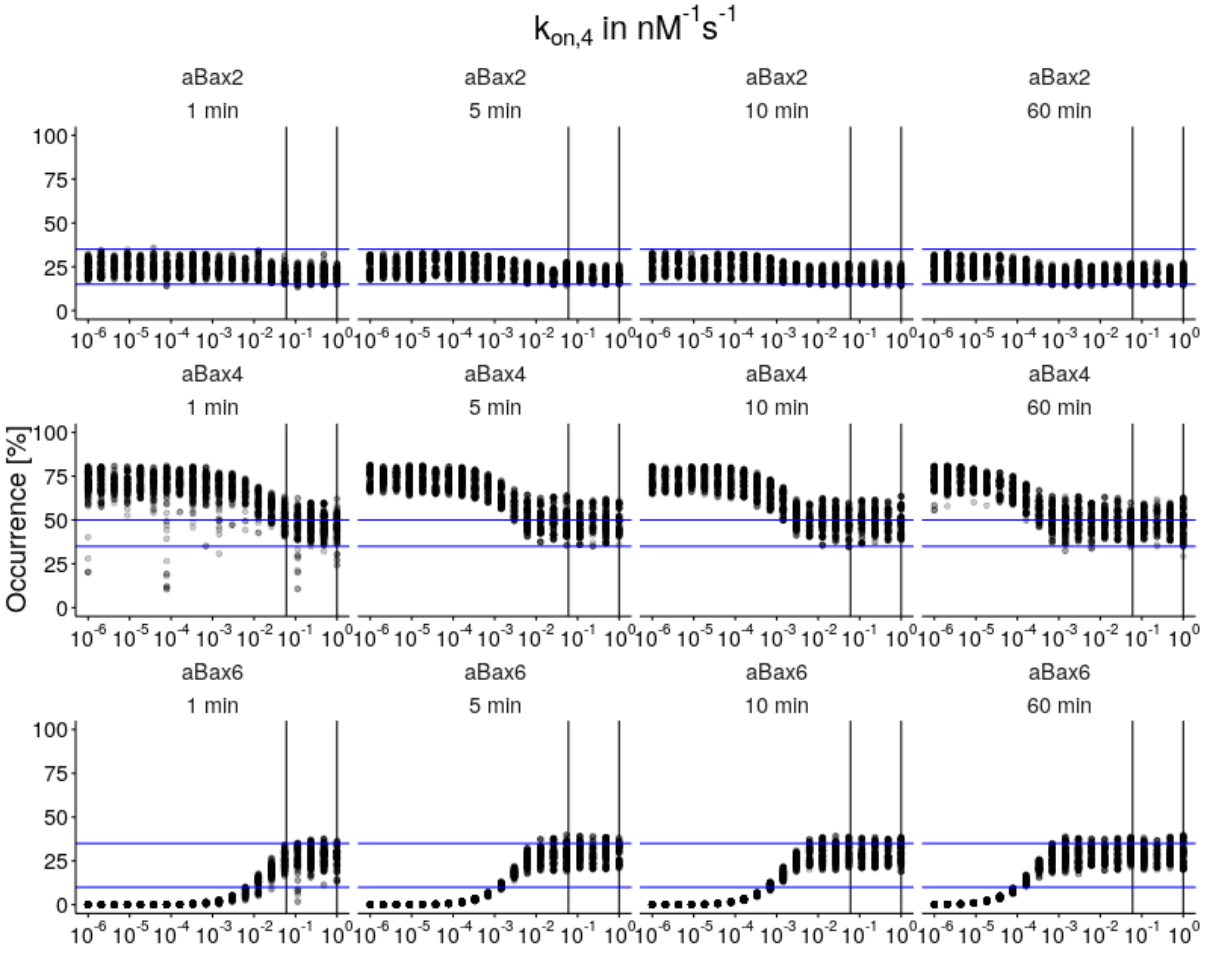

Figure 3.17: **Analysis of $k_{on,4}$ parameter range of trained core model** Simulation results using the starting conditions as in Fig. 3.2A,B and readout at the indicated time points. Shown are sampled parameterizations across the original assumed plausible range of parameter $k_{on,4}$ of the core model (before model training). Blue horizontal lines indicate experimentally valid range for the respective model outputs as estimated from original publication (Subburaj et al., 2015).

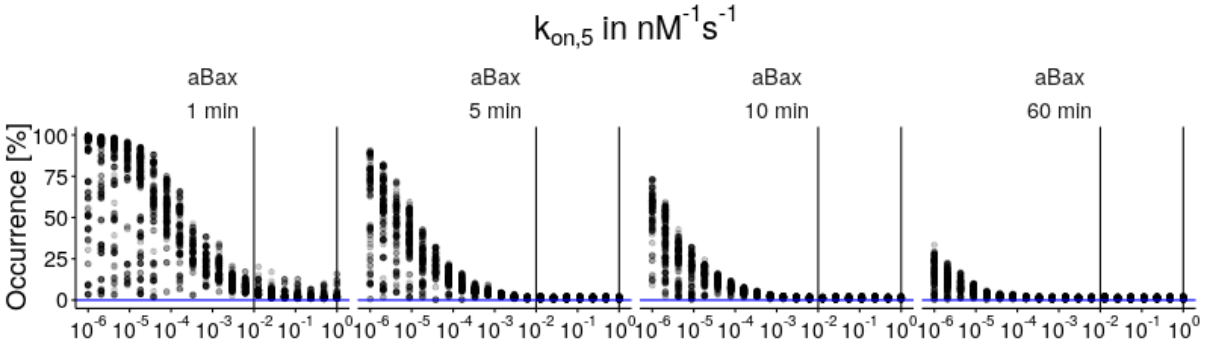

Figure 3.18: **Analysis of $k_{on,5}$ parameter range of trained core model** Simulation results using the starting conditions as in Fig. 3.2A,B and readout at the indicated time points. Shown are sampled parameterizations across the original assumed plausible range of parameter $k_{on,5}$ of the core model (before model training). Blue horizontal lines indicate experimentally valid range for the respective model outputs as estimated from original publication (Subburaj et al., 2015).

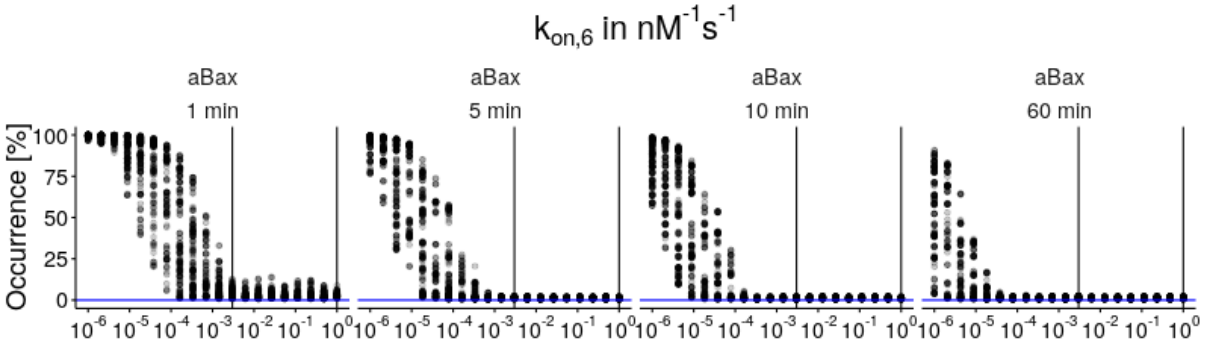

Figure 3.19: **Analysis of $k_{on,6}$ parameter range of trained core model** Simulation results using the starting conditions as in Fig. 3.2A,B and readout at the indicated time points. Shown are sampled parameterizations across the original assumed plausible range of parameter $k_{on,6}$ of the core model (before model training). Blue horizontal lines indicate experimentally valid range for the respective model outputs as estimated from original publication (Subburaj et al., 2015).

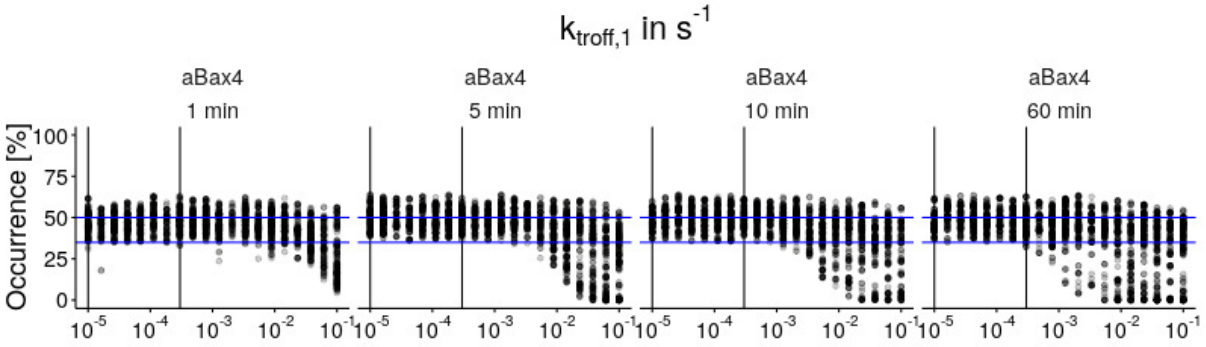

Figure 3.20: **Analysis of $k_{troff,1}$ parameter range of trained core model** Simulation results using the starting conditions as in Fig. 3.2A,B and readout at the indicated time points. Shown are sampled parameterizations across the original assumed plausible range of parameter $k_{troff,1}$ of the core model (before model training). Blue horizontal lines indicate experimentally valid range for the respective model outputs as estimated from original publication (Subburaj et al., 2015).

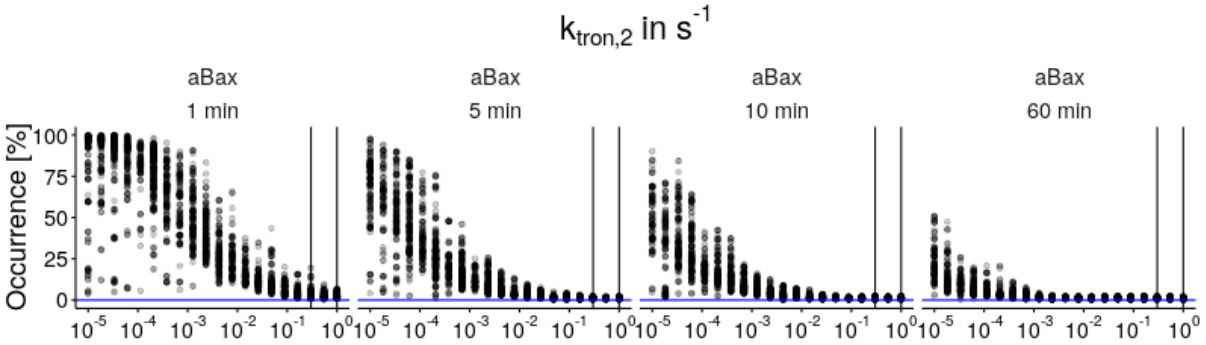

Figure 3.21: **Analysis of $k_{tron,2}$ parameter range of trained core model** Simulation results using the starting conditions as in Fig. 3.2A,B and readout at the indicated time points. Shown are sampled parameterizations across the original assumed plausible range of parameter $k_{tron,2}$ of the core model (before model training). Blue horizontal lines indicate experimentally valid range for the respective model outputs as estimated from original publication (Subburaj et al., 2015).

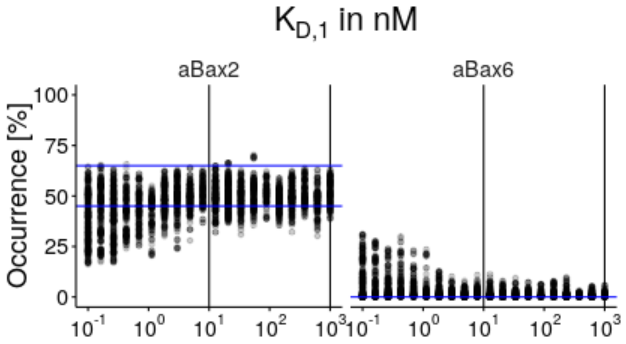

Figure 3.22: **Analysis of $K_{D,1}$ parameter range of complete model** Simulation results using the starting conditions as in Fig. 3.3E. Shown are sampled parameterizations across the parameter range of the core model of parameter $K_{D,1}$. Blue horizontal lines indicate experimentally valid range for the respective model outputs as estimated from original publication (Subburaj et al., 2015).

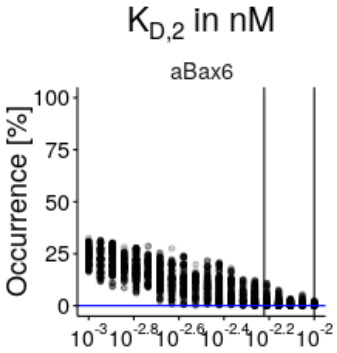

Figure 3.23: **Analysis of $K_{D,2}$ parameter range of complete model** Simulation results using the starting conditions as in Fig. 3.3E. Shown are sampled parameterizations across the parameter range of the core model of parameter $K_{D,2}$. Blue horizontal lines indicate experimentally valid range for the respective model outputs as estimated from original publication (Subburaj et al., 2015).

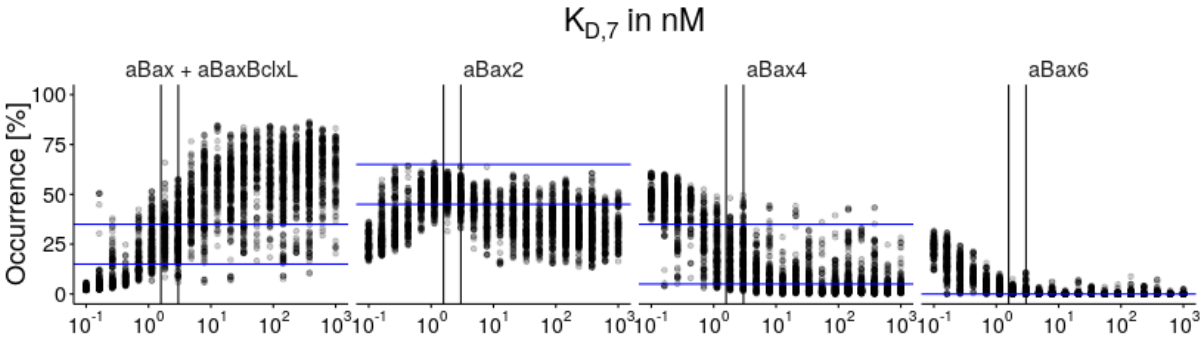

Figure 3.24: **Analysis of $K_{D,7}$ parameter range of complete model** Simulation results using the starting conditions as in Fig. 3.3E. Shown are sampled parameterizations across the parameter range of the core model of parameter $K_{D,7}$. Blue horizontal lines indicate experimentally valid range for the respective model outputs as estimated from original publication (Subburaj et al., 2015).

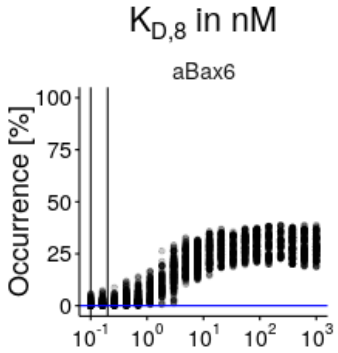

Figure 3.25: **Analysis of $K_{D,8}$ parameter range of complete model** Simulation results using the starting conditions as in Fig. 3.3E. Shown are sampled parameterizations across the parameter range of the core model of parameter $K_{D,8}$. Blue horizontal lines indicate experimentally valid range for the respective model outputs as estimated from original publication (Subburaj et al., 2015).

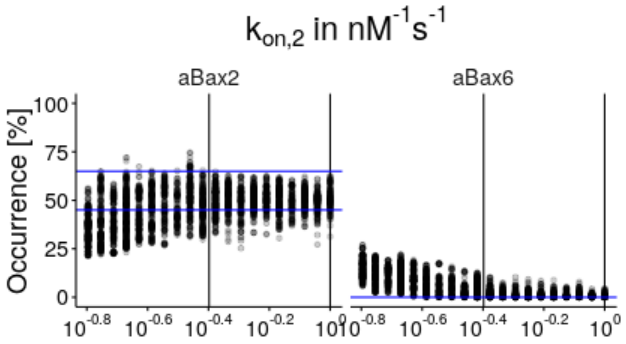

Figure 3.26: **Analysis of $k_{on,2}$ parameter range of complete model** Simulation results using the starting conditions as in Fig. 3.3E. Shown are sampled parameterizations across the parameter range of the core model of parameter $k_{on,2}$. Blue horizontal lines indicate experimentally valid range for the respective model outputs as estimated from original publication (Subburaj et al., 2015).

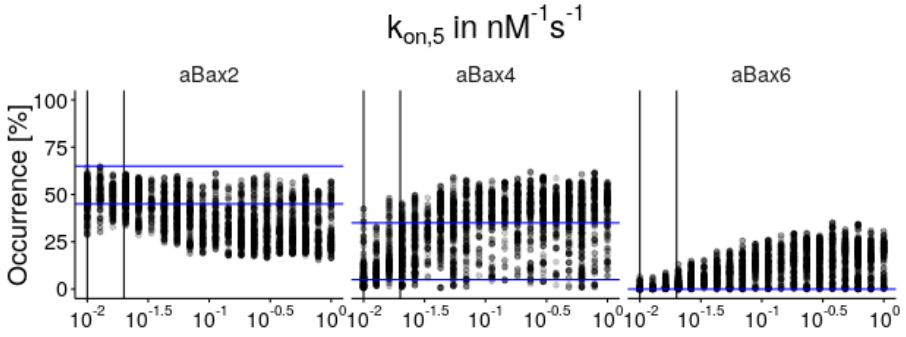

Figure 3.27: **Analysis of $k_{on,5}$ parameter range of complete model** Simulation results using the starting conditions as in Fig. 3.3E. Shown are sampled parameterizations across the parameter range of the core model of parameter $k_{on,5}$. Blue horizontal lines indicate experimentally valid range for the respective model outputs as estimated from original publication (Subburaj et al., 2015).

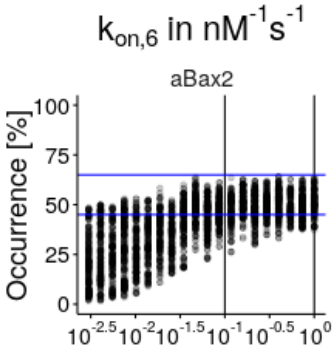

Figure 3.28: **Analysis of $k_{on,6}$ parameter range of complete model** Simulation results using the starting conditions as in Fig. 3.3E. Shown are sampled parameterizations across the parameter range of the core model of parameter $k_{on,6}$. Blue horizontal lines indicate experimentally valid range for the respective model outputs as estimated from original publication (Subburaj et al., 2015).

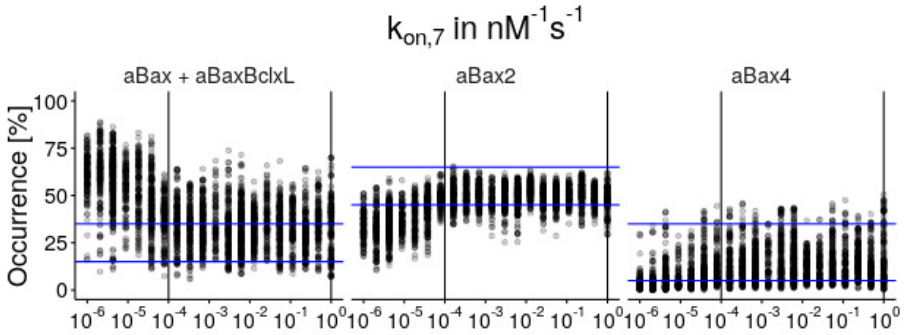

Figure 3.29: **Analysis of $k_{on,7}$ parameter range of complete model** Simulation results using the starting conditions as in Fig. 3.3E. Shown are sampled parameterizations across the parameter range of the core model of parameter $k_{on,7}$. Blue horizontal lines indicate experimentally valid range for the respective model outputs as estimated from original publication (Subburaj et al., 2015).

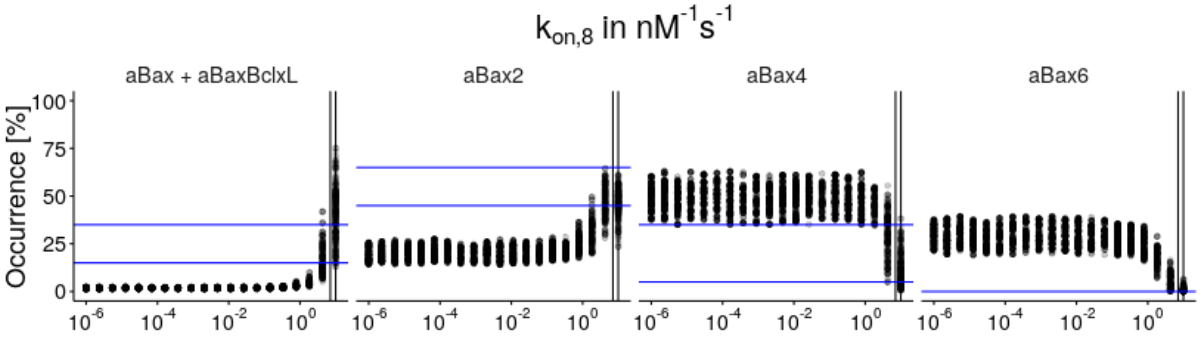

Figure 3.30: **Analysis of $k_{on,8}$ parameter range of complete model** Simulation results using the starting conditions as in Fig. 3.3E. Shown are sampled parameterizations across the parameter range of the core model of parameter $k_{on,8}$. Blue horizontal lines indicate experimentally valid range for the respective model outputs as estimated from original publication (Subburaj et al., 2015).

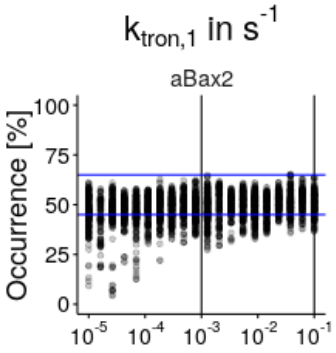

Figure 3.31: **Analysis of $k_{tron,1}$ parameter range of complete model** Simulation results using the starting conditions as in Fig. 3.3E. Shown are sampled parameterizations across the parameter range of the core model of parameter $k_{tron,1}$. Blue horizontal lines indicate experimentally valid range for the respective model outputs as estimated from original publication (Subburaj et al., 2015).

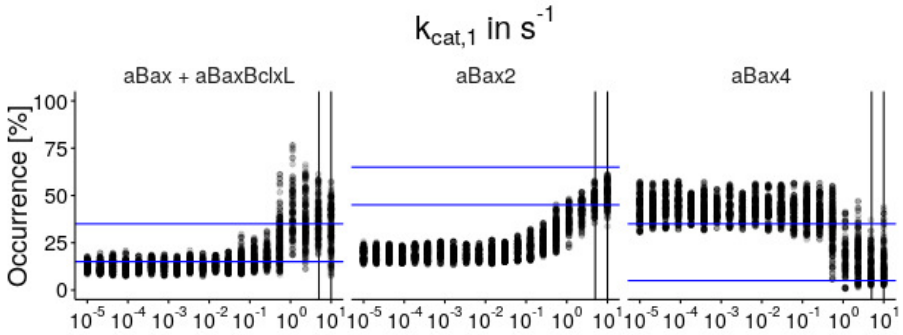

Figure 3.32: **Analysis of $k_{cat,1}$ parameter range of complete model** Simulation results using the starting conditions as in Fig. 3.3E. Shown are sampled parameterizations across the parameter range of the core model of parameter $k_{cat,1}$. Blue horizontal lines indicate experimentally valid range for the respective model outputs as estimated from original publication (Subburaj et al., 2015).

3.6.4 R function providing trajectories in parameter space

```
# k:                number of unknown input parameters
# p:                number of levels, has to be an even integer
# delta:            stepsize by which level is in/decreased (in
    standard uniform distribution)
# noTrajectories: number of trajectories generated

generateTrajectories <- function(k, p, delta, noTrajectories){
  # vector containing all possible levels between 0 and 1, given
      the number of levels
  levels <- seq(from=0, to=1, by=(1/(p-1)))
```

```
# defines the first number of levels allowed for the base
    vector,
# so that each generated point of trajectory is within [0,1]
startlevels <- (p/2)
# generate (k+1)xk matrix of 1s
ones <- seq(1, 1, length.out=(k+1)*k)
J <- matrix(ones, nrow=(k+1), ncol=k)

Jone <- matrix(seq(1, 1, length.out=(k+1)), nrow=(k+1), ncol
    =1)

# generate strictly lower triangular matrix of 1s
B <- J
B[upper.tri(J,diag=TRUE)] <- 0

# generate noTrajectories different possible trajectories
trajectory.list <- list()
trajectories.Outputs.df <- data.frame()

for(i in 1:noTrajectories){
  # sample base vector of parameter space
  base <- sample(levels[1:startlevels], k, replace = T)

  # generate k-dimensional diagonal matrix in which each
      element is either -1 or +1 with equal probability
  diagonal <- sample(c(-1, 1), k, replace = T)
  D <- diag(diagonal)

  # kxk random permutation matrix in which each row contains
      one element equal to 1,
  # all others are 0, an no two columns have 1s in the same
      position
  ones <- seq(1, 1, length.out=k)
  P <- diag(ones)
  permMatrix <- as(sample(k),"pMatrix")
  P <- P %*% permMatrix
```

```
    # generate trajectory; each row contains parameters for one
        model parameterization
    trajectory <- (Jone%*%base + (delta/2)*( (2*B-J)%*%D + J) )
        %*% P
    trajectory.list[[length(trajectory.list)+1]] <- trajectory
  }
  return(trajectory.list)
}
```

4 Quantitative interactome of a membrane Bcl-2 network identifies a hierarchy of complexes for apoptosis regulation

Stephanie Bleicken, Annika Hantusch, Kushal Kumar Das, Tancred Frickey, and Ana J. Garcia-Saez

Nature Communications, 8(1):73, July 2017

4.1 Abstract

The Bcl-2 proteins form a complex interaction network that controls mitochondrial permeabilization and apoptosis. The relative importance of different Bcl-2 complexes and their spatio-temporal regulation is debated. Using fluorescence cross-correlation spectroscopy to quantify the interactions within a minimal Bcl-2 network, comprised by cBid, Bax, and Bcl-xL, we show that membrane insertion drastically alters the pattern of Bcl-2 complexes, and that the C-terminal helix of Bcl-xL determines its binding preferences. At physiological temperature, Bax can spontaneously activate in a self-amplifying process. Strikingly, Bax also recruits Bcl-xL to membranes, which is sufficient to retrotranslocate Bax back into solution to secure membrane integrity. Our study disentangles the hierarchy of Bcl-2 complex formation in relation to their environment: Bcl-xL association with cBid occurs in solution and in membranes, where the complex is stabilized, whereas Bcl-xL binding to Bax occurs only in membranes and with lower affinity than to cBid, leading instead to Bax retrotranslocation.

4.2 Introduction

The proteins of the Bcl-2 family are key regulators of several cellular functions including mitochondrial dynamics and apoptosis (Youle and Strasser, 2008; García-Sáez, 2012; Czabotar et al., 2014). They form a complex network with multiple, parallel interactions that regulates the permeabilization of the mitochondrial outer membrane (MOM). Once the membrane is perforated, cytochrome *c* is released, which is considered the point of no return in the cell commitment to death. Because the Bcl-2 network lies at the heart of apoptosis regulation and is linked to diseases like cancer, Bcl-2 proteins are attractive targets in drug development (Czabotar et al., 2014; Delbridge and Strasser, 2015).

The Bcl-2 family is classified into three sub-groups: Bax and Bak are proapoptotic and directly mediate MOM permeabilization by opening pores at the MOM. Prosurvival proteins like Bcl-2, Bcl-xL, and Mcl-1 promote cell survival by inhibiting their proapoptotic counterparts. The BH3-only proteins have evolved to sense stress stimuli and to promote apoptosis either directly by activating Bax and Bak or indirectly by inhibiting the prosurvival Bcl-2 proteins (Youle and Strasser, 2008; García-Sáez, 2012).

In healthy cells, Bax is monomeric and shuttles continuously between the cytosol and the MOM (Schellenberg et al., 2013; Edlich et al., 2011). During apoptosis, it accumulates at the MOM and undergoes a conformational change that leads to membrane-insertion, oligomerization, and MOM permeabilization (Wolter et al., 1997; Eskes et al., 2000; An-

tonsson et al., 2000; Bleicken et al., 2014; Subburaj et al., 2015; Czabotar et al., 2013), which is accompanied by Bax assembly into a mixture of lines, rings, and arc-like structures (Salvador-Gallego et al., 2016; Grosse et al., 2016). The active membrane-embedded conformation is suggested to form a clamp-like structure that remodels the membrane and stabilizes pores of tunable size (Bleicken et al., 2014, 2013a, 2016). Bax activity is regulated by other Bcl-2 members, including cBid and Bcl-xL. Bid is inactive in the cytosol until it is cleaved by caspase 8 into the active form cBid, which consists of two fragments: p7 and tBid (Chou et al., 1999; Bleicken et al., 2012). cBid translocates to the MOM and promotes Bax activation (Eskes et al., 2000), as well as the insertion of Bcl-xL into the membrane (Bleicken et al., 2013b; Billen et al., 2008b; García-Sáez et al., 2009). Bcl-xL inhibits apoptosis via three incompletely understood modes (Fig. 4.1a). Mode 0 proposes that Bcl-xL shifts the equilibrium between membrane-bound and soluble Bax towards the soluble form (Schellenberg et al., 2013; Edlich et al., 2011). In Mode 1, Bcl-xL sequesters activator-type BH3 only proteins like cBid, and thereby prevents Bax activation (García-Sáez et al., 2009; Llambi et al., 2011). Mode 2 proposes inhibition by direct interaction of Bax and Bcl-xL. However, this is based on indirect evidence like co-immunoprecipitation, the use of chimeric proteins, or interaction-defective protein mutants (Llambi et al., 2011; Cheng et al., 1996; Hsu and Youle, 1997). In addition, Bcl-xL alters the way cBid and Bax remodel membranes (Bleicken et al., 2016).

Several models aim to explain how the Bcl-2 network controls MOM permeabilization. The indirect activation or de-repression model (Willis et al., 2007) implies that Bax is spontaneously active, unless it is bound to and inhibited by prosurvival Bcl-2 homologs. BH3 only proteins can compete with this interaction by binding to the prosurvival Bcl-2 family members, which releases Bax to induce MOM permeabilization. In contrast, the direct activation model (Kuwana et al., 2002; Letai et al., 2002) proposes that Bax is inactive until it interacts with an activator-type BH3-only protein, like cBid, which triggers membrane insertion and the conformational change. The unified (Llambi et al., 2011), the embedded together (Leber et al., 2007), and the hierarchical models (Chen et al., 2015) integrate the de-repression and the direct activation idea into one model.

To understand how the association between Bcl-2 members is orchestrated to regulate MOM permeabilization, a systems approach that provides detailed, quantitative understanding of the relative affinities between full-length Bcl-2 proteins, especially of their active, membrane-embedded forms, is necessary. Performing detailed interaction experiments in living cells is extremely difficult or impossible, due to at least four reasons: (i) the many interactions competing simultaneously, (ii) the difficulties to calculate protein concentrations in organelles of living cells, (iii) the presence of a mixture of different

regulatory post-translational modifications, (iv) and the use of fusions to green fluorescent protein (GFP) or similar fluorescent proteins, which due to their size could affect the function and interactions of the proteins of interest. To solve these limitations, we used here a bottom up approach based on a minimal interaction network composed of full-length cBid, Bax, and Bcl-xL that reproduces the functionality of the Bcl-2 family *in vitro*. Although the extrapolation to the physiological context needs to be done with extreme care, reconstituted systems allowed great advances in understanding the detailed molecular mechanisms of Bcl-2 function (Kuwana et al., 2002; Lovell et al., 2008; Gavathiotis et al., 2008). The main advantage of our approach is that it is chemically controlled so that the individual interactions between Bcl-2 members can be studied, whereas additional factors, as well as post-translational modifications are absent, or can be added separately when necessary.

Scanning fluorescence cross correlation spectroscopy (FCCS) allows to selectively detect interactions within membranes by removing signals from solution, which was not possible in earlier studies (Llambi et al., 2011; Lovell et al., 2008; Aranovich et al., 2012). This is a critical advantage as cBid, Bax, and Bcl-xL constantly shuttle between soluble and membrane-bound conformations, (Schellenberg et al., 2013; Edlich et al., 2011; Bleicken et al., 2012) and both environments should be considered separately. By applying FCCS on soluble and membrane-embedded proteins, we show that the interactions within the Bcl-2 family are spatially regulated. Soluble Bax is monomeric, while upon membrane insertion, it associates into homo-oligomers and hetero-oligomers with cBid and Bcl-xL. In contrast, cBid/Bcl-xL hetero-dimers are detected in solution and membranes. Bcl-xL also forms homo-dimers in solution and its C-terminal transmembrane region modulates the preference for interaction partners. Moreover, we show that membrane-associated Bax recruits soluble Bax and Bcl-xL to the membrane. Bax self-recruitment is a feed-forward mechanism to enhance Bax activity, whereas Bcl-xL recruitment is inhibitory by reducing the size of Bax oligomers via direct interaction and by translocating Bax back into solution. Our findings demonstrate that no additional components are necessary for Bcl-xL-mediated retro-translocation of Bax, which, based on our data, might be driven by Bcl-xL homo-dimerization in solution. This work has implications for the understanding of the Bcl-2 signaling network in its natural context and supports a new model for the integration of Bcl-2 interactions during apoptosis regulation.

4.3 Results

4.3.1 The majority of Bcl-xL molecules are dimers in solution

Here we used solution and scanning FCCS to quantify the concentrations, diffusion coefficients (D), and the interaction of cBid, Bax, and Bcl-xL (coupled to individual fluorophores) in solution and membranes. FCCS measures intensity fluctuations of fluorophores over time using the detection volume of a confocal microscope. On the basis of the intensity fluctuations over time auto-correlation (AC) and cross-correlation (CC) curves are calculated. The detection volumes of the two detection channels do not overlap perfectly, which affects the maximum CC detectable and as a result our CC values are slightly underestimated. The effect of channel cross talk and noise were calculated with free versions of the used dyes. In solution, the CC was below 2% (μ: 1.4, σ: 0.7; see Supplementary Fig. 4.9) and values above 2.8% (μ ±2σ, or 95% confidence) indicate protein interactions. More detailed information is given in Supplementary Methods and in (Ries et al., 2010).

We quantified the homo-interactions and hetero-interactions between cBid, Bax, and Bcl-xL in solution (Fig. 4.1b, c). Bax showed no interactions with itself, cBid or Bcl-xL, indicating that it was present as a monomeric protein. In contrast, the small but significant positive CC of Bcl-xL labeled with red and green dyes indicated the formation of Bcl-xL homo-complexes, most likely dimers, in line with (Jeong et al., 2004). In addition, Bcl-xL interacted with cBid, as shown before (García-Sáez et al., 2009; Aranovich et al., 2012). By using two cBid variants labeled at the N- (cBid-$_{p7R}$) or C-terminal fragment (cBid$_R$ or cBid$_G$), we found that the cBid/Bcl-xL complex contained both cBid fragments. In addition, no homo-oligomerization of cBid molecules was detected. Our results show that in solution three different complexes are formed: p7/tBid, Bcl-xL/Bcl-xL, and p7/tBid/Bcl-xL (Fig. 4.1d). Those complexes are potentially competing in the cytosolic environment and based on our data only Mode 1 of Bcl-xL inhibition takes place in solution. Contradictory results concerning the oligomeric state (monomeric vs. dimeric) of soluble Bcl-xL exist (Jeong et al., 2004; Yao et al., 2015; Muchmore et al., 1996; O'Neill et al., 2006; Denisov et al., 2007; Rajan et al., 2015). This is likely due to the use of C terminally truncated protein versions, which cannot dimerize (Jeong et al., 2004). Thus, the extent of Bcl-xL dimerization and its relevance remains obscure. The CC curves of Bcl-xL selfassociation showed low amplitudes, typical of weak interactions and supporting the existence of a major monomeric population (Fig. 4.1b, and Supplementary Fig. 4.10, K_D ~600 nM). Intriguingly, the D of Bcl-xL (Fig. 4.2a) was smaller than that of cBid and Bax, and varied strongly with protein concentration (Fig. 4.2a, b), suggesting a particle

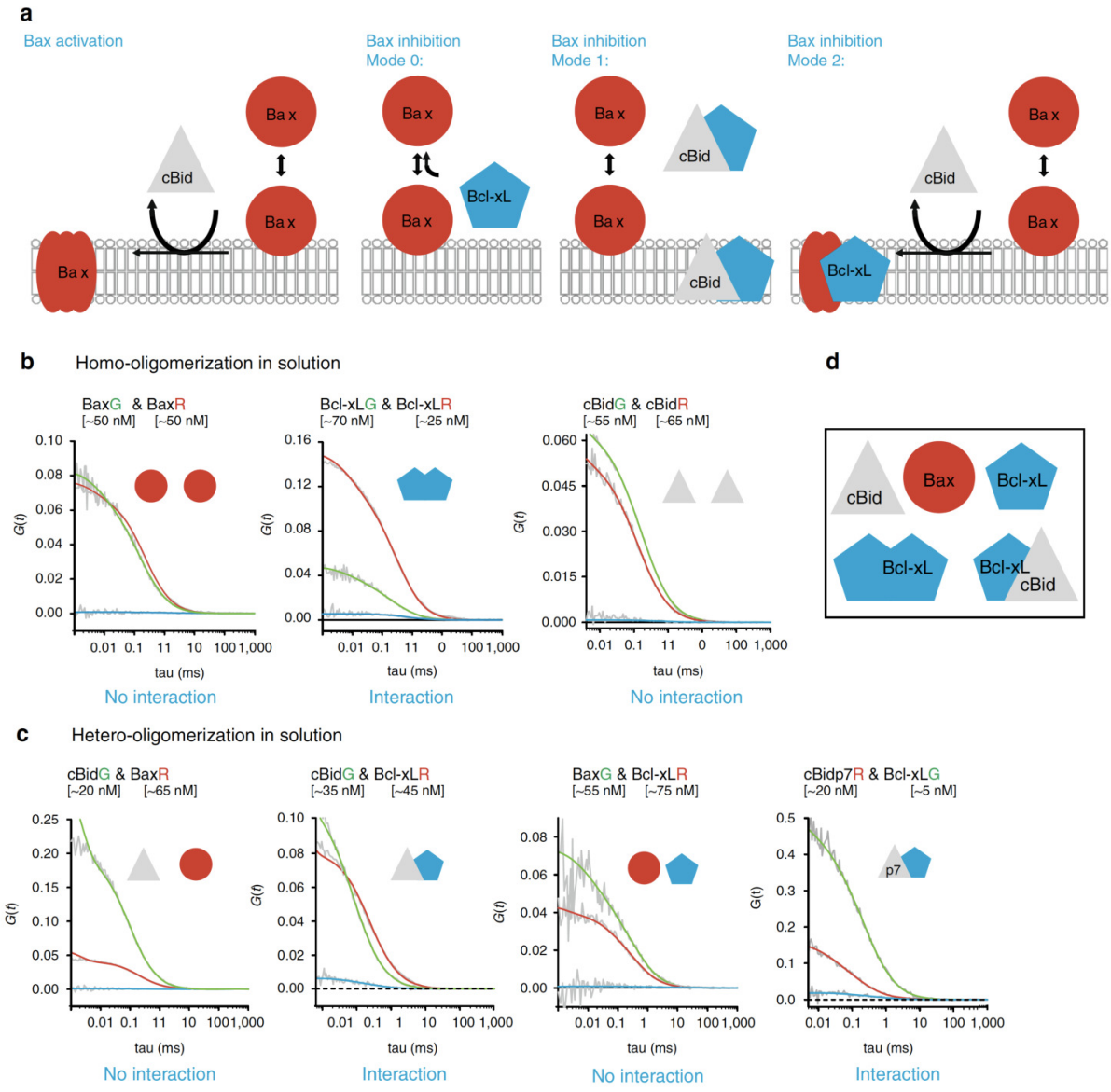

Figure 4.1: **Analysis of interactions between cBid, Bax, and Bcl-xL in solution. a**, Representation of current models on Bax activation and inhibition by cBid and Bcl-xL. **b**,**c**, Representative FCCS graphs of cBid, Bax, and Bcl-xL homo-hetero-oligomerization (B) and hetero-oligomerization in solution. For visual guidance: The amplitude of the AC curves is inversely proportional to the number of fluorophores, whereas the amplitude of the CC curves is proportional to the number of dual-color complexes. The decay of the AC and CC curves provides quantitative information on the diffusion properties of the particles and therefore of their size. All particle concentrations calculated from FCCS measurements refer to fluorescent particles that diffuse as a unit. Only Bcl-xL_G/Bcl-xL_R and $cBid_G$/Bcl-xL_R present positive CC amplitude (blue curve) indicative of interaction. The unfitted AC and CC curves are shown in grey ($n \geq 3$ independent experiments), and the fitted AC curves corresponding to the species labeled with green and red fluorophores and shown in green and red, respectively. We studied interactions at different protein concentrations up to 200 nM. **d**, Scheme of the five different monomeric and dimeric species that can be detected in solution. *FCCS* fluorescence cross correlation spectroscopy

size in line with high dimer content. The structures of the inactive, soluble conformations of cBid, Bax, and Bcl-xL (Chou et al., 1999; Muchmore et al., 1996; Suzuki et al., 2000) show protein radii in the range of 1.7-2.5 nm, transferring into a D of roughly 70-110 µm^2

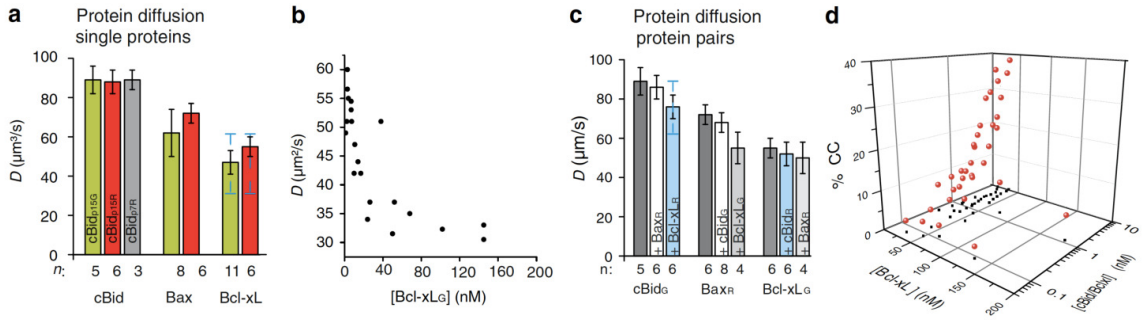

Figure 4.2: **Quantitative analysis of the interactions between cBid and Bcl-xL in solution. a**, D of cBid, Bax, and Bcl-xL labeled with Alexa488 or Atto488 (green columns), or Alexa633 or Atto655 (red columns). The grey column corresponds to $cBid_{p7R}$. Mean and error bars as s.d. are shown in black; the additional blue error bars for Bcl-xL indicate scattering of D values depending on concentration, n is indicated in the figure. **b**, The D of $Bcl\text{-}xL_G$ in dependence of the protein concentration ($n = 4$). **c**, Effect of protein co-incubation on the D of cBid, Bax, and Bcl-xL. Addition of $Bcl\text{-}xL_R$, induced a decrease in $cBid_G$ diffusion as expected from direct interaction ($n = 3$, mean and error bars as s.d. are shown in black); the additional blue error bar for cBid in presence of Bcl-xL indicates scattering of D values depending on the Bcl-xL/cBid ratio. **d**, The CC between $cBid_G$ and $Bcl\text{-}xL_R$ increased with protein concentration (data as red dots with black shadows in xy, $n = 6$)

s^{-1}. The D of cBid, Bax, and Bcl-xLΔCT fall in this range (Fig. 4.2a and $D_{Bcl\text{-}xL\Delta CT}$: 78 μm^2 s^{-1} see (García-Sáez et al., 2009)), whereas the full length Bcl-xL had a smaller D ($\sim$ 50 μm^2 s^{-1}), as would be expected for Bcl-xL dimers. These results indicated that, full length Bcl-xL was mainly dimeric in solution, whereas the C-terminal truncated version was monomeric (in agreement with (García-Sáez et al., 2009; Jeong et al., 2004)).

To test whether we could detect full-length Bcl-xL monomers in solution, we diluted the protein (Fig. 4.2b). Interestingly, the D of Bcl-xL grew at concentrations below 20 nM indicating an increase in the monomer population at lower concentrations in line with a high binding affinity between Bcl-xL monomers (low nano-molar K_D). In human cells, the concentration of Bcl-xL (10-1000 nM) and Bax (50-500 nM) was recently estimated (Lindner et al., 2013a), suggesting that at physiological concentrations Bcl-xL is mainly dimeric.

To further correlate particle mobility and interactions within the minimal Bcl-2 network, we tested how the presence of a second Bcl-2 protein affects the D of cBid, Bax, and Bcl-xL (Fig. 4.2c). As expected from the CC data, Bax diffusion was not affected by the presence of cBid or Bcl-xL and vice versa, whereas the mean D of cBid decreased in the presence of Bcl-xL, as expected for hetero-dimerization (p-value: 0.0089, unpaired two tailed t-test). In contrast, the D of Bcl-xL was barely affected by the presence of cBid (Fig. 4.2c), in line with Bcl-xL being homo- or hetero-dimeric in solution.

4.3.2 cBid can dissociate Bcl-xL homo-dimers

Next, we probed the competition between Bcl-xL homo-complexes and the hetero-complexes by adding increasing amounts of $cBid_G$ to $Bcl\text{-}xL_R$ and measuring the CC after 1 h incubation. As expected for hetero-dimer formation, the amount of two colored complexes increased with the cBid concentration (up to 40% CC, Fig. 4.2d). Hetero-dimerization of this pair in solution was reported before (García-Sáez et al., 2009; Llambi et al., 2011; Willis et al., 2007; Aranovich et al., 2012; Certo et al., 2006; Kim et al., 2006; Chen et al., 2005; Hockings et al., 2015; Kuwana et al., 2005), and in some cases quantified (with K_DâĂŹs: between 12 nM (Certo et al., 2006) and 350 nM (Hockings et al., 2015)). However, this can only be an effective value, as it does not take into account the presence of $Bcl\text{-}xL_R$ homo-dimers.

To understand the interaction between cBid and Bcl-xL quantitatively, we needed to determine the exact reactions taking place. In Fig. 4.3a, three possible scenarios are suggested. In the simplest scenario 1, cBid can only interact with Bcl-xL monomers and the formation of cBid/Bcl-xL and Bcl-xL/Bcl-xL complexes are competing. Scenario 2 differs from scenario 1 by an additional reaction, in which cBid is able to interact with Bcl-xL dimers, leading to the formation of a cBid/Bcl-xL hetero-dimer and one released Bcl-xL monomer. Scenario 3 considers instead that the interaction of cBid with a Bcl-xL dimer forms, a hetero-trimer, that can disassemble into two hetero-dimers after the addition of a second cBid molecule.

On the basis of these three scenarios, we designed an experiment that together with mathematical modeling allowed us to falsify one of the suggested scenarios. $Bcl\text{-}xL_R$ and $Bcl\text{-}xL_G$ were mixed and incubated for 120 min at room temperature (RT). Afterwards, the initial CC was measured (time -20 min) and the sample was divided into two equal parts. To one, we added unlabeled cBid in $\sim$ 10-fold excess (time 0 min) to shift the equilibrium towards cBid/Bcl-xL complexes. To the second one, we added buffer as negative control. In both samples, the CC was followed over time (Fig. 4.3b). To our surprise, addition of cBid led to a clear increase in the CC between $Bcl\text{-}xL_R$ and $Bcl\text{-}xL_G$, whereas the CC remained unchanged in the negative control. Thus, cBid provoked not only hetero-dimer formation (Fig. 4.2d), but additionally boosted the amount to two-colored Bcl-xL homo-dimers (Fig. 4.3b). This can be explained by the existence of stable Bcl-xL homo-dimers with very slow exchange rates, so that in absence of cBid monomer exchange hardly takes place. cBid addition provokes hetero-complex formation and the release of Bcl-xL monomers, which in turn form new Bcl-xL homo-dimers increasing the number of two-colored Bcl-xL homo-dimers. Thereby, the total number of Bcl-xL homo-dimers did not increase and homo-dimer and hetero-dimer formation is in equilibrium.

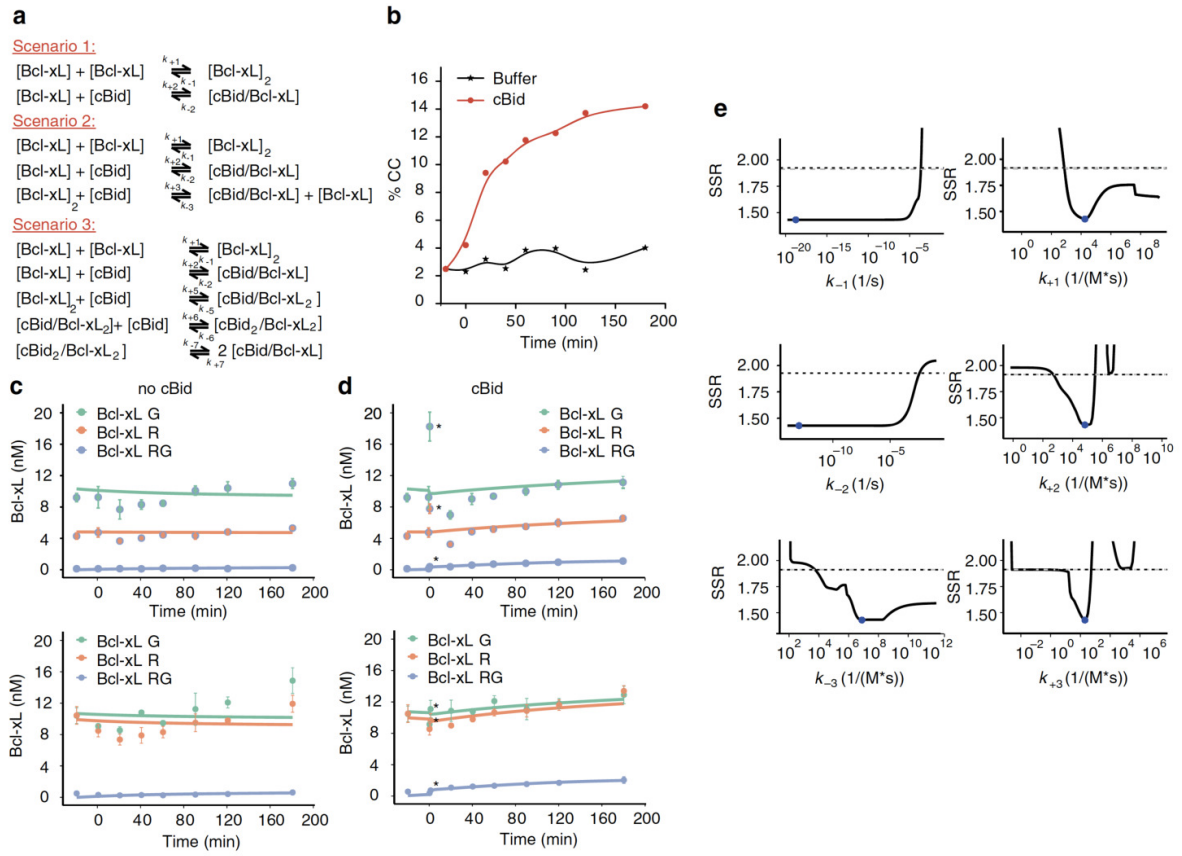

Figure 4.3: **Bcl-xL forms stable dimers in solution that exchange in presence of cBid. a**, Possible reaction scenarios between cBid and Bcl-xL in solution tested by modeling. **b**, FCCS kinetic experiment on Bcl-xL_R/Bcl-xL_G dimerization in absence and presence of cBid (exemplary experiment out of $n = 3$). **c**,**d**, Best fit of ODE model considering scenario 2 to the evolution of fluorescent Bcl-xL species based on the data shown in **b**. The upper and the lower panels show two independent experiments (mean and error bars as s.d. of three technical repetitions) with the Y-axis corresponding to the concentration of Bcl-xL particles. The first data point in presence of cBid is introduced as t = 1 min and highlighted in the figure by asterisk. This is applicable as each data point had a total FCS measurement time of 2 min. **e**, Likelihood profiles of model parameters that define rate constants. The fitted parameter is shown as a blue dot, the reoptimized SSR is shown as black line and the dashed grey line indicates the confidence limit. *FCCS* fluorescence cross correlation spectroscopy

4.3.3 Modeling cBid and Bcl-xL interactions in solution

To discriminate between the three reaction scenarios (Fig. 4.3a), we built mathematical models based on ordinary differential equations (ODEs), and analyzed the kinetics of association and dissociation of Bcl-xL molecules with themselves and with cBid. For scenario 1, a simple ODE system describing the two reversible interactions based on the law of mass action was fitted to the experimental data shown in Fig. 4.3b. The increase in two-colored Bcl-xL homo-dimers after cBid addition could not be reproduced by the model even when searching a large parameter space with a global optimization method (Supplementary Fig. 4.11). Thus, scenario 1 could be excluded.

In contrast, ODE modeling suggested that both scenarios 2 and 3 could quantitatively

reproduce the experimental data (Fig. 4.3a-d and Supplementary Fig. 4.12). Thus, ODE modeling supports the idea that cBid can interact with Bcl-xL monomers and dimers. To test whether scenario 2 or 3 are more likely, we used the difference in AkaikeâĂŹs information criterion (AIC), which considers the difference between the experimental data and the fit of the model as well as the number of parameters (model complexity). The differences in AIC values and the Akaike weights can then be used to select which scenario approximates the data best (Burnham et al., 2002). In our case, the values support scenario 2 over scenario 3 (Supplementary Table 4.2).

Finally, we performed a parameter identifiability analysis to examine and compare the velocity of all modeled association and dissociation reactions (Schaber, 2012) (Fig. 4.3e and Supplementary Figs. 4.13 and 4.14). For scenario 2, two of the parameters were identified with 95% confidence within the tested parameter range, and the other could be constrained in at least one direction based on the 95% confidence limit and a reoptimized sum of squared residuals (SSR, with a minimum SSR value for each parameter). On the basis of the likelihood profiles of the model corresponding to scenario 2 (Fig. 4.3e), we could conclude that conversion of Bcl-xL homo-dimers to cBid/Bcl-xL hetero-dimers via cBid addition is a slow process (k_{+3} 10-700 1/(M*s)). The slow association rate constant indicates that conformational changes are involved in the reaction leading to hetero-dimer formation (Schreiber et al., 2009). A comparison of the likelihood profiles for k_{-3} (exchange of cBid with Bcl-xL in a hetero-dimer to form a Bcl-xL homo-dimer) and k_{+1} (association of two Bcl-xL) further suggested that cBid binding to Bcl-xL may speed up Bcl-xL dimerization. The calculated weak K_D ($\sim$ 600 nM) for Bcl-xL homo-dimers (Supplementary Fig. 4.10) could then be explained by a very slow dissociation of Bcl-xL homo-dimers, causing the experimental system to reach an equilibrium much later than experimentally accessible. Thus the real K_D for Bcl-xL homo-dimerization would be much smaller (in the order of 10 nM), as suggested before (Fig. 4.2b). In summary, our modeling data excluded scenario 1, whereas scenario 2 and 3 were both plausible with scenario 2 being more likely.

4.3.4 In the membrane only Bax and Bcl-xL can self-associate

The active conformations of the Bcl-2 proteins are membrane-embedded. Thus, it is crucial to understand the protein interactions within the membrane. For this purpose, we measured scanning FCCS in giant unilamellar vesicles (GUVs) of two different lipid compositions (Methods and (Bleicken et al., 2014, 2013a,b; Lovell et al., 2008)): one is mimicking the MOM (MOM mix, $\sim$ 5% cardiolipin (CL)), whereas the other has a high CL content (30% CL) to enhance protein membrane binding and therefore the contrast

(Supplementary Fig. 4.15A). Both lipid mixtures have been studied before and Bax-induced membrane pores had similar properties in both (Bleicken et al., 2013a), whereas permeabilization was more efficient with the higher CL concentration (Bleicken et al., 2013a).

As a control for false-positive CC in the membrane, we measured the CC between Bcl-xL and a lipidic dye, two molecules that should not interact (Supplementary Fig. 4.15B). Based on this, we assumed that mean CC values above 20% (for 30% CL $\mu+/-2\sigma$ = 19% CC) indicated protein interactions in membranes. Some vesicles containing cBid and/or Bax exhibited bright spots, which we interpreted as membrane buds (Bleicken et al., 2016). Those vesicles were excluded from analysis as artificial CC can be detected (Supplementary Fig. 4.15C). Finally, to induce Bax and Bcl-xL membrane insertion, we used two methods: we added cBid (Bleicken et al., 2013b), or we applied a mild heat treatment (Subburaj et al., 2015; Hermann et al., 2014; Pagliari et al., 2005) to avoid effects of unlabeled cBid on the interactions measured.

After membrane insertion, the interaction network between cBid, Bax, and Bcl-xL strongly changed. Once inserted into the membrane, Bax formed homo-oligomers (in agreement with (Bleicken et al., 2014; Czabotar et al., 2013; Bleicken et al., 2013b; Lovell et al., 2008; Bleicken et al., 2010; Antonsson et al., 2001)) irrespectively of the activation method (Fig. 4.4a, c, d and (Subburaj et al., 2015)). In line with oligomer formation, the mean D of membrane-embedded Bax was clearly smaller than the D of cBid or Bcl-xL, whereas the CC between Bax molecules was much higher than the CC between cBid or Bcl-xL molecules (Fig. 4.4a and Supplementary Fig. 4.16A, B). Moreover, the mean CC between Bax molecules was higher and more disperse than expected for pure dimers (reaching 100% in some GUVs, Fig. 4.4c). This is in agreement with higher order oligomer formation and a broad distribution of oligomers sizes (Fig. 4.4e and Supplementary Fig.4.16C).

We did not detect Bcl-xL homo-dimers in presence of cBid (Fig. 4.4a, f and (Bleicken et al., 2013b)), but when Bcl-xL membrane-insertion was induced by heat, we observed a significant amount of CC in line with homo-complex formation. This demonstrates for the first time that the membrane-inserted Bcl-xL can self-associate when no other interaction partners are present (Fig. 4.4f). However, cBid and Bax were preferred interaction partners over the self-interaction. Finally, we could not detect cBid homo-dimers in the membrane (Fig. 4.4a). This is at odds with studies reporting cBid homo-oligomerization in membranes (Shivakumar et al., 2014). One reason could be cBid ability to reorganize membranes (Bleicken et al., 2016), which can lead to artificial oligomer detection (Supplemental Fig. 4.15c).

Of note, we published CC data on Bax and Bcl-xL homo-interactions in membranes before

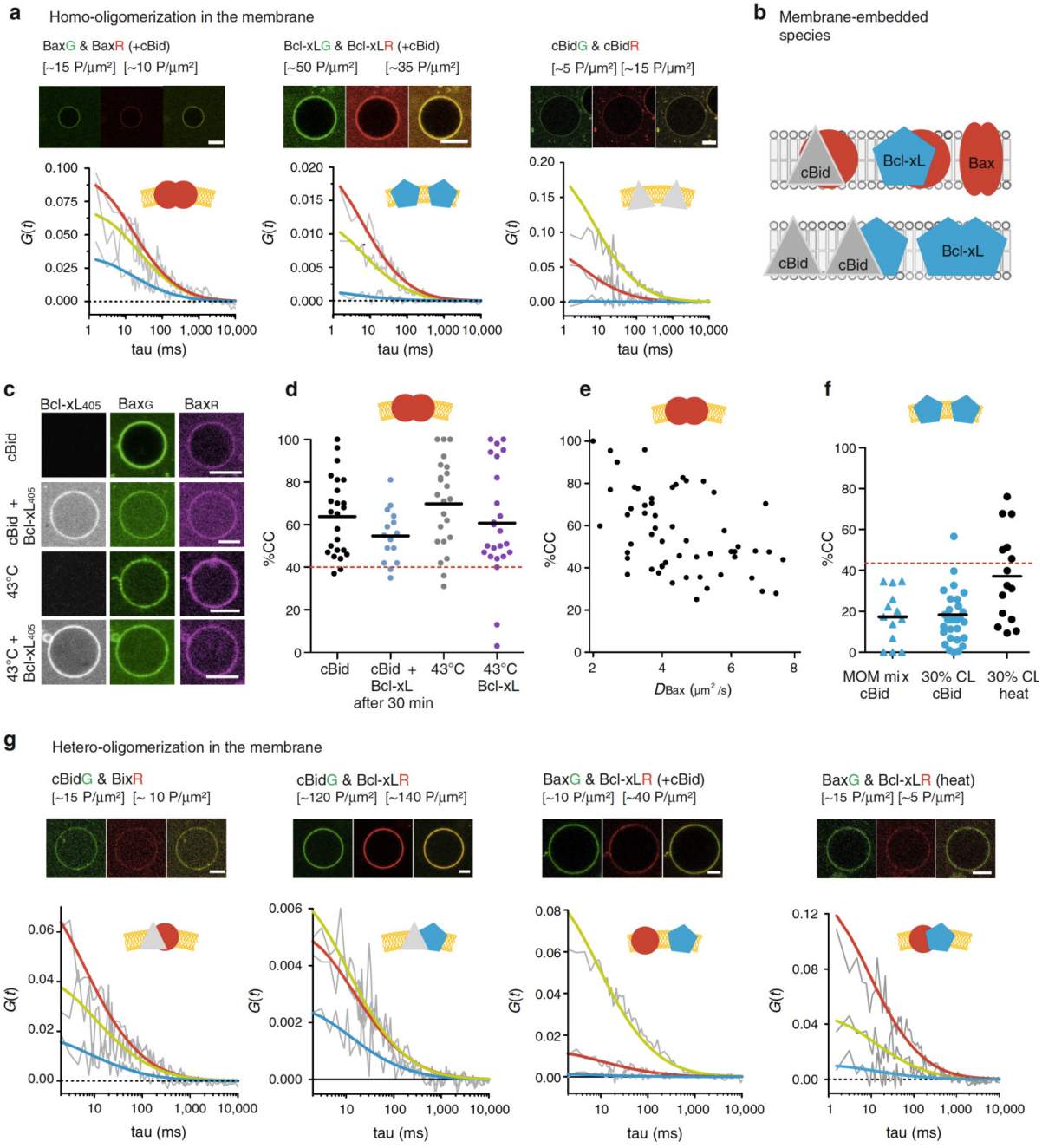

Figure legend on next page

(Bleicken et al., 2013b). Here, we included those data together with two new independent experimental repetitions, to compare the CC and D values with other complexes, as well as measurements under different conditions, e.g., absence of cBid (data used already in (Bleicken et al., 2013b) are included in Fig. 4.4e, f and Supplemental Fig. 4.16a, c). In summary, membrane-embedded Bax and Bcl-xL could be detected in homo-complexes and hetero-complexes, whereas cBid was present as a part of hetero-complexes or as a monomer.

Figure 4.4: **Analysis of the interactions between cBid, Bax and Bcl-xL within membranes.** **a**, Representative FCCS graphs and corresponding GUV images of cBid, Bax, and Bcl-xL homo-oligomerization in membranes (30% CL, Scale bar: 10 µm). Only the Bax_G/Bax_R pair presents positive CC amplitude indicative of interaction. The AC and CC curves are shown in grey, whereas the fitted curves are shown in green (green protein), red (red protein), or blue (complex). **b**, Scheme of the different species that can be detected in the membrane. **c**, Representative images of Bax_R, Bax_G, and $Bcl\text{-}xL_{405}$ binding to GUVs (30% CL, Scale bar: 10 µm) in presence of unlabeled cBid or after incubation at 43 °C. **d**, Comparison of the oligomerization expressed as %CC between Bax_G and Bax_R in individual GUVs after activation by cBid or 43 °C and in presence or absence of Bcl-xL405 (30% CL; n = 4). All data are from one batch of labeled Bax to ensure that the degree of labeling is the same under all conditions. The maximal possible %CC for dimer formation considering the degree of labeling and a Mendel-based distribution of red-red, red-green, and green-green complexes is indicated by the dotted red line. **e**, Relationship between CC and D of Bax_G and Bax_R activated by cBid in individual GUVs (30% CL; n = 5 independent experiments using three independent Bax batches; degree of labeling 80-100%). The CC values of three experiments were already published in (Bleicken et al., 2013b) (see also Supplemental Fig. 4.16A-C). **f**, Comparison of the CC between $Bcl\text{-}xL_G$ and $Bcl\text{-}xL_R$ in GUVs composed of the both lipid mixtures. Membrane insertion was induced by cBid or 43 °C. The dotted red line indicates the maximal %CC possible considering dimer formation (n = 3). Only one protein batch was used due to the same reasons as in **d**. Data from independent Bcl-xL batches are shown in Supplemental Fig. 4.16A, B. **g**, Representative FCCS graphs and corresponding GUV images of cBid, Bax, and Bcl-xL hetero-oligomerization in GUVs (30% CL; Scale bar: 10 µm; color code as in **a**. *FCCS* fluorescence cross correlation spectroscopy

4.3.5 In the membrane cBid-Bcl-xL complexes are stable and exclude p7

The only complex detected in solution and membranes was the cBid/Bcl-xL hetero-dimer. Upon membrane insertion, hetero-complex formation dominated over Bcl-xL homo-dimerization (Figs. 4.4a, f, g and 4.5a), which indicates a stronger interaction between cBid and Bcl-xL in membranes compared to solution. The mean CC between cBid/Bcl-xL in membranes was close to the maximum expected considering hetero-dimer formation (Fig. 4.5a), and it did not change significantly with lipid composition (Fig. 4.5b) or protein concentration (Fig. 4.5d). The mean D for cBid and Bcl-xL was ∼5 $\mu m^2\ s^{-1}$ (Fig. 4.5c), in line with previous work (Bleicken et al., 2013b; García-Sáez et al., 2009).

We also followed the kinetics of complex formation in individual GUVs (Fig. 4.5e and Supplementary Fig. 4.17) and found that the extent of association was high, stable over time, and independent of membrane permeabilization. This indicates again a very high binding affinity between cBid and Bcl-xL, and suggests that they insert into the membrane as a complex or, if there is recruitment, that it happens very fast. Thus, Mode 1 inhibition of MOMP will mainly happen in the membrane-bound state.

The soluble cBid/Bcl-xL complex contained tBid and the p7 fragment (Fig. 4.1c). To test if the same was true for the membrane-embedded complex, we used $cBid_{p7R}$. The

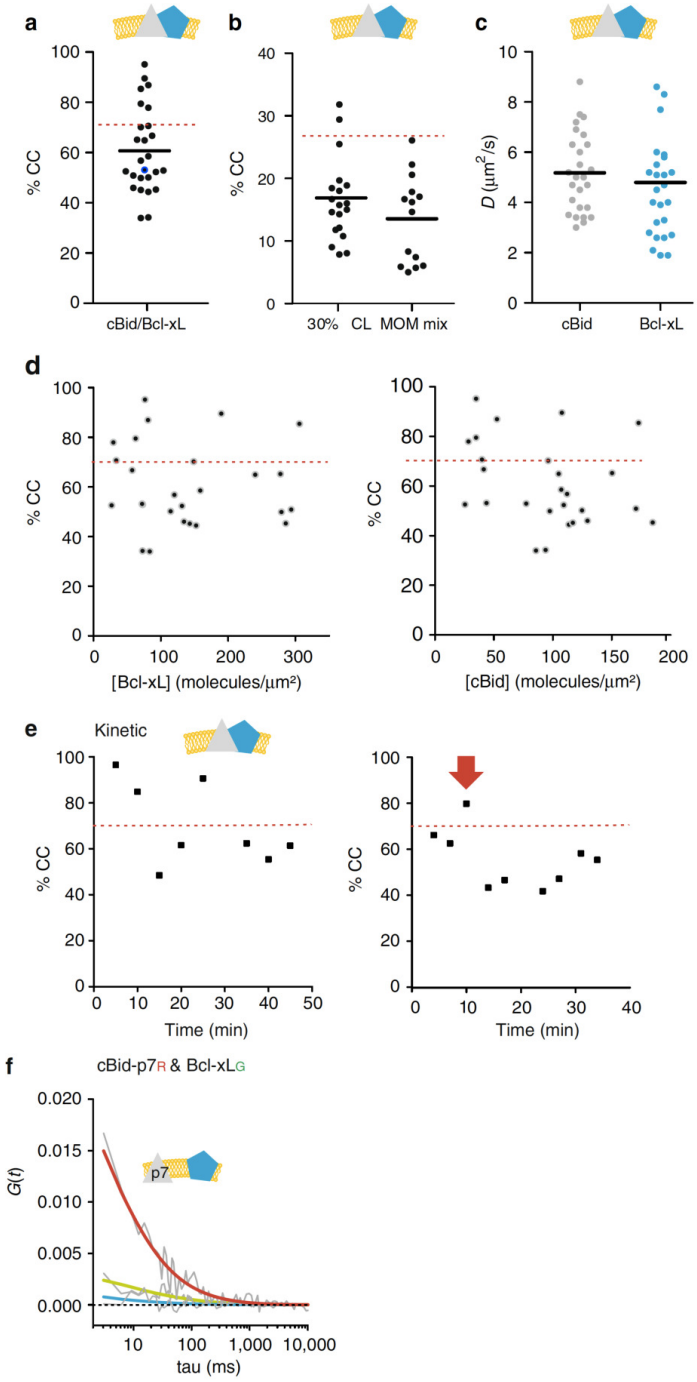

Figure 4.5: **Quantitative analysis of cBid-Bcl-xL association in membranes.** **a**, %CC between $cBid_G$ and $Bcl\text{-}xL_R$ in membranes (30% CL; n = 5). **b**, %CC between $cBid_G$ and $Bcl\text{-}xL_R$ in GUV membranes comparing both lipid mixtures (n = 3). **c**, *D* of $cBid_G$ and $Bcl\text{-}xL_R$ in individual 30% CL GUVs (n = 5). **d**, %CC vs. the $cBid_G$ or $Bcl\text{-}xL_R$ protein concentration in GUVs (30% CL; n = 5). **e**, Evolution of %CC between $cBid_G$ and $Bcl\text{-}xL_R$ in two individual GUVs as a function of time. The red arrow marks the time point at which the GUV was permeabilized (see also Supplemental Fig. 4.17). **f**, Representative FCCS graph of $cBid_{p7R}$ and $Bcl\text{-}xL_G$ interaction. The absence of positive CC indicates that the labeled proteins do not interact in the membrane (color code as in 4 A). In **a**, **d**, and **e**, the dotted red line indicates the maximal CC considering dimer formation and degree of labeling. *FCCS* fluorescence cross correlation spectroscopy

CC between labeled p7 and Bcl-xL was as low as in the negative controls (Fig. 4.5f) indicating that the membrane-embedded complex does not contain p7.

4.3.6 cBid-Bax interaction decreases upon Bax oligomerization

cBid has been proposed to interact transiently with Bax to catalyze its activation and membrane insertion (Czabotar et al., 2013; Lovell et al., 2008; Gavathiotis et al., 2008; Bleicken et al., 2010; Gavathiotis et al., 2010). A transient interaction seems necessary as the binding site of Bid to the Bax BH-groove is overlapping with one interaction interface between Bax monomers in the homo-oligomer (Czabotar et al., 2013). Detecting the cBid/Bax complex in membranes has remained challenging and could only be validated once (Lovell et al., 2008). Here, we could identify cBid/ Bax complexes as well (Fig. 4.6a), but the level of CC was much lower than for cBid/Bcl-xL complexes ($<$40% CC compared to $>$ 60% CC), indicating a low affinity or a short lifetime of the cBid/Bax complex.

We wondered if the dispersed CC data (Fig. 4.6a) could be the result of two populations of GUVs: one with high and one with low cBid and Bax interaction. On average, Bax clearly diffused slower than cBid (Fig. 4.6b), supporting this hypothesis. However, in GUVs with a high CC between cBid and Bax, cBid diffused similar to Bax (Fig. 4.6c), suggesting that Bax-oligomer assembly happened faster than cBid release. In addition, kinetic experiments revealed a decrease in the CC between cBid and Bax over time, in line with a transient interaction (Fig. 4.6d and Supplementary Fig. 4.18). Thus, the cBid-Bax complex in membranes is likely transient, and cBid is released after Bax homo-oligomerization.

4.3.7 In membranes Bcl-xL hetero-dimerizes with Bax, but prefers cBid

Although the inhibitory role of Bcl-xL via direct interaction with Bax (Mode 2) was first proposed more than two decades ago (Korsmeyer, 1995), the interaction between these two proteins has escaped detailed characterization. Here, despite the lack of association in solution (Fig. 4.1c), membrane-embedded Bax and Bcl-xL formed complexes (Fig. 4.6e). They were mainly detectable when membrane insertion was induced by mild heat treatment. In the presence of cBid, we could hardly detect Bax/Bcl-xL complexes (Fig. 4.6e-g and Supplementary Fig. 4.16D), likely due to the formation of competing cBid/Bcl-xL complexes (Fig. 4.5a). Performing these experiments was complicated as Bcl-xL excludes Bax from membranes (Schellenberg et al., 2013; Edlich et al., 2011; Bleicken

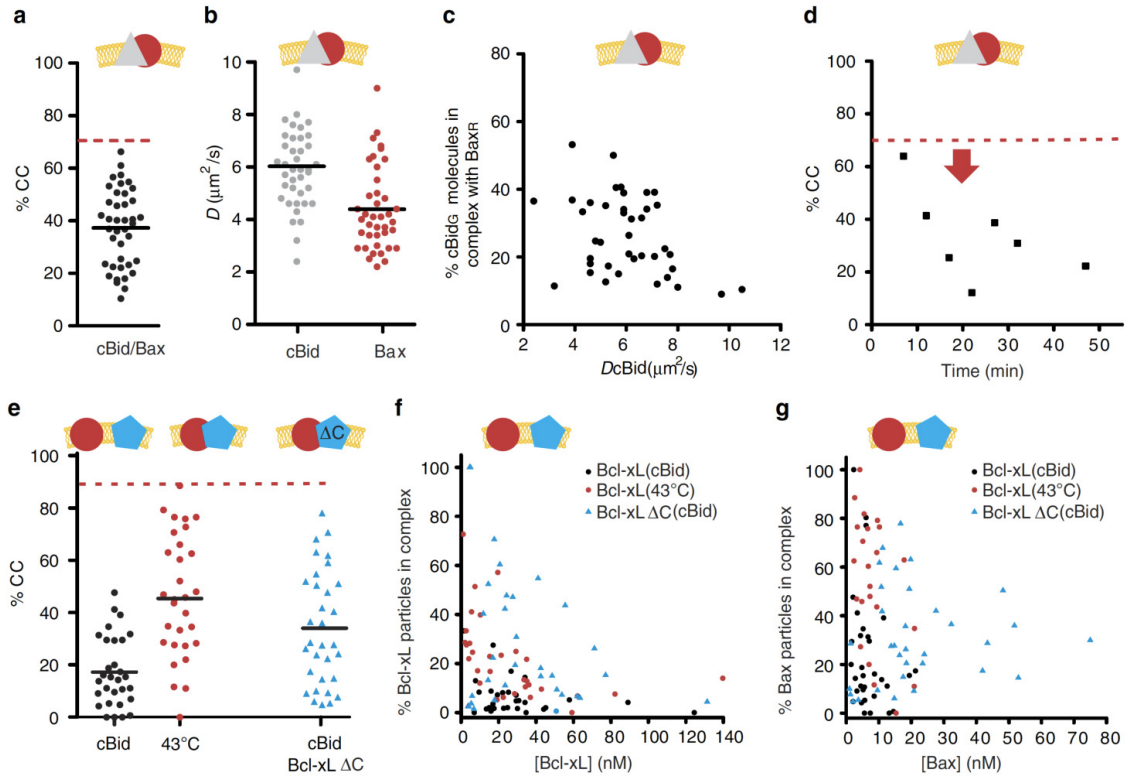

Figure 4.6: **Quantitative analysis of the interaction of Bax with cBid and Bcl-xL in membranes.** **a**,**b**, %CC (**a**) and D (**b**) of membrane-embedded $cBid_G$ and Bax_R in individual GUVs (30% CL; n = 8). **c**, Percentage of $cBid_G$ molecules in complex with Bax_R vs. the D of $cBid_G$ in individual GUVs (30% CL; n = 8). **d**, Temporal evolution of %CC between $cBid_G$ and Bax_R in a single GUV. The red arrow marks the time point at which the GUV was permeabilized (see also Supplemental Fig. 4.17). **e**, Comparison of %CC between membrane-embedded Bax_R (90% labeled) and Bcl-xL_G (100% labeled) or Bcl-xLΔCT$_G$ (90% labeled) in individual GUVs (30% CL). Protein insertion into the membrane was activated by cBid or heat, as indicated (n = 3). **f**, Percentage of membrane embedded Bcl-xL or Bcl-xLΔCT molecules in complex with Bax in relation to the absolute concentration of Bcl-xL (after activation by cBid (black dots) or heat (red dots)) or Bcl-xLΔCT (blue triangles) (n = 3). **g**, Percentage of membrane-embedded Bax molecules in complex with Bcl-xL (after activation by cBid (black dots) or heat (red dots)) or Bcl-xLΔCT (blue triangles) in relation to the absolute concentration of Bax (n = 3). The dotted red line in **a**, **d**, and **d** indicates the maximal possible CC considering the degree of labeling and dimer formation (n = 3). **e-g** Experiments done with one protein batch so that the results can be directly compared

et al., 2013b). To overcome this difficulty, we incubated cBid, Bax_G, and GUVs for 30 min prior to Bcl-xL_R addition, which allowed Bax to insert into the membrane before Bcl-xL was added. This experiment revealed two important facts. First, a direct interaction between Bax and Bcl-xL is possible, but takes place only in the membrane-bound state. Second, Bcl-xL interacts more strongly with cBid, when both partners are present, which indicates that Bcl-xL has a higher affinity for cBid than for Bax.

4.3.8 The presence of Bcl-xL reduces the size of Bax oligomers

These results raised the question of the functional impact of Bcl-xL on Bax oligomerization in membranes, which we addressed by comparing the CC between membrane-embedded Bax_G and Bax_R in presence and absence of Bcl-xL (Fig. 4.4c, d). To visualize Bcl-xL binding to GUVs, we used Bcl-xL_{405} (labeled with Alexa 405), which was imaged in a third detection channel. The experiment was done after inducing Bax and Bcl-xL membrane insertion either with heat or cBid. When heat was used, Bax_R, Bax_G, and Bcl-xL_{405} were added simultaneously to the GUVs, whereas when cBid was used, Bcl-xL_{405} was added after Bax oligomer formation. In both cases, Bcl-xL_{405} decreased the average CC between Bax molecules, indicating that Bcl-xL inhibited Bax oligomerization or reduced the oligomer size (Fig. 4.4d and (Subburaj et al., 2015)). This suggests that Bcl-xL is able to bind to the membrane-embedded, active conformation of Bax.
FCCS is an equilibrium method that cannot establish the order of events for single molecules or the stoichiometry within complexes. Thus, we cannot distinguish whether Bcl-xL binds to and disassembles large Bax oligomers or whether it preferentially binds to monomers or dimers, preventing them from forming larger oligomers. However, we observed that membrane-embedded Bcl-xL diffused slightly faster in presence of cBid than in presence of Bax (Supplementary Fig. 4.16E), which suggests that Bax/Bcl-xL hetero-complexes are bigger as cBid/BclxL dimers. This supports the idea that Bcl-xL is able to bind Bax oligomers, and suggests that one Bcl-xL molecule is able to inhibit more than one Bax molecule. However, we cannot discard the possibility that Bcl-xL preferentially binds Bax monomers.

4.3.9 Bcl-xL C-terminus regulates the preference of interactions

Until recently, most of the work done with recombinant Bcl-2 proteins used truncated proteins without the C-terminal membrane-anchoring helix. We tested the implications of this truncation on Bcl-2 interactions, because this helix has been related to homo-complex and hetero-complex formation, (Bleicken et al., 2014; Jeong et al., 2004; Zhang et al., 2016; Andreu-Fernández et al., 2017) and removal of the helix interfered with homo-dimerization (Jeong et al., 2004) as well as with Bax retro-translocation (Todt et al., 2013; O'Neill et al., 2016). To do so, we compared the interaction of Bax_R with full length Bcl-xL_G and Bcl-$xL\Delta CT_G$ (Fig. 4.6e-g). Similar to the full-length version, Bcl-$xL\Delta CT_G$ did not interact with Bax_R in solution (data not shown). However, in contrast to full-length Bcl-xL, the truncated protein failed to inhibit Bax membrane insertion, and once in the membrane, it interacted with Bax_R even in the presence cBid (Fig. 4.6e-g). This

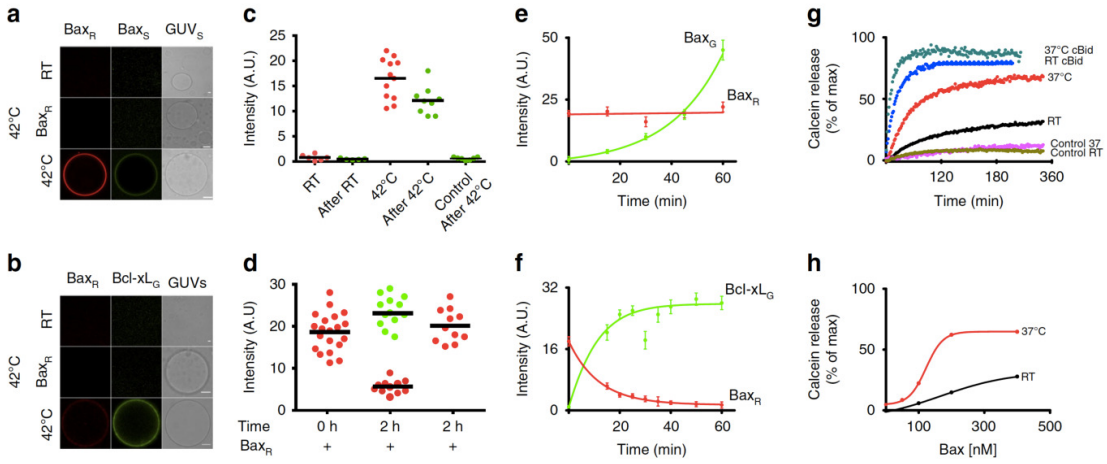

Figure 4.7: **Bax auto-activation and retrotranslocation in model membranes. a**, Bax_G binding to GUVs (30% CL) with or without membrane-embedded Bax_R at room temperature (RT) and after incubation at 42 °C for 30 min. (Scale bar: 10 µm). **b**, Binding of Bcl-xL_G to 30% CL GUVs containing or not Bax_R at RT and 42 °C for 30 min. **c**, Quantification of Bax_R (red dots) and Bax_G (green dots) binding to individual GUVs before and after incubation at RT or 42 °C. The control corresponds to samples treated at 42 °C but in the absence of Bax_R. (Black line represents mean of the distribution). **d**, Quantification of Bax_R (red dots) and Bcl-xL_G (green dots) binding to individual GUVs after heat activation (0 h after Bcl-xL addition) and after 2 h incubation at RT in presence and absence of Bcl-xL. (Black line represents mean of the distribution). **e**, Temporal evolution of Bax_R (previously bound by incubation at 42 °C) and Bax_G intensity on GUVs at RT. (Error bars represent s.d. of n = 3 experiments). **f**, Temporal evolution of Bax_R (previously bound by incubation at 42 °C) and Bcl-xL_G intensity on GUVs at RT. (Error bars represent s.d. of the average intensity of all GUVs in three experiments). **g**, Kinetics of calcein release from LUVs, comparing 200 nM Bax activity at ∼ 37 °C and RT in the presence and absence of 20 nM cBid. **h**, Dose response curve of % calcein release at varying Bax concentration at ∼ 37 °C as compared to RT. For all experiments n = 3

demonstrates that the C-terminal helix of Bcl-xL tunes the hierarchy of interactions with other Bcl-2 family members.

4.3.10 Membrane-bound Bax can recruit soluble Bax and Bcl-xL.

After analyzing the interactions between Bax, cBid, and Bcl-xL in solution and in membranes, we examined the translocation between both environments. We took advantage of direct visualization of protein binding to GUV membranes and investigated protein recruitment and retro-translocation. The presence of all three proteins leads to cBid and Bcl-xL translocation to the membrane, whereas Bax stays largely in solution (Bleicken et al., 2013b). Recently, it was suggested that membrane-bound Bax recruits soluble Bax via an auto-activation mechanism (Zhang et al., 2016). To test this hypothesis, we incubated 30% CL GUVs with Bax_R at 42 °C, inducing Bax_R association to the membrane (Fig. 4.7a, c). After cooling down, we added Bax_G molecules, incubated for 1 h at RT and imaged the vesicles. Bax_G bound to GUVs, confirming that membrane-bound Bax can recruit soluble Bax molecules (Fig. 4.7a, c, e). Binding did not happen when Bax_R was

absent or not treated with heat. To our surprise, membrane-associated Bax_R recruited not only soluble Bax_G but also soluble Bcl-xL_G to the membrane (Figs. 4.7b, d). The accumulation of Bcl-xL_G on the membrane was accompanied by a decrease in the mean fluorescence intensity of membrane-bound Bax_R (Fig. 4.7b, d), indicating that Bcl-xL_G promoted the release of Bax molecules from the membrane into solution. The kinetics of this association/dissociation processes are shown in Fig. 4.7e, f. Interestingly, Bax recruitment to the membrane increased with the amount of Bax associated to the membrane, supporting a positive feedback mechanism. In contrast, the association of Bcl-xL to the membrane was faster initially, when most Bax molecules were membrane-bound, and decreased with time as the concentration of Bax in the membrane decreased (Fig. 4.7e, f). Thus, membrane-bound Bax recruits Bcl-xL to the membrane without positive feedback or additional recruitment of Bcl-xL by Bcl-xL. Most importantly, our data show that Bcl-xL promotes the dissociation of Bax from the membrane in the absence of any additional component. To our knowledge, this is the first measurement of Bax retrotranslocation in recombinant systems.

These findings suggest that the energy barrier for Bax binding to the membrane, which is the limiting step in activation, is low. Indeed, in absence of all other Bcl-2 proteins, low expression of Bax in cells leads to its spontaneous activation, characterized by accumulation at the MOM and cell death (O'Neill et al., 2016). To determine the role of temperature in Bax activation, we performed vesicle content release assays at RT or 37 °C (Fig. 4.7g, h). Spontaneous activation of Bax was negligible at RT, whereas incubation at 37 °C induced significant permeabilization of the membrane even in absence of cBid. As expected, at both temperatures, addition of cBid led to full and faster membrane permeabilization. Altogether, these findings demonstrate that Bax can spontaneously activate at physiological temperature, which is amplified by a positive feedback mechanism.

4.4 Discussion

Here we report quantitative analysis of the interactions within a minimal Bcl-2 network that takes into account the spatial regulation of complexes in solution and membranes. One important finding is that the association of Bcl-2 proteins changes markedly upon membrane insertion, which is most likely due to the conformational changes associated with the process (Bleicken et al., 2014; Wang and Tjandra, 2013). In solution, Bax was monomeric, whereas cBid was present as a complex between its two fragments or associated with Bcl-xL. Bcl-xL itself hardly existed as a monomer, but formed homo-dimers and hetero-dimers with cBid (Fig. 4.8).

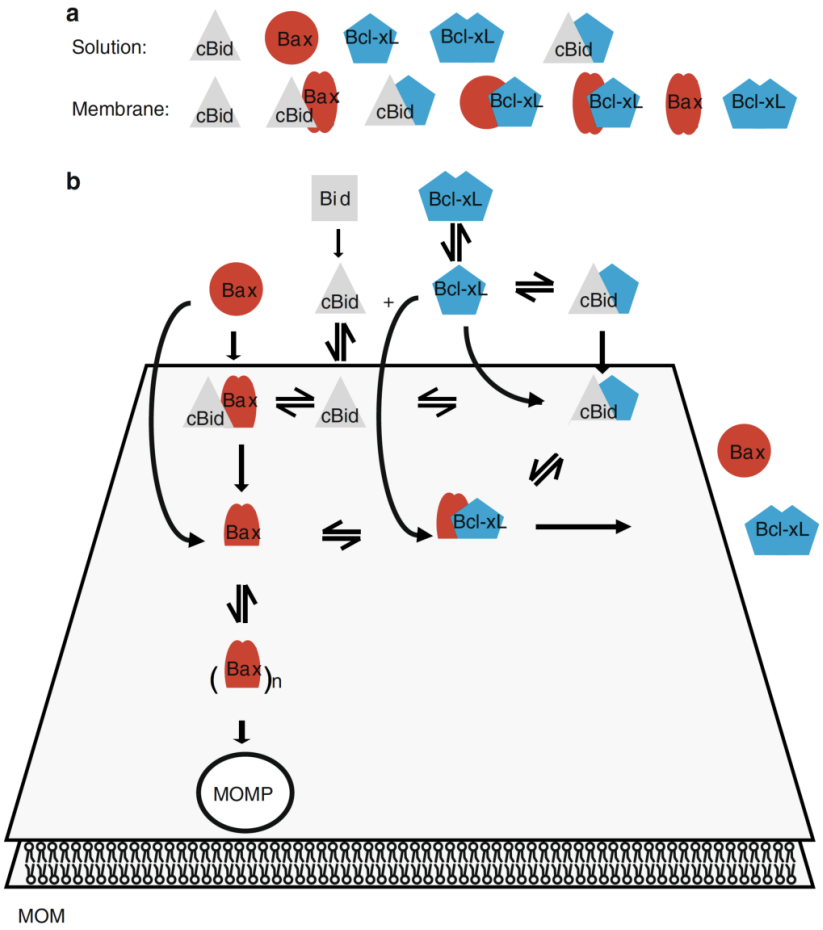

Figure 4.8: **Integrated model for the multiple interactions between Bcl-2 proteins in solution and in membranes to regulate MOM permeabilization.** **a**, Species detected in solution and membranes. Bax is schematically shown in two conformations corresponding to monomeric as filled red circles and the membraneembedded as two red, filled ovals. For the Bax/Bcl-xL complex, we showed that a complex containing oligomeric Bax exists, whereas we suggest the existence of the complex containing monomeric Bax. **b**, Schematic representation of an integrated model of Bcl-2 protein interaction network in solution and at the MOM. *MOM* mitochondrial outer membrane

The existence of soluble Bcl-xL and Bax homo-dimers is strongly debated. Bcl-xL homo-dimers were detected in cells (Jeong et al., 2004), but structural data are controversial (Yao et al., 2015; O'Neill et al., 2006; Denisov et al., 2007). Jeong et al. (Jeong et al., 2004) showed that the C-terminal helix of Bcl-xL is critical for homodimerization and suggested that the helix of one monomer would bind to the hydrophobic groove of the second one, enabling dimerization. We found this hypothesis intriguing, as the C-terminal helix would be shielded in the dimer (Supplementary Fig. 4.18), which could explain why a fraction of Bcl-xL is cytosolic in cells despite the membrane anchor. Our data support this model, as we detected stable Bcl-xL dimers that dissociated by the addition of cBid. In this scenario, the C-terminal helix and the BH3 domain of cBid compete for the same binding site (the BH groove) (Czabotar et al., 2013), which provides a molecular basis

for how cBid facilitates Bcl-xL membrane insertion by displacing the membrane anchor (Supplementary Fig. 4.18B).

In contrast to our results, the existence of soluble Bax homo-dimers and oligomers was recently reported (Garner et al., 2016; Sung et al., 2015). Garner et al. (Garner et al., 2016) detected autoinhibited Bax homo-dimers in the cytosol of the cell extracts of a number of cell lines, whereas in other cell lines, no Bax homo-dimers were found, suggesting that a very specific regulation might be necessary. Thus, the fact that we did not detect these dimers suggests that dimerization in solution requires additional factors (e.g., chaperones) or modifications absent in our system. Sung et al. (Sung et al., 2015) reported the oligomerization of soluble Bax upon incubation with BH3-only peptides at millimolar Bax concentrations. We never detected similar oligomers upon addition of cBid in the nanomolar (analyzed here) to micromolar (Bleicken et al., 2010) range. However, incubation of BaxΔC and BH3 peptides produced non-physiological swapped-dimers (Czabotar et al., 2013) and we cannot discard that the soluble Bax oligomers in (Sung et al., 2015) are multimers of swapped-dimers formed at very high protein concentrations.

Upon membrane insertion, the Bcl-2 interaction network strongly changed. Bax was always part of complexes with itself, with cBid, or with Bcl-xL, whereas Bcl-xL existed in complex with cBid or with Bax, or in the absence of both, as a mixture of monomers and homo-complexes (Fig. 4.8). This indicates that the affinity of Bcl-xL to itself is lower than the affinity to cBid or Bax molecules. A transient interaction between cBid and Bax has been proposed as part of the "hit-and-run" model. Here, we provide additional evidence for the cBid/Bax complex and for its dissociation upon Bax homo-oligomization. This is in line with the fact that one Bax oligomerization interface overlaps with the binding site for cBid (Czabotar et al., 2013).

Despite the many models proposed for the regulation of Bax activation by the other Bcl-2 proteins, the lack of direct detection of Bax/Bcl-xL complexes in membranes and the lack of a quantitative characterization of the different interactions had left a key question open. When all proteins are present, does Bcl-xL inhibit apoptosis mainly by blocking the activators, like cBid, or the executioners, like Bax? Our results point to the first, as the affinity between Bcl-xL and cBid is larger than between Bcl-xL and Bax. This also explains why BH3 mimetics are efficient inducing apoptosis. Most likely they would not be as effective if Bcl-xL/Bax interactions were the stronger ones. Remarkably, our data showed that deletion of the C-terminal anchor of Bcl-xL altered its interaction preferences. This is likely due to the participation of the C-terminal helix in interaction surfaces (Bleicken et al., 2014; Zhang et al., 2016; Andreu-Fernández et al., 2017). Our data are at odds with the claim that Mode 2 inhibition is more efficient than Mode 1 inhibition in

the unified model, but these studies where performed using C terminally truncated prosurvival Bcl-2 homologs (Llambi et al., 2011). Thus, caution should be exercised when interpreting experiments performed with truncated Bcl-2 members.

Our findings shed new light on Bax activation and inhibition. Recent work showed that in cells lacking all Bcl-2 proteins, Rb, and p53, reintroduction of Bax led to its spontaneous activation and cell death even at low Bax expression levels (O'Neill et al., 2016), in favor of the indirect activation model. However, the direct activation model is supported by the fact that Bax can be produced *in vitro* in an inactive form that can be activated by BH3-only activators to form membrane pores (Bleicken et al., 2013a; Lovell et al., 2008), as well as by the structural data of BH3 peptides bound to Bax (Czabotar et al., 2013). To reconcile both views, it is important to consider that activating Bax in absence of BH3 activators is also relatively easy: it can be achieved *in vitro* by exposure to mild heat (Subburaj et al., 2015; Pagliari et al., 2005), acidic pH (Cartron et al., 2004b), detergents (Kuwana et al., 2002), or proteins like Drp1 (Montessuit et al., 2010). This all argues for a low energy barrier for Bax activation, in the order of thermal energy at physiological temperature. Here, we show that without activator molecules Bax remains inactive at RT, but presents a significant membrane permeabilizing activity at 37 °C. Once in the membrane, Bax promotes recruitment of soluble Bax. In the context of the cell, a small fraction of Bax molecules could spontaneously become active, which could be kept in place by complex formation with prosurvival Bcl-2 homologs. In agreement with this, we show that membrane-bound, active Bax-recruited Bcl-xL to the membrane and formed complexes with it, which led to a release of Bax from the membrane back into solution and to a reduction in Bax oligomer size. The protein retro-translocation into solution also supports a low energy barrier for dissociation of Bax/Bcl-xL complexes from the membrane. This barrier could be overcome by the high affinity between Bcl-xL monomers in solution, providing the necessary driving force for Bax retro-translocation. Moreover, the fact that membrane-bound Bax can recruit Bax and Bcl-xL supports a common molecular mechanism for both processes that was so far unanticipated, and it demonstrates that Bcl-xL is sufficient to retro-translocate Bax from the membrane back into solution.

Our observations link so-far unconnected observations: the low fraction of Bax/Bcl-xL complexes naturally found in mitochondria (Chen et al., 2015); the finding that in cells lacking direct activators, Bax and Bak can still be activated and their activation depends on the absence of prosurvival Bcl-2 proteins (Chen et al., 2015; O'Neill et al., 2016); and the spontaneous minority MOM permeabilization observed when prosurvival Bcl-2 proteins are inhibited with ABT-737 (Ichim et al., 2015). It is important to consider that in cells, the Bcl-2 regulation network is much more complex and includes additional factors

and post-translational modifications that add a layer of complexity to the observations reported here. Moreover, beyond their function in MOMP, Bcl-2 proteins have been associated with regulatory functions in mitochondrial dynamics and Ca^{2+} homeostasis (Youle and Strasser, 2008; Youle and Karbowski, 2005; Karbowski et al., 2006; Vervliet et al., 2016). The underlying mechanisms are not completely understood, but several Bcl-2 proteins are proposed to interact with MOM or ER membrane proteins without inducing MOM permeabilization (Youle and Strasser, 2008; Youle and Karbowski, 2005; Karbowski et al., 2006; Vervliet et al., 2016). Therefore, the regulation of Bcl-2 protein function is more complex than considered so far, which could potentially also be examined with the system developed here.

On the basis of our findings, we propose a new, "integrated" model that explains how the multiple, parallel interactions between the Bcl-2 proteins are orchestrated to regulate apoptosis (Fig. 4.8). In absence of proapoptotic stimuli, Bax activation could proceed spontaneously. The membrane-bound Bax molecules could behave as seeding points for further Bax recruitment from solution in a positive feedback loop (here and (Subburaj et al., 2015; Chen et al., 2015; O'Neill et al., 2016)). Direct interaction with prosurvival Bcl-2 homologs in the membrane would inhibit MOM permeabilization by relocation of loosely bound Bax molecules from the membrane to the cytosol, and it would additionally block the oligomerization of membrane-embedded Bax. In the presence of proapoptotic stimuli, the activation of BH3-only proteins would be first inhibited by direct association with the prosurvival Bcl-2 proteins, for which they have a higher affinity. In this scenario, a low level of Bax activation would still be counterbalanced by excess prosurvival Bcl-2s, but would prime the cells to die (Letai et al., 2002; Certo et al., 2006). On the basis of literature data, continued stress would further increase the levels of BH3-only proteins. Above a certain threshold in the relative concentration of proapoptotic vs. prosurvival Bcl-2 proteins, the prosurvival Bcl-2 homologs would be engaged mostly with BH3-only proteins and would not be able to sustain the steady state of Bax activation/inactivation, which would turn the balance and switch towards Bax activation and MOM permeabilization. In situations with intense cellular stress, any additional excess of BH3-only proteins would create a pool of free direct activators that would promote a rapid and efficient activation of Bax and Bak, full MOM permeabilization, and cell death.

In summary, the minimal network reported here explains the spatial regulation of Bcl-2 complexes in solution and membranes. We disentangle the hierarchy of competing reactions, as well as the modulatory role of the membrane and the C-terminal anchor, which has implications for the prevalence of the different inhibition modes depending on the environment and proteins present. At physiological temperatures, a fraction of Bax

molecules spontaneously activates. These molecules can recruit to the membrane additional soluble Bax to promote MOM permeabilization, as well as soluble Bcl-xL, which inhibits Bax homo-oligomerization and releases Bax back into solution, thereby inhibiting MOM permeabilization. Altogether, these findings support an integrated model for Bcl-2 proteins that reconciles previously opposing experimental observations.

4.5 Methods

Protein production and labeling

Full length mouse Bid (wild type, Bid C30S, or Bid C126S), full length human Bax (wild type and Bax S4C, C62S, C126S), and full length human Bcl-xL (wild type and Bcl-xL S4C, C151A) were expressed in *E. coli* BL21/RILP cells (Stratagene, now Agilent, Santa Clara, CA). Bacterial cultures were started at 37 °C at $OD_{600} \sim 0.03$. Protein expression was induced with 1 mM IPTG at $OD_{600} \sim 0.5$ followed by 4 h incubation at 20 °C. Cells were harvested by centrifugation at 6000 xg for 20 min. The cell pellets were shock-frozen in liquid nitrogen and stored at -80 °C. Before purification, the cells were thawed on ice, resolved in buffer, and broken on ice by five passages though an Emulsiflex C5 (Avestin, Mannheim, Germany). Afterwards, ∼1-200 U DNase I were added per liter bacterial culture (Merck, Darmstadt, Germany) and the mixture was incubated 30 min on ice. Then unbroken cells and membranes were removed by centrifugation at 25,000 rpm (60 min at 4 °C; using a JA25.50 rotor in a Beckmann Avanti centrifuge (Beckman Coulter, Brea, CA). Bid variants were purified using Nickel-NTA beads (Qiagen, Hilden, Germany) as the protein has an N-terminal His tag (plasmid pET23-His-Bid). Purification was done using 5 ml Nickel-NTA beads loaded into an empty gravity flow column. Buffers and purification steps were done following the manufacturer instructions, and protein elution was done by step a gradient adding (Bleicken et al., 2014), 25, and 250 nM Imidazol (in buffer). Protein purity was tested by SDS-PAGE showing about 95% purity. Afterwards to buffer was replaced by the caspase 8 cleavage buffer (50 mM NaCl, 5 mM DTT, 0.5 mM EDTA, 25 mM HEPES, 5% Sucrose; pH 7.4) using dialysis. Bid was cleaved to cBid by 4 h incubation with caspase 8 (at RT, Bid/Caspase 8 ratio ∼1000:1; Caspase 8 was a gift J.-C. Martinou). Afterwards, a second purification (again based on Nickel-NTA) was done to remove Caspase 8, followed by an SDS PAGE performed to control protein purity (>95% see Supplemental Fig. 4.9E). Bax and Bcl-xL variants were expressed as intein-fusion proteins using the IMPACT-system from NEB (NEB, Ipswich, MA; plasmids pTYB1-BaxWT, pTYB1-Bax S4C, C62S, C126S, pTYB1-Bcl-xLWT, or pTYB1-Bcl-XL S4C, C151A). Buffers and purification were done following the manufacturer instructions.

Samples were always kept on ice or at 4 °C and the cleavage reaction was done ∼ 16 h at 4 °C. After elution protein purity was tested based on SDS-PAGE showing about ∼ 90% purity. To remove residual impurities the sample was further purified using an anion exchange column (using a HiTrap Q column from GE healthcare on an AKTA purifier FPLC system from GE healthcare). First, the buffer was exchanged to 20mM TRIS, pH 8 by dialysis to afterwards load the protein onto the column. The bound protein was washed with >20 column volumes (CV) of the buffer and then eluted with a gradient (8 CV) of high salt buffer (1 M NaCl, 20 mM TRIS, pH 8). The elution fractions were analyzed by SDS-PAGE (purity >95%, see Supplemental Fig. 4.9E) and finally, the buffer was exchanged using dialysis (to 150 mM NaCl, 20 mM TRIS, pH 7.5 or 150 mM NaCL, 20 mM HEPES, pH 7.5). The wild type proteins were aliquoted in 10 µl portions and shock-frozen in liquid nitrogen. Protein mutants were labeled before freezing (with Alexa 488-maleimide and Alexa 633-maleimide in the case of the cBid and ATTO 488-maleimide or ATTO 655-maleimide in the case of Bax and Bcl-xL). For labeling, the protein was incubated with threefold excess TCEP for 30 min on ice. Afterwards, a tenfold excess of the label was added and the sample incubated 2 h at 4 °C, before another fivefold excess of label was added and the sample incubated over night at 4 °C. Free label and protein were separated using desalting columns, and the degree of labeling was calculated using a combination of UV-VIS spectroscopy, Bradford assays, and ESI-LC-MS.

Composition of the lipid mixtures

The lipid mixture mimicking the MOM had a composition of 49% egg L-α-phosphatidyl choline (PC), 27% egg L-αphosphatidyl ethanolamine (PE), 10% bovine liver L-α-phosphatidyl inositol (PI), 10% 18:1 phosphatidyl serine (PS) and 4% CL (all percentages mol/-mol). Moreover lipid mixtures composed of 30% CL and 70% PC or 20% CL and 70% PC (mol/mol) were used. All lipids were purchased from Avanti polar lipids (Alabaster, AL) and mixed in chloroform. Afterwards the chloroform was evaporated overnight under vacuum and then flushed with nitrogen or argon gas and stored at -28 °C.

GUV formation and sample preparation

GUVs were produced by electro-formation and the experiments were done as described in (Bleicken et al., 2013b). Briefly, 5 µg lipid mixture dissolved in chloroform were spread on each platinum electrode of the electro-formation chamber and allowed to dry, before immersion in 300 mM sucrose. Electro-formation proceeded for 2 h at 10 Hz, followed by 30 min at 2 Hz. Overall, 75 to 100 µl of the GUVs suspension was added to a solution of buffer mixed with the proteins of interest in Lab-Tek 8-well chamber slides (NUNC) to a

final volume of 300 µl.
For experiments of Bax and Bcl-xL binding to GUVs, the sample mixtures were prepared in 8-well Lab-Tek chamber slides (NUNC) in buffer (150 mM NaCl, 20 mM Tris, pH 7.5) and 80 µl of GUV suspension, in total volume of 300 µl. The working concentration of Bax_R, Bax_G, and Bcl-xL_G were 0.5-200 nM, respectively. To monitor Bax auto-activation, Bax_R was incubated at 42 °C for 30 min, allowed to cool down to RT for 1 h, followed by subsequent addition of Bax_G at RT and incubation for 1 h. The binding of the proteins to GUVs was imaged using a LSM710 confocal microscope. For Bax retro-translocation in model membranes, Bax_R was heat activated at 42 °C for 30 min, cooled down to RT for 1 h, followed by the addition of Bcl-xL_G and incubation for 1 h at room temperature. To quantify the binding intensity of Bax_R, Bax_G, and Bcl-xL_G, the radial profile plugin of Image J was used with an integration angle of 60°. The background intensity was always taken into account for the intensity measurements. The curves were fitted using a nonlinear curve fitting function with sigmoidal dose response fit in Origin Lab.

Calcein permeabilization assay

LUVs composed of 80% PC and 20% CL were prepared by solving dried lipid mixtures in buffer (20 nM HEPES, pH 7.4 and 80 mM Calcein [fluorescein-bis-methyl-iminodiaceticacid at pH 7.5] with 4 mg mg^{-1} lipid) using intensive vortexing paused by five cycles of freezing and thawing. The multilamellar vesicles were passed 31 times through an extruder (Avestin) using membranes with 400 nm pore size (Avestin). Calcein was entrapped in the vesicles at a self-quenching concentration, so that its release in external medium was accompanied by an increase of the intensity of fluorescence. LUVs were incubated with different concentrations of Bax, varying from 0 to 400 nM at $\sim$ 37 °C in buffer (140 mM NaCl, 20 mM HEPES, 1 mM EDTA, pH 7.4) at room temperature with a lipid to protein concentration of >1:500 at the highest Bax concentration. The kinetics of calcein release were measured using a Tecan Infinite M200 microplate reader (Tecan, Männedorf, Switzerland).
The percentage of release R was calculated from the expression:

$$R = ((FS - F0) \div (Fmax - F0)) \times 100)$$

where, F0 is the initial fluorescence of LUVs, Fmax is the maximum fluorescence after addition of 5% TritonX-100, and FS is the equilibrium fluorescence in the sample of interest.

FCCS measurements

All FCCS experiments were performed using a LSM710 confocal microscope equipped with a Confocor3, a C-Apochromat 40 x N.A. 1.2 water immersion objective and laser to excite at 488 and 633 nm. Photons emitted from different fluorophores were separated by dichroic mirrors and detected by Avalanche photo diodes placed after suitable filters (for Atto/Alexa488, 505-540 nm band pass filter; for the far red dyes a >655 nm long pass filter). Each sample was measured at least 10,000x longer as their diffusion time to assure sufficient data points to generate the autocorrelation curves. To calculate the diffusion time (t_D), diffusion coefficients (D), protein concentration, and the cross-correlation, we assumed 3D Brownian diffusion and used the equations in Supplementary Table 4.1.
For solution FCS measurements, the proteins of interest were mixed with buffer (150 mM NaCl, 20 mM Tris, pH 7.5) in a total volume of 100-200 µl and incubated at least 30 min before measurements. Incubation and measurements were done in Lab-Tek 8-well chamber slides (NUNC) that were blocked with Casein (saturated solution in 150 mM NaCl, 20 mM TRIS, pH 7.5) before use. For all solution, FCCS measurements we did three technical repetitions and removed traces that contained large fluorescent particles disturbing the measurement. However, all n in the figure legends refer to experimental repetitions.
For scanning FCCS, we performed two-focus scanning FCCS measurements at 22 °C using a Confocor 3 module. Photon arrival times were recorded with a hardware correlator Flex 02-01D/C (http://correlator.com). We repeatedly scanned the detection volume with two perpendicular lines across a GUV equator (the distance between the two bleached lines d was measured on a film of dried fluorophores). Data analysis was performed with home-build software (García-Sáez et al., 2009). We binned the photon stream in 2 µs and arranged it as a matrix such that every row corresponded to one line scan. We corrected for membrane movements by calculating the maximum of a running average over several hundred line scans and shifting it to the same column. We fitted an average over all rows with a Gaussian and we added only the elements of each row between -2.5σ and 2.5σ to calculate the fluorescence intensity trace. We computed the auto-cross-correlation, spectral cross-correlation, and spatial cross-correlation curves from the intensity traces and excluded irregular curves resulting from instabilities and distortions. We fitted the auto-correlation and cross-correlation functions with a nonlinear least-squares global fitting algorithm as in (García-Sáez et al., 2009). The equations used are shown in Supplementary Table 4.1.
In scanning FCCS, each value measured refers to one GUV. In total, we did $n \geq 3$ independent experiments for each condition and interaction pair. In each experiment, we

measured several GUVs that are shown as individual data points. Overall, 25-50% of measured GUVs were not included in the analysis for three reasons: (1) The GUV moved out of the focal volume during the measurement time (300 s). (2) Identification of large aggregates/buds on the surface of the GUV (see Supplemental Fig. 4.15) that strongly affected the measurement. (3) Large changes in protein concentration in the membrane during the measurement. The experiments were set up as a way that GUVs were added with a lipid to protein ratio of ∼500:1 or higher.

Mathematical modeling

For each possible interaction scenario, an ODE-based model based on mass action kinetics was set up in COPASI (4.15, build 95) (Hoops et al., 2006). Differently labeled Bcl-xL proteins were included as separate species in the reactions.
Model parameters were fitted against four time courses of three different particle concentrations (Bcl-xL_G, Bcl-xL_R, and Bcl-xL_G/Bcl-xL_R) measured by FCS, with and without cBid addition. Bcl-xL_G particles denote Bcl-xL_G monomers and all possible multimers including at least one Bcl-xL_G (same for Bcl-xL_R particles). Bcl-xL_G/Bcl-xL_R particles denote any particles including at least one Bcl-xL_G and one Bcl-xL_R. Initial concentrations of monomeric and homo-dimeric Bcl-xL_G and Bcl-xL_R were included into parameter estimation (constrained between 0 and 10 nM).
For parameter fitting, first a global optimization method was applied by using the Evolutionary Programming algorithm in COPASI, where the population size was 10 times the number of parameters, and the maximum number of generations was 10 times the population size. To further improve the best parameter set found by the global optimization method, the local method "Hooke and Jeeves" from within COPASI was used with default parameter settings. This procedure was described in (Schaber et al., 2012).
The following objective function was used for parameter fitting (weighted SSR, sum of squared residuals):

$$SSR = \sum_{i,j} \omega_j \cdot (x_{i,j} - y_{i,j}(P))^2$$

with weight $\omega_j = \frac{1}{\langle x_j^2 \rangle}$; j = time course of one particle type; i = measurement at one time point; $x_{i,j}$ = measurement of one particle type at one time point; $y_{i,j}(P)$ = simulated value of one particle type at one time point given the parameter set P.
Bcl-xL_R and Bcl-xL_G were mixed and incubated 2 h at RT, before the first data point

was taken at t = -20. Afterwards, the sample was split into two parts: to one buffer was added at t = 0, to the other 400 nM cBid was added at t = 0, thereby the sample was diluted 1:1. The dilution was accounted for by assuming half particle concentrations in measurements at t = -20 min. To improve fit performance, measurement of buffer control sample at 0 min was added to the time course including cBid addition, which was possible because the time courses of buffer control and cBid addition were derived from the same reaction sample and only separated at t = 0 min. The value of cBid addition was set from t = 0 to 1 min, which is justifiable by relatively long measurement times of FCS for every time point (2 min per time point).

The experiments were corrected for unlabeled Bcl-xL proteins by adding an unlabeled Bcl-xL species to the ODE systems. Initial concentrations of unlabeled monomers, and (partially) unlabeled Bcl-xL dimers were calculated the following way, assuming that the label has no influence on association and dissociation behavior:

DOL•-labeling efficiency of Bcl-xL$_{\mathrm{G}}$ (B•); DOL○-labeling efficiency of Bcl-xL$_{\mathrm{R}}$ (B○)

unlabeled Bcl-xL monomer:

$$[B] = (1 - DOL_{B\circ}) \cdot \frac{[B\circ]}{DOL_{B\circ}} + (1 - DOL_{B\bullet}) \cdot \frac{[B\bullet]}{DOL_{B\bullet}}$$

unlabeled Bcl-xL homo-dimer:

$$[B - B] = (1 - DOL_{B\circ})^2 \cdot \frac{[B\circ - B\circ]}{DOL_{B\circ}^2} + (1 - DOL_{B\bullet})^2 \cdot \frac{[B\bullet - B\bullet]}{DOL_{B\bullet}^2}$$

Bcl-xL homo-dimer including one labeled Bcl-xL (correspondingly for B•-B):

$$[B\circ - B] = DOL_{B\circ}(1 - DOL_{B\circ}) \cdot 2 \cdot \frac{[B\circ - B\circ]}{DOL_{B\circ}^2}$$

The standard deviation shown in the particle time courses of Bcl-xL$_{\mathrm{G}}$-Bcl-xL$_{\mathrm{R}}$ particles was calculated the following way: 10,000 numbers were sampled from the cross-correlation (CC) value of Bcl-xL$_{\mathrm{G}}$ with Bcl-xL$_{\mathrm{R}}$ with a gaussian distribution around the measured mean with the measured standard deviation. The same procedure was applied vice versa (CC of Bcl-xL$_{\mathrm{R}}$ with Bcl-xL$_{\mathrm{G}}$). From these 20,000 values the mean and standard deviation were calculated. All ODE equations used are listed in Supplementary Table 4.3.

Differences in AIC$_{\mathrm{c}}$ (AIC corrected for small sample size) values and the Akaike weight w_{i} were calculated as following and as described elsewhere (Johnson and Omland, 2004): k = number of parameters; n = number of data points; R = number of tested models

$$AIC_c = 2k + n \cdot ln(SSR) + 2k \cdot \left(\frac{n}{n-k-1}\right)$$

$$\Delta_i = AIC_{c,i} - AIC_{c,min}$$

$$w_i = \frac{exp(-\Delta_i/2)}{\sum_{j=1}^{R} exp(-\Delta_j/2)}$$

Parameter identifiability analysis

Parameter identifiability analysis was performed and the 95% confidence regions of each parameter were determined as described in (Schaber, 2012). Briefly, the objective function was reoptimized for each parameter on discrete logarithmic steps surrounding the optimized parameter value p̂ with respect to all other parameters using the Hooke and Jeeves algorithm in COPASI. The confidence region was determined as described in (Schaber, 2012):
$P_{CR} = \left\{p : SSR(p) \leq SSR(\hat{p})\left(1 + \frac{k}{n-k}F^{\alpha}_{k,n-k}\right)\right\}$, where $F^{\alpha}_{k,n-k}$ is the upper α-critical value of the $F_{k,n-k}$ distribution.

4.6 Supplementary Information

4.6.1 Supplementary Figures

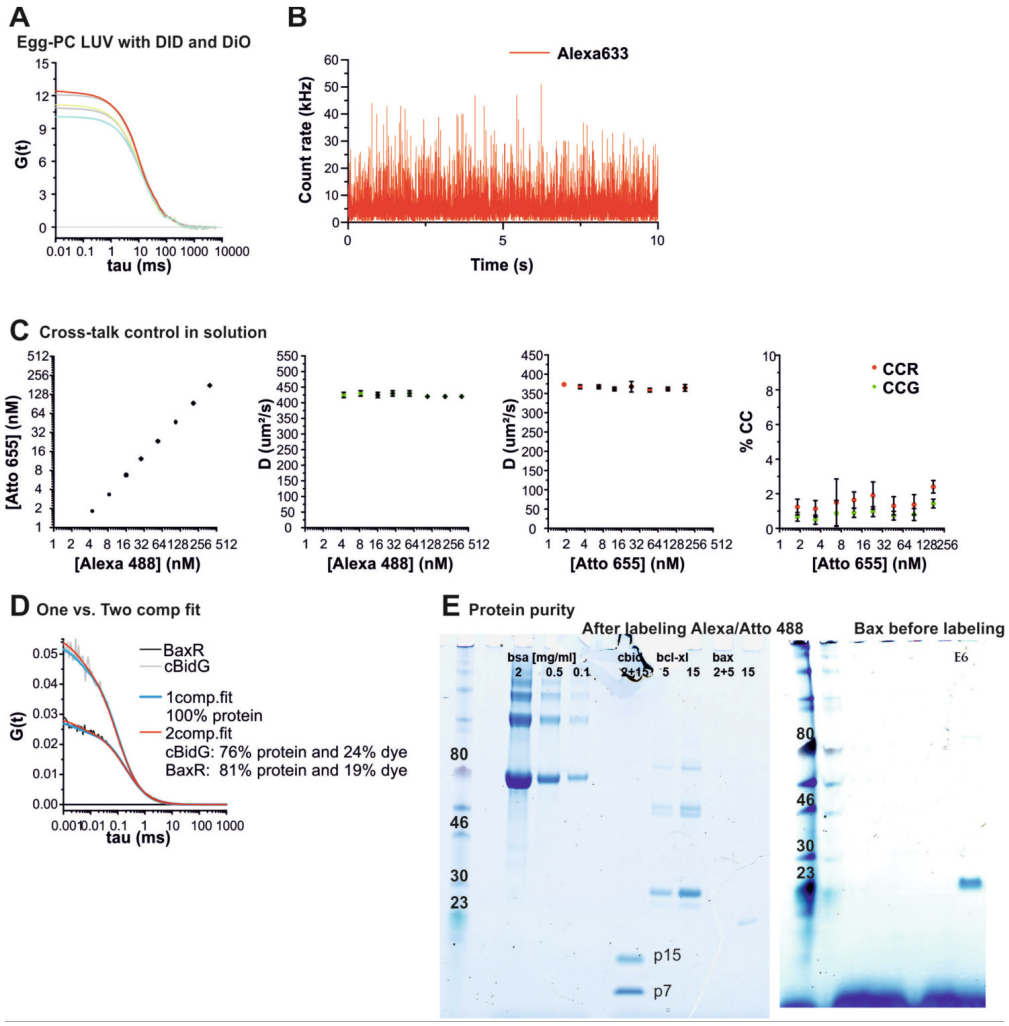

Figure 4.9: **Control measurements.** **A**, Exemplary AC and CC curves on egg PC LUVs containing >0.05% DiO and DiD. **B**, Exemplary fluorescence intensity trace on free Alexa633. **C**, Cross talk control using free Alexa488 and Atto655 mixed at different concentration. Shown is one (of n=3) exemplary experiment with mean and error bars as s.d. based on three technical repetitions. From n=3 independent experiments a %CC of μ:1.4, σ: 0.7 was calculated. The different graphs plot the protein concentration, the D of both molecules and the %CC. **D** Exemplary 1 component and 2 component fittings of the AC curves of Bax_R and $cBid_G$ in solution. **E**, SDS-PAGE of $cBid_G$, Bcl-xL_G and Bax_G and Bax before the labeling process as a visual guide for protein purity. More information in the Supplemental Methods.

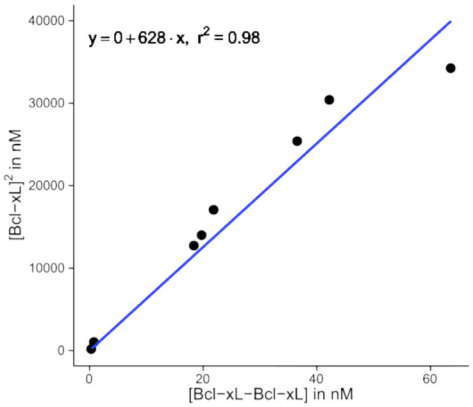

Figure 4.10: **Bcl-xL homodimerization as measured by FCS.** Theoretical K_D value of 628 nM calculated when assuming equilibrium conditions of Bcl-xL homodimerization of two differently labeled Bcl-xL proteins. Plotted is the squared concentration of free Bcl-xL proteins against the sum of all possible homodimeric Bcl-xL species (combinations of unlabeled and labeled proteins). Please note that the complex concentrations calculated from the labeling of the proteins and a Mendel-based distribution of red-red, green-green and red-green complexes, but not for partial overlap of the detection volumes. Data are from n=4 experiments.

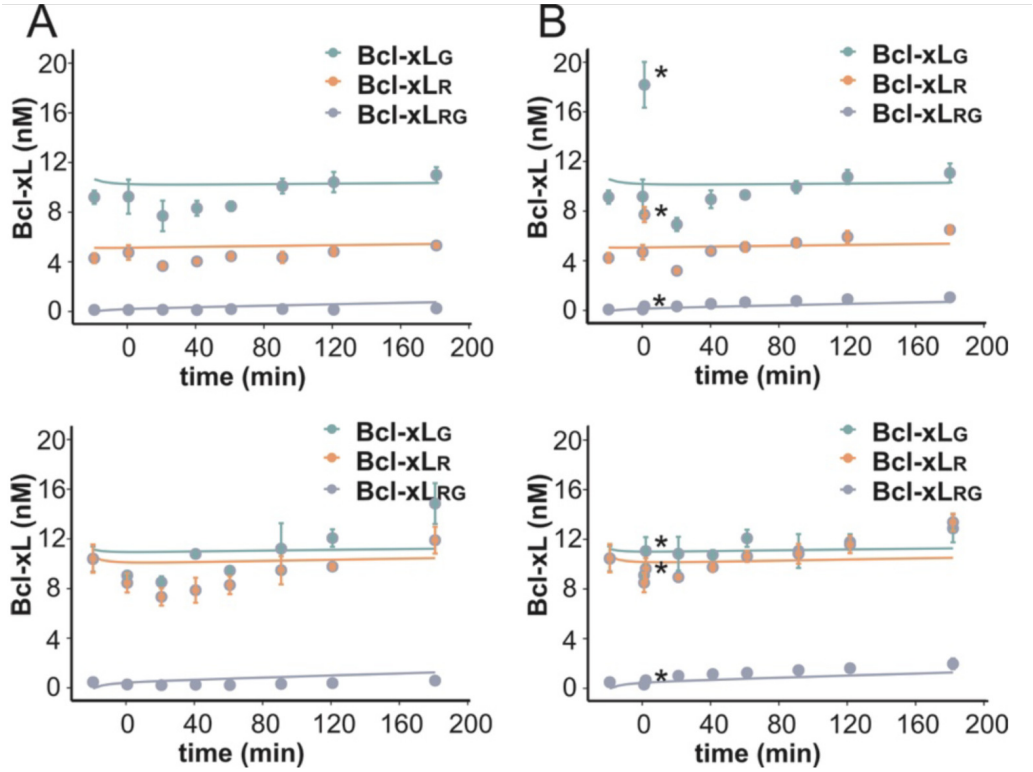

Figure 4.11: **Best fit of ODE model in scenario 1 to the kinetics of Bcl-xL dimerization measured by FCCS in Figure 4.3B. A**, Fitting to the control data after buffer addition and **B**, Fitting to the data after cBid addition. The upper and the lower panels show two independent experiments with mean and error bars as s.d. of three technical repetitions. To do the ODE fitting in B, we took the t=0 data point from A (without cBid). This is applicable as A and B present data of one sample split into two equal parts directly before measuring t=0. The first data point in presence of cBid is introduced as t=1min and highlighted in the figure by *. This is applicable as each data point had a total FCS measurement time of 2 min. The model corresponding to scenario 1 cannot qualitatively reproduce the occurrence of Bcl-xL_G-Bcl-xL_R dimer particles after addition of cBid. Instead, cross-correlating particles appear in same amounts irrespective of cBid addition.

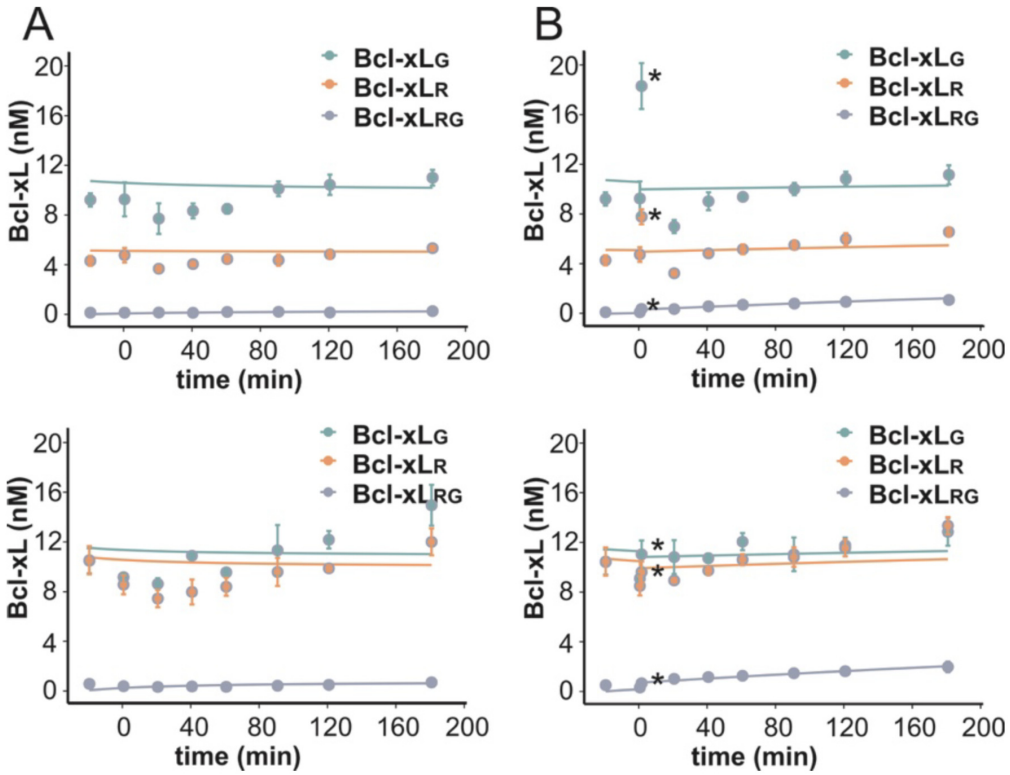

Figure 4.12: **Best fit of ODE model in scenario 3 to the kinetics of Bcl-xL dimerization measured by FCCS in Figure 4.3B. A**, Fitting to the control data after buffer addition and **B**, fitting to the data after cBid addition. The upper and the lower panel show two independent experiments with mean and error bars as s.d. of three technical repetitions. To do the ODE fitting in B, we took the t=0 data point from A (without cBid). This is applicable as A and B present data of one sample split into two equal parts directly before measuring t=0. The first data point in presence of cBid is introduced as t=1min and highlighted in the figure by *. This is applicable as each data point had a total FCS measurement time of 2 min.

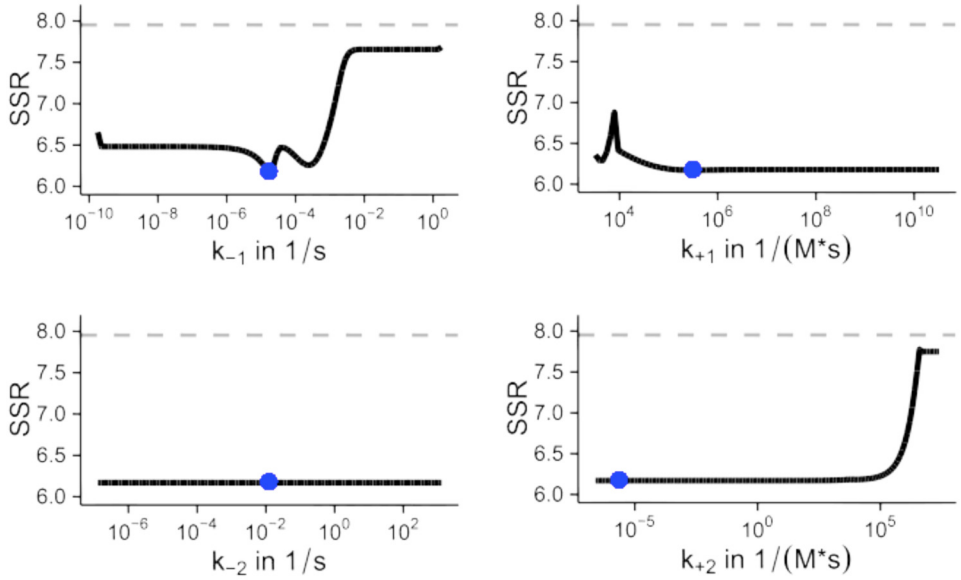

Figure 4.13: **Likelihood profiles of parameters defining rate constants of model of interaction scenario 1.** The fitted parameter is shown as blue dot, the re-optimized SSR is shown as black line and the dashed grey line indicates the confidence limit.

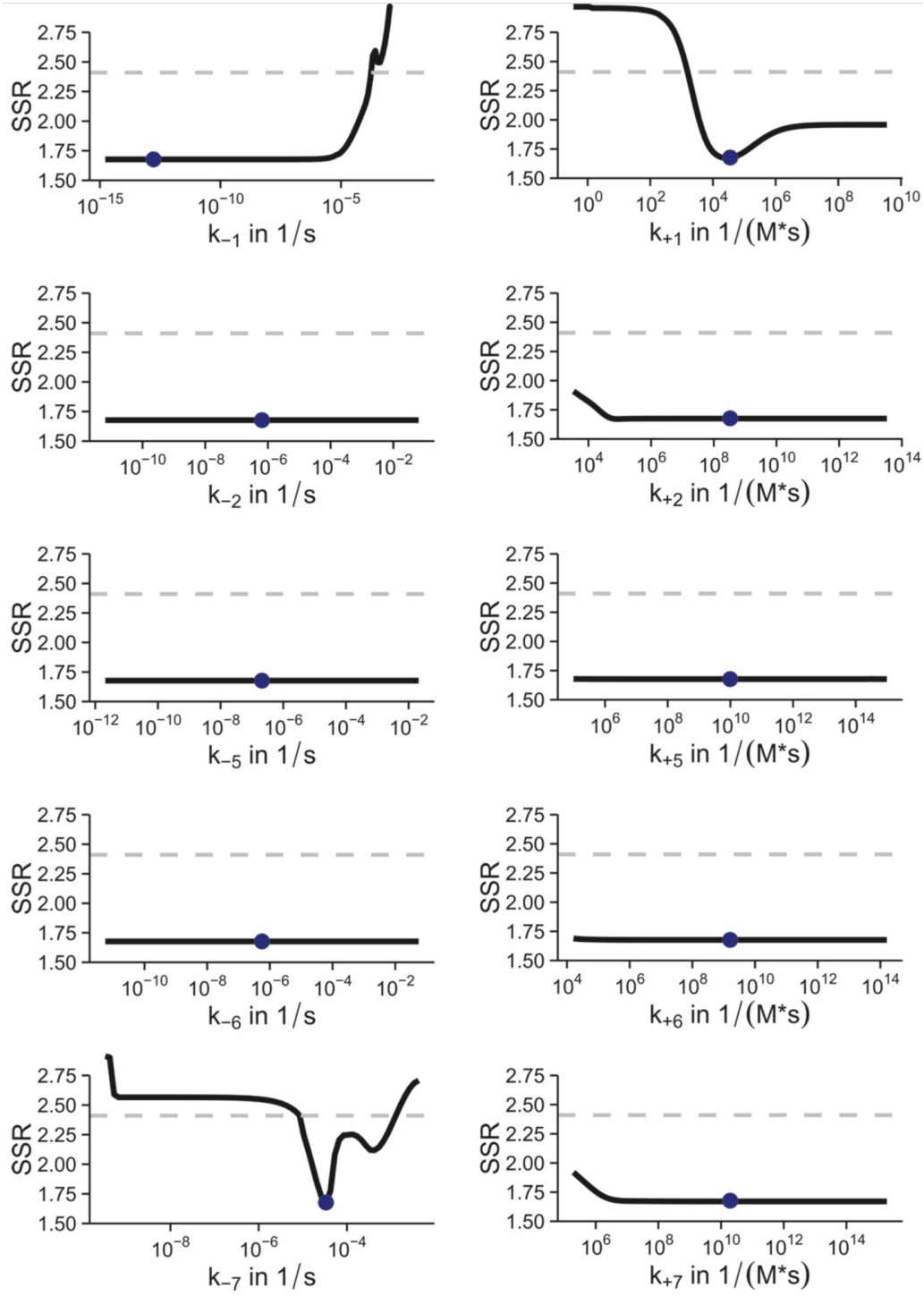

Figure 4.14: **Likelihood profiles of parameters defining rate constants of model of interaction scenario 3.** The fitted parameter is shown as blue dot, the re-optimized SSR is shown as black line and the dashed grey line indicates the confidence limit.

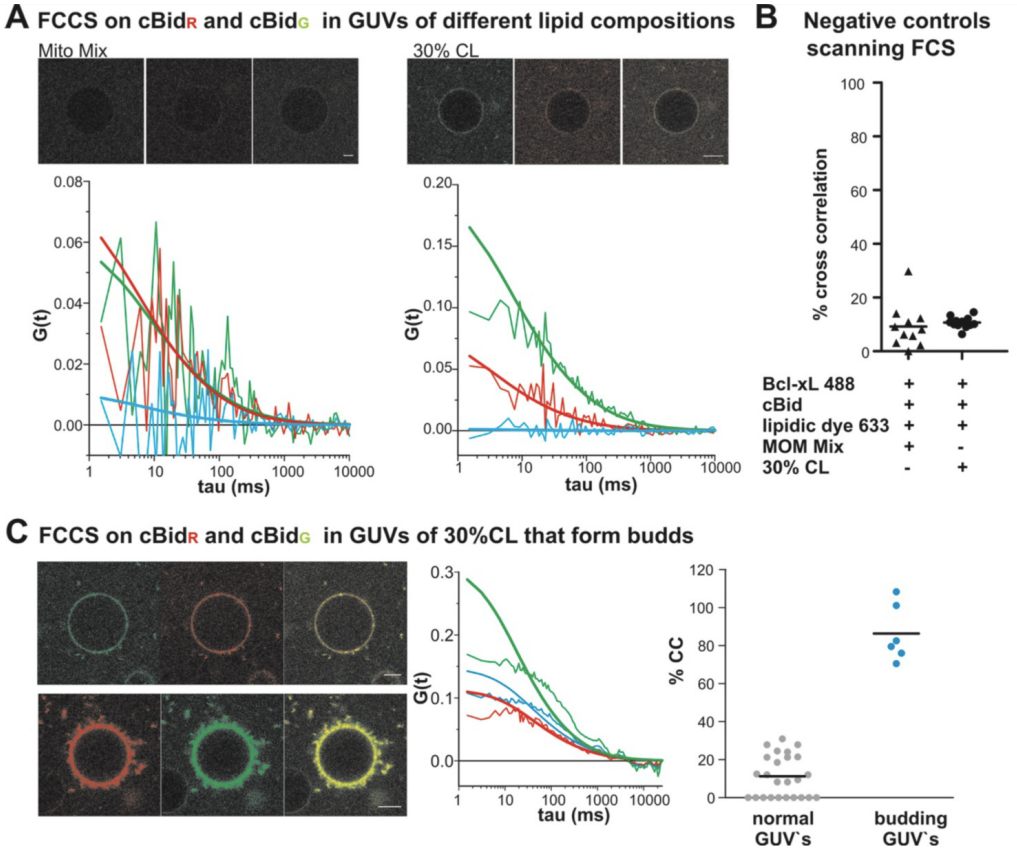

Figure 4.15: **Different test experiments in membranes. A**, AC- and CC curves of cBid molecules in GUVs using the lipid mixture mimicking the MOM or the 30% CL lipid mix. **B**, Negative controls for cross-correlation in membranes. As negative control the %CC between Bcl-xL$_G$ and DiD, two molecules not interacting was measured in both used lipid mixtures (n=3). **C**, Cross-correlation between cBid molecules in GUVs formed by 30% CL (n=4). Here, two different situations could be detected. GUVs with a smooth surface show a very low cross-correlation similar to the negative control (left panel upper GUV and right panel "normal GUVs". In contrast GUVs that show budding (left panel, lower GUV) showed high level of cross-correlation (right panel "budding GUVs"). Moreover, the AC and CC curves of budding GUVs showed a slow diffusion that could not be fitted properly to a 2D diffusion (middle panel). We assume that the curves describe the movements on buds on the GUV surface rather than single molecule diffusion in the membranes and as each bud contain likely several cBid molecules we detect a high %CC. Scale bar 10 µm.

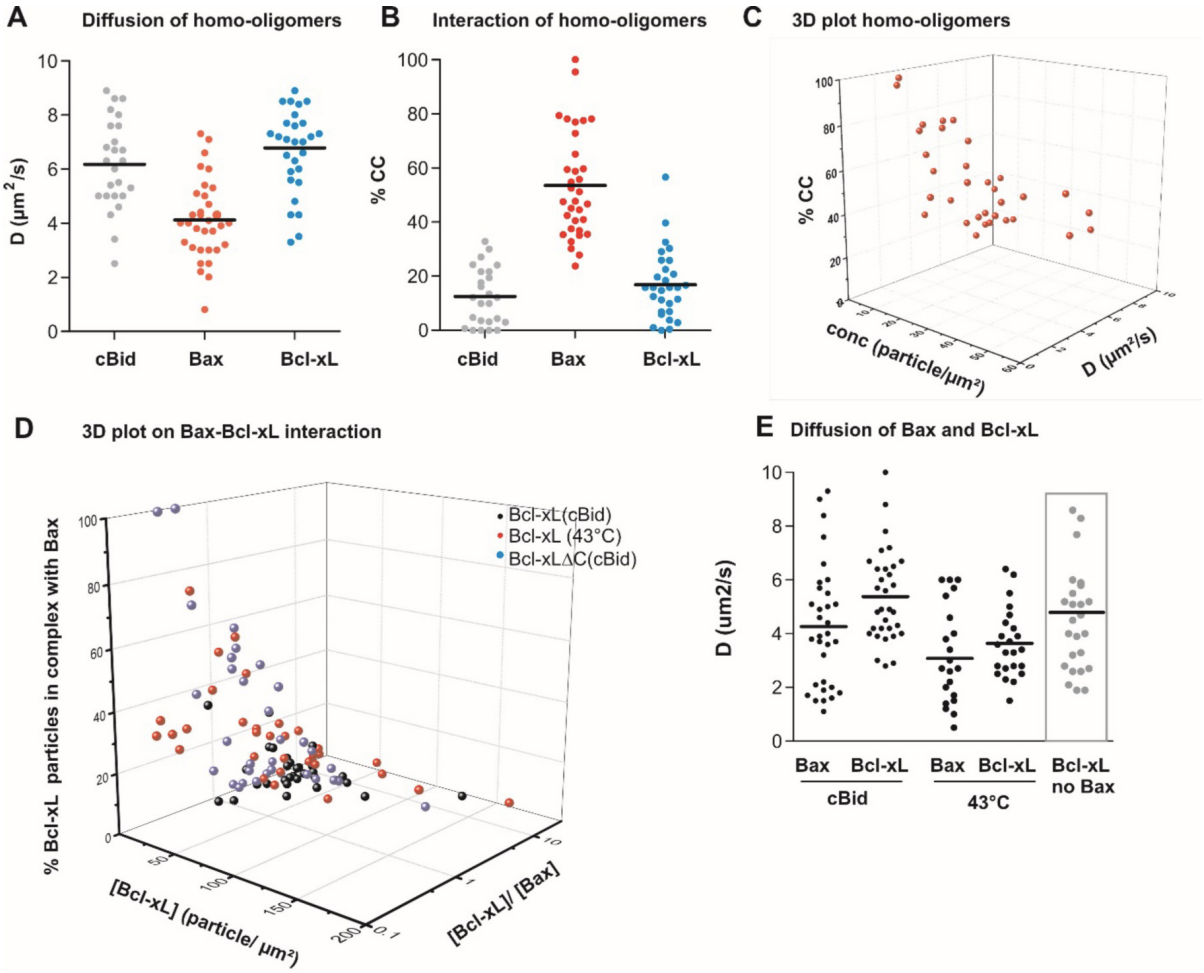

Figure 4.16: **Additional information on Bax homo- and hetero-oligomer formation in membranes. A-B**, Diffusion coefficients (A) and cross-correlation (B) of membrane embedded cBid and Bax and Bcl-xL homo-oligomers using GUVs of the 30% CL mix (cBid n=4; Bax n=5; Bcl-xL n=5). The CC values from 3 of 5 experiments studying Bax and Bcl-xL homo- interactions used here were already published in (Bleicken et al., 2013b). **C**, 3D graph of Bax-homo-oligomers in the membranes of individual GUVs plotting the relationship between concentration, diffusion and %CC (n=5). **D**, Related to Figure 4.6E. 3D graph plotting the relationship between Bax_R and $Bcl\text{-}xL_G$ concentration and percentage of Bcl-xL molecules in hetero-complexes with Bax. Data points from GUVs in which protein insertion was triggered by cBid are black dots; when heat was used red dots and when cBid and Bcl-xLΔCT were used blue dots. **E**, Related to Figure 4.6E. Diffusion coefficients of membrane embedded Bax_G and $Bcl\text{-}xL_R$ using GUVs of the 30% CL mix. Protein membrane-insertion was activated by cBid or heat. In data in the box show the diffusion coefficients of Bcl-xL in presence of only cBid taken from Figure 4.5A for comparison.

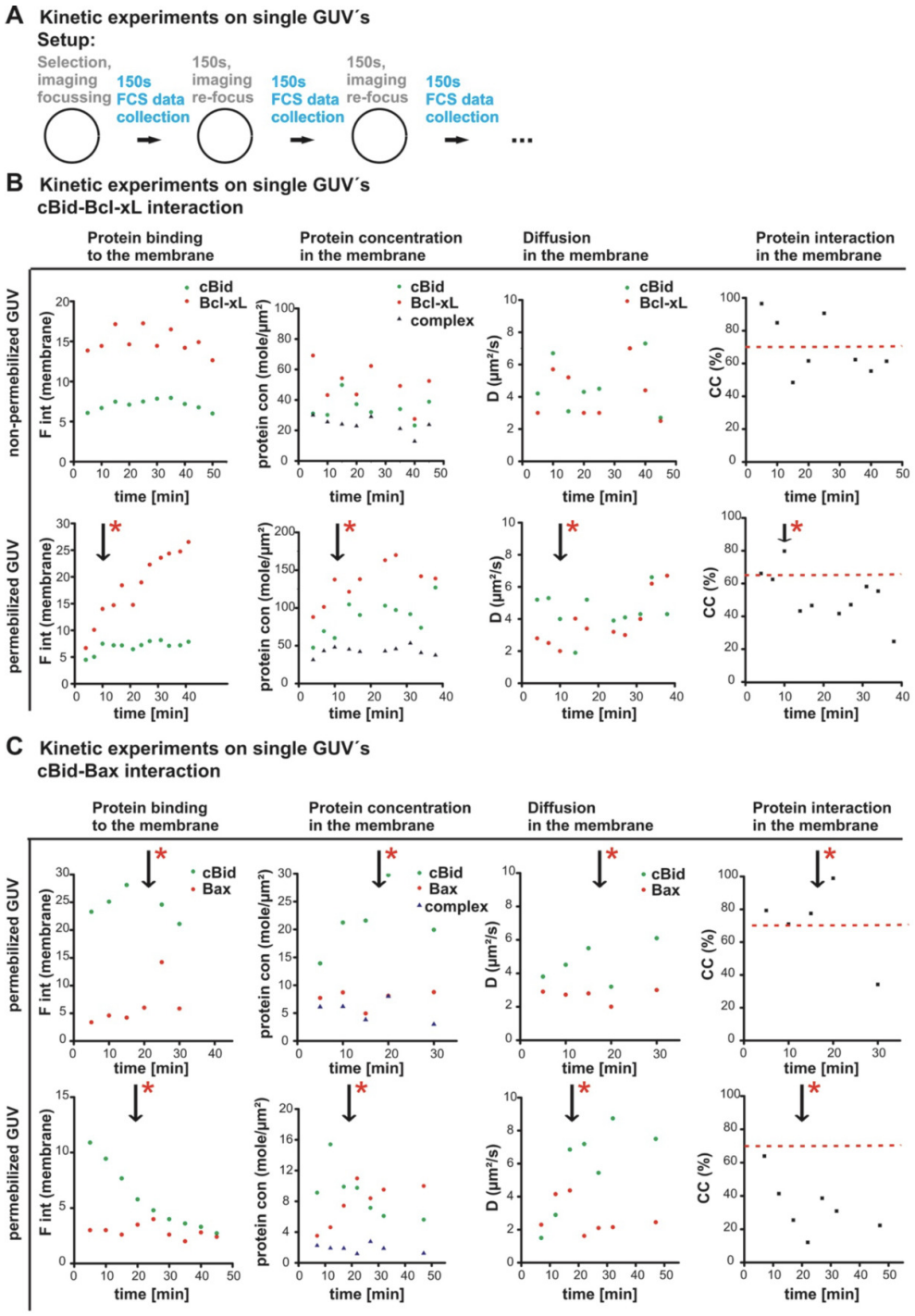

Figure 4.17: **Kinetic experiments of Bcl-2 protein interactions in membranes. A**, Schematic drawing on how the experiment was performed. **B-C**, Kinetic experiments of the interaction of $cBid_G$ with $Bcl\text{-}xL_R$ (B) or Bax_R (C). The first panel on the left shows changes in the fluorescence intensity of membrane embedded $cBid_G$, $Bcl\text{-}xL_R$ or Bax_R over time measured by imaging. The second panel shows changes in the protein and complex concentration over time measured by FCS. Concentration and fluorescence intensity are stable or rising except for $cBid_G$ in presence of Bax, where cBid molecules seem to be released from the membrane. The third panel follows D over time. For cBid-Bcl-xL D is relatively stable over time, while the D of cBid in presence of Bax can rise in line with cBid release from the complex. The right panel shows changes in the cross-correlation over time. The red line indicates the maximal possible cross-correlation and the arrow indicates the time point when the GUV was permeabilized.

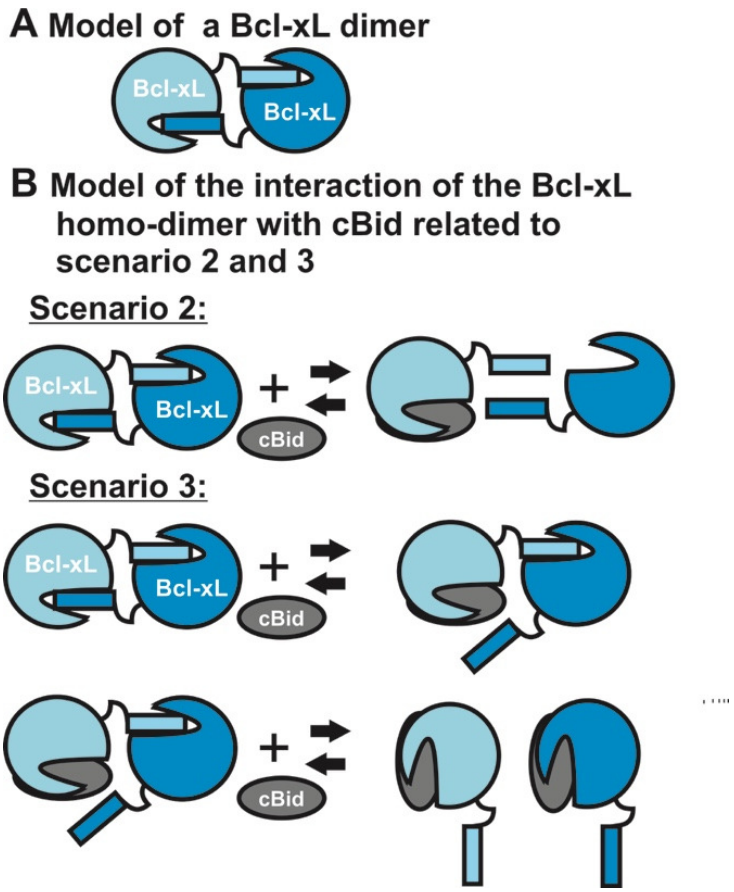

Figure 4.18: **Model of Bcl-xL dimerization.** **A**, Schematic drawing of a Bcl-xL homo-dimer. **B**, Schematic models of the interaction of cBid with a Bcl-xL homo-dimer related to Scenarios 2 and 3.

4.6.2 Supplementary Tables

Table 4.1: **Functions used for the FCS analysis** G is the autocorrelation and G_x the cross-correlation function; τ the lag time for correlation; $F(t)$ the fluorescence intensity as a function of time (t); $\langle\rangle$ corresponds to time averaging ($\delta F(t) = F(t) - \langle F(t)\rangle$); F_R and F_G are the fluorescence intensity in the red and green channels; C_{RG} is the concentration molecules in the two color complex; $C_{RG,t}$ the concentration of all particles having both colors; $G_{0,x}$ is the cross-correlation amplitude; $G_{0,R}$ ($G_{0,G}$) is the amplitude or the red (or green) autocorrelation curve; D is the diffusion coefficient; N is the average number of detected molecules; t_D is the average time the fluorophore stays in the focal volume; G_{12} is the spatial cross-correlation curve comparing the two foci; and d is the distance between the two foci.

Name	Function
Auto-correlation function	$G(\tau) = \frac{\langle \delta F(t) \delta F(t+\tau)\rangle}{\langle F(t)\rangle^2}$
Cross-correlation function	$G_x(\tau) = \frac{\langle \delta F_R(t)\, \delta F_G(t+\tau)\rangle}{\langle F_R(t)\rangle \langle F_G(t)\rangle}$
Fraction of molecules in two color complex	$C_{RG} = \frac{G_{0,x}}{G_{0,G}}$ or $C_{RG} = \frac{G_{0,x}}{G_{0,R}}$
Diffusion coefficient	$D = \frac{\omega_0^2 4 t_D}{4 t_D}$
3D diffusion for solution measurements	$G_{3D}(\tau) = \frac{1}{N}\left(1+\frac{\tau}{\tau_D}\right)^{-1} \frac{1}{\sqrt{1+\frac{\tau}{S^2\tau_D}}}$
Dual-focus scanning FCS for measurements in membranes	$G_{12}(\tau) = \frac{1}{C\pi s\omega_0}\left(1+\frac{4D\tau}{\omega_0^2}\right)^{-1/2}\left(1+\frac{4D\tau}{\omega_0^2 s^2}\right)^{-1/2} \exp\left(-\frac{d^2}{\omega_0^2+4D\tau}\right)$

Table 4.2: **SSR, AIC values and differences in AIC values of models of different interaction scenarios** k denote the number of fitted parameters, n the number of experimental data points the model was fitted to. AIC_c denotes the corrected Akaike information criterion as described in Materials and Methods.

Scenario	SSR	k	n	AIC_c	Δ_i	w_i
1	6.17037	12	90	215.83	121.93	3.3e-27
2	**1.4318**	**14**	**90**	**93.90**	**0**	**1.0**
3	1.67701	18	90	128.16	34.26	3.6e-08

Table 4.3: **Ordinary differential equations of different model scenarios** B0 denotes unlabeled Bcl-xL, B1 denotes Bcl-xL_R and C denotes cBid. Concentrations are denoted by [ ]. Kinetic rate constants are defined in Fig. 4.3A (k_+ denote k_{on} and k_- denote k_{off})

	Scenario 1	**Scenario 2**	**Scenario 3**
d([C]) dt	− (k2on · [C] · [B0]) + (k2off · [CB0]) - (k2on · [C] · [B1]) + (k2off · [CB1]) - (k2on · [C] · [B2]) + (k2off · [CB2])	- (k2on · [C] · [B1]) +(k2off · [CB1]) - (k2on · [C] · [B2]) +(k2off · [CB2]) -(k3on · [B1B1] · [C]) +(k3off · [CB1] · [B1]) -(k3on · [B2B2] · [C]) +(k3off · [CB2] · [B2]) -(k3on · [B1B2] · [C]) +(k3off · [CB1] · [B2]) -(k3on · [B1B2] · [C]) +(k3off · [CB2] · [B1]) -(k2on · [C] · [B0]) +(k2off · [CB0]) - (k3on · [B1B0] · [C]) +(k3off · [CB1] · [B0]) -(k3on · [B1B0] · [C]) +(k3off · [CB0] · [B1]) -(k3on · [B2B0] · [C]) +(k3off · [CB2] · [B0]) -(k3on · [B2B0] · [C]) +(k3off · [CB0] · [B2]) -(k3on · [B0B0] · [C]) +(k3off · [CB0] · [B0])	+(k5off · [CB2B2]) -(k5on · [B2B2] · [C]) +(k5off · [CB1B1]) -(k5on · [B1B1] · [C]) +(k5off · [CB0B0]) -(k5on · [B0B0] · [C]) -(k5on · [B1B2] · [C]) +(k5off · [CB1B2]) -(k5on · [B1B0] · [C]) +(k5off · [CB1B0]) -(k5on · [B2B0] · [C]) +(k5off · [CB2B0]) +(k2off · [CB0]) -(k2on · [C] · [B0]) +(k2off · [CB1]) -(k2on · [C] · [B1]) +(k2off · [CB2]) -(k2on · [C] · [B2]) -(k6on · [CB0B0] · [C]) +(k6off · [CB0B0C]) -(k6on · [CB1B1] · [C]) +(k6off · [CB1B1C]) -(k6on · [CB2B2] · [C]) +(k6off · [CB2B2C]) -(k6on · [CB1B2] · [C]) +(k6off · [CB1B2C]) -(k6on · [CB1B0] · [C]) +(k6off · [CB1B0C]) -(k6on · [CB2B0] · [C]) +(k6off · [CB2B0C])
d([B1]) dt	-(k1on · [B1] · [B2]) +(k1off · [B1B2]) -(k1on · [B1] · [B0]) +(k1off · [B1B0]) -(k2on · [C] · [B1]) +(k2off · [CB1]) -2 ·(k1on · [B1] · [B1]) + 2 ·(k1off · [B1B1])	-(k1on · [B1] · [B2]) +(k1off · [B1B2]) -(k2on · [C] · [B1]) +(k2off · [CB1]) -2 ·(k1on · [B1] · [B1]) + 2 ·(k1off · [B1B1]) +(k3on · [B1B1] · [C]) -(k3off · [CB1] · [B1]) +(k3on · [B1B2] · [C]) -(k3off · [CB2] · [B1]) -(k1on · [B1] · [B0]) +(k1off · [B1B0]) +(k3on · [B1B0] · [C]) -(k3off · [CB0] · [B1])	+ 2 ·(k1off · [B1B1]) -2 ·(k1on · [B1] · [B1]) +(k1off · [B1B0]) -(k1on · [B1] · [B0]) +(k1off · [B1B2]) -(k1on · [B1] · [B2]) +(k2off · [CB1]) -(k2on · [C] · [B1])
d([B2]) dt	-(k1on · [B1] · [B2]) +(k1off · [B1B2]) -(k1on · [B2] · [B0]) +(k1off · [B2B0]) -(k2on · [C] · [B2]) +(k2off · [CB2]) -2 ·(k1on · [B2] · [B2]) + 2 ·(k1off · [B2B2])	-(k1on · [B1] · [B2]) +(k1off · [B1B2]) -(k2on · [C] · [B2]) +(k2off · [CB2]) -2 ·(k1on · [B2] · [B2]) + 2 ·(k1off · [B2B2]) +(k3on · [B2B2] · [C]) -(k3off · [CB2] · [B2]) +(k3on · [B1B2] · [C]) -(k3off · [CB1] · [B1]) -(k1on · [B1] · [B0]) +(k1off · [B2B0]) +(k3on · [B2B0] · [C]) -(k3off · [CB0] · [B2])	+(k1off · [B2B0]) -(k1on · [B2] · [B0]) +(k1off · [B1B2]) -(k1on · [B1] · [B2]) +2 · (k1off · [B2B2]) -2 · (k1on · [B2] · [B2]) +(k2off · [CB2]) -(k2on · [C] · [B2])

d([B0]) dt	-(k1on · [B1] · [B0]) +(k1off · [B1B0]) -(k1on · [B2] · [B0]) +(k1off · [B2B0]) -2 ·(k1on · [B0] · [B0]) + 2 ·(k1off · [B0B0]) -(k2on · [C] · [B0]) +(k2off · [CB0])	-(k1on · [B1] · [B0]) +(k1off · [B1B0]) -(k1on · [B2] · [B0]) +(k1off · [B2B0]) -2 ·(k1on · [B0] · [B0]) + 2 ·(k1off · [B0B0]) -(k2on · [C] · [B0]) +(k2off · [CB0]) +(k3on · [B1B2] · [C]) -(k3off · [CB1] · [B0]) +(k3on · [B2B2] · [C]) -(k3off · [CB2] · [B0]) +(k3on · [B0B0] · [C]) -(k3off · [CB0] · [B0])	+(k1off · [B2B0]) -(k1on · [B2] · [B0]) +(k1off · [B1B0]) -(k1on · [B1] · [B0]) +(k2off · [CB0]) -(k2on · [C] · [B0]) +2 · (k1off · [B0B0]) -2 · (k1on · [B0] · [B])
d([CB1) dt	+(k2on · [C] · [B1]) -(k2off · [CB1])	+(k2on · [C] · [B1]) -(k2off · [CB1]) +(k3on · [B1B1] · [C]) -(k3off · [CB1] · [B1]) +(k3on · [B1B2] · [C]) -(k3off · [CB1] · [B2]) +(k3on · [B1B0] · [C]) -(k3off · [CB1] · [B0])	+ 2 · (k7off · [CB1B1C]) − 2 · (k7on · [CB1] · [CB1]) + (k7off · [CB1B2C]) − (k7on · [CB1] · [CB2]) + (k7off · [CB1B0C]) − (k7on · [CB1] · [CB0]) − (k2off · [CB1]) + (k2on · [C] · [B1])
d([CB2) dt	+(k2on · [C] · [B2]) -(k2off · [CB2])	+(k2on · [C] · [B2]) -(k2off · [CB2]) +(k3on · [B1B2] · [C]) -(k3off · [CB2] · [B2]) +(k3on · [B1B2] · [C]) -(k3off · [CB2] · [B1]) +(k3on · [B2B0] · [C]) -(k3off · [CB2] · [B0])	+ 2 · (k7off · [CB2B2C]) − 2 · (k7on · [CB2] · [CB2]) + (k7off · [CB1B2C]) − (k7on · [CB1] · [CB2]) + (k7off · [CB2B0C]) − (k7on · [CB2] · [CB0]) − (k2off · [CB2]) + (k2on · [C] · [B2)
d([CB0) dt	+(k2on · [C] · [B0]) -(k2off · [CB0])	+(k2on · [C] · [B0]) -(k2off · [CB0]) +(k3on · [B1B0] · [C]) -(k3off · [CB0] · [B2]) +(k3on · [B1B0] · [C]) -(k3off · [CB0] · [B2]) +(k3on · [B0B0] · [C]) -(k3off · [CB0] · [B0])	+ 2 · (k7off · [CB0B0C]) − 2 · (k7on · [CB0] · [CB0]) + (k7off · [CB1B0C]) − (k7on · [CB1] · [CB0]) + (k7off · [CB2B0C]) − (k7on · [CB2] · [CB0]) − (k2off · [CB0]) + (k2on · [C] · [B0)
d([B1B1) dt	+(k1on · [B1] · [B1]) -(k1off · [B1B1])	+(k1on · [B1] · [B1]) -(k1off · [B1B1]) - (k3on · [B1B1] · [C]) +(k3off · [CB1] · [B1])	-(k1off · [B1B1]) +(k1on · [B1] · [B1]) +(k5off · [CB1B1]) - (k5on · [B1B1] · [C])
d([B2B2) dt	+(k1on · [B2] · [B2]) -(k1off · [B2B2])	+(k1on · [B2] · [B2]) -(k1off · [B2B2]) - (k3on · [B2B2] · [C]) +(k3off · [CB2] · [B2])	+(k5off · [CB2B2]) - (k5on · [B2B2] · [C]) -(k1off · [B2B2]) +(k1on · [B2] · [B2])
d([B1B0) dt	+(k1on · [B1] · [B0]) -(k1off · [B1B0])	+(k1on · [B1] · [B0]) -(k1off · [B1B0]) - (k3on · [B1B0] · [C]) +(k3off · [CB1] · [B0]) - (k3on · [B1B0] · [C]) +(k3off · [CB0] · [B1])	-(k1off · [B1B0]) +(k1on · [B1] · [B0]) +(k5off · [CB1B0]) - (k5on · [B1B0] · [C])

d([B2B0) dt	+(k1on · [B2] · [B0]) -(k1off · [B2B0])	+(k1on · [B2] · [B0]) -(k1off · [B2B0]) - (k3on · [B2B0] · [C]) +(k3off · [CB2] · [B0]) - (k3on · [B2B0] · [C]) +(k3off · [CB0] · [B2])	-(k1off · [B2B0]) +(k1on · [B2] · [B0]) +(k5off · [CB2B1]) - (k5on · [B2B1] · [C])
d([B0B0) dt	+(k1on · [B0] · [B0]) -(k1off · [B0B0])	+(k1on · [B0] · [B0]) -(k1off · [B0B0]) - (k3on · [B0B0] · [C]) +(k3off · [CB0] · [B0])	-(k1off · [B0B0]) +(k1on · [B0] · [B0]) +(k5off · [CB0B0]) - (k5on · [B0B0] · [C])
d([B1B2) dt	+(k1on · [B1] · [B2]) -(k1off · [B1B2])	+(k1on · [B1] · [B2]) -(k1off · [B1B02) - (k3on · [B1B2] · [C]) +(k3off · [CB1] · [B2]) - (k3on · [B1B2] · [C]) +(k3off · [CB2] · [B1])	-(k1off · [B1B2]) +(k1on · [B1] · [B2]) +(k5off · [CB1B2]) - (k5on · [B1B0] · [C])
d([CB0B0) dt	-	-	-(k5off · [CB0B0]) + (k5on · [B0B0] · [C]) - (k6on · [B0B0] · [C]) +(k6off · [CB0B0C])
d([CB1B1) dt	-	-	-(k5off · [CB1B1]) + (k5on · [B1B1] · [C]) - (k6on · [B1B1] · [C]) +(k6off · [CB1B1C])
d([CB2B2) dt	-	-	-(k5off · [CB2B2]) + (k5on · [B2B2] · [C]) - (k6on · [CB2B2] · [C]) +(k6off · [CB2B2C])
d([CB1B2) dt	-	-	+(k5on · [B1B2]) - (k5off · [CB1B2]) - (k6on · [CB1B2] · [C]) +(k6off · [CB2B2C])
d([CB1B0) dt	-	-	+(k5on · [B1B0]) - (k5off · [CB1B0]) - (k6on · [CB1B0] · [C]) +(k6off · [CB2B0C])
d([CB2B0) dt	-	-	+(k5on · [B2B0] · [C]) - (k5off · [CB2B0]) - (k6on · [CB2B0] · [C]) +(k6off · [CB2B0C])
d([CB2B0C) dt	-	-	- (k7off · [CB0B0C]) +(k7on · [CB0] · [CBO]) + (k6on · [CB0B0] · [C]) -(k6off · [CB0B0C])
d([CB1B1C) dt	-	-	- (k7off · [CB1B1C]) +(k7on · [CB1] · [CB1]) + (k6on · [CB1B1] · [C]) -(k6off · [CB1B1C])
d([CB2B2C) dt	-	-	- (k7off · [CB2B2C]) +(k7on · [CB2] · [CB2]) + (k6on · [CB2B2] · [C]) -(k6off · [CB2B2C])
d([CB1B2C) dt	-	-	- (k7off · [CB1B2C]) +(k7on · [CB1] · [CB2]) + (k6on · [CB1B2] · [C]) -(k6off · [CB1B2C])
d([CB1B0C) dt	-	-	- (k7off · [CB1B0C]) +(k7on · [CB1] · [CB0]) + (k6on · [CB1B0] · [C]) -(k6off · [CB1B0C])
d([CB2B0C) dt	-	-	- (k7off · [CB2B0C]) +(k7on · [CB2] · [CB0]) + (k6on · [CB2B0] · [C]) -(k6off · [CB2B0C])

4.6.3 Supplementary Methods

Fundamentals and technical details of fluorescence correlation spectroscopy (FCS) and Fluorescence cross correlation spectroscopy (FCCS)

This is a short summary on the method and the experimental setup used in this study. For more information about the method please read the following reviews (Ries et al., 2010; Ries and Schwille, 2008; Ries et al., 2012).

FCCS measurements in solution

FCS measures the fluorescence fluctuations due to the diffusion of fluorophores or macromolecules (like proteins) with attached fluorophores through a small detection volume (<1 fL), which is here created by a confocal microscope. The raw data of the experiment are fluorescence intensity traces and based on those auto-correlation curves are calculated. The auto-correlation curves contain information about the diffusion properties and the concentrations of the molecules studied. To gain quantitative information, mathematical fitting with appropriate models thus provides the number of molecules in the detection volume and their average diffusion time. The use of reference measurements with free fluorescent dyes of known diffusion coefficients allows calibration of the size and shape of the detection volume and estimation of fluorophore concentrations and diffusion coefficient. They are also useful to ensure the proper alignment of the instrument when are performed before each measurement. Here, we used the same dyes that are attached to the proteins of interest in the calibration measurements.
In FCS, the confocal microscope requires a high quality optical setup containing: objectives with a high numerical aperture, suitable laser lines, components to produce very well-shaped, small and maximum overlapping detection volumes, sensitive detectors (with nanosecond resolution), filters to avoid channel cross-talk, and the equipment to collect and analyze the FCCS data. In our case we used a LSM 710 with a Confocor 3 unit (Zeiss, Jena, Germany), optimized for FCS measurements. As the method has single molecule sensitivity, the best results are achieved when in the range of one molecule (per channel) is present in the detection volume. This is the case at nanomolar concentrations, so that we used mainly protein concentrations between 5-100 nM.
In FCCS (fluorescence cross correlation spectroscopy), the proteins of interest are labeled with spectrally different fluorophores that can be simultaneously excited (here by a 488 nm and a 633 nm laser). The emitted light from the two fluorophores is separated by optical parts (here dichroic mirrors and filters) and the resulting fluorescence intensity signals are acquired simultaneously with two detectors. Then, auto- and cross-correlation

curves are calculated from the fluorescence intensity traces in both channels, which allow qualitative and quantitative assessment of the protein-protein-interactions.
The FCCS analysis of the data provides a percentage of cross-correlation (%CC) that can be used to calculate the extent of complex formation between the molecules of interest. For this, one needs to correct for: i) partial overlap of the detection volumes of both channels; ii) degree of labeling of the proteins of interest is; and iii) fraction of free dye molecules in the sample.
Our experiments were optimized to detect Alexa488 or Atto488 in the "green" channel and Alexa633 or Atto655 in the "red" channel. Both "green" dyes were excited by the 488 nm laser and are detected using a 505-540 nm band pass filter and an Avalanche-Photo-Diode (APD) as detector. The "red" dyes were excited by the 633 nm laser and detected using a >655 nm long pass filter and a second APD. The size of detection volume is directly proportional to the wavelength of the laser light. Thus, the detection volumes of both detection channels do not perfectly overlap, which precludes detecting 100% cross-correlation in both channels even when all molecules are fluorescently labeled and forming complexes. We performed test experiments to determine the maximal cross-correlation in each channel. An ideal sample to do so would be a stable molecule to which one red dye and one green dye is attached with 100% labeling efficiency, and no free dye present. Unfortunately, it was impossible for us produce or buy such a sample. Therefore, we used egg-PC vesicles (LUV) labeled with the two lipidic dyes: DID (exited by the 633 laser, emission maximum >655 nm) and DIO (excited by the 488 laser, emission maximum between 505-540 nm). Before the measurements, we passed the vesicle through a 200 nm filter to make them more homogenous in size. We detected >90% CC in the red channel and >75% CC in the green channel (Supplemental Fig. 4.9A), which provides an estimation of the partial overlap of both detection channels in our system. This is close to 100% crosscorrelation in both channels, considering that the reference sample does not contain 100% doubly labeled particles with a zero background of free dye. With an ideal test sample, it would be possible to correct for incomplete spectral overlap by introducing a correction factor. Therefore, in our calculations we slightly underestimate the cross-correlation values, but as all measurements are affected in the same way, this only changes the absolute numbers and not our conclusions.
We chose the fluorophores based on: 1) a reasonable quantum yield, 2) good photostability, 3) their relative small size, 4) no detectable tendency to aggregate under the used condition (Supp. Fig. 4.9B), 5) that the diffusion of the fluorophore is well described in literature and 6) that the proteins of choice were still functional after fluorophore attachment. Alexa 488 and 633 were used to label cBid and Atto 488 and 655 to label Bax

and Bcl-xL. None of those dyes showed signs of aggregation in their free form (example shown in Supplemental Fig. 4.9B) and the level of cross talk between the dye combinations used on the proteins was below 2% (Supp. Fig. 4.9C). An exception was the Alexa 488 /Alexa 633 pair (used only to study cBid homo-dimerization) with cross-talk levels up to 5%. However, as we did not detect any cBid homo-dimerization the higher cross-talk does not affect our conclusions. The free forms of the four dyes mentioned were also used to calculate the size and shape of the detection volumes.
For data quantification, the degree of labeling and the fraction of free dye in each protein sample were calculated. As shown in previous work, labeled cBid, Bax and Bcl-xL are active in membrane permeabilization (Bleicken et al., 2013b,a; Subburaj et al., 2015). We also did visualize the protein before and after labeling by SDS-PAGE (Supplemental Fig. 4.9E). The degree of labeling was estimated using absorption spectra and mass spectroscopy. For Bax and Bcl-xL, we calculated degrees of labeling between 80 and 100%, while cBid was labeled between 60 to 80% (concrete info given in the figure legends).
Most fluorophore molecules were covalently attached to the proteins. However, the dyes can also bind non-covalently to protein surfaces. As free dye and "non-covalently protein attached" dye molecules are in equilibrium, the sample dilution before the FCS measurement will release some non-covalently attached dyes. This fraction of free dye needs to be considered for data quantification, which was done here by two component fitting of the auto-correlation curves. In the fitting process, the diffusion time of the free dye (known from reference measurements performed directly before the actual measurement) was fixed to reduce the free parameters, so that the fraction of labeled protein and free dye could be estimated with good accuracy (Supplemental Fig. 4.9E). For Bax and Bcl-xL we calculated that the amount of free dye was ∼20%, for cBid the amount was a bit higher (∼ 20-30% for the green version and 30-40% for the red). The presence of non-covalently attached dyes is not unique to the Bcl-2 proteins. We have tested in our lab several other protein label combinations and after dilution to the low FCS concentration we were always able to detect some free dye molecules.

FCCS measurements in membranes

Due to the different viscosities of buffer solutions and lipid bilayers, membrane-embedded molecules diffuse slower than soluble ones, and they diffuse in two and not three dimensions. In addition, one important condition to measure FCS in membranes is to position the detection volume on the membrane plane. All this requires different measurement strategies, different fitting models and longer measurement times necessary. During the

long measurement time, the sample can be bleached and the membrane may move in and out of the detection volume, which both difficult the analysis of the FCS data. Moreover, due to the differences in refraction index, the use of calibration measurements acquired in solution is problematic when quantitatively analyzing FCS data from membranes. To solve these problems, an FCS variant called two-focus scanning FCCS was developed for membrane proteins by the Schwille group and their work also provides the necessary mathematical models to fit the data (Ries and Schwille, 2008; Ries et al., 2012).
In two-focus scanning FCCS, two parallel lines are repeatedly scanned perpendicular to and crossing the membrane of a GUV. As the laser is on the membrane only a fraction of the time, photobleaching is decreased. Moreover, the contributions of the membrane to the fluorescence intensity signal are aligned and integrated around the maximum, which allows corrections for slight movements of the membrane. If the distance between the two scanned lines is known, the data can be fitted with a mathematical model that provides directly diffusion coefficient and the structural parameter of the detection volume, so that calibration-free measurements are possible. Key for two-focus scanning FCCS measurements are stable GUVs, in which the proteins of interest insert, interact and diffuse. Optimally, the membrane should mimic the physiological situation. In previous work, we investigated several suitable lipid mixtures to study Bcl-2 proteins in GUVs. Here we chose two different mixtures, which are described in the main text. Fortunately, the free form of the dyes used here do not interact with the GUV membranes (Bleicken et al., 2013b,a, 2014), so that they do not need be considered for data quantification in FCS measurements in membranes.

Species used for model fitting to experimental data in different interaction scenarios

Scenario 1 and Scenario 2:

$$
\begin{aligned}
[\text{Bcl-xL}_{\text{G particles}}] = \quad & [\text{Bcl-xL}_\text{G}] + [\text{Bcl-xL}_\text{G}\text{-Bcl-xL}_\text{G}] + [\text{Bcl-xL}_\text{G}\text{-Bcl-xL}_\text{R}] + \\
& [\text{Bcl-xL}_\text{G}\text{-Bcl-xL}_0] + [\text{cBid-Bcl-xL}_\text{G}] \\
[\text{Bcl-xL}_{\text{R particles}}] = \quad & [\text{Bcl-xL}_\text{R}] + [\text{Bcl-xL}_\text{R}\text{-Bcl-xL}_\text{R}] + [\text{Bcl-xL}_\text{G}\text{-Bcl-xL}_\text{R}] + \\
& [\text{Bcl-xL}_\text{R}\text{-Bcl-xL}_0] + [\text{cBid-Bcl-xL}_\text{R}] \\
[\text{Bcl-xL}_\text{G}\text{-Bcl-xL}_{\text{R particles}}] = \quad & [\text{Bcl-xL}_\text{G}\text{-Bcl-xL}_\text{R}]
\end{aligned}
$$

Scenario 3:

$[\text{Bcl-xL}_{\text{G particles}}] =$ $[\text{Bcl-xL}_\text{G}] + [\text{Bcl-xL}_\text{G}\text{-Bcl-xL}_\text{G}] + [\text{Bcl-xL}_\text{G}\text{-Bcl-xL}_\text{R}] + [\text{Bcl-xL}_\text{G}\text{-Bcl-xL}_0] + [\text{cBid-Bcl-xL}_\text{G}] + [\text{cBid-Bcl-xL}_\text{G}\text{-Bcl-xL}_\text{G}] + [\text{cBid-Bcl-xL}_\text{G}\text{-Bcl-xL}_\text{R}] + [\text{cBid-Bcl-xL}_\text{G}\text{-Bcl-xL}_0] + [\text{cBid-Bcl-xL}_\text{G}\text{-Bcl-xL}_\text{G}\text{-cBid}] + [\text{cBid-Bcl-xL}_\text{G}\text{-Bcl-xL}_\text{R}\text{-cBid}] + [\text{cBid-Bcl-xL}_\text{G}\text{-Bcl-xL}_0\text{-cBid}]$

$[\text{Bcl-xL}_{\text{R particles}}] =$ $[\text{Bcl-xL}_\text{R}] + [\text{Bcl-xL}_\text{R}\text{-Bcl-xL}_\text{R}] + [\text{Bcl-xL}_\text{G}\text{-Bcl-xL}_\text{R}] + [\text{Bcl-xL}_\text{R}\text{-Bcl-xL}_0] + [\text{cBid-Bcl-xL}_\text{R}] + [\text{cBid-Bcl-xL}_\text{R}\text{-Bcl-xL}_\text{R}] + [\text{cBid-Bcl-xL}_\text{G}\text{-Bcl-xL}_\text{R}] + [\text{cBid-Bcl-xL}_\text{R}\text{-Bcl-xL}_0] + [\text{cBid- Bcl-xL}_\text{R}\text{- Bcl-xL}_\text{R}\text{-cBid}] + [\text{cBid-Bcl-xL}_\text{G}\text{- Bcl-xL}_\text{R}\text{-cBid}] + [\text{cBid-Bcl-xL}_\text{R}\text{-Bcl-xL}_0\text{-cBid}]$

$[\text{Bcl-xL}_\text{G}\text{-Bcl-xL}_{\text{R particles}}] =$ $[\text{Bcl-xL}_\text{G}\text{-Bcl-xL}_\text{R}]+[\text{cBid-Bcl-xL}_\text{G}\text{-Bcl-xL}_\text{R}] + [\text{cBid-Bcl-xL}_\text{G}\text{-Bcl-xL}_\text{R}\text{-cBid}]$

Calculation of Bcl-xL dimer and monomer concentrations from FCS measurements for plot in Suppl. Fig. 4.9 was performed the following way, assuming equilibrium conditions:

$\text{DOL}_{\text{B}\bullet}$ labelling efficiency of Bcl-xL_G (B•)
$\text{DOL}_{\text{B}\circ}$ labelling efficiency of Bcl-xL_R (B○)

measured values from FCS:
[B•-B○]
$[\text{B}\bullet]_{\text{tot}} = [\text{B}\bullet] + [\text{B}\bullet\text{-B}\bullet] + [\text{B}\bullet\text{-B}\circ] + [\text{B}\bullet\text{-B}]$
$[\text{B}\circ]_{\text{tot}} = [\text{B}\circ] + [\text{B}\circ\text{-B}\circ] + [\text{B}\bullet\text{-B}\circ] + [\text{B}\circ\text{-B}]$

values in plot:
$[\text{B}]_{\text{tot,free}} = [\text{B}\bullet] + [\text{B}\circ] + [\text{B}]$
$[\text{B-B}]_{\text{tot}} = [\text{B}\bullet\text{-B}\bullet] + [\text{B}\bullet\text{-B}\circ] + [\text{B}\circ\text{-B}\circ] + [\text{B}\bullet\text{-B}] + [\text{B}\circ\text{-B}] + [\text{B-B}]$

calculation of [B○](4.9), [B•](4.8), [B](4.7), [B•-B•](4.2), [B○-B○](4.3), [B-B](4.4), [B•-B](4.5), [B○-B](4.6):

$$K_D = \frac{[B\bullet]^2}{[B\bullet - B\bullet]} = \frac{[B\circ]^2}{[B\circ - B\circ]} = \frac{[B]^2}{[B - B]} = \frac{[B\bullet]\cdot[B\circ]}{[B\bullet - B\circ]} = \frac{[B\bullet]\cdot[B]}{[B\bullet - B]} = \frac{[B\circ]\cdot[B]}{[B\circ - B]} \quad (4.1)$$

(4.2)-(4.6) follow from (4.1)

$$[B\bullet - B\bullet] = \frac{[B\bullet]\cdot[B\bullet - B\circ]}{[B\circ]} \tag{4.2}$$

$$[B\circ - B\circ] = \frac{[B\circ]\cdot[B\bullet - B\circ]}{[B\bullet]} \tag{4.3}$$

$$[B - B] = \frac{[B]^2\cdot[B\bullet - B\circ]}{[B\bullet]\cdot[B\circ]} \tag{4.4}$$

$$[B\bullet - B] = \frac{[B]\cdot[B\bullet - B\circ]}{[B\circ]} \tag{4.5}$$

$$[B\circ - B] = \frac{[B]\cdot[B\bullet - B\circ]}{[B\bullet]} \tag{4.6}$$

$$[B] = [B\circ]\cdot\left(\frac{1}{DOL_{B\circ}} - 1\right) + [B\bullet]\cdot\left(\frac{1}{DOL_{B\bullet}} - 1\right) \tag{4.7}$$

from (4.1):

$$[B\bullet]_{tot} = [B\bullet] + \frac{[B\bullet]^2}{K_D} + \frac{[B\bullet]\cdot[B\circ]}{K_D} + \frac{[B\bullet]\cdot[B]}{K_D}$$

$$[B\bullet]_{tot} = [B\bullet]\cdot\left(1 + \frac{[B\bullet]}{K_D} + \frac{[B\circ]}{K_D} + \frac{[B]}{K_D}\right)$$

$$[B\circ]_{tot} = [B\circ]\cdot\left(1 + \frac{[B\circ]}{K_D} + \frac{[B\bullet]}{K_D} + \frac{[B]}{K_D}\right)$$

$$[B\bullet] = \frac{[B\bullet]_{tot}\cdot[B\circ]}{[B\circ]_{tot}} \tag{4.8}$$

rearranging $[B\circ]_{tot}$ leads to:

$$[B\circ] = [B\circ]_{tot} - [B\circ - B\circ] - [B\bullet - B\circ] - [B\circ - B]$$

(4.9) follows then from (4.3), (4.6), (4.7) and (4.8):

$$[B\circ] = [B\circ]_{tot} - \frac{[B\bullet - B\circ]\cdot[B\circ]_{tot}}{[B\bullet]_{tot}} - [B\bullet - B\circ] -$$
$$\frac{[B\circ]_{tot}\cdot[B\bullet - B\circ]\cdot\left(\frac{1}{DOL_{B\circ}} - 1 + \frac{[B\bullet]_{tot}}{DOL_{B\bullet}\cdot[B\circ]_{tot}} - \frac{[B\bullet]_{tot}}{[B\circ]_{tot}}\right)}{[B\bullet]_{tot}}$$

K_D was then determined by plotting $[B]_{tot,free}{}^2$ against $[B\text{-}B]_{tot}$ and determining the slope of the linear regression line.

5 Discussion

The aim of this project was to obtain a systems level understanding of the complex Bcl-2 protein family interactome and effector oligomerization. Novel insights into the molecular mechanisms taking place amongst Bcl-2 family members in solution and in membrane environments were obtained by mathematical modeling. The findings highlight that retrotranslocation of Bax by Bcl-xL plays a major role in mediating a sharp decision threshold for Bax oligomerization at subequimolar concentrations of Bcl-xL. Furthermore, modeling suggests that homodimers of Bcl-xL occurring in solution can be actively disrupted by tBid.
On a whole Bcl-2 interactome level, encompassing all 15 well-defined Bcl-2 family members, an interactive web service was developed that provides a comprehensive overview of published interaction studies. It provides tools for conveniently identifying consistently reported protein-protein interactions and highlights the dependence of outcomes on specific experimental conditions.
Likewise, this study stresses a number of open research questions requiring further investigation to complement the current understanding of Bcl-2 family mediated pore formation, especially in a cellular context.

5.1 Bcl-2-Ome and other resources on Bcl-2 protein family interactions

The interactive web service and database Bcl-2-Ome (Hantusch et al., 2017) provides state of the art data on the Bcl-2 interactome at highest curation quality. It integrates detailed information on experimental conditions, such as used buffers, which fundamentally affect Bcl-2 family signaling (Hsu and Youle, 1997; Dewson, 2015). Bcl-2-Ome thus allows the integration of entries which at first glance may seem conflicting. However, its strength is that each plausible interaction within Bcl-2 family members can be analyzed based on published experiments and is therefore not biased for or against specific findings and studies. It rather enables a convenient comparison of multiple studies, thereby providing information on reproducibly reported interactions and also giving an overview of poorly

defined or conflicting data on Bcl-2 family interactions.
Another Bcl-2 specific database, BCL2DB, has recently been reported (Rech de Laval et al., 2014). In contrast to Bcl-2-Ome, BCL2DB is focused on sequence analysis and structural data and does not contain interaction data. Other protein-protein interaction databases encompassing Bcl-2 family member interactions have been provided to the scientific community, such as the global interactome resources STRING (Szklarczyk et al., 2015) and IntAct (Orchard et al., 2014). STRING covers data from many organisms and origins and also predicted interactions. The strengths of STRING lie in its size and comprehensiveness through automated large scale data integration. However, an authentic detailed and reliable insight into the complexity of the Bcl-2 interactome is not possible in STRING as it does not allow a convenient analysis of underlying experimental conditions and published quantitative parameters such as KD values. It has, with respect to the Bcl-2 protein family, no comprehensive expert curation and is, by partially displaying false-positive/negative content (e.g. false Bad-Mc-1 interaction), not state of the art. IntAct, in comparison to STRING, is more comprehensive and comprises an attractive solution for obtaining an initial overview of the Bcl-2 interactome. Submissions to IntAct are possible and data underlie curation, albeit not by experts on the Bcl-2 family. In quantitative data and experimental details essential for the Bcl-2 interactome, it thus displays a lack of detail and accuracy. Importantly, Bcl-2-Ome uniquely also captures the transient but functionally crucial interactions of the effectors Bax and Bak with BH3-only proteins, which are essential for MOMP control.
Bcl-2-Ome content is entirely manually curated and validated, thereby outperforming the above named interactome resources in accuracy and detail. The functionalities of Bcl-2-Ome are therefore useful to a wide community of cell biologists, biochemists and systems biologists. Particularly the latter depend on high quality qualitative and quantitative data for the development of logical and deterministic mathematical models to understand the systems-level control of cellular death decisions by the Bcl-2 family. In summary, Bcl-2-Ome serves as a useful resource to a vast community of researchers and is expected to increase the awareness for the impact of experimental conditions on the observed results. It will benefit from further extension by novel studies on protein-protein interactions considering up-to-date mechanistic insights, such as membrane environments, posttranslational modifications and specific interactions sites. A user interface for the submission of new data is provided at http://for2036.uni-konstanz.de/Bcl2Ome/submit/index.php.

5.2 Bcl-2 family interactions in aqueous and membrane environments

The mitochondrial outer membrane is a critical player in the intrinsic apoptosis pathway. Bcl-2 family proteins can associate with the MOM and membrane integration brings about conformational changes in the proteins that alter their interaction profiles (Lindsay et al. (2011) and section 1.2). Available experimental data and mathematical modeling presented in this thesis hint at similarities as well as differences in the interaction mechanisms of the two multidomain family members Bax and Bcl-xL with BH3-only proteins. Binding of Bcl-xL to BH3-only proteins and membrane insertion of the prosurvival protein is so far less well understood than for the effector protein Bax.

Bax interacts with further family members mostly in the membrane, when its canonical binding groove is free for interactions with BH3 domains (Czabotar et al., 2014). The effector protein inserts its C-terminal α9 helix into the membrane upon binding to the MOM. The rest of the protein remains in a globular fold until activation of the protein induces a conformational change (Czabotar et al., 2013). In aqueous environments however, the C-terminal anchor of Bax is buried in its own hydrophobic binding groove (Suzuki et al., 2000). In healthy cells, Bax thus predominantly occurs as a monomer. Only its rear pocket would be accessible for an interaction with BH3-only proteins in the cytosol. This interaction was suggested to induce a conformational change in Bax, whereby its α9 helix is freed and membrane insertion facilitated (Gavathiotis et al., 2008, 2010).

The multidomain family member Bcl-xL can integrate into the membrane with its C-terminal transmembrane anchor (Yao et al., 2015). In solution however, Bcl-xL interestingly does not bury its membrane anchor by an intramolecular interaction, but by association with a further Bcl-xL molecule. In the homodimer, the hydrophobic transmembrane anchors bind to the hydrophobic binding groove of the other Bcl-xL molecule. When Bcl-xL is membrane bound, it does not homodimerize but interacts with other family members by heterodimerizations (Jeong et al., 2004).

This differing behavior of Bcl-xL and Bax raises two important questions: The first is, what molecular mechanisms convert Bcl-xL from a homodimeric cytosolic protein to a monomeric membrane bound protein? The second question is, do BH3-only proteins (and BH3 mimetics) differentially interact with the cytosolic and the membrane bound Bcl-xL species?

In reduced *in vitro* systems lacking further potentially influencing molecular players, Bcl-xL does not integrate into membranes without the presence of an effector or BH3-only protein (Billen et al., 2008b). Also *in cellulo* it was shown that BH3-only proteins can

induce Bcl-xL binding to the MOM (Jeong et al., 2004; Aranovich et al., 2012) and that Bcl-xL and Bax membrane binding are coregulated (Renault et al., 2015). Even BH3 mimetics induce Bcl-xL binding to the membrane, albeit less potently than BH3-only proteins (Aranovich et al., 2012). Thus, in the simplest scenario, BH3-only proteins, BH3 mimetics and Bcl-xL's C-terminal anchor all compete for binding to the same hydrophobic groove of a Bcl-xL molecule in solution. However, the work of Dr. Stephanie Bleicken presented in Figures 4.2b and 4.3b suggests that the interaction of two Bcl-xL molecules occurs with high affinity and has very low exchange rates. Addition of cBid (caspase-8 cleaved Bid) counterintuitively leads to higher exchange rates between differently labeled Bcl-xL species.

This observation cannot be explained by two simultaneously occurring bimolecular interactions. Instead, the comparison of mathematical models presented in this thesis supports a scenario in which cBid binds to Bcl-xL homodimers and thereby induces the release of one Bcl-xL molecule (Figure 4.3). This scenario implies that in aqueous environments cBid binds to an interaction site in Bcl-xL other than the hydrophobic binding groove.

The existence of an alternative binding site in Bcl-xL, as it exists in Bax (Gavathiotis et al., 2008), has not been shown to date, but is supported by the following observations. First of all, BH3-only proteins induce Bcl-xL binding to membranes, as they do promote Bax membrane binding (Jeong et al., 2004). Binding to a distinct interaction site in Bcl-xL might, as in the case of Bax, lead to conformational changes that expose its C-terminal transmembrane anchor and facilitate membrane insertion. A conformational change induced by interaction with the BH3-only protein might also explain the accelerated dissociation of Bcl-xL homodimers upon cBid addition in Figure 4.3.

It may seem puzzling at first sight that tBid could induce Bcl-xL monomerization and insertion into the membrane, thereby accelerating its prosurvival functions. However, such a mechanism could serve as a further level of regulation to prevent hypersensitivity of cells to low amounts of Bid cleavage. Due to Bcl-xL's capability to bind to the BH3-only protein in the cytosol as well as in the membrane, it might be able to outcompete tBid binding to Bax at subthreshold tBid concentrations.

An interaction between Bcl-xL and Bax only occurs in membranes, when Bax is in its active conformation and its BH3 domain is accessible for binding to the hydrophobic binding groove of Bcl-xL (Czabotar et al., 2013). The Bcl-xL specific small molecule inhibitor WEHI-539 was shown to efficiently disrupt Bcl-xL interaction with the effector protein in whole cells. However, although WEHI-539 binds to C-terminally truncated Bcl-xL in solution with high affinity, as do BH3-only proteins, treatment of whole cells with the small molecule did not interfere with the interaction of Puma or Bim with Bcl-xL

in membranes. In comparison to Bim and Puma, the complex of tBid with Bcl-xL was more sensitive to WEHI-539 treatment (Pécot et al., 2016). Similarly, ABT-737 competed with tBid, Bim and Bad for Bcl-xL binding in the cytoplasm. But in the membrane, it could only disrupt an association of Bcl-xL or Bcl-2 with tBid or Bad, and not an association with Bim. Also mutations in the BH3 domain of Bim could not disrupt its association with the two prosurvival proteins (Aranovich et al., 2012). Interactions of certain BH3-only proteins with Bcl-xL on further sites thus seem likely and require further investigation. A mechanistic and structural understanding of the regulatory interactions occurring within family members will be important to further elucidate the functions of seemingly redundant BH3-only proteins and to predict the efficacy of BH3 mimetics.

5.3 Molecular mechanisms controlling Bax activation and oligomerization

Bax membrane recruitment and oligomerization are tightly regulated in the cell. In healthy cells, a dynamic equilibrium between membrane-associated and cytosolic Bax exists (Schellenberg et al., 2013). Retrotranslocation of membrane bound Bax to the cytosol has been attributed to prosurvival proteins such as Bcl-xL, Bcl-2 and Mcl-1 (Edlich et al., 2011). Binding of the BH3 domain of Bax to the hydrophobic groove of Bcl-xL and an interaction with Bcl-xL's C-terminal domain seems to be required for Bax retrotranslocation (Todt et al., 2013). The work presented in this thesis highlights the importance of Bax retrotranslocation in the prosurvival function of Bcl-xL (Chapter 3).

Expanding knowledge on the kinetics of Bax oligomerization revealed that monomeric Bax that binds to the membrane rapidly homodimerizes and assembles into higher oligomeric species within minutes (Subburaj et al., 2015). Bcl-xL does not bind cytosolic Bax, but sequesters membrane-inserted active Bax. Thus, for Bcl-xL to prevent Bax oligomerization, binding to active Bax would have to be faster than the association of Bax with another active Bax molecule. Alternatively, if Bcl-xL does not rapidly bind to all active Bax molecules, the cell would need to tolerate the formation of a low amount of pores. This only seems plausible, if pores can be closed to prevent the release of proapoptotic molecules to the cytosol and caspase activation.

Indeed, experimental evidence points towards dynamic effector pore sizes. Pores that allow the passage of small globular proteins such as cytochrome *c* have been described to encompass varying amounts of Bax molecules (Saito et al., 2000; Xu et al., 2013; Kuwana et al., 2016). Importantly, Bax oligomers first seem to form larger pores that then relax to smaller pores (Bleicken et al., 2013a).

When Bax assembles into the dimeric building blocks of the oligomeric pores, its BH3 domain is inaccessible for interaction with a prosurvival protein. Thus, Bcl-xL and Bax compete for binding to this interaction site. When Bcl-xL interacts with Bax, it can mediate the retrotranslocation of Bax into the cytosol. Intriguingly, work presented in this thesis demonstrates that accounting for Bcl-xL mediated retrotranslocation was sufficient to remodel the disassembly of existing Bax pores, as had been observed experimentally (Figure 3.3). In contrast, neglecting retrotranslocation did not allow to reproduce the altered distribution of multimeric Bax species induced by Bcl-xL addition. Thus, the retrotranslocation of Bcl-xL might have a dual function. It reduces the amount of membrane bound active Bax molecules, as well as could enable the disassembly of existing oligomeric pores. The hydrophobic groove of Bcl-xL that mediates association with Bax also mediates retrotranslocation of the effector protein (Todt et al., 2013). This might explain why retrotranslocation by Bcl-xL and its importance in apoptosis regulation have been overlooked for long.

What remains unclear are the extent of retrotranslocation activity of other prosurvival proteins and their capability to disassemble pores. Further investigation of prosurvival mediated retrotranslocation, translocation and pore disassembly will aid in estimating the prosurvival potential of individual Bcl-2 family members. Likewise, the integration of Bax retrotranslocation processes into mathematical models will likely enhance their predictive capability.

5.4 Synergistic induction of MOMP and model extension

Efforts at the intersection of apoptosis and cancer research aim at efficiently inducing apoptotic cell death in cancerous cells. The specificity of targeted or standard chemotherapeutic drugs to tumor cells is of outstanding importance for later positive evaluation in clinical trials. Furthermore, a major obstacle for successful chemotherapy is to overcome intrinsic or acquired drug resistances in tumor tissue (Holohan et al., 2013). Combination therapy with two or more drugs can enhance efficacy of cancer cell treatment at lower doses of the single drugs (Hu et al., 2016; Jia et al., 2009). An increased cytotoxicity is achieved by the exploitation of synergistic effects, which arise when the effect of two drugs is bigger than the sum of the effect that would be achieved by the individual treatments (Tallarida, 2006).

In treatment strategies using inhibitors of oncogenic kinases, the molecular mechanisms leading to apoptosis induction might synergize at the level of the Bcl-2 protein family due

to the engagement of multiple family members by upstream signaling pathways (Hata et al., 2015). Highly tumor-specific drugs that lack sufficient cytotoxic effects, such as monomeric TRAIL, could be combined with other targeted therapeutics that are directed at signaling molecules of the apoptotic pathway (Lemke et al., 2014). Combination of TRAIL with cytotoxic chemotherapeutic agents such as Doxorubicin or Cisplatin was shown to result in activaton of multiple BH3-only proteins (Schneider-Jakob et al., 2010). In this thesis, mathematical modeling provided a rationale for the synergistic recruitment of Bax into pores induced by the combined stimulus of an activator and a sensitizer BH3-only protein (Figure 3.5). By binding to the prosurvival protein, the sensitizer can reduce the necessary amount of tBid to efficiently activate Bax.

In addition to the FDA-approved Bcl-2 specific inhibitor venetoclax, further highly selective BH3 mimetics currently become available (Kotschy et al., 2016). The heterogeneous responsiveness of tumours to distinct BH3 mimetics complicates the choice of the most efficient treatment option and to date no tools are available for the prediction of susceptibilities to BH3 mimetics alone or in combination. Different cancer and non-cancer cell types are differently susceptible to distinct BH3 mimetics, possibly linked to whether they reside in an apoptosis-primed, prosurvival protein-dependent state (Sarosiek and Letai, 2016). Additionally, exposure to BH3 mimetics can also cause conditions of ineffective MOMP induction, sublethal caspase activation and subsequent DNA damage and genomic instability (Ichim et al., 2015).

A predictive treatment response tool of BH3 mimetics leading to efficient cell death, cell survival or unfavorable oncogenic effects would thus be highly desirable. For this purpose, the mathematical modeling and quantitative analysis of molecular mechanisms of Bcl-2 family regulated MOMP on the cellular and single mitochondrial level will be necessary. Taking into account the crucial interaction mechanisms revealed in this study, a model encompassing the widely expressed and potent prosurvival regulators of cell death Bcl-2 and Mcl-1, as well as Bak activation and oligomerization, would complement such an investigation. A predictive response tool for BH3 mimetic treatment could in future studies be used to aid in stratifying patients, thereby supporting effective personalized treatment strategies.

Bibliography

D. Acehan, X. Jiang, D. G. Morgan, J. E. Heuser, X. Wang, and C. W. Akey. Three-Dimensional Structure of the Apoptosome. *Molecular Cell*, 9(2):423–432, February 2002.

J. G. Albeck, J. M. Burke, B. B. Aldridge, M. Zhang, D. A. Lauffenburger, and P. K. Sorger. Quantitative analysis of pathways controlling extrinsic apoptosis in single cells. *Molecular cell*, 30(1):11–25, April 2008a.

J. G. Albeck, J. M. Burke, S. L. Spencer, D. A. Lauffenburger, and P. K. Sorger. Modeling a Snap-Action, Variable-Delay Switch Controlling Extrinsic Cell Death. *PLoS Biology*, 6(12):e299, 2008b.

B. Alberts. *Molecular biology of the cell*. Garland Science, Taylor and Francis Group, New York, NY, sixth edition edition, 2015.

G. An, Q. Mi, J. Dutta-Moscato, and Y. Vodovotz. Agent-based models in translational systems biology. *Wiley Interdisciplinary Reviews: Systems Biology and Medicine*, 1(2): 159–171, September 2009.

V. Andreu-Fernández, M. Sancho, A. Genovés, E. Lucendo, F. Todt, J. Lauterwasser, K. Funk, G. Jahreis, E. Pérez-Payá, I. Mingarro, F. Edlich, and M. Orzáez. Bax transmembrane domain interacts with prosurvival Bcl-2 proteins in biological membranes. *Proceedings of the National Academy of Sciences of the United States of America*, 114 (2):310–315, January 2017.

B. Antonsson, S. Montessuit, S. Lauper, R. Eskes, and J.-C. Martinou. Bax oligomerization is required for channel-forming activity in liposomes and to trigger cytochrome c release from mitochondria. *Biochemical Journal*, 345(2):271–278, January 2000.

B. Antonsson, S. Montessuit, B. Sanchez, and J.-C. Martinou. Bax Is Present as a High Molecular Weight Oligomer/Complex in the Mitochondrial Membrane of Apoptotic Cells. *Journal of Biological Chemistry*, 276(15):11615–11623, April 2001.

A. Aouacheria, V. Rech de Laval, C. Combet, and J. M. Hardwick. Evolution of Bcl-2 homology motifs: homology versus homoplasy. *Trends in Cell Biology*, 23(3):103–111, March 2013.

A. Aranovich, Q. Liu, T. Collins, F. Geng, S. Dixit, B. Leber, and D. W. Andrews. Differences in the Mechanisms of Proapoptotic BH3 Proteins Binding to Bcl-XL and Bcl-2 Quantified in Live MCF-7 Cells. *Molecular Cell*, 45(6):754–763, March 2012.

H. Arokium, H. Ouerfelli, G. Velours, N. Camougrand, F. M. Vallette, and S. Manon. Substitutions of Potentially Phosphorylatable Serine Residues of Bax Reveal How They May Regulate Its Interaction with Mitochondria. *Journal of Biological Chemistry*, 282 (48):35104–35112, November 2007.

L. S. Babonis and M. Q. Martindale. Phylogenetic evidence for the modular evolution of metazoan signalling pathways. *Philosophical Transactions of the Royal Society of London. Series B, Biological Sciences*, 372(1713), February 2017.

R. Beroukhim, C. H. Mermel, D. Porter, G. Wei, S. Raychaudhuri, J. Donovan, J. Barretina, J. S. Boehm, J. Dobson, M. Urashima, K. T. Mc Henry, R. M. Pinchback, A. H. Ligon, Y.-J. Cho, L. Haery, H. Greulich, M. Reich, W. Winckler, M. S. Lawrence, B. A. Weir, K. E. Tanaka, D. Y. Chiang, A. J. Bass, A. Loo, C. Hoffman, J. Prensner, T. Liefeld, Q. Gao, D. Yecies, S. Signoretti, E. Maher, F. J. Kaye, H. Sasaki, J. E. Tepper, J. A. Fletcher, J. Tabernero, J. Baselga, M.-S. Tsao, F. Demichelis, M. A. Rubin, P. A. Janne, M. J. Daly, C. Nucera, R. L. Levine, B. L. Ebert, S. Gabriel, A. K. Rustgi, C. R. Antonescu, M. Ladanyi, A. Letai, L. A. Garraway, M. Loda, D. G. Beer, L. D. True, A. Okamoto, S. L. Pomeroy, S. Singer, T. R. Golub, E. S. Lander, G. Getz, W. R. Sellers, and M. Meyerson. The landscape of somatic copy-number alteration across human cancers. *Nature*, 463(7283):899–905, February 2010.

L. P. Billen, A. Shamas-Din, and D. W. Andrews. Bid: a Bax-like BH3 protein. *Oncogene*, 27 Suppl 1:S93–104, December 2008a.

L. P. Billen, C. L. Kokoski, J. F. Lovell, B. Leber, and D. W. Andrews. Bcl-XL Inhibits Membrane Permeabilization by Competing with Bax. *PLoS Biology*, 6(6):e147, June 2008b.

S. Bleicken, G. Hofhaus, B. Ugarte-Uribe, R. Schröder, and A. J. García-Sáez. cBid, Bax and Bcl-xL exhibit opposite membrane remodeling activities. *Cell Death and Disease*, 7(2):e2121, February 2016.

S. Bleicken, M. Classen, P. V. L. Padmavathi, T. Ishikawa, K. Zeth, H.-J. Steinhoff, and E. Bordignon. Molecular details of Bax activation, oligomerization, and membrane insertion. *The Journal of biological chemistry*, 285(9):6636–6647, February 2010.

S. Bleicken, A. J. García-Sáez, E. Conte, and E. Bordignon. Dynamic Interaction of cBid with Detergents, Liposomes and Mitochondria. *PLoS ONE*, 7(4):e35910, April 2012.

S. Bleicken, O. Landeta, A. Landajuela, G. Basañez, and A. J. García-Sáez. Proapoptotic Bax and Bak proteins form stable protein-permeable pores of tunable size. *The Journal of Biological Chemistry*, 288(46):33241–33252, November 2013a.

S. Bleicken, C. Wagner, and A. J. García-Sáez. Mechanistic Differences in the Membrane Activity of Bax and Bcl-xL Correlate with Their Opposing Roles in Apoptosis. *Biophysical Journal*, 104(2):421–431, January 2013b.

S. Bleicken, G. Jeschke, C. Stegmueller, R. Salvador-Gallego, A. J. García-Sáez, and E. Bordignon. Structural Model of Active Bax at the Membrane. *Molecular Cell*, 56 (4):496–505, November 2014.

S. Bleicken, A. Hantusch, K. K. Das, T. Frickey, and A. J. Garcia-Saez. Quantitative interactome of a membrane Bcl-2 network identifies a hierarchy of complexes for apoptosis regulation. *Nature Communications*, 8(1):73, July 2017.

C. Bogner, B. Leber, and D. W. Andrews. Apoptosis: embedded in membranes. *Current Opinion in Cell Biology*, 22(6):845–851, December 2010.

L. H. Boise, M. González-García, C. E. Postema, L. Ding, T. Lindsten, L. A. Turka, X. Mao, G. Nuñez, and C. B. Thompson. bcl-x, a bcl-2-related gene that functions as a dominant regulator of apoptotic cell death. *Cell*, 74(4):597–608, August 1993.

K. Breitschopf. Ubiquitin-mediated Degradation of the Proapoptotic Active Form of Bid. A FUNCTIONAL CONSEQUENCE ON APOPTOSIS INDUCTION. *Journal of Biological Chemistry*, 275(28):21648–21652, July 2000.

J. M. Brouwer, D. Westphal, G. Dewson, A. Y. Robin, R. T. Uren, R. Bartolo, G. V. Thompson, P. M. Colman, R. M. Kluck, and P. E. Czabotar. Bak Core and Latch Domains Separate during Activation, and Freed Core Domains Form Symmetric Homodimers. *Molecular Cell*, 55(6):938–946, September 2014.

K. P. Burnham, D. R. Anderson, and K. P. Burnham. *Model selection and multimodel inference: a practical information-theoretic approach*. Springer, New York, 2nd ed edition, 2002.

P.-F. Cartron, T. Gallenne, G. Bougras, F. Gautier, F. Manero, P. Vusio, K. Meflah, F. M. Vallette, and P. Juin. The First α Helix of Bax Plays a Necessary Role in Its Ligand-Induced Activation by the BH3-Only Proteins Bid and PUMA. *Molecular Cell*, 16(5):807–818, December 2004a.

P. F. Cartron, L. Oliver, E. Mayat, K. Meflah, and F. M. Vallette. Impact of pH on Bax alpha conformation, oligomerisation and mitochondrial integration. *FEBS letters*, 578 (1-2):41–46, December 2004b.

M. Certo, V. D. G. Moore, M. Nishino, G. Wei, S. Korsmeyer, S. A. Armstrong, and A. Letai. Mitochondria primed by death signals determine cellular addiction to anti-apoptotic BCL-2 family members. *Cancer Cell*, 9(5):351–365, May 2006.

B. A. Chabner and T. G. Roberts. Timeline: Chemotherapy and the war on cancer. *Nature Reviews Cancer*, 5(1):65–72, January 2005.

I. Chang, S. Majid, S. Saini, M. S. Zaman, S. Yamamura, T. Chiyomaru, V. Shahryari, S. Fukuhara, G. Deng, R. Dahiya, and Y. Tanaka. Hrk Mediates 2-Methoxyestradiol-Induced Mitochondrial Apoptotic Signaling in Prostate Cancer Cells. *Molecular Cancer Therapeutics*, 12(6):1049–1059, June 2013.

P. M. Chaudhary, M. T. Eby, A. Jasmin, A. Kumar, L. Liu, and L. Hood. Activation of the NF-κB pathway by Caspase 8 and its homologs. *Oncogene*, 19(39):4451–4460, September 2000.

C. Chen, J. Cui, H. Lu, R. Wang, S. Zhang, and P. Shen. Modeling of the Role of a Bax-Activation Switch in the Mitochondrial Apoptosis Decision. *Biophysical Journal*, 92(12):4304–4315, June 2007a.

C. Chen, J. Cui, W. Zhang, and P. Shen. Robustness analysis identifies the plausible model of the Bcl-2 apoptotic switch. *FEBS Letters*, 581(26):5143–5150, October 2007b.

H.-C. Chen, M. Kanai, A. Inoue-Yamauchi, H.-C. Tu, Y. Huang, D. Ren, H. Kim, S. Takeda, D. E. Reyna, P. M. Chan, Y. T. Ganesan, C.-P. Liao, E. Gavathiotis, J. J. Hsieh, and E. H. Cheng. An interconnected hierarchical model of cell death regulation by the BCL-2 family. *Nature Cell Biology*, 17(10):1270–1281, September 2015.

L. Chen, S. N. Willis, A. Wei, B. J. Smith, J. I. Fletcher, M. G. Hinds, P. M. Colman, C. L. Day, J. M. Adams, and D. C. S. Huang. Differential targeting of prosurvival Bcl-2 proteins by their BH3-only ligands allows complementary apoptotic function. *Molecular cell*, 17(3):393–403, February 2005.

W. W. Chen, M. Niepel, and P. K. Sorger. Classic and contemporary approaches to modeling biochemical reactions. *Genes & Development*, 24(17):1861–1875, September 2010.

E. H. Cheng, B. Levine, L. H. Boise, C. B. Thompson, and J. M. Hardwick. Bax-independent inhibition of apoptosis by Bcl-XL. *Nature*, 379(6565):554–556, February 1996.

E. H.-Y. Cheng. VDAC2 Inhibits BAK Activation and Mitochondrial Apoptosis. *Science*, 301(5632):513–517, July 2003.

X. Chi, J. Kale, B. Leber, and D. W. Andrews. Regulating cell death at, on, and in membranes. *Biochimica et Biophysica Acta (BBA) - Molecular Cell Research*, 1843(9): 2100–2113, September 2014.

J. J. Chou, H. Li, G. S. Salvesen, J. Yuan, and G. Wagner. Solution Structure of BID, an Intracellular Amplifier of Apoptotic Signaling. *Cell*, 96(5):615–624, March 1999.

N. Corazza, S. Jakob, C. Schaer, S. Frese, A. Keogh, D. Stroka, D. Kassahn, R. Torgler, C. Mueller, P. Schneider, and T. Brunner. TRAIL receptor–mediated JNK activation and Bim phosphorylation critically regulate Fas-mediated liver damage and lethality. *Journal of Clinical Investigation*, 116(9):2493–2499, September 2006.

S. Cory, A. W. Roberts, P. M. Colman, and J. M. Adams. Targeting BCL-2-like Proteins to Kill Cancer Cells. *Trends in Cancer*, 2(8):443–460, August 2016.

K. Cosentino and A. J. García-Sáez. Mitochondrial alterations in apoptosis. *Chemistry and Physics of Lipids*, 181:62–75, July 2014.

E. D. Crawford and J. A. Wells. Caspase Substrates and Cellular Remodeling. *Annual Review of Biochemistry*, 80(1):1055–1087, July 2011.

G. Csordás, P. Várnai, T. Golenár, S. Roy, G. Purkins, T. G. Schneider, T. Balla, and G. Hajnóczky. Imaging Interorganelle Contacts and Local Calcium Dynamics at the ER-Mitochondrial Interface. *Molecular Cell*, 39(1):121–132, July 2010.

P. E. Czabotar, E. F. Lee, M. F. van Delft, C. L. Day, B. J. Smith, D. C. S. Huang, W. D. Fairlie, M. G. Hinds, and P. M. Colman. Structural insights into the degradation of Mcl-1 induced by BH3 domains. *Proceedings of the National Academy of Sciences*, 104 (15):6217–6222, April 2007.

P. E. Czabotar, D. Westphal, G. Dewson, S. Ma, C. Hockings, W. D. Fairlie, E. F. Lee, S. Yao, A. Y. Robin, B. J. Smith, D. C. Huang, R. M. Kluck, J. M. Adams, and P. M. Colman. Bax Crystal Structures Reveal How BH3 Domains Activate Bax and Nucleate Its Oligomerization to Induce Apoptosis. *Cell*, 152(3):519–531, January 2013.

P. E. Czabotar, G. Lessene, A. Strasser, and J. M. Adams. Control of apoptosis by the BCL-2 protein family: implications for physiology and therapy. *Nature Reviews. Molecular Cell Biology*, 15(1):49–63, January 2014.

H. Dai, A. Smith, X. W. Meng, P. A. Schneider, Y.-P. Pang, and S. H. Kaufmann. Transient binding of an activator BH3 domain to the Bak BH3-binding groove initiates Bak oligomerization. *The Journal of cell biology*, 194(1):39–48, July 2011.

H. Dai, H. Ding, X. W. Meng, K. L. Peterson, P. A. Schneider, J. E. Karp, and S. H. Kaufmann. Constitutive BAK activation as a determinant of drug sensitivity in malignant lymphohematopoietic cells. *Genes & Development*, 29(20):2140–2152, October 2015.

K. K. Das, R. Shalaby, and A. J. García-Sáez. Determinants of BH3 Sequence Specificity for the Disruption of Bcl-xL/cBid Complexes in Membranes. *ACS Chemical Biology*, 12(4):989–1000, April 2017.

V. Del Gaizo Moore and A. Letai. BH3 profiling – Measuring integrated function of the mitochondrial apoptotic pathway to predict cell fate decisions. *Cancer Letters*, 332(2): 202–205, May 2013.

A. R. D. Delbridge and A. Strasser. The BCL-2 protein family, BH3-mimetics and cancer therapy. *Cell Death and Differentiation*, 22(7):1071–1080, July 2015.

A. R. D. Delbridge, S. Grabow, A. Strasser, and D. L. Vaux. Thirty years of BCL-2: translating cell death discoveries into novel cancer therapies. *Nature Reviews Cancer*, 16(2):99–109, January 2016.

J. Deng, N. Carlson, K. Takeyama, P. Dal Cin, M. Shipp, and A. Letai. BH3 Profiling Identifies Three Distinct Classes of Apoptotic Blocks to Predict Response to ABT-737 and Conventional Chemotherapeutic Agents. *Cancer Cell*, 12(2):171–185, August 2007.

A. Y. Denisov, T. Sprules, J. Fraser, G. Kozlov, and K. Gehring. Heat-induced dimerization of BCL-xL through alpha-helix swapping. *Biochemistry*, 46(3):734–740, January 2007.

A. Derakhshan, Z. Chen, and C. Van Waes. Therapeutic Small Molecules Target Inhibitor of Apoptosis Proteins in Cancers with Deregulation of Extrinsic and Intrinsic Cell Death Pathways. *Clinical Cancer Research*, 23(6):1379–1387, March 2017.

G. Dewson. Investigating Bak/Bax activating conformation change by immunoprecipitation. *Cold Spring Harbor Protocols*, 2015(5):472–476, May 2015.

D. N. Dhanasekaran and E. P. Reddy. JNK signaling in apoptosis. *Oncogene*, 27(48): 6245–6251, October 2008.

L. S. Dickens, R. S. Boyd, R. Jukes-Jones, M. A. Hughes, G. L. Robinson, L. Fairall, J. W. Schwabe, K. Cain, and M. MacFarlane. A Death Effector Domain Chain DISC Model Reveals a Crucial Role for Caspase-8 Chain Assembly in Mediating Apoptotic Cell Death. *Molecular Cell*, 47(2):291–305, July 2012.

J. Ding, B. H. M. Mooers, Z. Zhang, J. Kale, D. Falcone, J. McNichol, B. Huang, X. C. Zhang, C. Xing, D. W. Andrews, and J. Lin. After Embedding in Membranes Antiapoptotic Bcl-XL Protein Binds Both Bcl-2 Homology Region 3 and Helix 1 of Proapoptotic Bax Protein to Inhibit Apoptotic Mitochondrial Permeabilization. *Journal of Biological Chemistry*, 289(17):11873–11896, April 2014.

H. Du, J. Wolf, B. Schafer, T. Moldoveanu, J. E. Chipuk, and T. Kuwana. BH3 domains other than Bim and Bid can directly activate Bax/Bak. *The Journal of biological chemistry*, 286(1):491–501, January 2011.

L. Duprez, E. Wirawan, T. V. Berghe, and P. Vandenabeele. Major cell death pathways at a glance. *Microbes and Infection*, 11(13):1050–1062, November 2009.

H. Düssmann, M. Rehm, C. G. Concannon, S. Anguissola, M. Würstle, S. Kacmar, P. Völler, H. J. Huber, and J. H. M. Prehn. Single-cell quantification of Bax activation and mathematical modelling suggest pore formation on minimal mitochondrial Bax accumulation. *Cell death and differentiation*, 17(2):278–290, February 2010.

H. Düssmann, M. Rehm, D. Kögel, and J. H. M. Prehn. Outer mitochondrial membrane permeabilization during apoptosis triggers caspase-independent mitochondrial and caspase-dependent plasma membrane potential depolarization: a single-cell analysis. *Journal of Cell Science*, 116(Pt 3):525–536, February 2003.

F. Dyson. A meeting with Enrico Fermi. *Nature*, 427(6972):297–297, January 2004.

N. Echeverry, D. Bachmann, F. Ke, A. Strasser, H. U. Simon, and T. Kaufmann. Intracellular localization of the BCL-2 family member BOK and functional implications. *Cell Death and Differentiation*, 20(6):785–799, June 2013.

B. P. Eckelman, G. S. Salvesen, and F. L. Scott. Human inhibitor of apoptosis proteins: why XIAP is the black sheep of the family. *EMBO reports*, 7(10):988–994, October 2006.

J. Eder, R. Sedrani, and C. Wiesmann. The discovery of first-in-class drugs: origins and evolution. *Nature Reviews Drug Discovery*, 13(8):577–587, July 2014.

F. Edlich, S. Banerjee, M. Suzuki, M. M. Cleland, D. Arnoult, C. Wang, A. Neutzner, N. Tjandra, and R. J. Youle. Bcl-xL Retrotranslocates Bax from the Mitochondria into the Cytosol. *Cell*, 145(1):104–116, April 2011.

S. Einsele-Scholz, S. Malmsheimer, K. Bertram, D. Stehle, J. Johänning, M. Manz, P. T. Daniel, B. F. Gillissen, K. Schulze-Osthoff, and F. Essmann. Bok is a genuine multi-BH-domain protein that triggers apoptosis in the absence of Bax and Bak. *Journal of Cell Science*, 129(11):2213–2223, June 2016.

R. Eskes, S. Desagher, B. Antonsson, and J.-C. Martinou. Bid Induces the Oligomerization and Insertion of Bax into the Outer Mitochondrial Membrane. *Molecular and Cellular Biology*, 20(3):929–935, February 2000.

K. E. Ewings, K. Hadfield-Moorhouse, C. M. Wiggins, J. A. Wickenden, K. Balmanno, R. Gilley, K. Degenhardt, E. White, and S. J. Cook. ERK1/2-dependent phosphorylation of BimEL promotes its rapid dissociation from Mcl-1 and Bcl-xL. *The EMBO journal*, 26(12):2856–2867, June 2007.

M. Feoktistova, P. Geserick, B. Kellert, D. P. Dimitrova, C. Langlais, M. Hupe, K. Cain, M. MacFarlane, G. Häcker, and M. Leverkus. cIAPs block Ripoptosome formation, a RIP1/caspase-8 containing intracellular cell death complex differentially regulated by cFLIP isoforms. *Molecular Cell*, 43(3):449–463, August 2011.

Y. Fernández-Marrero, S. Bleicken, K. K. Das, D. Bachmann, T. Kaufmann, and A. J. Garcia-Saez. The membrane activity of BOK involves formation of large, stable toroidal pores and is promoted by cBID. *The FEBS Journal*, 284(5):711–724, March 2017.

B. E. Fitzwalter and A. Thorburn. Recent insights into cell death and autophagy. *FEBS Journal*, 282(22):4279–4288, November 2015.

J. L. Fox, F. Ismail, A. Azad, N. Ternette, S. Leverrier, M. J. Edelmann, B. M. Kessler, I. M. Leigh, S. Jackson, and A. Storey. Tyrosine dephosphorylation is required for Bak activation in apoptosis. *The EMBO Journal*, 29(22):3853–3868, November 2010.

Y. Fuchs and H. Steller. Programmed cell death in animal development and disease. *Cell*, 147(4):742–758, November 2011.

Y. Fuchs and H. Steller. Live to die another way: modes of programmed cell death and the signals emanating from dying cells. *Nature Reviews Molecular Cell Biology*, 16(6): 329–344, May 2015.

S. Fulda. Targeting extrinsic apoptosis in cancer: Challenges and opportunities. *Seminars in Cell & Developmental Biology*, 39:20–25, March 2015.

A. Funahashi, Y. Matsuoka, A. Jouraku, M. Morohashi, N. Kikuchi, and H. Kitano. CellDesigner 3.5: A Versatile Modeling Tool for Biochemical Networks. *Proceedings of the IEEE*, 96(8):1254–1265, August 2008.

L. Galluzzi, I. Vitale, J. M. Abrams, E. S. Alnemri, E. H. Baehrecke, M. V. Blagosklonny, T. M. Dawson, V. L. Dawson, W. S. El-Deiry, S. Fulda, E. Gottlieb, D. R. Green, M. O. Hengartner, O. Kepp, R. A. Knight, S. Kumar, S. A. Lipton, X. Lu, F. Madeo, W. Malorni, P. Mehlen, G. Nuñez, M. E. Peter, M. Piacentini, D. C. Rubinsztein, Y. Shi, H.-U. Simon, P. Vandenabeele, E. White, J. Yuan, B. Zhivotovsky, G. Melino, and G. Kroemer. Molecular definitions of cell death subroutines: recommendations of the Nomenclature Committee on Cell Death 2012. *Cell Death and Differentiation*, 19 (1):107–120, January 2012.

A. J. García-Sáez. The secrets of the Bcl-2 family. *Cell Death and Differentiation*, 19(11): 1733–1740, November 2012.

A. J. García-Sáez, J. Ries, M. Orzáez, E. Pérez-Payà, and P. Schwille. Membrane promotes tBID interaction with BCLXL. *Nature Structural & Molecular Biology*, 16(11):1178–1185, November 2009.

T. P. Garner, D. E. Reyna, A. Priyadarshi, H.-C. Chen, S. Li, Y. Wu, Y. T. Ganesan, V. N. Malashkevich, S. S. Almo, E. H. Cheng, and E. Gavathiotis. An Autoinhibited Dimeric Form of BAX Regulates the BAX Activation Pathway. *Molecular Cell*, 63(3): 485–497, August 2016.

S. Gaudet, S. L. Spencer, W. W. Chen, and P. K. Sorger. Exploring the Contextual Sensitivity of Factors that Determine Cell-to-Cell Variability in Receptor-Mediated Apoptosis. *PLoS Computational Biology*, 8(4):e1002482, April 2012.

E. Gavathiotis, M. Suzuki, M. L. Davis, K. Pitter, G. H. Bird, S. G. Katz, H.-C. Tu, H. Kim, E. H.-Y. Cheng, N. Tjandra, and L. D. Walensky. BAX activation is initiated at a novel interaction site. *Nature*, 455(7216):1076–1081, October 2008.

E. Gavathiotis, D. E. Reyna, M. L. Davis, G. H. Bird, and L. D. Walensky. BH3-Triggered Structural Reorganization Drives the Activation of Proapoptotic BAX. *Molecular Cell*, 40(3):481–492, November 2010.

B. Gibert and P. Mehlen. Dependence Receptors and Cancer: Addiction to Trophic Ligands. *Cancer Research*, 75(24):5171–5175, December 2015.

A. S. Gillings, K. Balmanno, C. M. Wiggins, M. Johnson, and S. J. Cook. Apoptosis and autophagy: BIM as a mediator of tumour cell death in response to oncogene-targeted therapeutics: BIM as a mediator of tumour cell death. *FEBS Journal*, 276(21):6050–6062, November 2009.

J. C. Goldstein, N. J. Waterhouse, P. Juin, G. I. Evan, and D. R. Green. The coordinate release of cytochrome c during apoptosis is rapid, complete and kinetically invariant. *Nature Cell Biology*, 2(3):156–162, March 2000.

A. M. Gonzalez-Angulo, B. T. J. Hennessy, and G. B. Mills. Future of personalized medicine in oncology: a systems biology approach. *Journal of Clinical Oncology: Official Journal of the American Society of Clinical Oncology*, 28(16):2777–2783, June 2010.

F. Gonzalvez, F. Pariselli, P. Dupaigne, I. Budihardjo, M. Lutter, B. Antonsson, P. Diolez, S. Manon, J.-C. Martinou, M. Goubern, X. Wang, S. Bernard, and P. X. Petit. tBid interaction with cardiolipin primarily orchestrates mitochondrial dysfunctions and subsequently activates Bax and Bak. *Cell Death and Differentiation*, 12(6):614–626, June 2005.

Y. Grabovsky and R. J. Tallarida. Isobolographic analysis for combinations of a full and partial agonist: curved isoboles. *The Journal of Pharmacology and Experimental Therapeutics*, 310(3):981–986, September 2004.

D. R. Green, L. Galluzzi, and G. Kroemer. Mitochondria and the Autophagy-Inflammation-Cell Death Axis in Organismal Aging. *Science*, 333(6046):1109–1112, August 2011.

D. R. Green and P. Fitzgerald. Just So Stories about the Evolution of Apoptosis. *Current Biology*, 26(13):R620–R627, July 2016.

M. T. Grijalba, A. E. Vercesi, and S. Schreier. Ca $^{2+}$ -Induced Increased Lipid Packing and Domain Formation in Submitochondrial Particles. A Possible Early Step in the Mechanism of Ca $^{2+}$ -Stimulated Generation of Reactive Oxygen Species by the Respiratory Chain †. *Biochemistry*, 38(40):13279–13287, October 1999.

L. Grosse, C. A. Wurm, C. Bru ser, D. Neumann, D. C. Jans, and S. Jakobs. Bax assembles into large ring-like structures remodeling the mitochondrial outer membrane in apoptosis. *The EMBO Journal*, 35(4):402–413, February 2016.

R. N. Gutenkunst, J. J. Waterfall, F. P. Casey, K. S. Brown, C. R. Myers, and J. P. Sethna. Universally Sloppy Parameter Sensitivities in Systems Biology Models. *PLoS Computational Biology*, 3(10):e189, 2007.

T. L. Haas, C. H. Emmerich, B. Gerlach, A. C. Schmukle, S. M. Cordier, E. Rieser, R. Feltham, J. Vince, U. Warnken, T. Wenger, R. Koschny, D. Komander, J. Silke, and H. Walczak. Recruitment of the linear ubiquitin chain assembly complex stabilizes the TNF-R1 signaling complex and is required for TNF-mediated gene induction. *Molecular Cell*, 36(5):831–844, December 2009.

D. Hanahan and R. A. Weinberg. The Hallmarks of Cancer. *Cell*, 100(1):57–70, January 2000.

A. Hantusch, T. Brunner, T. Frickey, and M. Rehm. Bcl-2-Ome – a database and interactive web service for dissecting the Bcl-2 interactome. *Cell Death and Differentiation*, 24(1):192–192, January 2017.

L. Happo, A. Strasser, and S. Cory. BH3-only proteins in apoptosis at a glance. *Journal of cell science*, 125(Pt 5):1081–1087, March 2012.

H. Harada, B. Becknell, M. Wilm, M. Mann, L. J.-s. Huang, S. S. Taylor, J. D. Scott, and S. J. Korsmeyer. Phosphorylation and Inactivation of BAD by Mitochondria-Anchored Protein Kinase A. *Molecular Cell*, 3(4):413–422, April 1999.

C. A. Harris and E. M. Johnson. BH3-only Bcl-2 family members are coordinately regulated by the JNK pathway and require Bax to induce apoptosis in neurons. *The Journal of Biological Chemistry*, 276(41):37754–37760, October 2001.

M. D. Haschka and A. Villunger. There is something about BOK we just don't get yet. *The FEBS Journal*, 284(5):708–710, March 2017.

M. D. Haschka, C. Soratroi, S. Kirschnek, G. Häcker, R. Hilbe, S. Geley, A. Villunger, and L. L. Fava. The NOXA–MCL1–BIM axis defines lifespan on extended mitotic arrest. *Nature Communications*, 6:6891, April 2015.

A. N. Hata, J. A. Engelman, and A. C. Faber. The BCL2 Family: Key Mediators of the Apoptotic Response to Targeted Anticancer Therapeutics. *Cancer Discovery*, 5(5): 475–487, May 2015.

E. Hermann, S. Bleicken, Y. Subburaj, and A. J. García-Sáez. Automated analysis of giant unilamellar vesicles using circular Hough transformation. *Bioinformatics*, 30(12): 1747–1754, June 2014.

M. J. Herold, J. Zeitz, C. Pelzer, C. Kraus, A. Peters, G. Wohlleben, and I. Berberich. The Stability and Anti-apoptotic Function of A1 Are Controlled by Its C Terminus. *Journal of Biological Chemistry*, 281(19):13663–13671, May 2006.

C. Hockings, K. Anwari, R. L. Ninnis, J. Brouwer, M. O'Hely, M. Evangelista, M. G. Hinds, P. E. Czabotar, E. F. Lee, W. D. Fairlie, G. Dewson, and R. M. Kluck. Bid chimeras indicate that most BH3-only proteins can directly activate Bak and Bax, and show no preference for Bak versus Bax. *Cell Death & Disease*, 6:e1735, April 2015.

B. Hoesel and J. A. Schmid. The complexity of NF-κB signaling in inflammation and cancer. *Molecular Cancer*, 12(1):86, 2013.

C. Holohan, S. Van Schaeybroeck, D. B. Longley, and P. G. Johnston. Cancer drug resistance: an evolving paradigm. *Nature Reviews Cancer*, 13(10):714–726, September 2013.

D. Holtom and E. Fisher. *Enjoy writing your science thesis or dissertation! a step by step guide to planning and writing dissertations and theses for undergraduate and graduate science students*. Imperial College Press, London, repr edition, 2006. OCLC: 837634836.

S. Hoops, S. Sahle, R. Gauges, C. Lee, J. Pahle, N. Simus, M. Singhal, L. Xu, P. Mendes, and U. Kummer. COPASI–a COmplex PAthway SImulator. *Bioinformatics*, 22(24): 3067–3074, December 2006.

S. Y. Hsu, A. Kaipia, E. McGee, M. Lomeli, and A. J. Hsueh. Bok is a pro-apoptotic Bcl-2 protein with restricted expression in reproductive tissues and heterodimerizes with selective anti-apoptotic Bcl-2 family members. *Proceedings of the National Academy of Sciences of the United States of America*, 94(23):12401–12406, November 1997.

S. Y. Hsu, P. Lin, and A. J. W. Hsueh. BOD (Bcl-2-Related Ovarian Death Gene) Is an Ovarian BH3 Domain-Containing Proapoptotic Bcl-2 Protein Capable of Dimerization with Diverse Antiapoptotic Bcl-2 Members. *Molecular Endocrinology*, 12(9):1432–1440, September 1998.

Y. T. Hsu and R. J. Youle. Nonionic detergents induce dimerization among members of the Bcl-2 family. *The Journal of Biological Chemistry*, 272(21):13829–13834, May 1997.

Q. Hu, D. Wu, W. Chen, Z. Yan, C. Yan, T. He, Q. Liang, and Y. Shi. Molecular determinants of caspase-9 activation by the Apaf-1 apoptosome. *Proceedings of the National Academy of Sciences*, 111(46):16254–16261, November 2014.

Q. Hu, W. Sun, C. Wang, and Z. Gu. Recent advances of cocktail chemotherapy by combination drug delivery systems. *Advanced Drug Delivery Reviews*, 98:19–34, March 2016.

H. J. Huber, H. Duessmann, J. Wenus, S. M. Kilbride, and J. H. M. Prehn. Mathematical modelling of the mitochondrial apoptosis pathway. *Biochimica Et Biophysica Acta*, 1813 (4):608–615, April 2011.

M. Hucka, A. Finney, H. M. Sauro, H. Bolouri, J. C. Doyle, H. Kitano, A. P. Arkin, B. J. Bornstein, D. Bray, A. Cornish-Bowden, A. A. Cuellar, S. Dronov, E. D. Gilles, M. Ginkel, V. Gor, I. I. Goryanin, W. J. Hedley, T. C. Hodgman, J.-H. Hofmeyr, P. J. Hunter, N. S. Juty, J. L. Kasberger, A. Kremling, U. Kummer, N. Le Novère, L. M. Loew, D. Lucio, P. Mendes, E. Minch, E. D. Mjolsness, Y. Nakayama, M. R. Nelson, P. F. Nielsen, T. Sakurada, J. C. Schaff, B. E. Shapiro, T. S. Shimizu, H. D. Spence, J. Stelling, K. Takahashi, M. Tomita, J. Wagner, J. Wang, and SBML Forum. The systems biology markup language (SBML): a medium for representation and exchange of biochemical network models. *Bioinformatics (Oxford, England)*, 19(4):524–531, March 2003.

M. A. Hughes, I. R. Powley, R. Jukes-Jones, S. Horn, M. Feoktistova, L. Fairall, J. W. Schwabe, M. Leverkus, K. Cain, and M. MacFarlane. Co-operative and Hierarchical Binding of c-FLIP and Caspase-8: A Unified Model Defines How c-FLIP Isoforms Differentially Control Cell Fate. *Molecular Cell*, 61(6):834–849, March 2016.

G. Ichim, J. Lopez, S. U. Ahmed, N. Muthalagu, E. Giampazolias, M. E. Delgado, M. Haller, J. S. Riley, S. M. Mason, D. Athineos, M. J. Parsons, B. van de Kooij, L. Bouchier-Hayes, A. J. Chalmers, R. W. Rooswinkel, A. Oberst, K. Blyth, M. Rehm, D. J. Murphy, and S. W. Tait. Limited Mitochondrial Permeabilization Causes DNA Damage and Genomic Instability in the Absence of Cell Death. *Molecular Cell*, 57(5): 860–872, March 2015.

A. Inoue-Yamauchi, P. S. Jeng, K. Kim, H.-C. Chen, S. Han, Y. T. Ganesan, K. Ishizawa, S. Jebiwott, Y. Dong, M. C. Pietanza, M. D. Hellmann, M. G. Kris, J. J. Hsieh, and E. H. Cheng. Targeting the differential addiction to anti-apoptotic BCL-2 family for cancer therapy. *Nature Communications*, 8:16078, July 2017.

S.-Y. Jeong, B. Gaume, Y.-J. Lee, Y.-T. Hsu, S.-W. Ryu, S.-H. Yoon, and R. J. Youle. Bcl-xL sequesters its C-terminal membrane anchor in soluble, cytosolic homodimers. *The EMBO Journal*, 23(10):2146–2155, May 2004.

J. Jia, F. Zhu, X. Ma, Z. Cao, Z. W. Cao, Y. Li, Y. X. Li, and Y. Z. Chen. Mechanisms of drug combinations: interaction and network perspectives. *Nature Reviews. Drug Discovery*, 8(2):111–128, 2009.

J. B. Johnson and K. S. Omland. Model selection in ecology and evolution. *Trends in Ecology & Evolution*, 19(2):101–108, February 2004.

M. Karbowski, K. L. Norris, M. M. Cleland, S.-Y. Jeong, and R. J. Youle. Role of Bax and Bak in mitochondrial morphogenesis. *Nature*, 443(7112):658–662, October 2006.

G. Karlebach and R. Shamir. Modelling and analysis of gene regulatory networks. *Nature Reviews Molecular Cell Biology*, 9(10):770–780, October 2008.

T. Kaufmann, S. Schlipf, J. Sanz, K. Neubert, R. Stein, and C. Borner. Characterization of the signal that directs Bcl-x $_{l}$, but not Bcl-2, to the mitochondrial outer membrane. *The Journal of Cell Biology*, 160(1):53–64, January 2003.

H. Kim, M. Rafiuddin-Shah, H.-C. Tu, J. R. Jeffers, G. P. Zambetti, J. J.-D. Hsieh, and E. H.-Y. Cheng. Hierarchical regulation of mitochondrion-dependent apoptosis by BCL-2 subfamilies. *Nature Cell Biology*, 8(12):1348–1358, December 2006.

H. Kim, H.-C. Tu, D. Ren, O. Takeuchi, J. R. Jeffers, G. P. Zambetti, J. J.-D. Hsieh, and E. H.-Y. Cheng. Stepwise activation of BAX and BAK by tBID, BIM, and PUMA initiates mitochondrial apoptosis. *Molecular cell*, 36(3):487–499, November 2009.

E. Klipp, W. Liebermeister, C. Wierling, A. Kowald, H. Lehrach, and R. Herwig, editors. *Systems biology: a textbook*. Wiley-VCH, Weinheim, 1. reprint edition, 2010.

E. Klipp, W. Liebermeister, C. Wierling, and A. Kowald. *Systems biology: a textbook*. Wiley-VCH Verlag GmbH & Co. KGaA, Weinheim, second, completely revised and enlarged edition edition, 2016. OCLC: 909797011.

A. J. Kocab and C. S. Duckett. Inhibitor of apoptosis proteins as intracellular signaling intermediates. *FEBS Journal*, 283(2):221–231, January 2016.

S. J. Korsmeyer. Regulators of cell death. *Trends in genetics: TIG*, 11(3):101–105, March 1995.

A. Kotschy, Z. Szlavik, J. Murray, J. Davidson, A. L. Maragno, G. Le Toumelin-Braizat, M. Chanrion, G. L. Kelly, J.-N. Gong, D. M. Moujalled, A. Bruno, M. Csekei, A. Paczal, Z. B. Szabo, S. Sipos, G. Radics, A. Proszenyak, B. Balint, L. Ondi, G. Blasko, A. Robertson, A. Surgenor, P. Dokurno, I. Chen, N. Matassova, J. Smith, C. Pedder, C. Graham, A. Studeny, G. Lysiak-Auvity, A.-M. Girard, F. Gravé, D. Segal, C. D. Riffkin, G. Pomilio, L. C. A. Galbraith, B. J. Aubrey, M. S. Brennan, M. J. Herold, C. Chang, G. Guasconi, N. Cauquil, F. Melchiore, N. Guigal-Stephan, B. Lockhart, F. Colland, J. A. Hickman, A. W. Roberts, D. C. S. Huang, A. H. Wei, A. Strasser, G. Lessene, and O. Geneste. The MCL1 inhibitor S63845 is tolerable and effective in diverse cancer models. *Nature*, 538(7626):477–482, October 2016.

C. Kreutz, A. Raue, and J. Timmer. Likelihood based observability analysis and confidence intervals for predictions of dynamic models. *BMC Systems Biology*, 6(1):120, 2012.

B. Ku, C. Liang, J. U. Jung, and B.-H. Oh. Evidence that inhibition of BAX activation by BCL-2 involves its tight and preferential interaction with the BH3 domain of BAX. *Cell Research*, 21(4):627–641, April 2011.

H. Y. Kueh, Y. Zhu, and J. Shi. A simplified Bcl-2 network model reveals quantitative determinants of cell-to-cell variation in sensitivity to anti-mitotic chemotherapeutics. *Scientific Reports*, 6:36585, November 2016.

T. Kuwana, M. R. Mackey, G. Perkins, M. H. Ellisman, M. Latterich, R. Schneiter, D. R. Green, and D. D. Newmeyer. Bid, Bax, and lipids cooperate to form supramolecular openings in the outer mitochondrial membrane. *Cell*, 111(3):331–342, November 2002.

T. Kuwana, L. Bouchier-Hayes, J. E. Chipuk, C. Bonzon, B. A. Sullivan, D. R. Green, and D. D. Newmeyer. BH3 domains of BH3-only proteins differentially regulate Bax-mediated mitochondrial membrane permeabilization both directly and indirectly. *Molecular cell*, 17(4):525–535, February 2005.

T. Kuwana, N. H. Olson, W. B. Kiosses, B. Peters, and D. D. Newmeyer. Pro-apoptotic Bax molecules densely populate the edges of membrane pores. *Scientific Reports*, 6: 27299, June 2016.

J. Lauterwasser, F. Todt, R. M. Zerbes, T. N. Nguyen, W. Craigen, M. Lazarou, M. van der Laan, and F. Edlich. The porin VDAC2 is the mitochondrial platform for Bax retrotranslocation. *Scientific Reports*, 6:32994, September 2016.

B. Leber, J. Lin, and D. W. Andrews. Embedded together: the life and death consequences of interaction of the Bcl-2 family with membranes. *Apoptosis: An International Journal on Programmed Cell Death*, 12(5):897–911, May 2007.

K. Lei and R. J. Davis. JNK phosphorylation of Bim-related members of the Bcl2 family induces Bax-dependent apoptosis. *Proceedings of the National Academy of Sciences of the United States of America*, 100(5):2432–2437, March 2003.

J. Lemke, S. von Karstedt, J. Zinngrebe, and H. Walczak. Getting TRAIL back on track for cancer therapy. *Cell Death and Differentiation*, 21(9):1350–1364, September 2014.

E. S. Leshchiner, C. R. Braun, G. H. Bird, and L. D. Walensky. Direct activation of full-length proapoptotic BAK. *Proceedings of the National Academy of Sciences of the United States of America*, 110(11):E986–995, March 2013.

A. Letai, M. C. Bassik, L. D. Walensky, M. D. Sorcinelli, S. Weiler, and S. J. Korsmeyer. Distinct BH3 domains either sensitize or activate mitochondrial apoptosis, serving as prototype cancer therapeutics. *Cancer Cell*, 2(3):183–192, September 2002.

A. G. Letai. Diagnosing and exploiting cancer's addiction to blocks in apoptosis. *Nature Reviews. Cancer*, 8(2):121–132, February 2008.

H. Li, H. Zhu, C.-j. Xu, and J. Yuan. Cleavage of BID by Caspase 8 Mediates the Mitochondrial Damage in the Fas Pathway of Apoptosis. *Cell*, 94(4):491–501, August 1998.

J. Li, T. McQuade, A. B. Siemer, J. Napetschnig, K. Moriwaki, Y.-S. Hsiao, E. Damko, D. Moquin, T. Walz, A. McDermott, F. K.-M. Chan, and H. Wu. The RIP1/RIP3

Necrosome Forms a Functional Amyloid Signaling Complex Required for Programmed Necrosis. *Cell*, 150(2):339–350, July 2012.

W. Liebermeister, E. Noor, A. Flamholz, D. Davidi, J. Bernhardt, and R. Milo. Visual account of protein investment in cellular functions. *Proceedings of the National Academy of Sciences*, 111(23):8488–8493, June 2014.

A. U. Lindner, C. G. Concannon, G. J. Boukes, M. D. Cannon, F. Llambi, D. Ryan, K. Boland, J. Kehoe, D. A. McNamara, F. Murray, E. W. Kay, S. Hector, D. R. Green, H. J. Huber, and J. H. M. Prehn. Systems analysis of BCL2 protein family interactions establishes a model to predict responses to chemotherapy. *Cancer research*, 73(2):519–528, January 2013a.

A. U. Lindner, J. H. M. Prehn, and H. J. Huber. The indirect activation model of mitochondrial outer membrane permeabilisation (MOMP) initiation requires a trade-off between robustness in the absence of and sensitivity in the presence of stress. *Molecular bioSystems*, 9(9):2359–2369, September 2013b.

A. U. Lindner, M. Salvucci, C. Morgan, N. Monsefi, A. J. Resler, M. Cremona, S. Curry, S. Toomey, R. O'Byrne, O. Bacon, M. Stühler, L. Flanagan, R. Wilson, P. G. Johnston, M. Salto-Tellez, S. Camilleri-Broët, D. A. McNamara, E. W. Kay, B. T. Hennessy, P. Laurent-Puig, S. Van Schaeybroeck, and J. H. M. Prehn. BCL-2 system analysis identifies high-risk colorectal cancer patients. *Gut*, September 2016.

J. Lindsay, M. D. Esposti, and A. P. Gilmore. Bcl-2 proteins and mitochondria—Specificity in membrane targeting for death. *Biochimica et Biophysica Acta (BBA) - Molecular Cell Research*, 1813(4):532–539, April 2011.

F. Llambi, T. Moldoveanu, S. W. Tait, L. Bouchier-Hayes, J. Temirov, L. L. McCormick, C. P. Dillon, and D. R. Green. A Unified Model of Mammalian BCL-2 Protein Family Interactions at the Mitochondria. *Molecular Cell*, 44(4):517–531, November 2011.

F. Llambi, Y.-M. Wang, B. Victor, M. Yang, D. M. Schneider, S. Gingras, M. J. Parsons, J. H. Zheng, S. A. Brown, S. Pelletier, T. Moldoveanu, T. Chen, and D. R. Green. BOK Is a Non-canonical BCL-2 Family Effector of Apoptosis Regulated by ER-Associated Degradation. *Cell*, 165(2):421–433, April 2016.

J. Lopez and S. W. G. Tait. Mitochondrial apoptosis: killing cancer using the enemy within. *British Journal of Cancer*, 112(6):957–962, March 2015.

J. F. Lovell, L. P. Billen, S. Bindner, A. Shamas-Din, C. Fradin, B. Leber, and D. W. Andrews. Membrane binding by tBid initiates an ordered series of events culminating in membrane permeabilization by Bax. *Cell*, 135(6):1074–1084, December 2008.

F. Luciano, A. Jacquel, P. Colosetti, M. Herrant, S. Cagnol, G. Pages, and P. Auberger. Phosphorylation of Bim-EL by Erk1/2 on serine 69 promotes its degradation via the proteasome pathway and regulates its proapoptotic function. *Oncogene*, 22(43):6785–6793, October 2003.

M. P. Luna-Vargas and J. E. Chipuk. The deadly landscape of pro-apoptotic BCL-2 proteins in the outer mitochondrial membrane. *The FEBS Journal*, 283(14):2676–2689, July 2016.

S. Ma, C. Hockings, K. Anwari, T. Kratina, S. Fennell, M. Lazarou, M. T. Ryan, R. M. Kluck, and G. Dewson. Assembly of the Bak apoptotic pore: a critical role for the Bak protein α6 helix in the multimerization of homodimers during apoptosis. *The Journal of Biological Chemistry*, 288(36):26027–26038, September 2013.

D. Machado, R. S. Costa, M. Rocha, E. C. Ferreira, B. Tidor, and I. Rocha. Modeling formalisms in Systems Biology. *AMB Express*, 1(1):45, 2011.

S. Malladi, M. Challa-Malladi, H. O. Fearnhead, and S. B. Bratton. The Apaf-1•procaspase-9 apoptosome complex functions as a proteolytic-based molecular timer. *The EMBO Journal*, 28(13):1916–1925, July 2009.

T. Mandal, S. Shin, S. Aluvila, H.-C. Chen, C. Grieve, J.-Y. Choe, E. H. Cheng, E. J. Hustedt, and K. J. Oh. Assembly of Bak homodimers into higher order homooligomers in the mitochondrial apoptotic pore. *Scientific Reports*, 6(1), November 2016.

G. Mariño, M. Niso-Santano, E. H. Baehrecke, and G. Kroemer. Self-consumption: the interplay of autophagy and apoptosis. *Nature Reviews Molecular Cell Biology*, 15(2): 81–94, January 2014.

K. D. Mason, M. R. Carpinelli, J. I. Fletcher, J. E. Collinge, A. A. Hilton, S. Ellis, P. N. Kelly, P. G. Ekert, D. Metcalf, A. W. Roberts, D. C. Huang, and B. T. Kile. Programmed Anuclear Cell Death Delimits Platelet Life Span. *Cell*, 128(6):1173–1186, March 2007.

J. P. Mathai, M. Germain, R. C. Marcellus, and G. C. Shore. Induction and endoplasmic reticulum location of BIK/NBK in response to apoptotic signaling by E1a and p53. *Oncogene*, 21(16):2534–2544, April 2002.

M. P. Mattson, M. Gleichmann, and A. Cheng. Mitochondria in Neuroplasticity and Neurological Disorders. *Neuron*, 60(5):748–766, December 2008.

U. Maurer, C. Charvet, A. S. Wagman, E. Dejardin, and D. R. Green. Glycogen Synthase Kinase-3 Regulates Mitochondrial Outer Membrane Permeabilization and Apoptosis by Destabilization of MCL-1. *Molecular Cell*, 21(6):749–760, March 2006.

O. Micheau, S. Lens, O. Gaide, K. Alevizopoulos, and J. Tschopp. NF- B Signals Induce the Expression of c-FLIP. *Molecular and Cellular Biology*, 21(16):5299–5305, August 2001.

O. Micheau and J. Tschopp. Induction of TNF receptor I-mediated apoptosis via two sequential signaling complexes. *Cell*, 114(2):181–190, July 2003.

T. Moldoveanu, Q. Liu, A. Tocilj, M. Watson, G. Shore, and K. Gehring. The X-Ray Structure of a BAK Homodimer Reveals an Inhibitory Zinc Binding Site. *Molecular Cell*, 24(5):677–688, December 2006.

T. Moldoveanu, C. R. Grace, F. Llambi, A. Nourse, P. Fitzgerald, K. Gehring, R. W. Kriwacki, and D. R. Green. BID-induced structural changes in BAK promote apoptosis. *Nature Structural & Molecular Biology*, 20(5):589–597, April 2013.

S. Montessuit, S. P. Somasekharan, O. Terrones, S. Lucken-Ardjomande, S. Herzig, R. Schwarzenbacher, D. J. Manstein, E. Bossy-Wetzel, G. Basañez, P. Meda, and J.-C. Martinou. Membrane remodeling induced by the dynamin-related protein Drp1 stimulates Bax oligomerization. *Cell*, 142(6):889–901, September 2010.

S. W. Muchmore, M. Sattler, H. Liang, R. P. Meadows, J. E. Harlan, H. S. Yoon, D. Nettesheim, B. S. Chang, C. B. Thompson, S. L. Wong, S. L. Ng, and S. W. Fesik. X-ray and NMR structure of human Bcl-xL, an inhibitor of programmed cell death. *Nature*, 381(6580):335–341, May 1996.

P. A. J. Muller and K. H. Vousden. p53 mutations in cancer. *Nature Cell Biology*, 15(1): 2–8, January 2013.

N. C. I. NCI. National Cancer Institute, NIH Fact Sheet - Cancer, March 2013.

D. Nijhawan, M. Fang, E. Traer, Q. Zhong, W. Gao, F. Du, and X. Wang. Elimination of Mcl-1 is required for the initiation of apoptosis following ultraviolet irradiation. *Genes & Development*, 17(12):1475–1486, June 2003.

L. O'Connor, A. Strasser, L. A. O'Reilly, G. Hausmann, J. M. Adams, S. Cory, and D. C. Huang. Bim: a novel member of the Bcl-2 family that promotes apoptosis. *The EMBO journal*, 17(2):384–395, January 1998.

E. Oda, R. Ohki, H. Murasawa, J. Nemoto, T. Shibue, T. Yamashita, T. Tokino, T. Taniguchi, and N. Tanaka. Noxa, a BH3-only member of the Bcl-2 family and candidate mediator of p53-induced apoptosis. *Science (New York, N.Y.)*, 288(5468): 1053–1058, May 2000.

K. J. Oh, S. Barbuto, K. Pitter, J. Morash, L. D. Walensky, and S. J. Korsmeyer. A Membrane-targeted BID BCL-2 Homology 3 Peptide Is Sufficient for High Potency Activation of BAX *in Vitro*. *Journal of Biological Chemistry*, 281(48):36999–37008, December 2006.

Z. N. Oltval, C. L. Milliman, and S. J. Korsmeyer. Bcl-2 heterodimerizes in vivo with a conserved homolog, Bax, that accelerates programed cell death. *Cell*, 74(4):609–619, August 1993.

J. W. O'Neill, M. K. Manion, B. Maguire, and D. M. Hockenbery. BCL-XL dimerization by three-dimensional domain swapping. *Journal of Molecular Biology*, 356(2):367–381, February 2006.

K. L. O'Neill, K. Huang, J. Zhang, Y. Chen, and X. Luo. Inactivation of prosurvival Bcl-2 proteins activates Bax/Bak through the outer mitochondrial membrane. *Genes & Development*, 30(8):973–988, April 2016.

J. T. Opferman. Apoptosis in the development of the immune system. *Cell Death and Differentiation*, 15(2):234–242, February 2008.

J. T. Opferman. Attacking cancer's Achilles heel: antagonism of anti-apoptotic BCL-2 family members. *The FEBS Journal*, 283(14):2661–2675, July 2016.

S. Orchard, M. Ammari, B. Aranda, L. Breuza, L. Briganti, F. Broackes-Carter, N. H. Campbell, G. Chavali, C. Chen, N. del Toro, M. Duesbury, M. Dumousseau, E. Galeota, U. Hinz, M. Iannuccelli, S. Jagannathan, R. Jimenez, J. Khadake, A. Lagreid, L. Licata, R. C. Lovering, B. Meldal, A. N. Melidoni, M. Milagros, D. Peluso, L. Perfetto, P. Porras, A. Raghunath, S. Ricard-Blum, B. Roechert, A. Stutz, M. Tognolli, K. van Roey, G. Cesareni, and H. Hermjakob. The MIntAct project–IntAct as a common curation platform for 11 molecular interaction databases. *Nucleic Acids Research*, 42(Database issue):D358–363, January 2014.

E. Ottina, D. Tischner, M. J. Herold, and A. Villunger. A1/Bfl-1 in leukocyte development and cell death. *Experimental cell research*, 318(11):1291–1303, July 2012.

L. J. Pagliari, T. Kuwana, C. Bonzon, D. D. Newmeyer, S. Tu, H. M. Beere, and D. R. Green. The multidomain proapoptotic molecules Bax and Bak are directly activated by heat. *Proceedings of the National Academy of Sciences of the United States of America*, 102(50):17975–17980, December 2005.

Y.-P. Pang, H. Dai, A. Smith, X. W. Meng, P. A. Schneider, and S. H. Kaufmann. Bak Conformational Changes Induced by Ligand Binding: Insight into BH3 Domain Binding and Bak Homo-Oligomerization. *Scientific Reports*, 2(1), December 2012.

S.-Y. Park and I.-S. Kim. Engulfment signals and the phagocytic machinery for apoptotic cell clearance. *Experimental & Molecular Medicine*, 49(5):e331, May 2017.

J. Pécot, L. Maillet, J. Le Pen, C. Vuillier, S. d. C. Trécesson, A. Fétiveau, K. A. Sarosiek, F. J. Bock, F. Braun, A. Letai, S. W. Tait, F. Gautier, and P. P. Juin. Tight Sequestration of BH3 Proteins by BCL-xL at Subcellular Membranes Contributes to Apoptotic Resistance. *Cell Reports*, 17(12):3347–3358, December 2016.

R. M. Perciavalle and J. T. Opferman. Delving deeper: MCL-1's contributions to normal and cancer biology. *Trends in Cell Biology*, 23(1):22–29, January 2013.

M. E. Peter. Programmed cell death: Apoptosis meets necrosis. *Nature*, 471(7338): 310–312, March 2011.

R. M. Pitti, S. A. Marsters, S. Ruppert, C. J. Donahue, A. Moore, and A. Ashkenazi. Induction of Apoptosis by Apo-2 Ligand, a New Member of the Tumor Necrosis Factor Cytokine Family. *Journal of Biological Chemistry*, 271(22):12687–12690, May 1996.

H. Puthalakath and A. Strasser. Keeping killers on a tight leash: transcriptional and post-translational control of the pro-apoptotic activity of BH3-only proteins. *Cell Death and Differentiation*, 9(5):505–512, May 2002.

H. Puthalakath, A. Villunger, L. A. O'Reilly, J. G. Beaumont, L. Coultas, R. E. Cheney, D. C. Huang, and A. Strasser. Bmf: a proapoptotic BH3-only protein regulated by interaction with the myosin V actin motor complex, activated by anoikis. *Science (New York, N.Y.)*, 293(5536):1829–1832, September 2001.

H. Puthalakath, D. C. Huang, L. A. O'Reilly, S. M. King, and A. Strasser. The Proapoptotic Activity of the Bcl-2 Family Member Bim Is Regulated by Interaction with the Dynein Motor Complex. *Molecular Cell*, 3(3):287–296, March 1999.

S. Rajan, M. Choi, Q. T. Nguyen, H. Ye, W. Liu, H. T. Toh, C. Kang, N. Kamariah, C. Li, H. Huang, C. White, K. Baek, G. Grüber, and H. S. Yoon. Structural transition in Bcl-xL and its potential association with mitochondrial calcium ion transport. *Scientific Reports*, 5:10609, May 2015.

A. Raue, C. Kreutz, T. Maiwald, J. Bachmann, M. Schilling, U. Klingmuller, and J. Timmer. Structural and practical identifiability analysis of partially observed dynamical models by exploiting the profile likelihood. *Bioinformatics*, 25(15):1923–1929, August 2009.

A. Raue, J. Karlsson, M. P. Saccomani, M. Jirstrand, and J. Timmer. Comparison of approaches for parameter identifiability analysis of biological systems. *Bioinformatics*, 30(10):1440–1448, May 2014.

V. Rech de Laval, G. Deléage, A. Aouacheria, and C. Combet. BCL2db: database of BCL-2 family members and BH3-only proteins. *Database: The Journal of Biological Databases and Curation*, 2014:bau013, 2014.

M. Rehm, H. J. Huber, C. T. Hellwig, S. Anguissola, H. Dussmann, and J. H. M. Prehn. Dynamics of outer mitochondrial membrane permeabilization during apoptosis. *Cell Death and Differentiation*, 16(4):613–623, April 2009.

M. Rehm and J. H. M. Prehn. Systems modelling methodology for the analysis of apoptosis signal transduction and cell death decisions. *Methods (San Diego, Calif.)*, 61(2):165–173, June 2013.

M. Rehm, H. Düssmann, and J. H. M. Prehn. Real-time single cell analysis of Smac/-DIABLO release during apoptosis. *The Journal of Cell Biology*, 162(6):1031–1043, September 2003.

T. T. Renault, O. Teijido, F. Missire, Y. T. Ganesan, G. Velours, H. Arokium, F. Beaumatin, R. Llanos, A. Athané, N. Camougrand, M. Priault, B. Antonsson, L. M. Dejean, and S. Manon. Bcl-xL stimulates Bax relocation to mitochondria and primes cells to ABT-737. *The International Journal of Biochemistry & Cell Biology*, 64:136–146, July 2015.

J. Ries, T. Weidemann, and P. Schwille. 2.11 Fluorescence Correlation Spectroscopy. In *Comprehensive Biophysics*, pages 210–245. Elsevier, 2012. DOI: 10.1016/B978-0-12-374920-8.00219-8.

J. Ries and P. Schwille. New concepts for fluorescence correlation spectroscopy on membranes. *Physical Chemistry Chemical Physics*, 10(24):3487, 2008.

J. Ries, Z. Petrášek, A. J. García-Sáez, and P. Schwille. A comprehensive framework for fluorescence cross-correlation spectroscopy. *New Journal of Physics*, 12(11):113009, November 2010.

A. W. Roberts, M. S. Davids, J. M. Pagel, B. S. Kahl, S. D. Puvvada, J. F. Gerecitano, T. J. Kipps, M. A. Anderson, J. R. Brown, L. Gressick, S. Wong, M. Dunbar, M. Zhu, M. B. Desai, E. Cerri, S. Heitner Enschede, R. A. Humerickhouse, W. G. Wierda, and J. F. Seymour. Targeting BCL2 with Venetoclax in Relapsed Chronic Lymphocytic Leukemia. *New England Journal of Medicine*, 374(4):311–322, January 2016.

J. Rodriguez and Y. Lazebnik. Caspase-9 and APAF-1 form an active holoenzyme. *Genes & Development*, 13(24):3179–3184, 1999.

W. P. Roos, A. D. Thomas, and B. Kaina. DNA damage and the balance between survival and death in cancer biology. *Nature Reviews Cancer*, 16(1):20–33, December 2015.

S. S. Roy, A. M. Ehrlich, W. J. Craigen, and G. Hajnóczky. VDAC2 is required for truncated BID-induced mitochondrial apoptosis by recruiting BAK to the mitochondria. *EMBO reports*, 10(12):1341–1347, December 2009.

S. Sahle, P. Mendes, S. Hoops, and U. Kummer. A new strategy for assessing sensitivities in biochemical models. *Philosophical Transactions of the Royal Society A: Mathematical, Physical and Engineering Sciences*, 366(1880):3619–3631, October 2008.

M. Saito, S. J. Korsmeyer, and P. H. Schlesinger. BAX-dependent transport of cytochrome c reconstituted in pure liposomes. *Nature Cell Biology*, 2(8):553–555, August 2000.

A. Saltelli, editor. *Global sensitivity analysis: the primer*. John Wiley, Chichester, England ; Hoboken, NJ, 2008.

R. Salvador-Gallego, M. Mund, K. Cosentino, J. Schneider, J. Unsay, U. Schraermeyer, J. Engelhardt, J. Ries, and A. J. Garcia-Saez. Bax assembly into rings and arcs in apoptotic mitochondria is linked to membrane pores. *The EMBO Journal*, 35(4):389–401, February 2016.

K. A. Sarosiek and A. Letai. Directly targeting the mitochondrial pathway of apoptosis for cancer therapy using BH3 mimetics - recent successes, current challenges and future promise. *The FEBS Journal*, 283(19):3523–3533, October 2016.

C. Scaffidi, S. Fulda, A. Srinivasan, C. Friesen, F. Li, K. J. Tomaselli, K. M. Debatin, P. H. Krammer, and M. E. Peter. Two CD95 (APO-1/Fas) signaling pathways. *The EMBO journal*, 17(6):1675–1687, March 1998.

J. Schaber. Easy parameter identifiability analysis with COPASI. *Biosystems*, 110(3): 183–185, December 2012.

J. Schaber, R. Baltanas, A. Bush, E. Klipp, and A. Colman-Lerner. Modelling reveals novel roles of two parallel signalling pathways and homeostatic feedbacks in yeast. *Molecular Systems Biology*, 8:622, 2012.

B. Schellenberg, P. Wang, J. A. Keeble, R. Rodriguez-Enriquez, S. Walker, T. W. Owens, F. Foster, J. Tanianis-Hughes, K. Brennan, C. H. Streuli, and A. P. Gilmore. Bax Exists in a Dynamic Equilibrium between the Cytosol and Mitochondria to Control Apoptotic Priming. *Molecular Cell*, 49(5):959–971, March 2013.

A. Schinzel, T. Kaufmann, M. Schuler, J. Martinalbo, D. Grubb, and C. Borner. Conformational control of Bax localization and apoptotic activity by Pro168. *The Journal of Cell Biology*, 164(7):1021–1032, March 2004.

S. Schneider-Jakob, N. Corazza, A. Badmann, D. Sidler, R. Stuber-Roos, A. Keogh, S. Frese, M. Tschan, and T. Brunner. Synergistic induction of cell death in liver tumor cells by TRAIL and chemotherapeutic drugs via the BH3-only proteins Bim and Bid. *Cell Death and Disease*, 1(10):e86, October 2010.

G. Schreiber, G. Haran, and H.-X. Zhou. Fundamental Aspects of Protein-Protein Association Kinetics. *Chemical Reviews*, 109(3):839–860, March 2009.

M. Schwickart, X. Huang, J. R. Lill, J. Liu, R. Ferrando, D. M. French, H. Maecker, K. O'Rourke, F. Bazan, J. Eastham-Anderson, P. Yue, D. Dornan, D. C. S. Huang, and V. M. Dixit. Deubiquitinase USP9x stabilizes MCL1 and promotes tumour cell survival. *Nature*, 463(7277):103–107, January 2010.

R. Sender, S. Fuchs, and R. Milo. Revised Estimates for the Number of Human and Bacteria Cells in the Body. *PLOS Biology*, 14(8):e1002533, August 2016.

A. Shamas-Din, S. Bindner, X. Chi, B. Leber, D. W. Andrews, and C. Fradin. Distinct lipid effects on tBid and Bim activation of membrane permeabilization by pro-apoptotic Bax. *Biochemical Journal*, 467(3):495–505, May 2015.

S. Shivakumar, M. Kurylowicz, N. Hirmiz, Y. Manan, O. Friaa, A. Shamas-Din, P. Masoudian, B. Leber, D. W. Andrews, and C. Fradin. The Proapoptotic Protein tBid Forms Both Superficially Bound and Membrane-Inserted Oligomers. *Biophysical Journal*, 106(10):2085–2095, May 2014.

R. M. Siegel, D. A. Martin, L. Zheng, S. Y. Ng, J. Bertin, J. Cohen, and M. J. Lenardo. Death-effector filaments: novel cytoplasmic structures that recruit caspases and trigger apoptosis. *The Journal of Cell Biology*, 141(5):1243–1253, June 1998.

J. Silke and P. Meier. Inhibitor of Apoptosis (IAP) Proteins-Modulators of Cell Death and Inflammation. *Cold Spring Harbor Perspectives in Biology*, 5(2):a008730–a008730, February 2013.

C. E. Sims and N. L. Allbritton. Analysis of single mammalian cells on-chip. *Lab on a Chip*, 7(4):423, 2007.

M. R. Sprick and H. Walczak. The interplay between the Bcl-2 family and death receptor-mediated apoptosis. *Biochimica et Biophysica Acta (BBA) - Molecular Cell Research*, 1644(2-3):125–132, March 2004.

Z. Su, Z. Yang, Y. Xu, Y. Chen, and Q. Yu. Apoptosis, autophagy, necroptosis, and cancer metastasis. *Molecular Cancer*, 14(1):48, 2015.

Y. Subburaj, K. Cosentino, M. Axmann, E. Pedrueza-Villalmanzo, E. Hermann, S. Bleicken, J. Spatz, and A. J. García-Sáez. Bax monomers form dimer units in the membrane that further self-assemble into multiple oligomeric species. *Nature Communications*, 6: 8042, August 2015.

L. Sun, H. Wang, Z. Wang, S. He, S. Chen, D. Liao, L. Wang, J. Yan, W. Liu, X. Lei, and X. Wang. Mixed Lineage Kinase Domain-like Protein Mediates Necrosis Signaling Downstream of RIP3 Kinase. *Cell*, 148(1-2):213–227, January 2012.

T.-C. Sung, C.-Y. Li, Y.-C. Lai, C.-L. Hung, O. Shih, Y.-Q. Yeh, U.-S. Jeng, and Y.-W. Chiang. Solution Structure of Apoptotic BAX Oligomer: Oligomerization Likely Precedes Membrane Insertion. *Structure (London, England: 1993)*, 23(10):1878–1888, October 2015.

M. Suzuki, R. J. Youle, and N. Tjandra. Structure of Bax: coregulation of dimer formation and intracellular localization. *Cell*, 103(4):645–654, November 2000.

D. Szklarczyk, A. Franceschini, S. Wyder, K. Forslund, D. Heller, J. Huerta-Cepas, M. Simonovic, A. Roth, A. Santos, K. P. Tsafou, M. Kuhn, P. Bork, L. J. Jensen, and C. von Mering. STRING v10: protein-protein interaction networks, integrated over the tree of life. *Nucleic Acids Research*, 43(D1):D447–D452, January 2015.

S. W. G. Tait and D. R. Green. Mitochondria and cell death: outer membrane permeabilization and beyond. *Nature Reviews Molecular Cell Biology*, 11(9):621–632, September 2010.

R. J. Tallarida. An Overview of Drug Combination Analysis with Isobolograms. *Journal of Pharmacology and Experimental Therapeutics*, 319(1):1–7, July 2006.

C. Tan, P. J. Dlugosz, J. Peng, Z. Zhang, S. M. Lapolla, S. M. Plafker, D. W. Andrews, and J. Lin. Auto-activation of the Apoptosis Protein Bax Increases Mitochondrial Membrane Permeability and Is Inhibited by Bcl-2. *Journal of Biological Chemistry*, 281(21):14764–14775, May 2006.

T. Tenev, K. Bianchi, M. Darding, M. Broemer, C. Langlais, F. Wallberg, A. Zachariou, J. Lopez, M. MacFarlane, K. Cain, and P. Meier. The Ripoptosome, a signaling platform that assembles in response to genotoxic stress and loss of IAPs. *Molecular Cell*, 43(3): 432–448, August 2011.

F. Todt, Z. Cakir, F. Reichenbach, R. J. Youle, and F. Edlich. The C-terminal helix of Bcl-xL mediates Bax retrotranslocation from the mitochondria. *Cell Death and Differentiation*, 20(2):333–342, February 2013.

F. Todt, Z. Cakir, F. Reichenbach, F. Emschermann, J. Lauterwasser, A. Kaiser, G. Ichim, S. W. Tait, S. Frank, H. F. Langer, and F. Edlich. Differential retrotranslocation of mitochondrial Bax and Bak. *The EMBO Journal*, 34(1):67–80, January 2015.

T. Tokar and J. Ulicny. The Mathematical Model of the Bcl-2 Family Mediated MOMP Regulation Can Perform a Non-Trivial Pattern Recognition. *PLoS ONE*, 8(12):e81861, December 2013.

T. Tokar, Z. Turcan, and J. Ulicny. Boolean network-based model of the Bcl-2 family mediated MOMP regulation. *Theoretical biology & medical modelling*, 10:40, 2013.

Y. Tsujimoto, L. R. Finger, J. Yunis, P. C. Nowell, and C. M. Croce. Cloning of the chromosome breakpoint of neoplastic B cells with the t(14;18) chromosome translocation. *Science (New York, N.Y.)*, 226(4678):1097–1099, November 1984a.

Y. Tsujimoto, J. Yunis, L. Onorato-Showe, J. Erikson, P. C. Nowell, and C. M. Croce. Molecular cloning of the chromosomal breakpoint of B-cell lymphomas and leukemias with the t(11;14) chromosome translocation. *Science (New York, N.Y.)*, 224(4656): 1403–1406, June 1984b.

B. Tummers and D. R. Green. Caspase-8: regulating life and death. *Immunological Reviews*, 277(1):76–89, May 2017.

R. T. Uren, M. O'Hely, S. Iyer, R. Bartolo, M. X. Shi, J. M. Brouwer, A. E. Alsop, G. Dewson, and R. M. Kluck. Disordered clusters of Bak dimers rupture mitochondria during apoptosis. *eLife*, 6, February 2017.

A. J. Valentijn, J.-P. Upton, N. Bates, and A. P. Gilmore. Bax targeting to mitochondria occurs via both tail anchor-dependent and -independent mechanisms. *Cell Death and Differentiation*, 15(8):1243–1254, August 2008.

T. Vanden Berghe, A. Linkermann, S. Jouan-Lanhouet, H. Walczak, and P. Vandenabeele. Regulated necrosis: the expanding network of non-apoptotic cell death pathways. *Nature Reviews. Molecular Cell Biology*, 15(2):135–147, February 2014.

T. Vervliet, J. B. Parys, and G. Bultynck. Bcl-2 proteins and calcium signaling: complexity beneath the surface. *Oncogene*, 35(39):5079–5092, September 2016.

C. Vivo, W. Liu, and V. C. Broaddus. c-Jun N-terminal Kinase Contributes to Apoptotic Synergy Induced by Tumor Necrosis Factor-related Apoptosis-inducing Ligand plus DNA Damage in Chemoresistant, p53 Inactive Mesothelioma Cells. *Journal of Biological Chemistry*, 278(28):25461–25467, July 2003.

N. Volkmann, F. M. Marassi, D. D. Newmeyer, and D. Hanein. The rheostat in the membrane: BCL-2 family proteins and apoptosis. *Cell Death and Differentiation*, 21 (2):206–215, February 2014.

S. von Karstedt, A. Montinaro, and H. Walczak. Exploring the TRAILs less travelled: TRAIL in cancer biology and therapy. *Nature Reviews Cancer*, 17(6):352–366, May 2017.

H. Walczak, R. E. Miller, K. Ariail, B. Gliniak, T. S. Griffith, M. Kubin, W. Chin, J. Jones, A. Woodward, T. Le, C. Smith, P. Smolak, R. G. Goodwin, C. T. Rauch, J. C. Schuh, and D. H. Lynch. Tumoricidal activity of tumor necrosis factor-related apoptosis-inducing ligand in vivo. *Nature Medicine*, 5(2):157–163, February 1999.

P. Wang, J. Lindsay, T. W. Owens, E. J. Mularczyk, S. Warwood, F. Foster, C. H. Streuli, K. Brennan, and A. P. Gilmore. Phosphorylation of the Proapoptotic BH3-Only Protein Bid Primes Mitochondria for Apoptosis during Mitotic Arrest. *Cell Reports*, 7(3):661–671, May 2014.

Q. Wang, S.-Y. Sun, F. Khuri, W. J. Curran, and X. Deng. Mono- or Double-Site Phosphorylation Distinctly Regulates the Proapoptotic Function of Bax. *PLoS ONE*, 5(10):e13393, October 2010.

Y. Wang and N. Tjandra. Structural Insights of tBid, the Caspase-8-activated Bid, and Its BH3 Domain. *Journal of Biological Chemistry*, 288(50):35840–35851, December 2013.

N. J. Waterhouse, J. C. Goldstein, O. von Ahsen, M. Schuler, D. D. Newmeyer, and D. R. Green. Cytochrome C Maintains Mitochondrial Transmembrane Potential and Atp Generation after Outer Mitochondrial Membrane Permeabilization during the Apoptotic Process. *The Journal of Cell Biology*, 153(2):319–328, April 2001.

A. Weber, M. Heinlein, J. Dengjel, C. Alber, P. K. Singh, and G. Häcker. The deubiquitinase Usp27x stabilizes the BH3-only protein Bim and enhances apoptosis. *EMBO reports*, 17(5):724–738, May 2016.

M. C. Wei, T. Lindsten, V. K. Mootha, S. Weiler, A. Gross, M. Ashiya, C. B. Thompson, and S. J. Korsmeyer. tBID, a membrane-targeted death ligand, oligomerizes BAK to release cytochrome c. *Genes & Development*, 14(16):2060–2071, August 2000.

R. Weinlich, A. Oberst, H. M. Beere, and D. R. Green. Necroptosis in development, inflammation and disease. *Nature Reviews Molecular Cell Biology*, 18(2):127–136, December 2016.

I. E. Wertz, S. Kusam, C. Lam, T. Okamoto, W. Sandoval, D. J. Anderson, E. Helgason, J. A. Ernst, M. Eby, J. Liu, L. D. Belmont, J. S. Kaminker, K. M. O'Rourke, K. Pujara, P. B. Kohli, A. R. Johnson, M. L. Chiu, J. R. Lill, P. K. Jackson, W. J. Fairbrother, S. Seshagiri, M. J. C. Ludlam, K. G. Leong, E. C. Dueber, H. Maecker, D. C. S. Huang, and V. M. Dixit. Sensitivity to antitubulin chemotherapeutics is regulated by MCL1 and FBW7. *Nature*, 471(7336):110–114, March 2011.

S. R. Wiley, K. Schooley, P. J. Smolak, W. S. Din, C.-P. Huang, J. K. Nicholl, G. R. Sutherland, T. D. Smith, C. Rauch, C. A. Smith, and R. G. Goodwin. Identification and characterization of a new member of the TNF family that induces apoptosis. *Immunity*, 3(6):673–682, December 1995.

F. Wilfling, A. Weber, S. Potthoff, F.-N. Vögtle, C. Meisinger, S. A. Paschen, and G. Häcker. BH3-only proteins are tail-anchored in the outer mitochondrial membrane and can initiate the activation of Bax. *Cell death and differentiation*, 19(8):1328–1336, August 2012.

S. N. Willis, L. Chen, G. Dewson, A. Wei, E. Naik, J. I. Fletcher, J. M. Adams, and D. C. S. Huang. Proapoptotic Bak is sequestered by Mcl-1 and Bcl-xL, but not Bcl-2, until displaced by BH3-only proteins. *Genes & development*, 19(11):1294–1305, June 2005.

S. N. Willis, J. I. Fletcher, T. Kaufmann, M. F. van Delft, L. Chen, P. E. Czabotar, H. Ierino, E. F. Lee, W. D. Fairlie, P. Bouillet, A. Strasser, R. M. Kluck, J. M. Adams, and D. C. S. Huang. Apoptosis initiated when BH3 ligands engage multiple Bcl-2 homologs, not Bax or Bak. *Science (New York, N.Y.)*, 315(5813):856–859, February 2007.

J. Wilson-Annan, L. A. O'Reilly, S. A. Crawford, G. Hausmann, J. G. Beaumont, L. P. Parma, L. Chen, M. Lackmann, T. Lithgow, M. G. Hinds, C. L. Day, J. M. Adams, and D. C. Huang. Proapoptotic BH3-only proteins trigger membrane integration of prosurvival Bcl-w and neutralize its activity. *The Journal of Cell Biology*, 162(5):877–888, September 2003.

K. G. Wolter, Y. T. Hsu, C. L. Smith, A. Nechushtan, X. G. Xi, and R. J. Youle. Movement of Bax from the cytosol to mitochondria during apoptosis. *The Journal of Cell Biology*, 139(5):1281–1292, December 1997.

C.-C. Wu, S. Lee, S. Malladi, M.-D. Chen, N. J. Mastrandrea, Z. Zhang, and S. B. Bratton. The Apaf-1 apoptosome induces formation of caspase-9 homo- and heterodimers with distinct activities. *Nature Communications*, 7:13565, November 2016.

G. S. Wu, T. F. Burns, E. R. McDonald, W. Jiang, R. Meng, I. D. Krantz, G. Kao, D. D. Gan, J. Y. Zhou, R. Muschel, S. R. Hamilton, N. B. Spinner, S. Markowitz, G. Wu, and W. S. el Deiry. KILLER/DR5 is a DNA damage-inducible p53-regulated death receptor gene. *Nature Genetics*, 17(2):141–143, October 1997.

M. L. Würstle, E. Zink, J. H. M. Prehn, and M. Rehm. From computational modelling of the intrinsic apoptosis pathway to a systems-based analysis of chemotherapy resistance: achievements, perspectives and challenges in systems medicine. *Cell Death & Disease*, 5:e1258, 2014.

M. L. Würstle and M. Rehm. A Systems Biology Analysis of Apoptosome Formation and Apoptosis Execution Supports Allosteric Procaspase-9 Activation. *Journal of Biological Chemistry*, 289(38):26277–26289, September 2014.

X.-P. Xu, D. Zhai, E. Kim, M. Swift, J. C. Reed, N. Volkmann, and D. Hanein. Three-dimensional structure of Bax-mediated pores in membrane bilayers. *Cell Death and Disease*, 4(6):e683, June 2013.

W. S. Yang, J.-K. Ko, S.-O. Park, H.-Y. Choi, Y.-N. Kim, and C.-W. Kim. C-terminal region of Bfl-1 induces cell death that accompanies caspase activation when fused with GFP. *Journal of Cellular Biochemistry*, 94(6):1234–1247, April 2005.

Y. Yao, L. M. Fujimoto, N. Hirshman, A. A. Bobkov, A. Antignani, R. J. Youle, and F. M. Marassi. Conformation of BCL-XL upon Membrane Integration. *Journal of Molecular Biology*, 427(13):2262–2270, July 2015.

H. You, M. Pellegrini, K. Tsuchihara, K. Yamamoto, G. Hacker, M. Erlacher, A. Villunger, and T. W. Mak. FOXO3a-dependent regulation of Puma in response to cytokine/growth factor withdrawal. *The Journal of Experimental Medicine*, 203(7):1657–1663, July 2006.

R. J. Youle and M. Karbowski. Mitochondrial fission in apoptosis. *Nature Reviews. Molecular Cell Biology*, 6(8):657–663, August 2005.

R. J. Youle and A. Strasser. The BCL-2 protein family: opposing activities that mediate cell death. *Nature reviews. Molecular cell biology*, 9(1):47–59, January 2008.

J. Yu, L. Zhang, P. M. Hwang, K. W. Kinzler, and B. Vogelstein. PUMA Induces the Rapid Apoptosis of Colorectal Cancer Cells. *Molecular Cell*, 7(3):673–682, March 2001.

B. J. Zarnegar, Y. Wang, D. J. Mahoney, P. W. Dempsey, H. H. Cheung, J. He, T. Shiba, X. Yang, W.-c. Yeh, T. W. Mak, R. G. Korneluk, and G. Cheng. Noncanonical NF-κB activation requires coordinated assembly of a regulatory complex of the adaptors cIAP1, cIAP2, TRAF2 and TRAF3 and the kinase NIK. *Nature Immunology*, 9(12): 1371–1378, December 2008.

J. Zha, H. Harada, E. Yang, J. Jockel, and S. J. Korsmeyer. Serine Phosphorylation of Death Agonist BAD in Response to Survival Factor Results in Binding to 14-3-3 Not BCL-XL. *Cell*, 87(4):619–628, November 1996.

Z. Zhang, S. Subramaniam, J. Kale, C. Liao, B. Huang, H. Brahmbhatt, S. G. Condon, S. M. Lapolla, F. A. Hays, J. Ding, F. He, X. C. Zhang, J. Li, A. Senes, D. W. Andrews,

and J. Lin. BH3-in-groove dimerization initiates and helix 9 dimerization expands Bax pore assembly in membranes. *The EMBO Journal*, 35(2):208–236, January 2016.

J. Zhao, S. Jitkaew, Z. Cai, S. Choksi, Q. Li, J. Luo, and Z.-G. Liu. Mixed lineage kinase domain-like is a key receptor interacting protein 3 downstream component of TNF-induced necrosis. *Proceedings of the National Academy of Sciences*, 109(14):5322–5327, April 2012.

H. Zhou, Q. Hou, Y. Chai, and Y. Hsu. Distinct domains of Bcl-X are involved in Bax and Bad antagonism and in apoptosis inhibition. *Experimental Cell Research*, 309(2): 316–328, October 2005.